Ion channels and calcium signaling in kidney disease

DISSERTATION ZUR ERLANGUNG DES DOKTORGRADES
DER NATURWISSENSCHAFTEN (DR.RER.NAT.)
DER FAKULTÄT FÜR BIOLOGIE UND VORKLINISCHE MEDIZIN
DER UNIVERSITÄT REGENSBURG

vorgelegt von
Khaoula Talbi
aus
Tunis, Tunisia

im Jahr
2022

DAS PROMOTIONSGESUCH WURDE EINGEREICHT AM:
28.10.22
DIE ARBEIT WURDE ANGELEITET VON:
PROF. DR. RAINER SCHREIBER

UNTERSCHRIFT:

DIE ARBEIT WURDE ANGELEITET VON: PROF. DR. RAINER SCHREIBER

PRÜFUNGSAUSSCHUSS:

VORSITZENDER: PROF. DR. RICHARD WARTH

1. GUTACHTER: PROF. DR. RAINER SCHREIBER

2. GUTACHTER: DR. MED. BJÖRN BUCHHOLZ

3. PRÜFERIN: PROF. DR. CHRISTINE ZIEGLER

ERSATZPERSON: PROF. DR. CHARLOTTE WAGNER

SUMMARY

Autosomal dominant polycystic kidney disease (ADPKD) is characterized by the development of bilateral cysts, which grow over many years and compromise the function of adjacent renal tissue, leading to a gradual decline in kidney function and ultimately, renal failure. ADPKD is induced by mutations in two different genes, namely PKD1 and PKD2 While PKD1 encodes an orphan receptor (polycystin-1; PC-1), Pkd2 encodes a non-selective cation channel which is permeable for Ca^{2+} (polycystin-2; PC-2). PC-1 and PC-2 form a functional complex which modulates intracellular calcium. Cyst development and growth in ADPKD are driven by enhanced cell proliferation and chloride secretion. The calcium (Ca^{2+}) activated chloride channel TMEM16A (Anoctamin 1) was shown to be central in interrupting Ca^{2+} signaling, and increasing proliferation and Cl^- secretion in mice with ADPKD, caused by lack of expression of PC-1. It was unclear whether lack of expression of PC-2 leads to a similar increase of TMEM16A-dependent Ca^{2+} signaling as does the lack of PC-1 expression. In the present work we demonstrate that the loss of both Pkd1 or Pkd2 leads to enhanced release of Ca^{2+} from the endoplasmic reticulum (ER) Ca^{2+} store, upon purinergic stimulation by ATP. Abnormal Ca^{2+} signaling due to abrogation of either PC-1 or PC-2 relies on expression of TMEM16A, as demonstrated by siRNA-mediated knockout of TMEM16A.

In numerous previous *in vitro* studies, upregulation of the cystic fibrosis transmembrane conductance regulator (CFTR), an adenosine 3',5'-cyclic monophosphate (cAMP)-activated chloride channel, was proposed to be crucial for ADPKD. However, this has never been confirmed *in vivo*. Using double knockout mice ($Pkd1^{-/-}/Cftr^{-/-}$), we provide strong evidence that CFTR is not required for cyst development in Pkd1-knockout mice. ADPKD mice lacking expression of CFTR still demonstrate upregulation of ion currents and cell proliferation, and develop large renal cysts, supporting the use of inhibitors for TMEM16A but not CFTR for the treatment of ADPKD.

Men develop a more severe ADPKD phenotype compared to women, and have an earlier onset of end stage renal disease (ESRD). Consistently, male gender was shown to be associated with a more severe cyst development in different experimental settings. This gender-dependent disease progression is thought to originate from the differences in sex hormones. We therefore investigated the mechanisms by which androgens and estrogens contribute to differences in disease severity, and whether this mechanism involve TMEM16A. We found that differences in male vs. female ADPKD are paralleled by differences in intracellular Ca^{2+} signaling, and that androgen-induced upregulation of Ca^{2+} influx channels is probably the cause for enhanced activity of TMEM16A, and the more severe disease phenotype observed in males.

Calmodulin (CAM) is a mediator of intracellular Ca^{2+} signaling and contradicting reports exist on CAM-dependent regulation of TMEM16A. CAM is a highly conserved Ca^{2+}-binding

messenger which is known to modulate the activity of a wide range of proteins. We indeed found that CAM induced activation of TMEM16A, when TMEM16A was overexpressed, while cells, which express TMEM16A endogenously, do not show a CAM-dependent regulation of TMEM16A. We found evidence that CAM interaction with TMEM16A modulates the Ca^{2+} sensitivity of TMEM16A. Enhanced Ca^{2+} sensitivity of overexpressed TMEM16A explains its enhanced activity at basal intracellular Ca^{2+} levels. These results correspond well to a recent report demonstrating pre-association of CAM with TMEM16A, which mediates sensitization of TMEM16A towards intracellular Ca^{2+}. We therefore propose that regulatory properties of TMEM16A detected in overexpression studies, should be validated for endogenously expressed TMEM16A.

In an earlier report, our team demonstrated that the TMEM16A paralogue TMEM16J also modulates calcium signaling by depleting the (ER) Ca^{2+} store. Interestingly, the TMEM16J gene is located in a genomic region that negatively regulates immune responses. Mutations within this locus are linked to hyper-inflammatory diseases in various organs and rejection of renal grafts. The function of TMEM16J in immune cells and tissues is currently unknown. A genome wide association study identified a TMEM16J variant, TMEM16J-T604A, as a risk factor for chronic kidney disease (CKD). We found that TMEM16J is an ER-resident ion channel which regulates Ca^{2+} signaling, while its ion channel function is disrupted in TMEM16J-T604A. Moreover, we demonstrated that TMEM16J and TMEM16J-T604A modulate synthesis and release of pro-inflammatory cytokines through regulation of intracellular Ca^{2+} signals, thereby providing a possible link to chronic inflammation and CKD. These results identify TMEM16J as a novel promising target for the treatment of CKD and chronic inflammation in general.

ZUSAMMENFASSUNG

Die autosomal-dominante polyzystische Nierenerkrankung (ADPKD) ist durch die Entwicklung bilateraler Zysten gekennzeichnet, die über viele Jahre hinweg wachsen und die Funktion des angrenzenden Nierengewebes beeinträchtigen. Dies führt zu einer allmählichen Abnahme der Nierenfunktion und schließlich zum Nierenversagen. ADPKD wird durch Mutationen in zwei verschiedenen Genen, nämlich PKD1 und PKD2 ausgelöst. Während PKD1 für einen Orphan-Rezeptor (Polycystin-1; PC-1) kodiert, kodiert PKD2 für einen nicht-selektiven Kationenkanal, der Ca^{2+} durchlässig ist (Polycystin-2; PC-2). PC-1 und PC-2 bilden einen funktionellen Komplex, der das intrazelluläre Kalzium moduliert. Zystenentwicklung und -wachstum bei ADPKD werden durch verstärkte Zellproliferation und Chloridsekretion angetrieben. Es konnte bei ADPKD- Mäusen gezeigt werden, dass aufgrund der fehlenden Expression von PC-1 der Kalzium (Ca^{2+}) aktivierte Chloridkanal TMEM16A (Anoctamin 1) eine zentrale Rolle bei der Erhöhung des intrazellulären Ca^{2+}-Signals, und der Zunahme der Proliferation und Chlorid-Sekretion spielt. Es war unklar, ob eine fehlende Expression von PC-2 zu einem ähnlichen Anstieg des TMEM16A-abhängigen intrazellulären Ca^{2+}-Signals führt, wie das Fehlen der Expression von PC-1. In der vorliegenden Arbeit konnten wir zeigen, dass bei purinerger ATP- Stimulation der Verlust sowohl von Pkd-1 als auch der von Pkd-2 zu einer erhöhten Freisetzung von Ca^{2+} aus dem Ca^{2+}-Speicher des endoplasmatischen Retikulums (ER) führt. Dieses erhöhte intrazelluläre Ca^{2+}-Signal hängt von der Expression von TMEM16A ab, wie durch siRNA-vermittelte Ausschaltung von TMEM16A gezeigt werden konnte.

In zahlreichen früheren *in vitro*-Studien wurde eine erhöhte Expression von CFTR (Cystic Fibrosis Transmembrane conductance Regulator), eines durch Adenosin-3',5'-zyklisches Monophosphat (cAMP) aktivierten Chloridkanals, als entscheidend für Entstehung von ADPKD angesehen. Dies wurde jedoch nie *in vivo* bestätigt. Mit Hilfe von Doppel-Knockout-Mäusen ($Pkd1^{-/-}/Cftr^{-/-}$) konnten wir eindeutig nachweisen, dass CFTR für die Zystenbildung bei Pkd-1-Knockout-Mäusen nicht erforderlich ist. ADPKD-Mäuse, denen die Expression von CFTR fehlt, zeigen immer noch erhöhte Ionenströme und eine erhöhte Zellproliferation und entwickeln große Nierenzysten. Diese Ergebnisse unterstützen den Einsatz von TMEM16A- Inhibitoren gegenüber CFTR- Inhibitoren zur Behandlung von ADPKD.

Männer entwickeln einen schwereren ADPKD-Phänotyp als Frauen und weisen ein früheres Auftreten von Nierenerkrankungen im Endstadium (ESRD) auf. Übereinstimmend wurde gezeigt, dass das männliche Geschlecht in verschiedenen Versuchsanordnungen mit einer schwereren Zystenentwicklung verbunden ist. Es wird angenommen, dass dieser geschlechtsabhängige Krankheitsverlauf auf die Geschlechtshormone zurückzuführen ist. Wir untersuchten daher die Mechanismen, durch die Androgene und Östrogene zu den Unterschieden in der Schwere der Erkrankung beitragen, und ob diese Mechanismen TMEM16A betreffen. Wir fanden heraus, dass die Unterschiede zwischen männlicher und

weiblicher ADPKD mit Unterschieden im intrazellulären Ca^{2+}-Signal einhergehen und dass wahrscheinlich eine androgen bedingte Hochregulierung von Ca^{2+}-Einstromkanälen die Ursache für die erhöhte Aktivität von TMEM16A ist und die beobachteten schwereren Krankheitsverläufen bei Männern erklärt.

Calmodulin (CAM) ist ein Vermittler des intrazellulären Ca^{2+}-Signals. Es gibt widersprüchliche Berichte über die CAM-abhängige Regulierung von TMEM16A. CAM ist ein hoch konservierter Ca^{2+}-bindender Botenstoff, von dem bekannt ist, dass er die Aktivität einer Vielzahl von Proteinen moduliert. In der Tat haben wir festgestellt, dass CAM die Aktivierung von TMEM16A induziert, wenn TMEM16A überexprimiert wird, während Zellen, die TMEM16A endogen exprimieren, keine CAM-abhängige Regulation von TMEM16A zeigen. Wir fanden Hinweise darauf, dass die Interaktion von CAM mit TMEM16A die Ca^{2+}-Empfindlichkeit von TMEM16A moduliert. Die erhöhte Ca^{2+}-Empfindlichkeit von überexprimiertem TMEM16A erklärt seine erhöhte Aktivität bei basalen intrazellulären Ca^{2+}-Spiegeln. Diese Ergebnisse stimmen gut mit einem kürzlich erschienenen Bericht über die Interaktion von CAM mit TMEM16A überein, die eine Sensibilisierung von TMEM16A gegenüber intrazellulärem Ca^{2+} bewirkt. Wir empfehlen deshalb, dass die regulatorischen Eigenschaften von TMEM16A, die in Überexpressionsstudien nachgewiesen wurden, für endogen exprimiertes TMEM16A validiert werden sollten.

In einer früheren Veröffentlichung hat unser Team gezeigt, dass der TMEM16A-Paralog TMEM16J auch das intrazellulären Ca^{2+}-Signal moduliert, indem er den Ca^{2+}-Speicher des endoplasmatischen Retikulums (ER) leert. Interessanterweise befindet sich das TMEM16J-Gen in einer genomischen Region, die die Immunantwort negativ reguliert. Mutationen innerhalb dieses Lokus werden mit hyperinflammatorischen Erkrankungen in verschiedenen Organen und der Abstoßung von Nierentransplantaten in Verbindung gebracht. Die Funktion von TMEM16J in Immunzellen und -geweben ist derzeit noch unbekannt. In einer genomweiten Assoziationsstudie wurde eine TMEM16J-Variante, TMEM16J-T604A, als Risikofaktor für chronische Nierenerkrankungen (CKD) identifiziert. Wir fanden heraus, dass TMEM16J ein im ER ansässiger Ionenkanal ist, der das intrazellulären Ca^{2+}-Signal reguliert. Dagegen ist die Ionen- Kanalfunktion bei TMEM16J-T604A gestört. Darüber hinaus konnten wir nachweisen, dass TMEM16J und TMEM16J-T604A die Synthese und Freisetzung von pro-inflammatorischen Zytokinen durch die Regulierung intrazellulärer Ca^{2+}-Signale modulieren und damit eine mögliche Verbindung zu chronischen Entzündungen und CKD herstellen. Diese Ergebnisse identifizieren TMEM16J als einen neuen, vielversprechenden pharmakologischen Angriffspunkt für die Behandlung von CKD und chronischen Entzündungen.

PREFACE

The following work is the result of the combination of published papers under the form of book chapters. Therefore, the reader may encounter variations (e.g. mouse nomenclature), according to the guidelines of the different journals.

The chapters consist of the following manuscripts:

Chapter 2: Cabrita, I., **Talbi, K**., Kunzelmann, K., & Schreiber, R. (2021). Loss of PKD1 and PKD2 share common effects on intracellular Ca^{2+} signaling. *Cell calcium*, *97*, 102413.

Chapter 3: **Talbi K**, Cabrita I, Kraus A, Hofmann S, Skoczynski K, Kunzelmann K, Buchholz B, Schreiber R. The chloride channel CFTR is not required for cyst growth in an ADPKD mouse model. *FASEB J*. 2021 Oct;35(10):e21897

Chapter 4: **Talbi, K**., Cabrita, I., Schreiber, R., & Kunzelmann, K. (2021). Gender-Dependent Phenotype in Polycystic Kidney Disease Is Determined by Differential Intracellular Ca^{2+} Signals. *International journal of molecular sciences*, *22*(11), 6019.

Chapter 5: **Talbi, K**., Ousingsawat, J., Centeio, R., Schreiber, R., & Kunzelmann, K. (2021). Calmodulin-Dependent Regulation of Overexpressed but Not Endogenous TMEM16A Expressed in Airway Epithelial Cells. *Membranes*, *11*(9), 723.

Chapter 6: Schreiber, R., **Talbi, K.**, Ousingsawat, J., & Kunzelmann, K. (2023). A TMEM16J variant leads to dysregulated cytosolic calcium which may lead to renal disease. *FASEB J*, *37*(1), e22683.

INDEX

LIST OF ABBREVIATIONS

ADCY	Adenylyl cyclase
ADCY1	Adenylate cyclase 1
ADPKD	Autosomal Dominant Polycystic Kidney Disease
AQP2	Aquaporin 2
AR	Androgen receptor
AVP	Arginine-vasopressin
ATP	Adenosine triphosphate
BBR	Benzbromarone
CA	Cyproterone acetate
CaCCs	Ca^{2+}-activated chloride channel
CAM	Calmodulin
cAMP	Adenosine 3',5'-cyclic monophosphate
CaMKII	CAM-dependent kinase
CDK1	Cyclin kinase D1
CPA	Cyclopiazonic acid
CKD	Chronic kidney disease
CF	Cystic fibrosis
CFTR	Cystic fibrosis transmembrane conductance regulator
CREB	cAMP response element binding protein
DAG	Diacylglycerol
DHT	Dihydrotestosterone
DLG1	Discs Large MAGUK Scaffold Protein 1
EGF	Epidermal growth factor
EGFR	Epidermal growth factor receptor
EPAC	Exchange protein directly activated by cAMP
ER	Endoplasmic reticulum
ERK	Extracellular signal-regulated kinase
Esr	Estrogen receptor
ESRD	End-Stage Renal Disease
EST	Estradiol
ESYT1	Synaptotagmin-1
GFR	Glomerular filtration Rate
GPCR	G-protein coupled receptor
GWAS	Genome wide association study

HIF-1α	Hypoxia-inducible transcription factor-1α
I/F	Forskolin
IL-1R	Interleukin-1 receptor
IP3	Inositol trisphosphate
IP3R	Inositol trisphosphate receptor
Isc	Short circuit currents
LPS	Lipopolysaccharides
MAPK	Mitogene-activated protein kinase kinase
MPTE	Mouse primary proximal tubular epithelial
mTOR	Mechanistic target of rapamycin
NBD	Nucleotide-binding domain
NKCC	Sodium/potassium/chloride co-transporter
Orai1	Ca^{2+} release-activated calcium channel protein 1
PC-	Polycystin-1
PC-2	Polycystin-2
PDE	Cyclic nucleotide phosphodiesterase
PKA	Protein kinase A
PKD	Polycystic kidney disease
PKP3	Plakophilin 3
PLC	Phospholipase C
PM	Plasma membrane
PMCA	Plasma membrane Ca^{2+} ATPase
PIP_2	Phosphatidyl inositol-diphosphate
RAAS	Renin-angiotensin-aldosterone system
RD	Regulatory domain
ROCC	Receptor-operated Ca^{2+} channels
RyR	Ryanodine receptor
SERCA	Sarco-endoplasmic reticulum Ca^{2+} ATPase
shRNA	Small hairpin RNA
SNPs	Single nucleotide polymorphisms
SIGIRR	Single Ig IL-1-related receptor
siRNA	Small interfering RNA
SOCC	Store-operated Ca^{2+} channels
SOCE	Store operated calcium entry
STIM1	Stromal-interacting molecule 1
TGF-α	Transforming growth factor alpha
TLR	Toll-like receptor

TMD	Transmembrane domain
TMEM16	Transmembrane protein 16
TRP	Transient Receptor Potential
TRPV	Transient receptor potential channels, vanilloid subtype
VGCC	Voltage gated calcium channel
VOCC	Voltage-operated Ca^{2+} channels
V2R	Vasopressin receptor 2
YFP	Yellow fluorescent protein

LIST OF FIGURES

LIST OF TABLES

CHAPTER 1 | INTRODUCTION

AUTOSOMAL DOMINANT POLYCYSTIC KIDNEY DISEASE

Autosomal Dominant Polycystic Kidney Disease (ADPKD) is the most prevalent hereditary kidney disease as it accounts for one in 1000 to one in 2500 individuals in the general population [1]. ADPKD is characterized by a relentlessly progressive decline in renal function due to continuous development of fluid-filled cysts throughout the kidney. The enlargement of these cysts displaces and destroys adjacent renal parenchymal tissue, leading to compromised kidney function. Loss of renal function progresses over the course of many years and leads to End-Stage Renal Disease (ESRD) by the sixth decade of life in around 50% of cases [2]. ADPKD is often associated with major complications such as hypertension, gross haematuria, acute and chronic pain, nephrolithiasis, in addition to the development of hepatic and pancreatic cysts [3].

Male sex has been identified as a risk factor for ADPKD progression and severity. In humans, male patients have an earlier onset of ESRD when compared to women [4,5]. Sex differences in biology start during foetal development and continue after puberty. These differences are the result of the combined effect of genetic and hormonal events. In fact, cell metabolism is programmed by the autonomous effect of sex chromosomes, in addition to the effect of gonadal hormones [6]. Sex hormones originate from a common precursor, cholesterol, which is transformed by several enzymes to generate androgens and estrogens. Circulating estrogens are produced mainly in the ovaries, while in males, androgens are synthetized in the testes and adrenal glands [7]. Beside their role in the male and female reproductive system, sex hormones are relevant for several other organs and physiological processes, such as the cardiovascular and immune system, musculoskeletal system, lipid and protein metabolism, as well as the cognitive function [8-11]. Regarding the kidney, several characteristics and functions as well as multiple renal diseases display significant sex differences.

Studies have demonstrated that ADPKD progression and severity are influenced by sex hormones in different experimental models. In a heterozygous rat model, only male rats developed severe interstitial inflammation and fibrosis and azotemia [12]. Testosterone treatment in the same experimental model resulted in an increased ADPKD severity in females. Orchiectomy, which is the removal of one or both testicles, reduced renal enlargement and the drop in glomerular filtration rate (GFR), whereas testosterone treatment revoked these effects. Conversely, ovariectomy led to a decrease in GFR [13,14]. Furthermore, it has been shown that androgen receptors (AR) and estrogen receptors (Esr) are expressed in renal tissue, making it reasonable to conclude that that sex steroids influence the progression of ADPKD and might explain the difference in disease severity between the two sexes.

ADPKD is predominantly caused by germinal mutations touching either the PKD1 gene on chromosome 16 (16p13.3) encoding polycystin-1 (PC-1) (78% of cases) [15], or PKD2 on chromosome 4 (4q21) encoding polycystin-2 (PC-2) (15% of cases) [16], with PKD2-related ADPKD (type-2 ADPKD) having typically a later onset and a milder phenotype in comparison to PKD1-related ADPKD (type-1 ADPKD) [17]. In mice, homozygous mutations of Pkd1 or Pkd2 are lethal at the embryonic stage [18,19], and are thought to be similarly non-viable in humans.

Although considered dominant, ADPKD behaves in a recessive manner at the cellular level. The wildtype copy of PC-1 or PC-2 in the patient's cells allows for normal kidney development and function until adulthood, despite the presence of the mutated allele. A cyst will start to develop only once a “second hit” somatic mutation has taken place in a renal tubular cell, causing the wildtype copy to lose its function. Thus, each cyst forms separately as a result of a distinct somatic mutation, in addition to the germline mutation, which may explain the progressive nature of ADPKD [20]. This “two-hit” model for cystogenesis in ADPKD has been further supported by studies identifying loss of heterozygosity in kidney cysts of type 1 ADPKD patients [21] and in kidney and liver cysts of type 2 ADPKD patients [22]. Other studies suggest that in addition to the germline and somatic mutation, a “third-hit” such as renal injury is required to trigger and hasten cystogenesis during adulthood [23-25].

Polycystins modulate calcium signaling

PC-1 is a large protein encompassing 11 transmembrane segments, an extensive extracellular N-terminus containing multiple motifs for protein modifications and signaling events, and a short cytoplasmic C-terminus that contains a coiled coil domain and several protein cleavage sites [26,27]. PC-1 is abundant in kidney epithelial cells during foetal development. However, its expression decreases in adult kidney tissue [28]. This fairly large protein plays a role in epithelial cells differentiation and maturation and has been localized to lateral membranes of cells in contact. Indeed, PC-1 has several motifs involved in protein-protein associations, suggesting that this polycystin might mediate cell-cell and cell-matrix interactions, in addition to interacting with other proteins [15,29,30]. PC-1 has also been localized to primary cilia, a complex organelle present on most cell types including renal epithelial cells, and implicated in cystic kidney diseases [31]. It is generally accepted that PC-1 functions as a cell surface receptor, although some studies reported that expression of PC-1 alone was enough to allow for Ca^{2+} permeable nonselective cation currents [32-34].

PC-2 is a Transient Receptor Potential (TRP) channels family member and is expressed in all cell types mainly in the endoplasmic reticulum (ER), but it is also present at the plasma membrane (PM) and primary cilia. This protein is composed of intracellular N-terminus, 6 transmembrane domains, a pore-forming loop, and a cytoplasmic C-terminal domain that includes a coiled-coil motif, an ER retention tag and a Ca^{2+}-binding EF-hand [27,35]. PC-2

functions as a non-selective Ca^{2+}-permeable cation channel, and its open probability depends on the cytosolic Ca^{2+} concentration [36,37]. Opening of the channel requires the binding of Ca^{2+} to the EF-hand, which acts as a cytosolic Ca^{2+}-sensor [38]. Permeability to Ca^{2+} was shown to change depending on whether it was measured in the ER or in primary cilia [34], which shows that PC-2 channel activity and permeability is modulated by interactions with other proteins, depending on its subcellular location.

Indeed, PC-2, in addition to its role as cation channel, also modulates Ca^{2+} signaling via binding to other proteins at the ER and PM, with the most important partner being PC-1. A cryogenic electron microscopy (Cryo-EM) study revealed that PC-1 binds 3 PC-2 proteins to form a complex (Fig 1.1A-B). When in a complex, positively charged residues from segment 6 (S6) of PC-1 protrude into the pore formed by the PC-2 subunits, most likely leading to poor Ca^{2+} conductance [39] (Fig 1.1C).

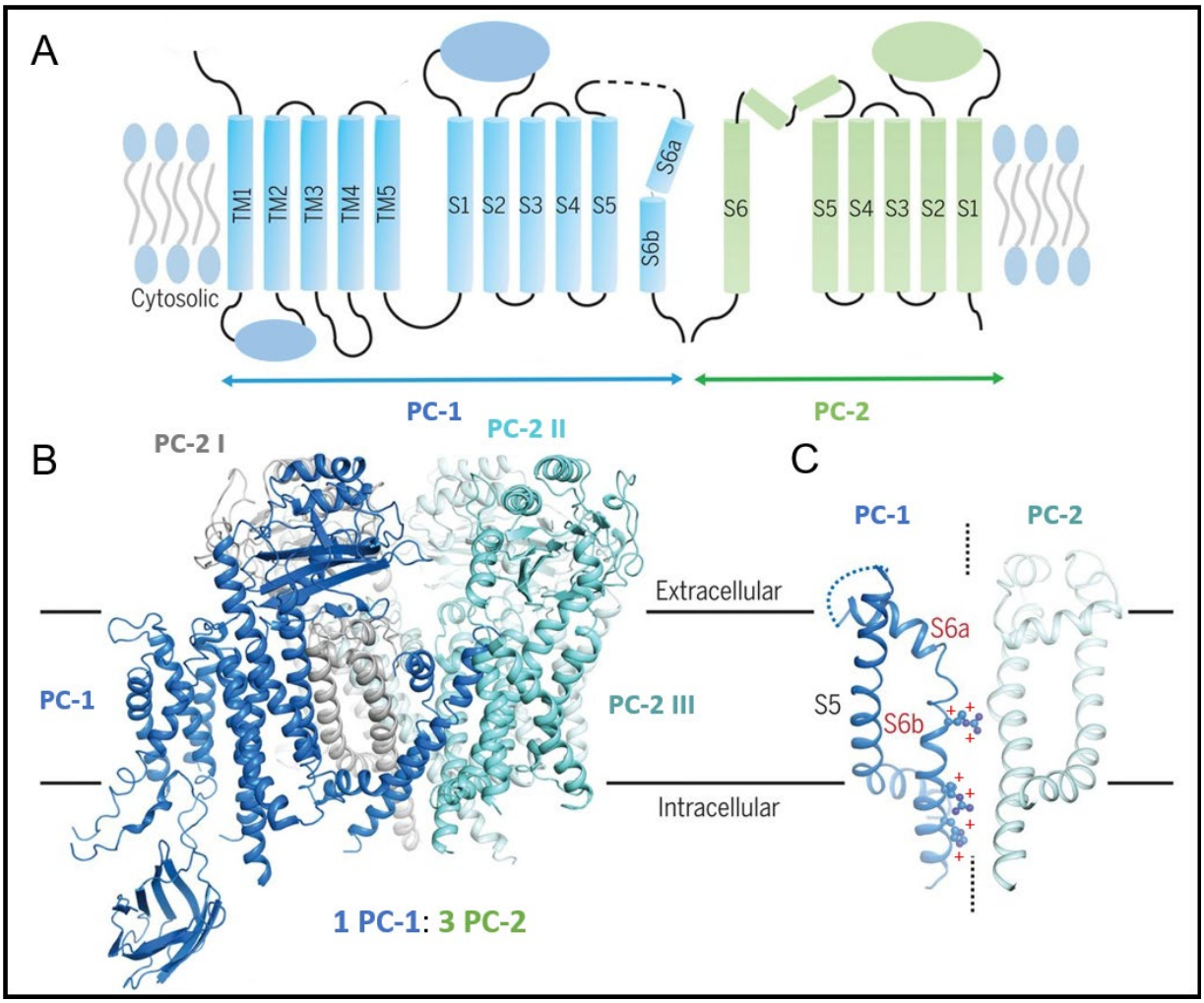

Figure 1.1 | *Polycystin-1 and polycystin-2 complex structure.*

Cryo-EM structure of human PC-1/PC-2 complex. A) Topological illustration of PC-1 and PC-2. B) Organisation of the PKD1/PKD2 complex. The complex is formed by 1 PC-1 subunit and 3 PC-2 subunits (PC-2 I, PC-2 II and PC-2 III). C) Conventional conformation of the S6 segment of PC-1 showing

positively charged residues directed towards the channel pore formed by the PC-2 subunit. Adapted from [39].

It has been proposed by multiple studies that PC-2 and the PC-1/PC-2 complex function as mechanosensory Ca^{2+} channels in primary cilia and can be mechanically stimulated to regulate the Ca^{2+} concentration and related signaling cascades in response to fluid stress [40-42]. This widely supported theory however has been challenged by a study that demonstrated the absence of ciliary Ca^{2+} signaling following exposure to flow stimulus [43]. Further investigations are hence required to have a full understanding of the role of polycystins in primary cilia. Polycystins were also shown to interact with the ER-resident Ca^{2+} channel Inositol trisphosphate receptor (IP3R). The PC-2 C-terminal tail competes with the IP3R ligand, IP3, to bind IP3R and induce ER-Ca^{2+}store release, whilst PC-1 seems to inhibit this PC-2/IP3R interaction by promoting stromal interaction molecule 1 (STIM-1) binding to IP3R instead [44,45]. Additionally, PC-2 interacts with the ryanodine receptor (RyR), an important ER-Ca^{2+} release channel, in its open state to negatively regulate Ca^{2+} release in the presence of Ca^{2+} [46] (Fig 1.2).

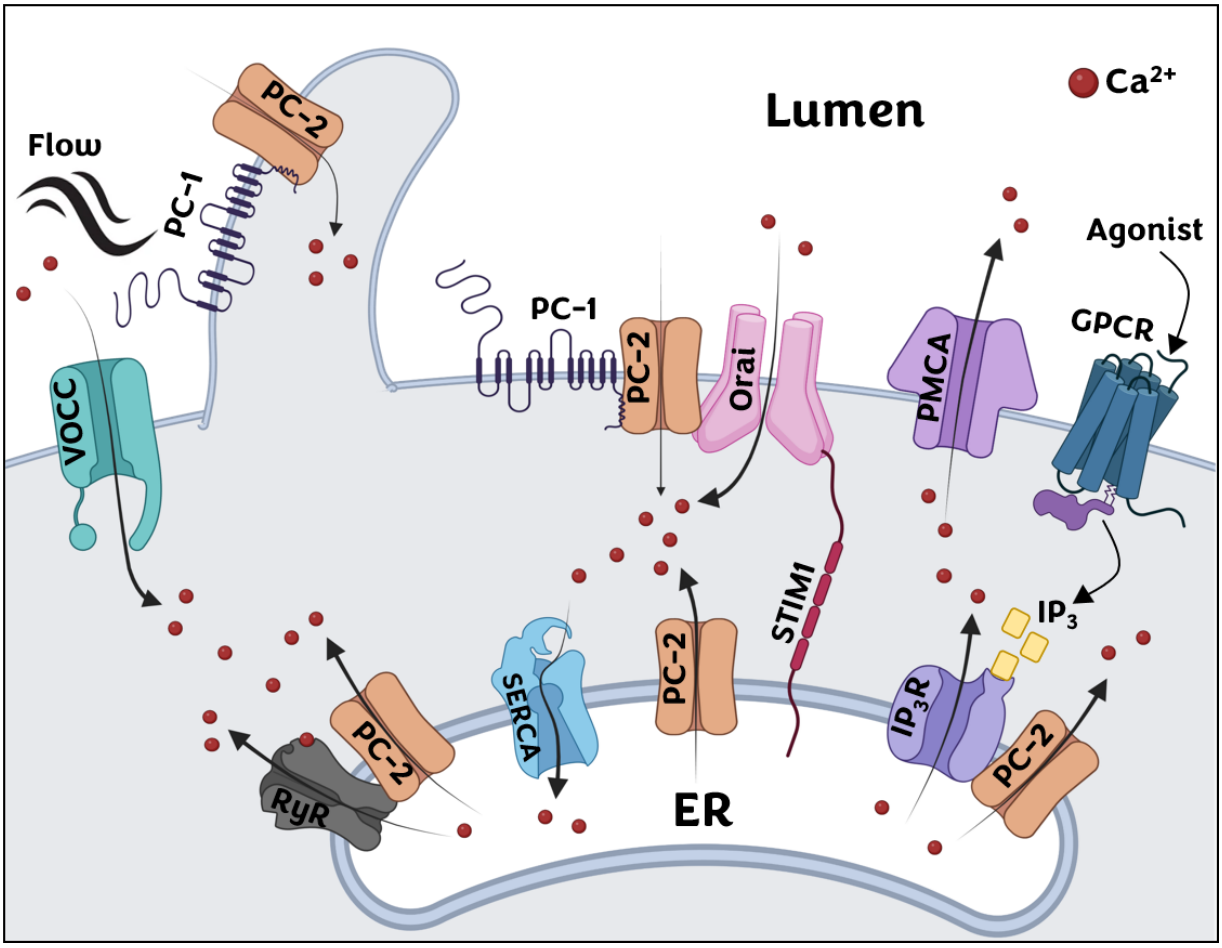

Figure 1.2 | *Proposed pathways for Ca^{2+} regulation by polycystins in kidney epithelial cells.*
Polycystin-2 (PC-2) is a Ca^{2+} permeable ion channel. At the ER, it mediates Ca^{2+} leakage to the cytosol, interacts with IP3R to prolong its activity and regulates ryanodine receptor (RyR) activation by Ca^{2+} influx.

At the plasma membrane, PC-2 activity is regulated by polycystin-1 (PC-1). In primary cilia, PC-1 may function as a receptor and activate PC-2 and subsequent Ca^{2+} influx following mechanic stress. Created with BioRender.com.

Considering the extensive involvement of polycystins in calcium homeostasis, it is not surprising that mutations to PC-1 or PC-2 disrupt Ca^{2+} signaling in ADPKD. Mutations to PC-2 lead to loss of its Ca^{2+} permeable channel function and regulatory function, while mutations to PC-1 affect the regulation of PC-2 activity [47]. Calcium signaling regulates a wide range of cellular pathways, including cell proliferation, survival and apoptosis, all of which are disrupted in ADPKD, leading to cyst formation and growth.

Cyst growth is driven by enhanced proliferation and chloride secretion

In ADPKD, an important fraction of cyst growth originates from the collecting ducts but can potentially involve proximal and distal tubules as well. Cytogenesis starts with a small saccular dilation in a renal tubule, which expands overtime to form a fluid-filled cavity. Once it reaches ~2 mm in diameter, the cyst pinches off the parent tubule to form an anatomically independent fluid-filled sac, which continues to grow at the rate of ~5% per year driven by further proliferation of epithelial cells lining the cyst lumen, in conjunction with transepithelial fluid secretion [48,49]. Cystic epithelial cells are not completely differentiated but are in constant proliferative mode, allowing the cyst to expand [50].

Cell proliferation is enhanced in ADPKD

Proliferation is an important physiological process which allows cell populations to grow through cell division. A wide network of protein kinases and growth factors control cell cycle and proliferation. The extracellular signal-regulated kinase (ERK) is one the most studied mitogen-activated protein kinases (MAPKs) pathways. It is activated following binding of growth factors or cytokines to their respective receptors. The signaling cascade includes B-Raf, mitogen-activated protein kinase kinase (MEK) and ERK, and ends with the activation of transcription of target genes involved in proliferation [51].

Growth factors such as epidermal growth factor (EGF), transforming growth factor alpha (TGF-α) and EGF receptor (EGFR) are overexpressed and at times mislocalized in ADPKD, driving increased proliferation and cyst formation [52]. In addition, tissue levels of adenosine 3′ 5′-cyclic monophosphate (cAMP) are elevated in PKD animal models [53,54] and have been shown to promote cyst growth [55]. In normal renal cells, cAMP inhibits proliferation by inhibiting Raf-1 and thus the RAS-RAF-MEK-ERK proliferation cascade, while in cells from ADPKD cysts, it activates B-Raf which triggers cell proliferation [56]. Interestingly, disrupted intracellular Ca^{2+} signaling was shown to switch cells from the cAMP proliferation-inhibited phenotype, to a cAMP

proliferation-stimulated phenotype [57]. Other cAMP targets which promote cell growth and proliferation are cAMP response element binding protein (CREB), mechanistic target of rapamycin (mTOR), Wnt-β-catenin and STAT3 signaling [27,58]. Intracellular cAMP concentration is regulated by the balanced activity of two enzymes: adenylyl cyclase (ADCY) and cyclic nucleotide phosphodiesterase (PDE). ADCY is a plasma membrane-bound enzyme that mediates ATP conversion into cAMP and is activated downstream from G-protein coupled receptors (GPCRs). Vasopressin receptor 2 (V2R) is the main regulator of ADCY activity and cAMP production in the collecting ducts. PKD1 haploinsufficiency was shown to induce increased arginine-vasopressin (AVP) signaling, resulting in enhanced phosphorylation and recruitment of aquaporin-2 (AQP-2) channels. Inhibition of V2R pathway by several antagonists lowered renal cAMP concentrations and delayed cyst development in various ADPKD rodent models [48]. The highly selective V2R antagonist Tolvaptan has been approved in several countries for the treatment of ADPKD patients [59].

Increased proliferation is paralleled with an increased apoptosis in cystic cells. Kidneys from ADPKD patients and a PKD rat model showed increased activity of apoptosis-inducing factors [60]. Enhanced apoptosis might result from enhanced mTOR signaling which, in addition to proliferation, regulates programmed cell death. Apoptosis seems to play a crucial role in cytogenesis. When induced in cultured tubular cells, apoptosis resulted in cyst formation, whereas the inhibition of the apoptotic factor caspase decreased proliferation of tubular epithelia and consequently inhibited cyst growth and renal failure [61].

Chloride secretion in ADPKD

Chloride secretion is the driving force for fluid secretion by ADPKD cyst cells [62,63]. Cl^- efflux is accompanied by paracellular sodium (Na^+) transport and water movement through aquaporins into the cyst lumen following transepithelial potential and osmotic gradients. Apical Cl^- secretion stimulates basolateral Cl^- uptake by the sodium/potassium/chloride co-transporter (NKCC), [52] which in turn requires basolateral recycling of K^+ and Na^+ via the Ca^{2+}-activated K^+ channel KCa3.1 and the Na^+/K^+ ATPase, respectively. Albaquami et al. have shown that KCa3.1 plays an important role in maintaining a negative intracellular membrane potential which creates the electrochemical driving force for Cl^- efflux [64]. KCa3.1 can be activated by cAMP and protein kinase A (PKA) which might be relevant in the context of ADPKD [48]. Similarly, the Na^+/K^+ ATPase establishes and maintains Na^+ and K^+ gradients, which control membrane potential and cell volume [65]. Interestingly, it has been demonstrated that PC-1, through its C-terminal tail, interacts with the α-subunit of Na^+/K^+ ATPase and might regulate its activity in the kidney [66]. Ca^{2+}-dependent Cl^-secretion at the apical membrane of cyst-lining cells was shown to be largely mediated by the Ca^{2+}-activated Cl^- channel TMEM16A [67], while the cAMP-dependent chloride channel CFTR is thought to mediate cAMP-dependent Cl^- secretion into the cyst lumen [68,69].

CHLORIDE CHANNELS IN ADPKD

The cystic fibrosis transmembrane conductance regulator role in ADPKD

The cystic fibrosis transmembrane conductance regulator (CFTR) is a member of the ATP-binding cassette (ABC) protein superfamily, most members of which are active pumps shuttling substrates across cell membranes. CFTR is composed of 2 transmembrane domains (TMD1 and TMD2) and 2 cytoplasmic nucleotide-binding domains (NBD1 and NBD2) characteristic of all ABC proteins, in addition to the regulatory domain (RD) unique to CFTR. Each transmembrane domain comprises 6 α-helices, which assemble to form the Cl^- pore. CFTR activity is regulated by cAMP activation and ATP-dependent gating. In its native form, the RD inhibits channel activity, and the inhibition is lifted through cAMP-dependent phosphorylation of its serine residues via PKA. NBDs from a ' head to tail ' dimer following ATP binding and the cytoplasmic Cl^- pathway opens. ATP binding and hydrolysis thus mediate channel gating. CFTR N- and C- termini are cytoplasmic, with the latter containing a PDZ domain-binding motif [58,70]. PDZ domains are modular protein interaction domains of 80-90 amino acids which allow interactions with PDZ domain proteins such as Na^+/H^+ exchange regulatory factors and the actin binding protein Ezrin. These interactions may participate into CFTR forming a macromolecular functional complex, involving regulatory proteins as well as other ion channels [70].

In humans, CFTR is encoded by a gene of 189 kb located in chromosome 7q31.2. Cystic fibrosis is the most common autosomal recessive airway disease among the Caucasian population and is caused by mutations to the CFTR gene, the most common being the F508del which results in altered CFTR glycosylation and a subsequent protein trafficking defect [71].
CFTR is expressed at the apical membrane of all secretory epithelia including airways, liver, kidney, sweat and pancreatic glands, colonic crypts and the male reproductive tract. In addition, CFTR might be expressed in non-epithelial cells, as well as the central and peripheral nervous system [72,73]. In the mouse kidney, CFTR is expressed mainly in the apical surface of proximal tubules. In rats, it has been located to proximal and distal tubules. In human kidney, CFTR is expressed in the proximal and distal tubules, as well as the thin limbs of Henle's loop and the collecting ducts [58]. CFTR is expressed at the apical membrane of the β-intercalated cells of the collecting ducts, where it participates, along with the Cl^-/HCO_3^- exchanger pendrin (SLC26A4), in bicarbonate (HCO_3^-) secretion, essential for acid–base homeostasis [74].

CFTR mediates cAMP-dependent chloride secretion in ADPKD

In the collecting ducts, CFTR is mainly activated through GPCRs such as V2R which, once activated, stimulates cAMP synthesis by ADCY. cAMP can alternatively bind exchange protein directly activated by cAMP (EPAC) and activate the Ca^{2+} sensitive adenylate cyclase-1 (ADCY1) through ER-Ca^{2+} store release (Fig 1.3).

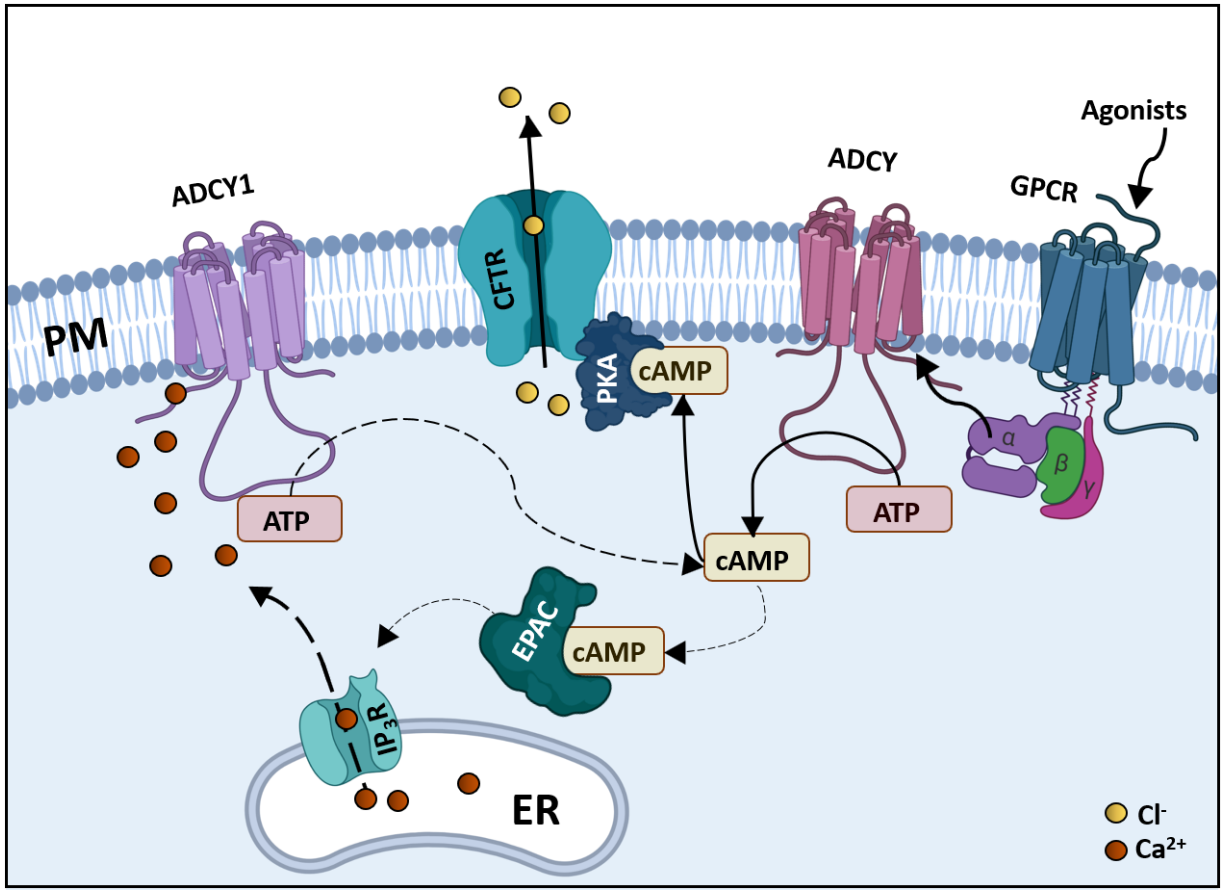

Figure 1.3 | GPCR-dependent activation of CFTR.
In cyst epithelial cells, CFTR is proposed to be activated following GPCR (V2R) stimulation, which activates adenylate cyclase (ADCY) to convert ATP into cAMP. cAMP activates protein kinase A (PKA) which mediates phosphorylation and subsequent activation of CFTR. Additionally, CFTR can be activated by cAMP synthesis through the Ca^{2+}-sensitive ADCY1, which is activated glands by ER-Ca^{2+} release through IP3R following cAMP binding to the cAMP sensor EPAC. Created with BioRender.com

In ADPKD, CFTR is expressed at the apical membrane of cyst-lining cells [68]. A model for cyst formation portraying CFTR as the main channel mediating Cl^- and fluid secretion in ADPKD has stemmed from the homology between the cystic epithelium and other secretory epithelia, in addition to numerous *in vitro* studies. For example, Cl^- secretion stimulated by forskolin, which activates ADCY, was inhibited by antisense oligonucleotide against CFTR [75]. Furthermore, CFTR blockers such as CFTR-inh-172 and GlyH-101 reduced cAMP stimulated Cl^- currents and cyst growth in MDCK cells [76,77], in embryonic kidney cyst models, as well as in neonatal and kidney-specific Pkd1 knockout models [77]. Such results suggested the following mechanism for cyst growth in ADPKD; Mutations to PKD1 or PKD2 disrupt the formation of the functional PC-1/PC-2 complex. The decrease in residual activity of this complex, once below a certain critical threshold, triggers a series of cellular changes including cell dedifferentiation, enhanced proliferation, and defects in the extracellular matrix. Increased activity of GPCRs, including V2R, and consequential increase in cAMP stimulate proliferation via activation of the

Ras/Raf-1/MEK/ERK pathway through PKA, which additionally activates cAMP-dependent ion channels, namely CFTR, resulting in Cl^- and fluid secretion and cyst expansion [48,78].

However, evidence for an alternative Cl^- conductive pathway in ADPKD cysts exists as well. Cystic fibrosis, which is characterized by a non-functional CFTR protein, and ADPKD are two diseases that can coexist in human patients [79,80], indicating that renal cysts still develop in absence of CFTR function. CFTR expression at the apical membrane of cyst-lining epithelia was reported to be significantly heterogenous, possibly due to cell dedifferentiation [68,75]. Therefore, it was hypothesised that Cl^- secretion is either mediated by only a subset of cells differentiated enough to express CFTR, or alternatively, other Cl^- transporters might be involved [58]. Additionally, renal tubular epithelial cells secrete ATP into the lumen following mechanic or chemical stimulation, activating multiple purinergic receptors to regulate ion and water transport in kidney tubules [81]. This purinergic signaling microenvironment is dramatically enhanced in PKD cysts [82], and has been demonstrated to stimulate Ca^{2+}-activated Cl^- currents and thus cyst growth in ADPKD [83,84]. Indeed, in more recent studies, the Ca^{2+}-activated Cl^- channel TMEM16A was proven to have a central role in ADPKD cyst formation [67,85,86].

TMEM16A drives cyst growth in ADPKD

Ca^{2+}-activated chloride channels (CaCCs) are a class of Cl^- channels expressed ubiquitously in invertebrates and mammals, and are known to mediate several physiological functions, including smooth muscle cell contraction, transepithelial fluid transport and sensory transduction. These channels are normally closed in resting conditions and are activated in response to increased intracellular Ca^{2+} concentrations. CaCCs are also voltage-dependent. In the presence of permissive Ca^{2+} concentrations, membrane depolarization further increases their currents [87]. In 2008, CaCC was reported to be TMEM16A (Anoctamin 1) by 3 independent research teams [88-90]. The transmembrane protein 16 (TMEM16) family consists of 10 paralogue members (TMEM16A-K), also known as anoctamins (Anoctamin1-10). This protein family includes Ca^{2+}-activated ion channels and phospholipid scramblases. Among the 10 members, TMEM16A is the most studied, considering that dysregulated expression or function of this anoctamin is involved in several pathological conditions. TMEM16A, like the rest of the TMEM16 proteins, is a homodimer containing 10 transmembrane α-helices, 2 Ca^{2+}-binding sites and an ion conduction pore within each subunit, in addition to the cytosolic long N- and short C-termini. The ion pore is formed by nonpolar and hydrophilic residues of α3-7 and has an hourglass shape. α7 and α8, together with α6, form the highly conserved Ca^{2+} binding sites (Fig 1. 4A). Triggered by Ca^{2+}-binding, α6 changes conformation and physically separates from α4, opening the pore in a transient fashion [91-93].

TMEM16A regulation by calmodulin

Several agents and stimuli have been reported to regulate TMEM16A function, including temperature, cholesterol, phosphoinositides, and calmodulin [94]. Calmodulin (CAM) is Ca^{2+} signal transducer protein that is highly conserved in all eucaryotic cells [95]. It regulates essential physiological processes including neural plasticity [96], smooth muscle contraction [97] and proliferation [98]. CAM is composed of 2 globular domains (N- and C-terminal lobes) each containing two Ca^{2+} binging EF-hands. This ubiquitous protein can bind and regulate target proteins in its Ca^{2+} free state (apo-CAM), or in its Ca^{2+}-bound state (holo-CAM). The regulatory function of CAM is mediated either directly by protein-to-protein contact, or indirectly via CAM-dependent kinase (CaMKII).

Whether CAM regulates Ca^{2+}-dependent TMEM16A activation is still largely debated. CAM-dependent regulation of TMEM16A is reminiscent to that of the small conductance Ca^{2+}-activated K+ channels (SK). In an olfactory cell line, CAM was shown to be indispensable for CaCC activation, where transfection with dominant CAM mutant led to a strong inhibition of Cl^- currents [99]. Another study reported that CAM co-immunoprecipitates with the TMEM16A (abc) but not the (ac) isoform. Furthermore, CAM-inhibitors significantly attenuated TMEM16A currents [100]. However, studies arguing against the implication of CAM in channel activation present strong arguments as well. Immunoprecipitation assays revealed only a weak and unstable TMEM16A-CAM complex [101,102]. Purified TMEM16A reconstituted in liposomes recapitulated Ca^{2+}-dependent channel activity without the need for CAM [101]. In addition, CAM was not among the network of TMEM16A regulatory proteins identified through a highly sensitive quantitative proteomic approach [103]. Importantly, Yang et al., have reported that TMEM16A activation does not require CAM, however, they found that, similar to SK channels, CAM was tethered to TMEM16A N-terminus even in the absence of Ca^{2+} (apo-CAM). They have concluded that CAM is not a Ca^{2+} sensor for TMEM16A, but instead, it can regulate the channel activity by modulating its Ca^{2+} sensitivity depending on intracellular Ca^{2+} concentrations [104,105]. Different experimental models and conditions may contribute to the contradicting results mentioned above, which implies that TMEM16A activation and regulation mechanisms require validation in well controlled physiological conditions.

TMEM16A was strongly expressed in Madin-Darby canine kidney (MDCK) cyst models, in embryonic kidney cyst models and in human ADPKD tissue [85]. Similarly, Cabrita et al. demonstrated increased TMEM16A expression in a Pkd1-knockout mouse model. Additional knockout of TMEM16A remarkably reduced cyst formation and kidney size, indicating a central role for this Cl^- channel in the overall pathology of ADPKD. This report demonstrated that TMEM16A's role in ADPKD is mediated by at least 3 main mechanisms: increased Ca^{2+} signaling, Ca^{2+}-dependent chloride secretion and enhanced cell proliferation [67].

TMEM16A drives enhanced proliferation in ADPKD

TMEM16A is involved in the pathology of several types of cancer, especially of epithelial origin. In breast cancer, intestinal cancer, liver cancer and pancreatic cancer, increased TMEM16A expression promotes cell proliferation and tumor growth by enhancing epidermal growth factor receptor (EGFR) signaling. TMEM16A was also reported to modulate progression of prostate, glioma and gastric cancer by affecting TNF-α, NF-κB and TGF-β signaling, respectively. Additionally, TMEM16A was shown to stimulate the RAS/RAF/MEK/ERK pathway activation in head and neck squamous cell carcinoma (SCCHN) [106]. In a Pkd1-knockout mouse model, enhanced TMEM16A expression was shown to mediate enhanced cell proliferation. Additional knockout of TMEM16A in this ADPKD experimental model abolished increased proliferation and cyst development [67]. Hence, TMEM16A, in addition to mediating Cl^- secretion, is a potent promoter of abnormal cell proliferation driving cyst growth in ADPKD.

TMEM16A mediates Ca^{2+}-dependent chloride secretion in ADPKD

TMEM16A is preferentially activated by compartmentalized Ca^{2+} signaling following purinergically induced ER-Ca^{2+} store release (Fig 1.4B) [107]. TMEM16A mediates a time- and voltage-dependent current and displays a high Ca^{2+} sensitivity with an EC_{50} of approximately 0,4-1 µM at positive membrane potentials. Saturating Ca^{2+} concentrations beyond 1µM ,however, stimulate a linear current-voltage (I/V) relationship instead of the typical outwardly rectifying I/V [93].

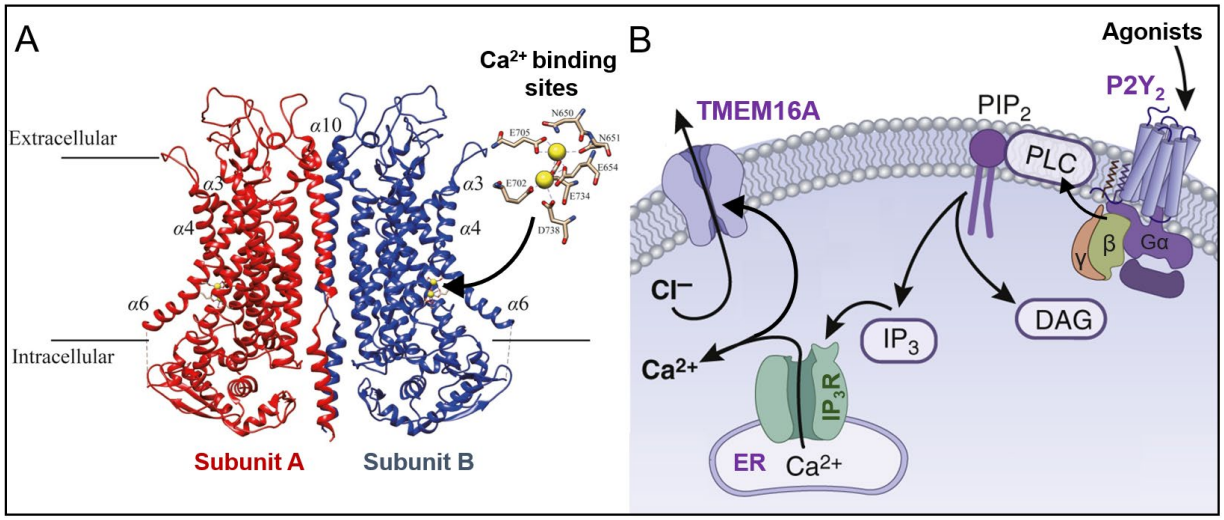

Figure 1.4 | ***TMEM16A structure and Ca^{2+}-dependent activation.***

A) Ca^{2+}-bound structural conformation of the mouse TMEM16A dimer (subunits A and B) determined by high-resolution Cryo-EM. Each monomer contains 10 transmembrane α-helices and 2 Ca^{2+} (yellow balls)-binding sites. Ca^{2+}-binding sites are formed by residues N650, N651 and E654 from α6, E702, E705 from α7, and E734 and D738 from α8. **B)** TMEM16A activation by purinergic stimulation; The GPCR $P2Y_2$ is activated following binding to an agonist, which activates Phospholipase C (PLC) to synthetize IP3 and diacylglycerol (DAG) from phosphatidyl inositol-diphosphate (PIP_2). IP_3 binds the

Inositol-1,4,5-triphosphate receptor (IP_3R) which in turn mediates Ca^{2+} release from the ER. Ca^{2+} binds and activates TMEM16A and its chloride (Cl^-) conductance. Adapted from [108,109].

TMEM16A is expressed in multiple epithelial tissues such as the respiratory epithelium, the salivary and pancreatic glands and the intestinal and kidney epithelium. Numerous studies have revealed the involvement of TMEM16A in pathological conditions such as asthma, cystic fibrosis, diarrhea and cancer [108]. Ca^{2+} is one of the two main messengers involved in ADPKD, which suggests an important role for CaCCs and Ca^{2+}-dependent Cl^- secretion in this disease. In the kidney, TMEM16A has been mainly located to the proximal tubules, in addition to the collecting ducts, podocytes and primary cilia. In the proximal tubules where it is apically expressed, TMEM16A contributes to effective proton secretion and protein reabsorption by counterbalancing Vacuolar-type H^+-ATPase (V-ATPase) activity through apical Cl^- conductance [110]. Nephron-specific knockout of TMEM16A in mice leads to a reduced number of glomeruli, albuminuria and renal damage, pointing to the role of TMEM16A in nephrogenesis and albumin reabsorption [111]. Additionally, TMEM16A is involved in the formation and maintenance of primary cilia [112].

TMEM16A modulates calcium signaling

Ca^{2+} is a signaling messenger responsible for the regulation of central physiological processes such as muscle contraction, proliferation and apoptosis. While the cytoplasmic Ca^{2+} concentration is kept at ~10^{-7} M, the extracellular Ca^2 concentration is ~$2x10^{-3}$ M. High Ca^{2+} concentrations are toxic to the cell and thus, under physiological conditions, Ca^{2+} signaling is kept transient by multiple cellular mechanisms [113]. Calcium signaling is initiated following stimulation of cell-surface receptors such as GPCRs. $P2Y_2$ is a GPCR that, once stimulated by an agonist (ATP), binds PLC which in turn cleaves PIP_2 to IP_3 and DAG. IP_3 binds the Inositol-1,4,5-triphosphate receptor (IP_3R) triggering Ca^{2+} release from the ER. Another pathway for ER-Ca^{2+} store release is through the ryanodine receptor (RyR), which is activated following Ca^{2+} entry from the extracellular milieu to the cytosol. Ca^{2+} influx through the PM is mediated by several types of influx channels, including receptor-operated (ROCC), voltage-operated (VOCC) and store-operated (SOCC) Ca^{2+} channels. Depletion of the ER Ca^{2+} store is detected by the ER-Ca^{2+} sensor STIM1, which interacts with PM Ca^{2+} channels like the Ca^{2+} release-activated calcium channel protein 1 (Orai1) or TRP channels, triggering Ca^{2+} entry into the cytoplasm in a process known as store operated calcium entry (SOCE). Once Ca^{2+} signaling is achieved, resting Ca^{2+} concentrations are restored through the function of the Na^+/Ca^{2+} exchanger and the plasma membrane Ca^{2+} ATPase (PMCA) pump, which traffic Ca^{2+} out of the cell. ER Ca^{2+} store is re-filled through the sarco-endoplasmic reticulum Ca^{2+} ATPase (SERCA) pump, which mediates uptake of Ca^{2+} from the cytosol to the internal ER Ca^{2+} stores (Fig 1.5).

PM-ER junctions have been described in several cell types and are known to regulate

Ca^{2+} transport, organelle morphology and ER function [114]. Wolf et al,. have shown that the TMEM16 homologue in yeast, Ist2, is located in the ER where it mediates tethering of the ER to the PM via its basic C-terminus [115]. Cabrita et al.,[116] have demonstrated that TMEM16A co-localizes and interacts with IP_3R, allowing the ER to be in close proximity of TMEM16A-rich PM microdomains.

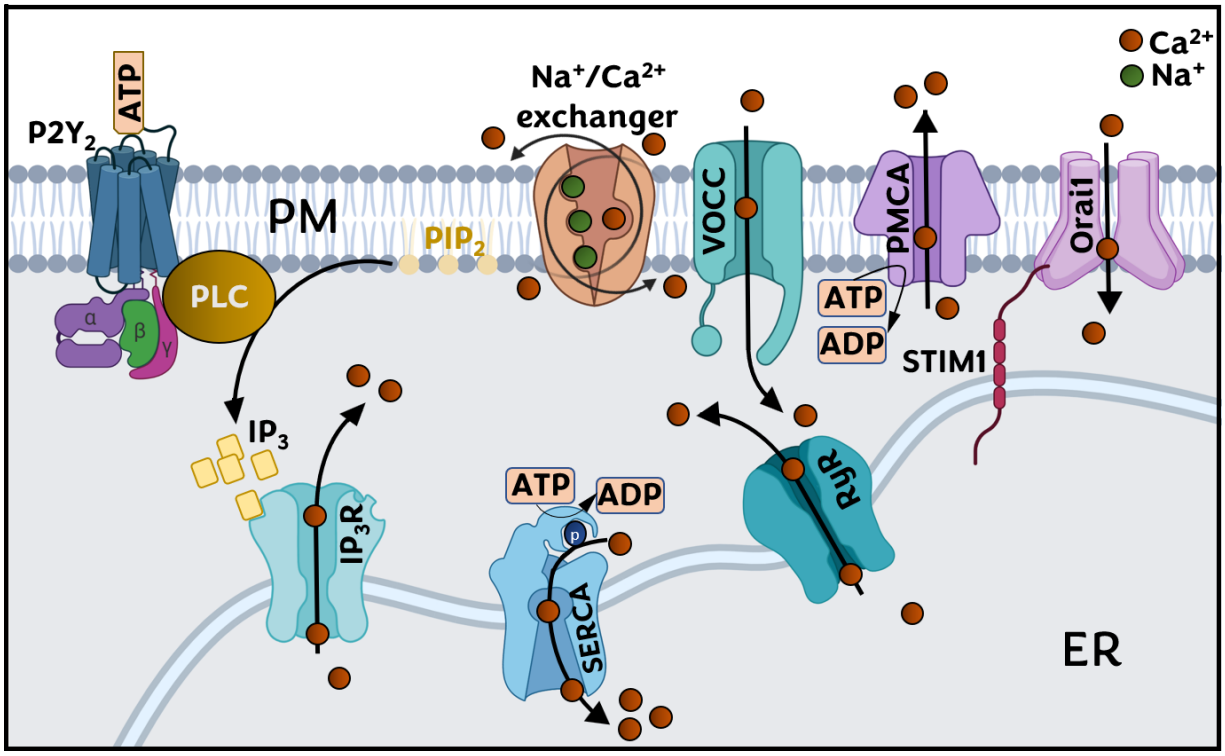

Figure 1.5 | ***Components of calcium signaling and homeostasis.***
Following adenosine triphosphate (ATP) binding, the cell surface GPCR $P2Y_2$ activates phospholipase C (PLC) which converts phosphatidyl inositol-diphosphate (PIP_2) into IP_3 and diacylglycerol (DAG). IP3 binds IP3R and stimulates ER Ca^{2+}-store release. Ryanodine receptor (RyR) is an ER located Ca^{2+}-permeable channel activated by extracellular Ca^{2+}-influx through voltage-gated Ca^{2+}channel (VGCC). Stromal-interacting molecule 1 (STIM1) senses ER Ca^{2+} depletion and activates calcium channel protein 1 (Orai1) and calcium influx. Once the signaling is achieved, ER Ca^{2+} is re-filled through the sarco-endoplasmic reticulum Ca^{2+} ATPase (SERCA) pump and the resting cytoplasmic Ca^{2+} concentration is re-established via Ca^{2+} efflux through the plasma membrane Ca^{2+} ATPase (PMCA) pump and the Na^+/Ca^{2+} exchanger. Created with BioRender.com.

Unlike the Cl^- channel TMEM16B, which is activated by a global Ca^{2+} increase and only weakly stimulated through GPCRs, the authors have reported that TMEM16A is preferentially activated through GPCR-induced Ca^{2+} store release instead of extracellular Ca^{2+} influx [116]. In line with these results, TMEM16A was reported to be activated by ER-Ca^{2+} store release but not by Ca^{2+} influx through VGCC in small nociceptive dorsal root ganglia neurons [117]. Such a compartmentalized signaling is achieved by tethering of the ER to PM-lipid rafts where TMEM16A is expressed via TMEM16A/IP_3R interaction. Additionally, TMEM16A interacts with

ERLIN1, a lipid raft- and ER-expressed protein. The resulting microdomain enables TMEM16A activation in response to local Ca^{2+} signals instead of global Ca^{2+} increases [118]. Importantly, enhanced TMEM16A expression was shown to increase Ca^{2+} signaling in ADPKD [67].

TMEM16J MODULATES Ca^{2+} SIGNALING

Not only TMEM16A, but also other TMEM16 proteins are known to modulate Ca^{2+} signaling. TMEM16D is expressed in the ER and was shown to lower the ER-Ca^{2+}store, interact directly with Orai1 and stimulate SOCE. Cl^- conductance by TMEME16A and TMEM16B depolarizes the membrane, which supports Ca^{2+} release from the ER through IP_3Rs or RyRs. TMEM16B not only conducts Cl^-, but is also Ca^{2+} permeable, and can mediate Ca^{2+} influx through the PM following its activation by extracellular Ca^{2+} influx. TMEM16J attenuates ER store filling and ATP-induced Ca^{2+} store release [119]. TMEM16J is expressed intracellularly and was shown to inhibit ATP-stimulated TMEM16A currents. In addition, experimentally-induced PM expression of TMEM16J generated a whole cell current, revealing an intracellular ion conductance function. Taken together, these data suggest that TMEM16J negatively regulates calcium signaling, potentially through an ion conductance function affecting ER-Ca^{2+} store filling. However, the exact subcellular location and function of TMEM16J is still not fully known. Interestingly, a TMEM16J variant has been linked to chronic kidney disease (CKD) [120].

TMEM16J in Chronic kidney disease

A genome wide association study (GWAS) based on estimated glomerular filtration rate (eGFR) identified the TMEM16J variant, T604A, and the Single Ig IL-1-related receptor (SIGIRR) as a risk factor for CKD [120]. A patient is diagnosed with CKD if they present a GFR lower than 60ml/min/1.73 m^2 or if they show signs of renal injury for more than 3 months. Markers for kidney damage include albuminuria and urinary and kidney tissue abnormalities. CKD has a complex pathophysiology with multiple underlying causes, all leading towards kidney failure, the main ones being diabetes, hypertension, chronic glomerulonephritis, polycystic kidney disease and autoimmune diseases [121].

Inflammation is a complex biological response triggered by a variety of stimuli, such as foreign agents or damaged cells. Persistent inflammatory responses lead to chronic inflammation, which induces fibrosis and tissue damage and has been associated with CKD [122,123]. Hence, the duration and extent of the immune response are maintained under control by several regulatory mechanisms [124]. A genetic region encoding Plakophilin 3 (PKP3), SIGIRR and TMEM16J was shown to negatively regulate the immune response. Mutations in this genetic locus are associated with inflammatory diseases, such as tuberculosis [125]. PKP3 belongs to the armadillo protein family and is expressed in the nucleus and desmosomes [126,127].

This protein plays a role in binding the filaments of the cytoskeleton and in the maintenance of cell-cell adhesion, and was shown to regulate acute tissue-specific immune responses in mice [128]. SIGIRR is expressed in immune cells, such as dendritic cells and T-cells, in addition to kidney, liver and gut epithelial cells [124]. The role SIGIRR plays in regulating immunity is well investigated and understood. This transmembrane protein negatively regulates Toll-like receptor (TLR)/IL-1R signalling, activation of which triggers the innate immune response through pathways involving downstream protein kinases, NF-κB translocation to the nucleus and consequent activation of MAPKs and proinflammatory cytokines production [129]. Ca^{2+} is a central messenger in the immune system as it is involved in proliferation, differentiation and apoptosis of immune cells. Additionally, Ca^{2+} indirectly modulates protein expression by regulating multiple signaling molecules involved in the regulation of gene transcription. Nuclear Ca^{2+} is essential for cAMP response element-binding protein (CREB) activation. In addition, cytoplasmic Ca^{2+} induces the activation and translocation of NF-κB and MAPKs to the nucleus [130]. Furthermore, IL-2 secretion by T-lymphocytes following their activation during an immune response is largely promoted by PLC activation, IP3 synthesis and subsequent ER-Ca^{2+} store release and SOCE [131,132]. Ca^{2+} signalling is hence largely involved in immune response regulation. TMEM16J involvement in inflammation and kidney disease, therefore, may relate to its effects on Ca^{2+} signaling.

AIMS OF THE STUDY

Throughout this project, we examined the function of TMEM16A, CFTR and TMEM16J ion channels in kidney disease in order to identify promising new pharmacological targets for the treatment of ADPKD and CKD. Calcium homeostasis is disrupted in ADPKD, and it is well known that TMEM16A regulates Ca^{2+} signaling. In chapter two, modulation of Ca^{2+} signaling by polycystins, as well as the contribution of TMEM16A are addressed. Our team had previously demonstrated the importance of TMEM16A in ADPKD. However, the role of CFTR had never been confirmed *in vivo.* In chapter three, we made use of a kidney specific Pkd1/Cftr double-knockout mouse to assess the role of CFTR in ADPKD. There are considerable differences between male and female regarding the severity of ADPKD. This was also observed during our studies on the ADPKD mouse model. In Chapter four, we therefore examined potential mechanisms behind the more severe phenotype observed in males. In chapter five, we explored the regulation of TMEM16A by calmodulin and identified a regulatory artefact in cells overexpressing TMEM16A. The paralogous protein TMEM16J is involved in the negative regulation of the immune response, and a variant, TMEM16J-T604A, was recently identified as a risk factor for CKD. We therefore explored, in chapter six, the implication of TMEM16J in Ca^{2+} signaling and immunity, and put forward a mechanism by which TMEM16J-T604A may predispose to inflammation and CKD.

CHAPTER 2 | LOSS OF PKD1 AND PKD2 SHARE COMMON EFFECTS ON INTRACELLULAR Ca^{2+} SIGNALING

Abstract

In polycystic kidney disease (PKD) multiple bilateral renal cysts gradually enlarge causing a decline in renal function. Transepithelial chloride secretion through cystic fibrosis transmembrane conductance regulator (CFTR) and TMEM16A (anoctamin 1) drive cyst enlargement. We demonstrated recently that a loss of PKD1 increases expression and function of TMEM16A in murine kidneys and in mouse M1 collecting duct cells. The data demonstrated that TMEM16A contributes essentially to cyst growth by upregulating intracellular Ca^{2+} signaling. Enhanced expression of TMEM16A and Ca^{2+} signaling increased both cell proliferation and fluid secretion, which suggested inhibition of TMEM16A as a novel therapy in ADPKD. About 15 % of all ADPKD cases are caused by mutations in PKD2. To analyze the effects of loss of function of PKD2 on Ca^{2+} signaling, we knocked-down *Pkd2* in mouse primary renal epithelial cells in the present study, using viral transfection of shRNA. Unlike in *Pkd1-/-* cells, knockdown of PKD2 lowered basal Ca^{2+} and augmented store-operated Ca^{2+} entry, which was both independent of TMEM16A. However, disease causing purinergic Ca^{2+} store release was similar to that observed in *Pkd1-/-* renal epithelial cells. The present data suggest pharmacological inhibition of TMEM16A as a treatment in ADPKD caused by mutations in both *PKD1* and *PKD2*.

Keywords: Pkd1, Pkd2, ADPKD, renal cysts, TMEM16A, anoctamin 1, Ca^{2+} activated Cl^- channel

Published in: Cabrita, I., **Talbi, K**., Kunzelmann, K., & Schreiber, R. (2021). Loss of PKD1 and PKD2 share common effects on intracellular Ca^{2+} signaling. *Cell calcium*, *97*, 102413

Own experimental contribution: Isolation of renal primary cells, viral transfection, intracellular Ca^{2+} measurements.
Own written contribution: Original draft preparation.
Other contributions: Designed experiments and analysed data.

Introduction

Loss of function mutations in the polycystic kidney disease genes *PKD1* and *PKD2* lead to autosomal dominant polycystic kidney disease (ADPKD). This common inherited disease affects about 1 in 1000, and accounts for up to 10% of end-stage renal disease, which is due to continuous renal cyst enlargement and compression of adjacent healthy parenchyma [133]. ADPKD is caused in 85 % and 15 % by mutations in *PKD1* (encoding polycystin-1) and *PKD2* (encoding polycystin-2), respectively. Our recent studies demonstrated the crucial role of TMEM16A for renal cyst growth in mice lacking expression of PKD1. We showed that loss of PKD1 increased expression of TMEM16A and CFTR, which caused induced Cl^- secretion in murine kidneys [67]. Moreover, upregulation of TMEM16A caused a pronounced increase in cell proliferation and thus TMEM16A contributes essentially to renal cyst formation.

As meanwhile shown for naïve epithelial cells from intestine, airways, and kidney, as well as macrophages, nociceptive sensory neurons, and a number of different cell lines, TMEM16 proteins control intracellular Ca^{2+} signals in subcellular compartments [116,117,134-136]. Enhanced intracellular Ca^{2+} signaling is also found in renal epithelial cells isolated from cystic kidneys of *Pkd1*-knockout mice and human cysts grown in vitro [67,137]. In contrast, enhanced Ca^{2+} signaling, cell proliferation and CFTR expression was abolished in *Pkd1/Tmem16a* double knockout mice. Moreover, inhibition of TMEM16A *in vivo* and *in vitro* abolished enhanced cell proliferation and largely reduced cyst growth. Thus, pharmacological inhibition of TMEM16A was proposed as a novel treatment in ADPKD [67].

Enhanced Ca^{2+} store release triggered by purinergic stimulation was found in primary renal epithelial cells isolated from *Pkd1-/-* mice and in mouse M1 collecting duct cells after knockdown of PKD1. A small increase in basal intracellular Ca^{2+} concentration ($[Ca^{2+}]_i$) was observed, along with enhanced Ca^{2+} entry after store depletion by cyclopiazonic acid. These changes were directly related to enhanced expression and function of TMEM16A, and were suppressed by knockout or pharmacological inhibition of TMEM16A [67]. We therefore asked in the present study, i) whether loss of expression of polycystin-2 (PKD2) leads to a similar increase in TMEM16A-expression in primary renal epithelial cells and ii) whether loss of PKD2 (polycystin-2) is paralleled by a similar upregulation of purinergic Ca^{2+} signaling. In agreement with earlier data obtained in M1 mouse collecting duct cells [86], the present data from primary renal epithelial cells suggest a similar role of TMEM16A in ADPKD caused by loss of PKD2.

Materials and Methods

Animals. Animal experiments were approved by the local institutional review board and all animal experiments complied with the United Kingdom Animals Act, 1986, and associated guidelines, EU Directive 2010/63/EU for animal experiments. Experiments were approved by

the local Ethics Committee of the Government of Unterfranken/Wuerzburg (AZ: 55.2-2532-2-823-26). Mice with a floxed *Pkd1* allele were generously provided by Prof. Dr. Dorien J.M. Peters (Department of Human Genetics, Leiden University Medical Center, Leiden, The Netherlands) [23]. Animals were hosted on a 12:12 h light:dark cycle under constant temperature (24 ± 1 °C) in standard cages. They were fed a standard diet with free access to tap water. Generation of mice with a tamoxifen inducible, kidney epithelium-specific *Pkd1*-deletion were described recently [138]. Mice carrying loxP-flanked conditional alleles of *Pkd1* were crossed with KSP-Cre mice in a C57BL/6 background (KspCreER^{T2};*Pkd1*$^{lox;lox}$; abbreviated as *Pkd1*$^{-/-}$). Mice carrying loxP-flanked alleles of *Tmem16a* [110] were crossed to generate KspCreER^{T2};*Pkd1*$^{lox;lox}$;*Tmem16a*$^{lox;lox}$ double-knockout mice (abbreviated as *Pkd1*$^{-/-}$*/T16a*$^{-/-}$*).* Primers for genotyping are listed in Table 1. We used C57BL/6 *Pkd1*$^{-/-}$ and *Pkd1*$^{-/-}$*/T16a*$^{-/-}$ males in the age of 8–10 weeks in the experiments.

Animal treatment. Conditional knockout was induced in *Pkd1*$^{-/-}$ (n = 8) and *Pkd1*$^{-/-}$*/T16a*$^{-/-}$ (n = 8) mice by administrating tamoxifen (2 mg/kg body weight) dissolved in 5% ethanol and 95 % neutral oil, daily at postnatal days PN 20–22. Non-induced *Pkd1*$^{-/-}$ (n = 8) served as controls. All animals were sacrificed 8-10 weeks after induction with tamoxifen and kidneys were analyzed [67].

Table 2.1 | *Primers used for genotyping.*

Primer	Gene	Sequence 5-3’
m*PKD1* loxPF	*Pkd1*	ACCCTTCCCTGAGCCTCCAC
m*PKD1* loxPR	*Pkd1*	CCACAGGGGAAGCCATCATA
F427 Va	*Ksp*	CATTCTCTCCCACTGAATGGA
F427 Vb	*Ksp*	ACAGAGTGGGGTTTGTGTCTG
inv	*Ksp*	AACTGTCCCCTTGTCATACCC
16aCKOf	*Tmem16a*	GGCTCTATCAATGTTCTGTTC
16aCKOr1	*Tmem16a*	CTCAAGTCCTCAAGTCCCAGTC

Cells and viral transduction. Renal medullary and cortical primary cells were isolated like described recently [67] and cultured at 37 °C/5% CO_2 in DMEM/ F12 supplemented with 1% FBS, 1% Pen/Strep, 1% L-Glutamine (200 mM), 1% ITS (100×), 50 nM hydrocortisone, 5 nM triiodothyronine, and 5 nM Epidermal Growth Factor (Sigma Taufkirchen, Germany). Primary cells were transduced to downregulate *Pkd2*. Cells were infected with lentiviral recombinant vectors containing the shRNA of mouse *Pkd2* (5´-GCATCTTGACCTACGGCATGA) with YFP_{I152L}, as previously described [139,140]. Stable transfected renal primary cells were maintained in the presence of 5 µg/ml of Puromycin (Thermo Fisher Scientific, Darmstadt, Germany).

TMEM16A was downregulated by murine siRNA transfection (5´-AGAUGUACACGUAGUCACCgg, Silencer Select, ambion, USA) into renal primary cells using standard methods (Lipofectamine, Invitrogen, Germany). Successful downregulation was confirmed by RT-PCR.

Western blotting. Protein was isolated from renal medullary and cortical primary cells using a sample buffer containing 25 mM Tris–HCl, 150 mM NaCl, 1% Nonidet P-40, 5% glycerol, 1 mM EDTA, and 1% protease inhibitor mixture (Roche, Mannheim, Germany). Equal amounts of protein were separated using a 4–20% Mini-PROTEAN TGX Stain-Free (Bio-Rad) for detection of PKD1 and 8% sodium dodecyl sulfate (SDS) polyacrylamide gel for PKD2. Proteins were transferred to a polyvinylidene difluoride membrane (GE Healthcare Europe GmbH, Munich, Germany) using a semi-dry transfer unit (Bio-Rad). Membranes were incubated with primary anti-PKD1 (Polycystin-1 (7E12), Santa Cruz; 1:500) mouse antibody or anti-PKD2 (Polycystin-2 (D-3), Santa Cruz; 1:500) mouse antibody, overnight at 4 °C. Proteins were visualized using horseradish peroxidase-conjugated secondary antibody and ECL detection. Beta-Actin was used as a loading control.

Measurement of $[Ca^{2+}]i$. Measurements of the global cytosolic Ca^{2+} concentration were performed as described recently [67]. Primary cells were isolated from four mice and for each mice 3 coverslips with 20 to 50 cells were loaded with 2 µM Fura2-AM (to measure global cytosolic Ca^{2+} changes) and 0.02% pluronic Pluronic F-127 (Invitrogen, Darmstadt, Germany) in Ringer solution (mmol/l: NaCl 145; KH_2PO_4 0.4; K_2HPO_4 1.6; Glucose 5; $MgCl_2$ 1; Ca^{2+}-Gluconat 1.3) at room temperature for 1 h. Fluorescence was detected at 37°C, using an inverted microscope Axiovert 100 (Zeiss, Jena, Germany) and a high speed polychromator system (Visi-Chrome, Puchheim, Germany). The results were obtained at 340/380 nm fluorescence ratio (after background subtraction). After calibration intracellular Ca^{2+} concentrations were calculated as described in [86].

Materials and statistical analysis: All compounds used were of highest available grade of purity. Student's *t* test for unpaired samples and one-way ANOVA, followed by a Bonferroni were used for statistical analysis. $P < 0.05$ was accepted as significant difference. Data are expressed as mean ± SEM.

Results

Reduced basal Ca^{2+} and augmented Ca^{2+} store release in renal medullary epithelial cells lacking expression of PKD2.

Previous data demonstrated an upregulation of receptor-mediated intracellular Ca^{2+} signals in renal epithelial cells isolated from mice wit*h kidney-specific knockdown of* PKD1. *Here we*

examined how shRNA-knockdown of PKD2 in renal epithelial cells isolated from wild type (*Pkd1+/+*) or PKD1-knockout animals (*Pkd1-/-*) affects intracellular Ca^{2+} signaling. As reported previously, kidneys of *Pkd1-/-* mice demonstrated strongly attenuated expression of PKD1 (Fig. 1A). Expression of PKD2 was potently knocked-down by shRNA in cells isolated from renal medulla of *Pkd1+/+, Pkd1-/-* and *Pkd1-/-/Tmem16a-/-* double knockout mice (Fig. 1B,C).

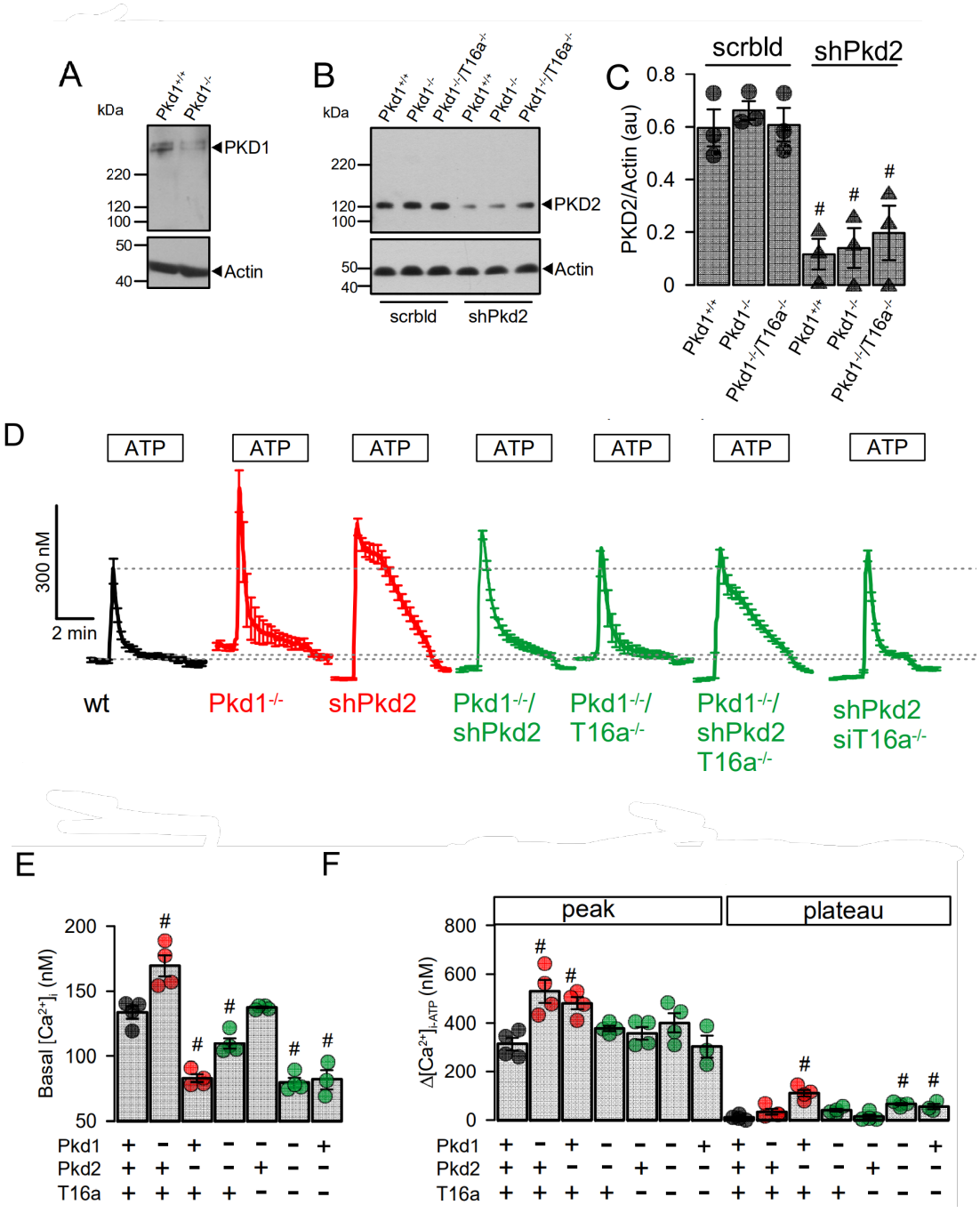

Figure 2.1 | *Reduced basal Ca^{2+} and augmented Ca^{2+} store release and SOCE by downregulation of PKD2 in primary medullary epithelial cells.*

A) Western blotting indicates knockdown of PKD1 (450 kDa) in primary epithelial cells isolated from kidneys of *Pkd1-/-* mice 10 weeks after tamoxifen induction at postnatal days 20–22. **B,C)** Western blotting indicates significant knockdown of PKD2 (120 kDa) by small hairpin (sh) RNA in cells isolated

from renal medulla of *Pkd1+/+, Pkd1-/-* and *Pkd1-/-/Tmem16a-/-,* in comparison with cells transfected with scrambled ($^{\#}P$ = 0.0044, $^{\#}P$ = 0.0023, and $^{\#}P$ = 0.0141, respectively). Western blots were performed n = 3 animals. Protein loading was not normalized among the lanes. **D)** Summary traces of ATP (100 µM)-induced Ca^{2+} increase measured by Fura2 in mouse medullary epithelial cells. Increased ATP-induced Ca^{2+} store release in red and normal Ca^{2+} store release in green, in comparison with *Pkd1+/+* in black **E)** Basal Ca^{2+} is increased in cells from mice lacking PKD1 and decreased in cells lacking PKD2, compared with *Pkd1+/+* cells ($^{\#}P$ = 0.0004 and $^{\#}P$ < 0.0001, $^{\#}P$ = 0.0194, $^{\#}P$ < 0.0001 and $^{\#}P$ < 0.0017, respectively). **F)** ATP-induced Ca^{2+} increase is larger in *Pkd1-/-* cells and shRNA-knockdown of PKD2 in cells isolated from *Pkd1+/+*, compared with *Pkd1+/+* cells ($^{\#}P$ = 0.0014 and $^{\#}P$ = 0.0148, respectively). Increased levels of SOCE were observed in cells from *Pkd1+/+* and *Pkd1-/-/ T16a-/-* transfected with shPkd2 ($^{\#}P$ < 0.0001 and $^{\#}P$ = 0.0063, respectively) when compared to *Pkd1+/+* cells. (n = 32-224 cells from 4 independent cultures of 3-4 animals each). Mean and error bars indicating ±SEM. $^{\#}$One-way ANOVA and Tukey's post-hoc test comparing with scrambled or *Pkd1+/+* as indicated.

We measured intracellular Ca^{2+} concentrations using Fura2. Compared to *Pkd1+/+* cells, basal $[Ca^{2+}]_i$ was slightly but significantly enhanced in *Pkd1-/-* cells, whereas basal $[Ca^{2+}]_i$ was reduced in cells lacking expression of PKD2 (*shPkd2*) (Fig. 1D, red traces). Notably, eliminating expression polycystin-1 and -2 together moved basal Ca^{2+} towards normal values (Fig. 1D, E, green traces). Additional knockout of TMEM16A reduced increased basal $[Ca^{2+}]_i$ in *Pkd1-/-* cells to normal value, whereas knockout of TMEM16A did not correct lower basal $[Ca^{2+}]_i$ in *Pkd1-/-/shPkd2* and *shPkd2* cells. The data confirm earlier results showing that upregulation of TMEM16A increases basal Ca^{2+} levels in *Pkd1-/-* cells [67].

Data also indicate that loss in PKD2 attenuates basal $[Ca^{2+}]_i$, in primary renal epithelial cells despite upregulation of TMEM16A (Fig. 2A,B). This is in contrast to our previous observations in M1 cell line. Here, knockdown of *Pkd2* slightly increase basal $[Ca^{2+}]_i$ in M1 cells, which was sensitive to TMEM16A expression [86]. Lower basal $[Ca^{2+}]_i$ could be due to reduced activity of Ca^{2+} leakage channels in the endoplasmic reticulum (ER) and/or lower ER Ca^{2+} store content in *shPkd2* cells. As PKD2 is a nonselective cation channel permeable for Ca^{2+} that is also expressed in the ER, it probably serves as a leakage channel [141].

We stimulated the cells with the purinergic agonist ATP, which induced a Ca^{2+} peak (store release) and Ca^{2+} plateau (SOCE) increase (Fig. 1D). Corresponding to our previous studies, elimination of *Pkd1* augmented ATP-induced store release [67,86]. Also *shPkd2* cells demonstrated a larger rise in $[Ca^{2+}]_i$, however, the absolute peak $[Ca^{2+}]_i$ increase was lower than in *Pkd1-/-* cells (Fig. 1D,F). Eliminating expression of both PKD1 and/or PKD2 and knockout of TMEM16A almost normalized purinergic Ca^{2+} store release. Notably, knockout of PKD2 induced an impressive prolongation of the Ca^{2+} plateau, suggesting augmented SOCE. This was not observed in *Pkd1-/-* cells, and was much reduced in *Pkd1-/-* and/or *shPkd2* cells. Because additional knockout of TMEM16A-expression did not affect the plateau phase, enhanced SOCE observed in *shPkd2* cells is independent of TMEM16A (Fig. 1D,F).

Loss of expression of PKD1 or PKD2 causes similar changes in intracellular Ca^{2+} signaling in medullary and cortical renal epithelial cells.

In ADPKD renal cysts are derived primarily from the medullary part, but also occur in the renal cortex [133]. We therefore examined whether loss of expression of PKD1 and PKD2 in cortical epithelial cells causes similar changes in intracellular Ca^{2+}. Knockdown of PKD2 in primary cortical cells was equally effective as in medullary cells (Fig. 2C,D).

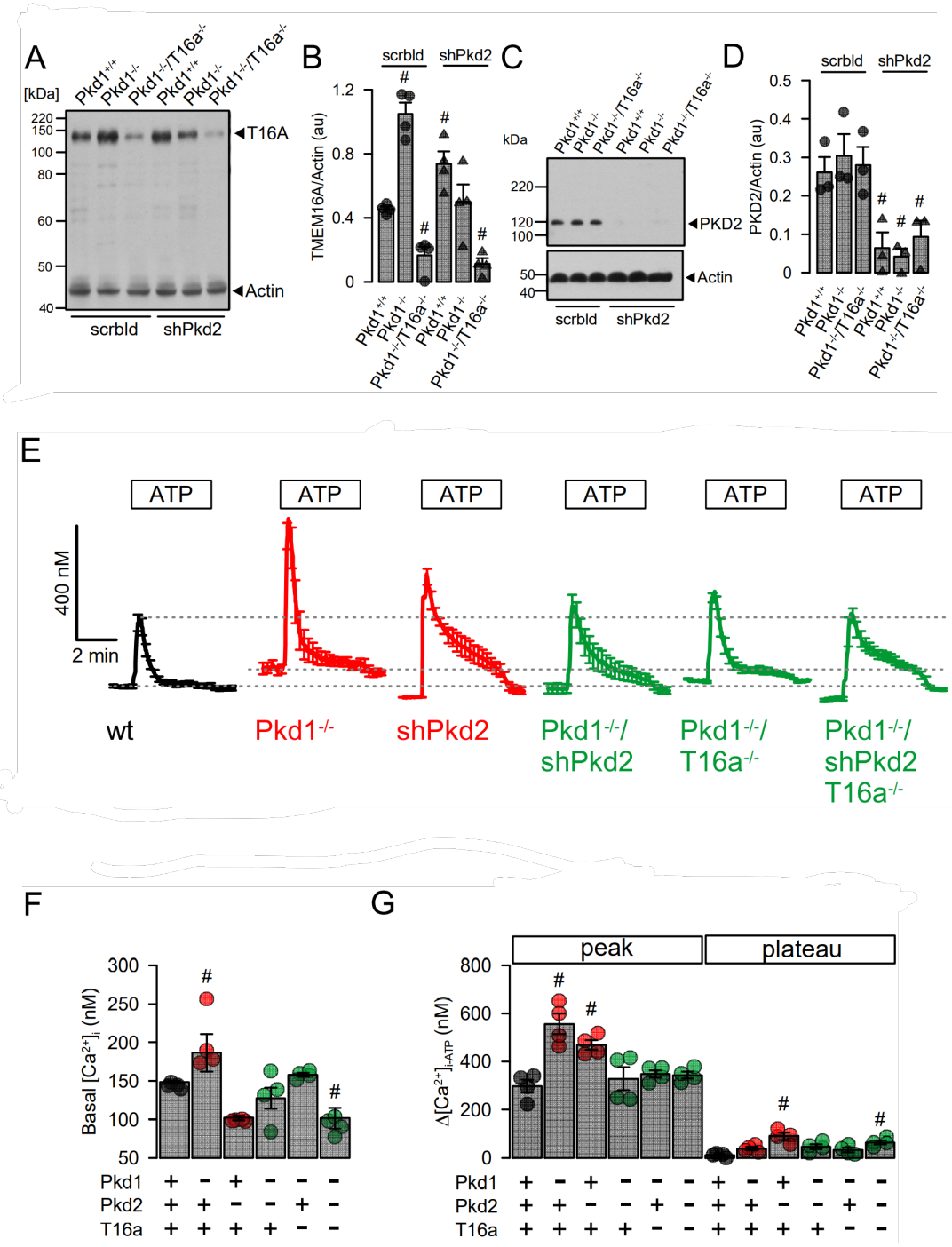

Figure 2.2 | ***Reduced basal Ca^{2+} and augmented Ca^{2+} store release and SOCE in cortical renal epithelial cells lacking PKD2. Upregulation of TMEM16A is essential for enhanced Ca^{2+} signaling upon knockdown of PKD1 and PKD2***

(**A, B)** Western blot indicating significant upregulation of TMEM16A by knockout of PKD1 or PKD2 and

significant down regulation by knockout of TMEM16A ($^{\#}P$ = 0.003, $^{\#}P$ = 0.006, $^{\#}P$ = 0.03 and #P = 0,004). **C,D)** Western blotting indicates significant knockdown of PKD2 (120 kDa) by small hairpin (sh) RNA in cells isolated from renal cortex of *Pkd1+/+, Pkd1-/-* and *Pkd1-/-/Tmem16a-/-*, in comparison with cells transfected with scrambled ($^{\#}P$ = 0.026, $^{\#}P$ = 0.012, and $^{\#}P$ = 0.042, respectively). Western blots were performed n = 3 animals. Protein loading was not normalized among the lanes. **E)** Summary traces of ATP (100 µM)-induced Ca^{2+} increase measured by Fura2 in mouse cortical epithelial cells. Increased ATP-induced Ca^{2+} store release in red and normal Ca^{2+} store release in green, in comparison with *Pkd1+/+*. **F)** Basal Ca^{2+} is increased in cells from mice lacking PKD1 ($^{\#}P$ = 0.0109) and present a strong tendency of decrease in cells lacking PKD2 expression ($^{\#}P$ = 0.047), compared with *Pkd1+/+* cells. **G)** ATP-induced Ca^{2+} increase is larger in *Pkd1-/-* cells and shRNA-knockdown of PKD2 in cells isolated from *Pkd1+/+*, compared with *Pkd1+/+* cells ($^{\#}P$ = 0.0002 and $^{\#}P$ = 0.0104, respectively). Increased levels of SOCE were observed in cells from *Pkd1+/+* and *Pkd1-/-/T16a-/-* transfected with shPkd2 ($^{\#}P$ = 0.0002 and $^{\#}P$ = 0.0099, respectively) in comparison *Pkd1+/+* cells. (n = 28-44 cells from 4 independent cultures of 4 animals each). Mean and error bars indicating ±SEM. $^{\#}$One-way ANOVA and Tukey's post-hoc test comparing with scrambled or *Pkd1+/+* as indicated.

Basal Ca^{2+} levels and ATP-induced Ca^{2+} rise were similar in cortical and medullary epithelial cells (Fig. 2E-G). Moreover, changes in basal $[Ca^{2+}]_i$ and ATP-induced Ca^{2+} signaling by knockout of PKD1 or PKD2 or simultaneous loss of PKD1, PKD2, and TMEM16A expression, were basically identical to the changes observed in medullary epithelial cells (Fig. 2E-G).

Knockout of PKD1 or PKD2 affects store release and SOCE.

To better understand Ca^{2+} signals observed in the absence of PKD1 or PKD2, we performed store release experiments, using extracellular Ca^{2+} free solution and the inhibitor of the sarco/endoplasmic reticulum Ca^{2+}-ATPase (SERCA), cyclopiazonic acid (CPA). Notably, in renal medullary cells lacking expression of PKD1 but not of PKD2, removal of extracellular Ca^{2+} reduced basal Ca^{2+} levels, suggesting Ca^{2+} influx under resting conditions in PKD1 cells [67] (Fig. 3A). Depletion of the Ca^{2+} store by CPA caused a transient rise in cytosolic Ca^{2+} that was augmented in *Pkd1-/-* cells, but was reduced in *shPkd2* cells (Fig. 3A,4A).

The results again suggest reduced Ca^{2+} store filling in the absence of PKD2. Ca^{2+} entry after re-adding of Ca^{2+} to the extracellular bath solution, was augmented in both cells lacking expression of PKD1 and/or PKD2 (Fig. 3A). Remarkably, simultaneous knockdown of both PKD1 and PKD2 cancelled-out the changes observed by single knockout of PKD1 or PKD2 (Fig. 3B,C). Moreover, eliminating expression of TMEM16A also corrected CPA-induced store release and Ca^{2+} influx in *Pkd1-/-* cells. Essentially the same results were obtained from renal cortical epithelial cells (Fig. 4).

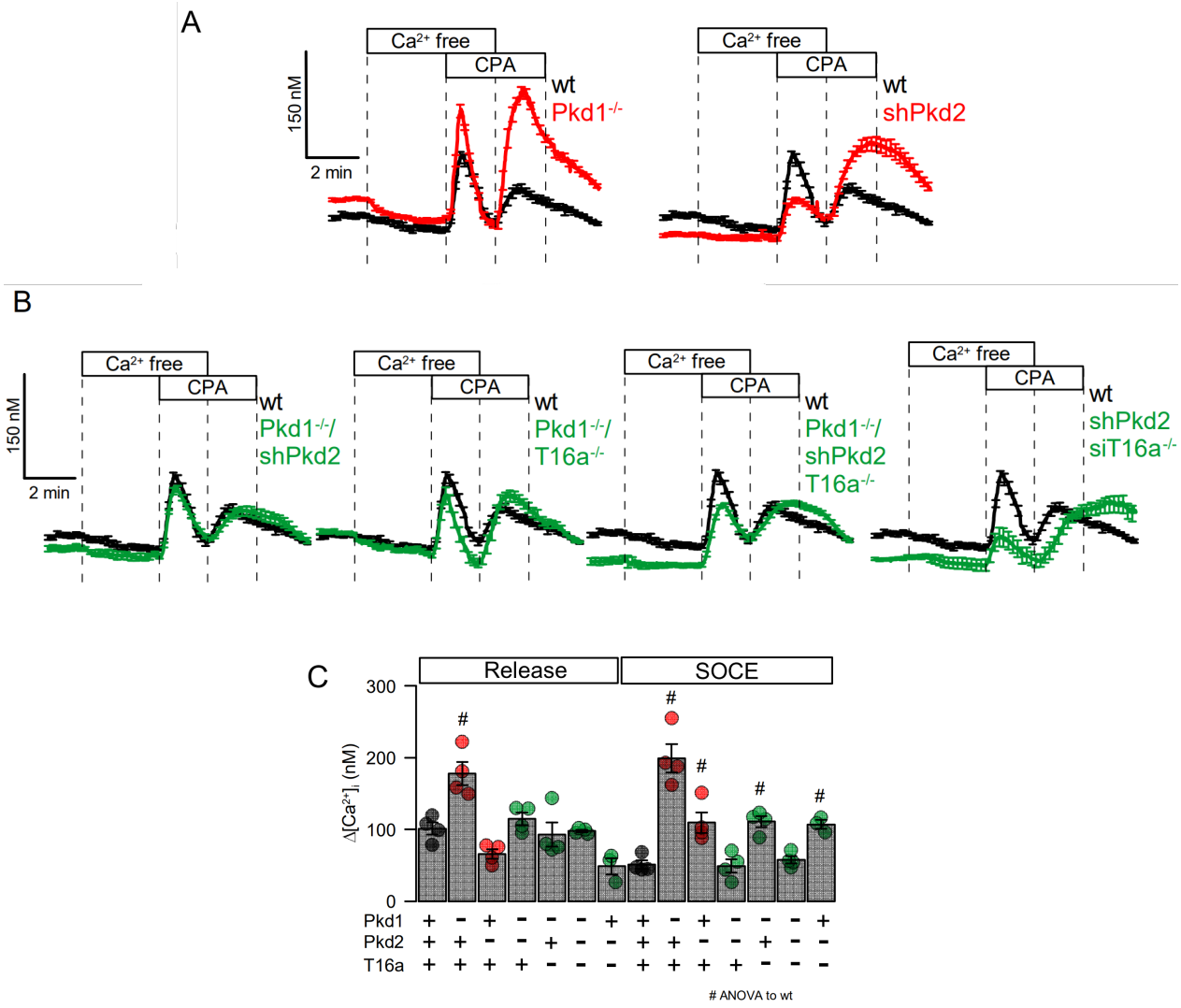

Figure 2.3 | *TMEM16A is essential for effects in Ca^{2+} store release and SOCE by knockout of PKD1 or PKD2 in medullary renal epithelial cells.*

A) Original recordings of abnormal cyclopiazonic acid (CPA, 10 µM) induced store release and SOCE in red and **B)** normal Ca^{2+} signals in green, when compared with *Pkd1+/+* (black) measured by Fura2 in mouse primary medullary epithelial cells. **C)** Summary for cyclopiazonic acid induced store release and SOCE. Ca^{2+} store depletion is enhanced in *Pkd1-/-* cells ($^{\#}P = 0.0016$) and decreased in knockout PKD2, in comparison with Pkd1+/+. Knockout of PKD1 or PKD2 result in increased SOCE ($^{\#}P = 0.0001$, $^{\#}P = 0.0395$, $^{\#}P = 0.003$ and $^{\#}P = 0.001$ respectively) in comparison with *Pkd1+/+* cells. (n = 30-236 cells from 4 independent cultures of 3-4 animals each). Mean and error bars indicating ±SEM. $^{\#}$One-way ANOVA and Tukey's post-hoc test comparing with *Pkd1+/+* cells.

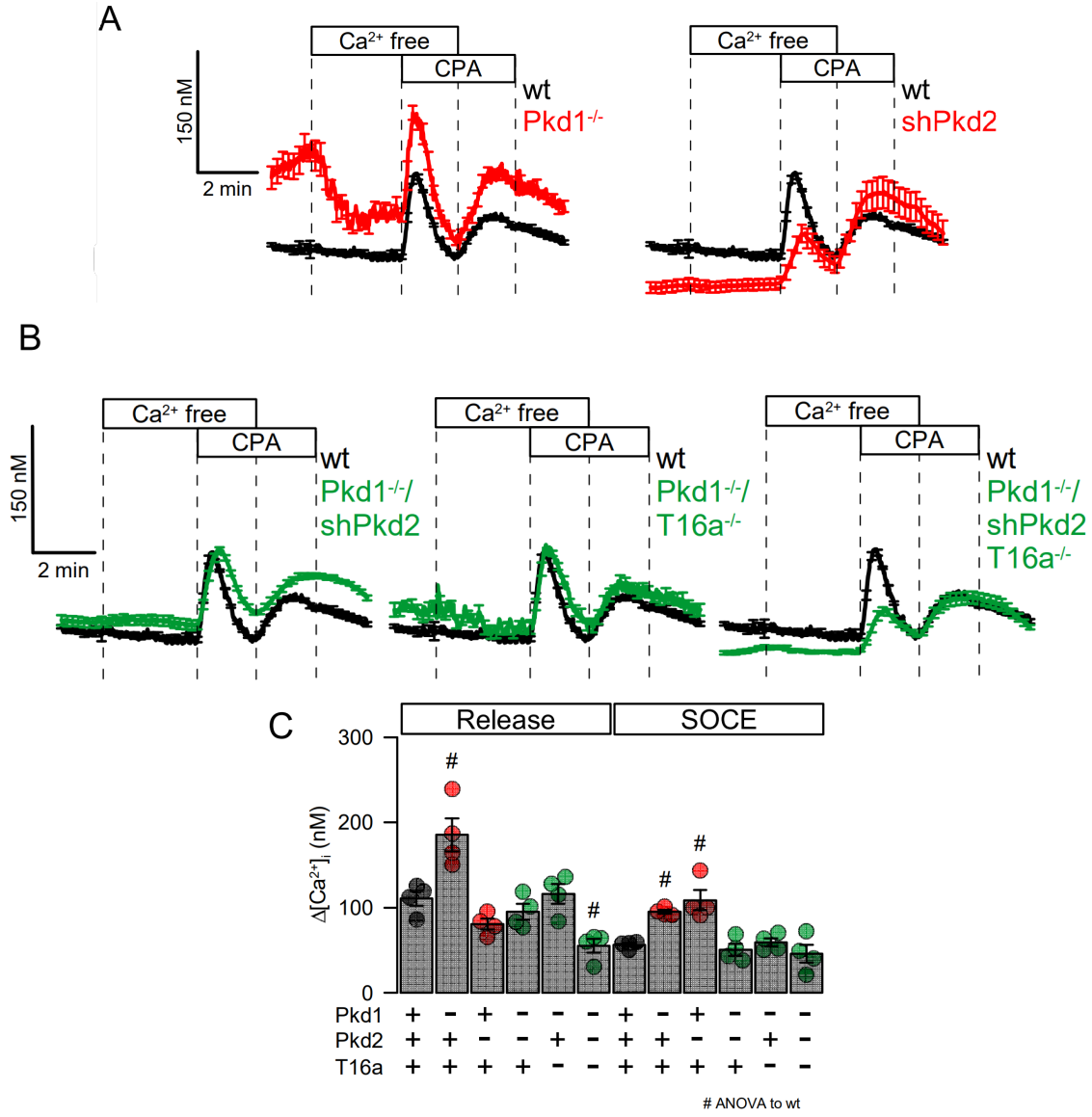

Figure 2.4 | *TMEM16A is essential for effects in Ca^{2+} store release and SOCE by knockout of PKD1 or PKD2 in cortical renal epithelial cells.*

A) Original recordings for affected cyclopiazonic acid (CPA, 10 µM) induced store release and SOCE in red and **B)** normal signaling in green, in comparison with *Pkd1+/+* (black) measured by Fura2 in mouse primary cortical epithelial cells. **C)** Summary for cyclopiazonic acid induced store release and SOCE. Ca^{2+} store depletion is enhanced in *Pkd1-/-* cells ($^{\#}P = 0.0025$), decreased in *shPkd2* cells and further decreased with triple knockout of PKD1, PKD2 and TMEM16A ($^{\#}P = 0.0283$). Comparison with Pkd1+/+ cell (black) Knockout of PKD1 or PKD2 result in increased SOCE ($^{\#}P = 0.0185$ and $^{\#}P = 0.0011$, respectively) in comparison with *Pkd1+/+* cells. (n = 46-62 cells from 4 independent cultures of 4 animals each). Mean and error bars indicating ±SEM. #One-way ANOVA and Tukey's post-hoc test comparing with *Pkd1+/+* cells.

Taken together the present comparison between knockout of PKD1 or PKD2 in mouse renal epithelial cells suggests partially divergent effects on intracellular Ca^{2+} signals. However, expression of TMEM16A is upregulated and purinergic Ca^{2+} store release is augmented in both *Pkd1-/-* and *shPkd2* cells. Disease-causing purinergic Ca^{2+} increase is suppressed by

additional knockdown *of TMEM16A in* both *Pkd1-/-* and *shPkd2* cells. Because the function of TMEM16A is essential for cyst development, pharmacological inhibition of TMEM16A is recommended as a therapy of ADPKD caused by loss of function of PKD1 and PKD2 [67].

Inhibition of TMEM16A by benzbromarone reduces augmented Ca^{2+} store release and SOCE by downregulation of PKD2 in primary medullary epithelial cells.

Benzbromarone is a well-established FDA-approved drug and a potent inhibitor of TMEM16A. Our previous studies show that benzbromarone inhibits cell proliferation in M1 renal organoids and cyst progression in ADPKD mouse model [67,86]. Pre-incubation of control medullary epithelial cells (wt, treated with scrambled shRNA) with 10 µM benzbromarone has no effect on reduced basal Ca^{2+} by knockdown of Pkd2 by shRNA (Fig. 5 A,B), but inhibits ATP-induced store release in wt and PKD2 knockdown cells (Fig. 5B,C).

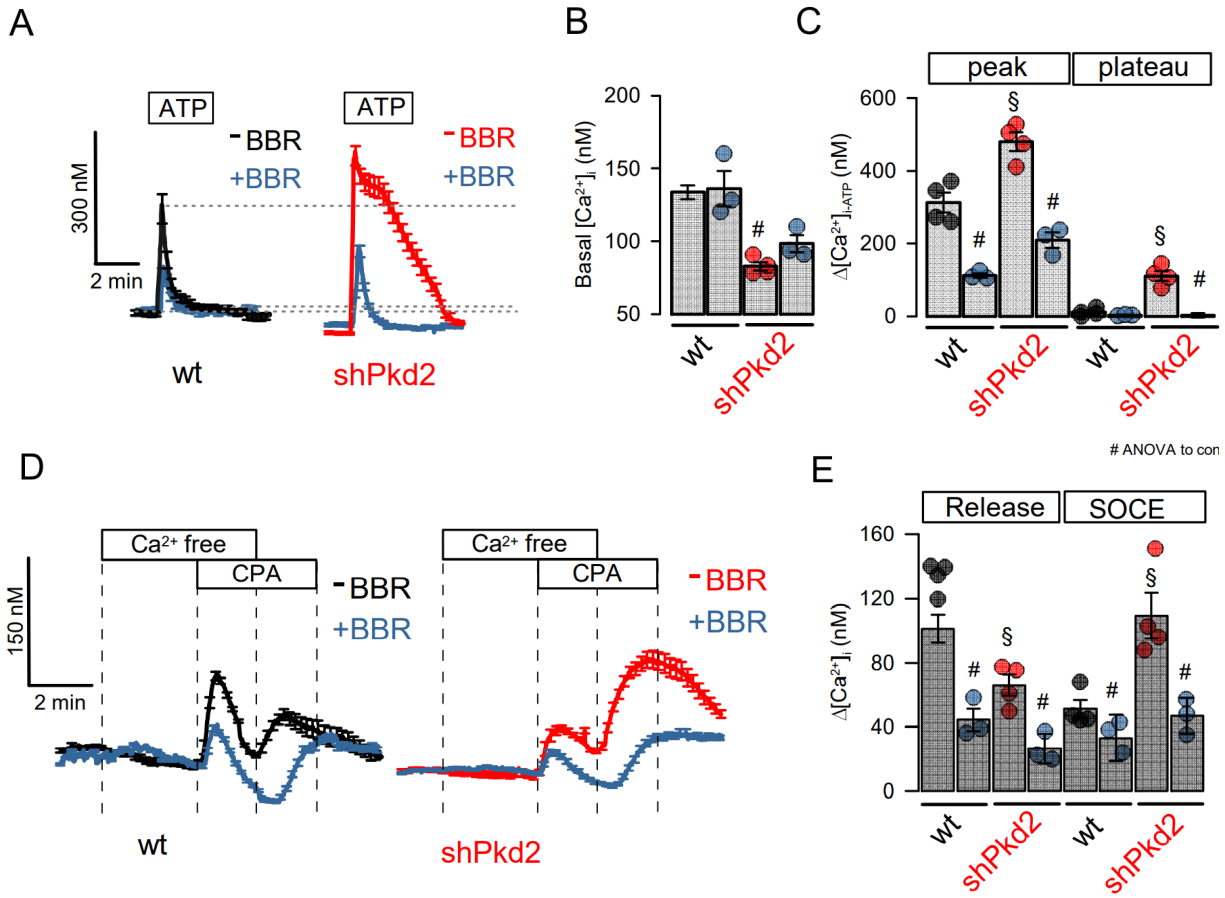

Figure 2.5 | ***Inhibition of TMEM16A by benzbromarone reduce augmented Ca^{2+} store release and SOCE by downregulation of PKD2 in primary medullary epithelial cells.***

A) Summary traces of ATP (100 µM)-induced Ca^{2+} increase measured by Fura2 in wild type (wt, sh-scrambeld) and Pkd2 knockdown (shPkd2) mouse medullary epithelial cells of untreated (-BBR) and 3 min pre-incubated cells with 10 µM benzbromarone (+BBR). **B)** Basal Ca^{2+} is reduced by Pkd2 knockdown ($^{\#}P$ = 0.01) but not affected by benzbromarone. **C)** Pkd2 knockdown increase ATP-induced store release ($^{\S}P$ = 0.016). ATP-induced Ca^{2+} increase is inhibited by benzbromarone in wt and PKD2 knockdown cells ($^{\#}P$ = 0.0017 and $^{\#}P$ = 0.0015, respectively). Increased levels of SOCE in cells

transfected with shPkd2 ($^{\S}P$ = 0.0005) are inhibited by benzbromerone ($^{\#}P$ < 0.0015). **D)** Original recordings of cyclopiazonic acid (CPA, 10 µM) induced store release and SOCE of untreated (-BBR) and 3 min pre-incubated cells with 5 µM benzbromarone (+BBR). **E)** Summary for cyclopiazonic acid induced store release and SOCE. Ca^{2+} store depletion is decreased in *shPkd2* cells ($^{\S}P$ = 0.02). Benzbromerone inhibits Ca^{2+} store depletion of wt and shPkd2 cells ($^{\#}$P = 0.01 and $^{\#}$P = 0.01, respectively). Knockout of PKD2 result in increased SOCE ($^{\#}$P = 0.008) in comparison with wt cells. Benzbromerone inhibits SOCE of wt and shPkd2 cells ($^{\#}$P = 0.01 and $^{\#}$P = 0.01, respectively). (n = 108-235 cells from 3 independent cultures of 3-4 animals each). Mean and error bars indicating ±SEM. §, #One-way ANOVA and Tukey's post-hoc test.

In addition, the increase of SOCE by PKD2 knockdown was also inhibited by benzbromarone (Fig. 5A,C). Furthermore, CPA - induced store release and SOCE are reduced by benzbromarone in wt and PKD2 knockdown cells (Fig. 5D,E). These results underline that pharmacological inhibition of TMEM16A could be used as a therapy of ADPKD.

Discussion

In the kidney, the Ca^{2+} activated Cl^- channel TMEM16A is expressed at low levels, but is upregulated in human and mouse polycystic kidneys [67,110,137]. Our previous work suggested that upregulation of TMEM16A supports cyst growth by increasing receptor-activated Ca^{2+} signals, which are responsible for enhanced cell proliferation [67,86]. It is well known that loss of PKD1 and PKD2 cause a change in transcription. This is in part due to activation of the TAZ/Wnt-β-catenin/c-MYC axis [142,143], and through deregulation of a number of other genes that control transcription [144] as well as Hippo targeted gene expression [145]. Importantly, TMEM16A-expression is upregulated by the STAT-signaling pathway, which has also been shown to be activated in ADPKD [146]. Finally, a systems biology approach identified changes in protein expression in ADPKD, among them TMEM16A, which we reported in our recent paper [67,147]. All of these changes lead to an increase in cell proliferation, and a switch of the renal tubular epithelium from reabsorption towards Cl^- secretion. In the normal unaffected collecting duct, TMEM16A is found only in apical membranes of ß-intercalated cells [148]. In contrast, in the cyst epithelium of ADPKD, TMEM16A is expressed also in principal cells [67,137].

Along with TMEM16A, also CFTR is found to be upregulated in principle cells. Importantly, TMEM16A and CFTR do not operate independently but TMEM16A upregulates membrane expression of CFTR and the activity of CFTR, by enhancing submembraneous Ca^{2+} levels [116,117,135,149-151]. Thus, not only enhanced proliferation but also induction of electrolyte secretion into the cyst lumen is responsible for continuous cyst growth and compression of the healthy functional parenchyma. Purinergic Ca^{2+} signaling is highly relevant in this pathogenic process, and along with TMEM16A also expression of P2Y2-receptors is enhanced in ADPKD

[152]. Unlike previously thought, not CFTR but TMEM16A appears to be the dominating secretory channel in ADPKD [67,86]. However, the impact of TMEM16A on intracellular Ca^{2+} signaling and cell proliferation are most relevant for disease progression [67,86].

Changes in intracellular Ca^{2+} signaling in ADPKD have been found in many previous studies, although with sometimes controversial results [43,153,154]. In *Pkd1*$^{-/-}$ cells we found enhanced basal intracellular [Ca^{2+}] along with augmented purinergic Ca^{2+} signals, in contrast to Yamaguchi et al, who reported lower intracellular Ca^{2+} levels [67,155]. Enhanced basal $[Ca^{2+}]_i$, and purinergic increase in $[Ca^{2+}]_i$, correlated well to enhanced basal and ATP-activated Cl^- transport, found in the present and in our previous study [67]. Essentially all results obtained in tissues from PKD1-knockout mice could be reproduced by PKD1-knockout in mouse M1 collecting duct cells [86]. In M1 cells, both knockout of PKD1 or PKD2 by shRNA induced expression of TMEM16A, augmented cell proliferation and cyst growth *in vitro*, increased electrolyte secretion, and enhanced intracellular Ca^{2+} signals.

Generally speaking, Ca^{2+} signals were less pronounced in *shPkd2* when compared to *Pkd1-/-* cells [86]. The present data now confirm these subtle differences caused by a lack of PKD1 vs. lack of PKD2 in primary renal epithelial cells. The data confirm that loss of PKD1 leads to i) enhanced basal $[Ca^{2+}]_i$, ii) augmented purinergic Ca^{2+} store release, and iii) no change in SOCE. The changes are clearly related to upregulation of TMEM16A, as shown here and in the previous report [67]. In contrast, loss of PKD2 caused i) lower basal $[Ca^{2+}]_i$, ii) augmented purinergic store release, and iii) enhanced SOCE. Lower basal $[Ca^{2+}]_i$, and enhanced SOCE seem to be independent of TMEM16A. In contrast, enhanced purinergic Ca^{2+} signals in cells lacking PKD1 are TMEM16A-dependent.

Based on the present findings we hypothesize that renal epithelial cells possibly have different Ca^{2+} stores as described earlier [156]. Some Ca^{2+} stores are triggered by purinergic stimulation and are controlled by TMEM16A, but are independent of PKD1 and PKD2, while others dependent on PKD1 and PKD2. Under normal conditions as present in wild type cells, both Ca^{2+} stores are functionally not distinguishable. In cells lacking Pkd1, upregulation of TMEM16A causes augmented Ca^{2+} release enhanced CPA-sensitive Ca^{2+} reuptake. Higher basal Ca^{2+} may be caused through ER located PKD2 leakage channels, contributing to enhanced Ca^{2+} influx (SOCE, Fig. 3A, Fig. 4A), which is TMEM16A dependent (Fig. 3B,C; Fig. 4B,C). In cells lacking Pkd2, Ca^{2+} influx is also accelerated but Ca^{2+} store release and basal Ca^{2+} levels may be independent of TMEM16A (Fig. 3B,C; Fig. 4B,C). Nevertheless, lack of PKD2 increases expression of TMEM16A which upregulates purinergic release in other stores (Fig. 2A). The complex regulation of intracellular Ca^{2+} signals by different Ca^{2+} stores currently does not allow a complete understanding of the contribution of all components, TMEM16A, PKD1, and PKD2, to the overall Ca^{2+} output signal. Nevertheless, both loss of PKD1 and of PKD2 lead to augmented purinergic Ca^{2+} signals that cause augmented cell proliferation and growth of renal cysts.

Interestingly, the disease-related increase in purinergic $[Ca^{2+}]_i$ signals was attenuated in PKD1/2 double knockout cells, which corresponds well to the milder phenotype reported in double knockout mice, or observed with loss of the primary cilium. Interestingly, a recent study described cyclin-dependent kinase 1 activity as a driver of cyst growth in polycystic kidney disease [144]. This corresponds well to the upregulation of cyclin D1-expression by enhanced expression of TMEM16A in head and neck cancers [106].

Plasma membrane tethering of the ER by TMEM16A and increase in compartmentalized Ca^{2+} signals close to the plasma membrane provide a mechanism for TMEM16A-dependent cyst formation [116,157]. To what degree Cl^- movement through TMEM16A contributes to the changes in local $[Ca^{2+}]_i$, remains obscure, as compartmentalized Ca^{2+} was difficult to measure in primary cells and because cell growth in the presence of TMEM16A blockers leads to degradation of TMEM16A [67,158]. Nevertheless, TMEM16A-dependent changes in intracellular Cl^- was shown to operate as an intracellular signal [159-161]. Interestingly, the Muallem lab found that also TMEM16H tethers the ER and the plasma membrane for assembly of Ca^{2+} signaling complexes [162]. These contact sides are highly relevant for cell signaling and ion transport [163]. Along this line, extended synaptotagmin-1 (ESYT1), another membrane tether, was found to be associated with TMEM16A [150]. Finally, the TMEM16A-homologue Ist2 operates as an ER-tether in yeast and even produced Ca^{2+} activated Cl^- currents when expressed in HEK293 cells [118].

Taken together, the present data and previous reports indicate that loss of PKD1 or PKD2 lead to subtle differences in intracellular Ca^{2+}, which are independent of TMEM16A in *shPkd2* cells. However, both *Pkd1-/-* and *shPkd2* caused upregulation of TMEM16A-expression that leads to augmented purinergic Ca^{2+} signals. Pathologic Ca^{2+} signaling is abolished with deletion or inhibition of TMEM16A, thereby correcting abnormal proliferation and ion secretion, which inhibits cyst development [67,86]. Therefore, pharmacological inhibition of TMEM16A is suitable to treat ADPKD caused by mutations in both *PKD1* and *PKD2*.

Acknowledgements

Supported by the Deutsche Forschungsgemeinschaft (DFG, German Research Foundation), project number 387509280, SFB 1350 (project A3). We are grateful to Prof. Dr. Dorien J.M. Peters (Department of Human Genetics, Leiden University Medical Center, Leiden, The Netherlands) for providing us with animals with a floxed *Pkd1* allele.

CHAPTER 3 | THE CHLORIDE CHANNEL CFTR IS NOT REQUIRED FOR CYST GROWTH IN AN ADPKD MOUSE MODEL

Abstract

Autosomal dominant polycystic kidney disease (ADPKD) is characterized by the development of bilateral renal cysts which enlarge continuously, leading to compression of adjacent intact nephrons. The growing cysts lead to a progressive decline in renal function. Cyst growth is driven by enhanced cell proliferation and chloride secretion into the cyst lumen. Chloride secretion is believed to occur mainly by the cAMP-activated cystic fibrosis transmembrane conductance regulator (CFTR), with some contribution by the calcium-activated chloride channel TMEM16A. However, our previous work suggested TMEM16A as a major factor for renal cyst formation. The contribution of CFTR to cyst formation has never been demonstrated in in an adult ADPKD mouse model. We used mice with an inducible tubule-specific Pkd1-knockout, which consistently develop polycystic kidneys upon deletion of Pkd1. Cellular properties, ion currents and cyst development in these mice were compared with that of mice carrying a co-deletion of Pkd1 and Cftr. Knockout of Cftr did not reveal any significant impact on cyst formation in the ADPKD mouse model. Furthermore, knockout of Cftr did not attenuate the largely augmented cell proliferation observed in Pkd1 knockout kidneys. Patch clamp analysis on primary renal epithelial cells lacking expression of Pkd1 indicated an only marginal contribution of CFTR to whole cell Cl^- currents, which were clearly dominated by calcium-activated TMEM16A currents. In conclusion, CFTR does not essentially contribute to renal cyst formation in mice caused by deletion of Pkd1. Enhanced cell proliferation and chloride secretion is caused primarily by upregulation of the calcium-activated chloride channel TMEM16A.

Keywords: ADPKD, CFTR, cyst growth, proliferation, TMEM16A

Published in: Talbi K, Cabrita I, Kraus A, Hofmann S, Skoczynski K, Kunzelmann K, Buchholz B, Schreiber R. The chloride channel CFTR is not required for cyst growth in an ADPKD mouse model. FASEB J. 2021 Oct;35(10):e21897.

Own experimental contribution: Isolation of renal primary cells, whole cell Patch Clamp, kidney perfusion, protein isolation from whole kidney lysate.
Own written contribution: Original draft preparation.
Other contributions: Designed experiments and analysed data.

Introduction

Autosomal dominant polycystic kidney disease (ADPKD) is a frequent monogenic kidney disease often resulting in end stage renal failure [164]. It is caused by mutations in either PKD1 (~85%) encoding polycystin-1 or PKD2 (~15%) encoding polycystin-2 [164]. ADPKD is characterized by the development of multiple bilateral renal cysts which enlarge continuously over years and decades [165]. Continuous cyst enlargement leads to compression of adjacent intact tissue which results in decline of renal function [165]. Cyst growth is driven by increased cell proliferation and chloride transport into the cyst lumen accompanied by fluid transport secretion [165,166].

Chloride conductance has been early demonstrated in monolayers of human ADPKD cyst cells [167,168]. Fluid secretion was stimulated by adenylyl cyclase agonists like forskolin, and also by the phosphodiesterase inhibitor 3-isobutyl-1-methylxanthine (IBMX) [62,63]. The analogy between observations in ADPKD cyst epithelial cells and those in other secretory epithelial cells, suggested that CFTR chloride channels mediate cAMP-stimulated Cl^- secretion in ADPKD cysts [169]. CFTR belongs to the ATP-binding cassette (ABC) superfamily of integral membrane transporters [170]. CFTR is regulated by cAMP-dependent phosphorylation of the regulatory (R) domain via PKA resulting in transepithelial Cl^- transport [170]. Mutations of CFTR are known to cause cystic fibrosis, a common lethal autosomal recessive disease [171]. Expression of CFTR has been detected in isolated primary ADPKD cells and ADPKD kidney extracts, with a staining pattern suggesting localization in the apical membrane of cyst-lining cells [169].

Cl^- currents were observed in isolated ADPKD cyst cells, which were activated by forskolin or stable analogues of cAMP. These currents could be inhibited by diphenylamine-2-carboxylate, and by antisense oligonucleotide against human CFTR [75,169]. Moreover, specific inhibitors of CFTR like the thiazolidinone inhibitor CFTRinh-172, which stabilizes the channel closed state, inhibited cyst growth of MDCK cells and in cAMP-stimulated metanephric kidney cultures [172,173]. Interestingly, the CFTR inhibitors tetrazolo-CFTRinh-172 and Ph-GlyH-101 suppressed MDCK cyst enlargement without affecting cell proliferation [172]. In addition, both inhibitors retarded cyst growth in a metanephric kidney cyst model and in a neonatal kidney-specific Pkd1 knockout (KspCre;$Pkd1^{flox/-}$) mouse model [172]. However, the role of CFTR to polycystic kidney kidney disease has not been demonstrated *in vivo* in a suitable animal model. Such a model probably reflects better the long-standing course of the disease in humans. Furthermore, a significant heterogeneity in CFTR expression has been reported in isolated primary cyst cells from ADPKD patient [75,169,174]. Notably, a milder cystic phenotype has been reported in three patients with ADPKD and cystic fibrosis, when compared to their siblings suffering from ADPKD alone [175,176]. However, the potential protective effect by cystic fibrosis in ADPKD has not been confirmed in a subsequent report [80].

In our previous reports, we identified the calcium-activated chloride channel TMEM16A to be significantly involved in cyst growth in ADPKD [85,177]. In ADPKD, expression of TMEM16A is upregulated in the apical membrane of human cyst-lining cells [85]. Knockdown of TMEM16A (Anoctamin1; ANO1) in cyst-forming MDCK cells significantly inhibited ATP-dependent, i.e. calcium-activated chloride currents [85]. ATP is released by renal epithelial cells and accumulates in the cyst fluid of human ADPKD cysts [178,179]. Pharmacological inhibition of TMEM16A and morpholinos directed against TMEM16A inhibited cyst growth in metanephric kidney cultures [85]. Importantly, tubule-specific knockout of TMEM16A as well as pharmacological inhibition by the TMEM16A-inhibitors Ani9, as well as benzbromarone, and niclosamide, inhibited cyst growth in an adult Pkd1 orthologous mouse model [177]. In addition, both, knockout and inhibition of TMEM16A inhibited cyst cell proliferation markedly [85,177]. This is explained by suppression of the pro-proliferative and pro-cancerous function of TMEM16A [180,181]. The unmasked importance of TMEM16A for ADPKD asks for the proportionate contribution of CFTR to cyst formation in ADPKD. In the present study, we therefore co-deleted Cftr together with Pkd1 in adult mice, and analyzed how this would affect cyst growth, proliferation and ion currents. The data demonstrate uncompromised cyst development by deletion of CFTR. Thus, CFTR is not required for cyst formation in the examined adult ADPKD mouse model.

Materials and Methods

Animals. Animal experiments were approved by the local institutional review board and the local Ethics Committee of the Government of Unterfranken/Wuerzburg (AZ: 55.2-2532-2-328, and AZ: 55.2.2-2532-2-853). All experiments complied with the United Kingdom Animals Act, 1986, and associated guidelines, EU Directive 2010/63/EU for animal experiments. Animals were hosted on a 12:12 hours light:dark cycle under constant temperature (24 ± 1 C°) in standard cages. They were fed a standard diet with free access to tap water. Generation of mice with a tamoxifen-inducible, kidney epithelium-specific Pkd1-deletion were described recently [182]. Mice carrying loxP-flanked conditional alleles of Pkd1 were crossed with KSP-Cre mice in a C57BL/6 background (KspCreER^{T2};Pkd1$^{lox;lox}$; abbreviated as Pkd1$^{-/-}$). Mice carrying loxP-flanked Exon 10 alleles of Cftr were crossed to generate KspCreER^{T2};Pkd1$^{lox;lox}$;Cftr$^{lox;lox}$ double knockout mice in a C57BL/6 background (abbreviated as Pkd1$^{-/-}$/Cftr$^{-/-}$). Primers for genotyping are listed in Supplemental Table 1.

Animal treatment. Conditional knockout was induced in male Pkd1$^{-/-}$ (n = 5) and Pkd1$^{-/-}$/Cftr$^{-/-}$ mice (n=7) by intraperitoneal injection of tamoxifen (2 mg/kg body weight) dissolved in 5 % ethanol and 95 % neutral oil, daily at postnatal days PN 20 - 22. Non-induced KspCreER^{T2};Pkd1$^{lox;lox}$ mice (n = 5, abbreviated as Pkd1$^{+/+}$) served as controls. All animals were sacrificed 10 weeks after induction with tamoxifen and kidneys were analyzed. In addition, and

in accordance with pre-defined abort criteria, two mice were sacrificed 6 and 8 weeks after induction, respectively.

Isolation of renal medullary primary cells. Mice were sacrificed and kidneys were removed and kept in ice-cold DMEM/F12 medium (Thermo Fisher Scientific, Darmstadt, Germany). The renal capsule was removed under germ-free conditions. Medulla was separated and chopped into smaller pieces of tissue using a sharp razor blade (Heinz Herenz, Hamburg, Germany). Tissues were incubated in Hanks balanced salt solution/DMEM/F12 (Life Technologies/Gibco, Karlsruhe, Germany) containing 1 mg/ml collagenase type 2 (Worthington, Lakewood, USA) for 20 min at 37° C. The digested tissue was passed through a 100 µm cell strainer (Merck KGaA, Darmstadt, Germany), transferred to a 50 ml falcon tube and washed with ice cold PBS. After centrifugation at 600 g for 4 min / 4° C, tubules were resuspended. After washing with ice-cold PBS, tubules were maintained at 37 °C / 5 % CO_2 in DMEM/F12 supplemented with 1 % fetal bovine serum, 1 % Penicillin/Streptomycin, 1 % L-Glutamine (200 mM), 1 % ITS (100x), 50 nM hydrocortisone, 5 nM triiodothyronine, and 5 nM Epidermal Growth Factor (all Sigma-Aldrich, Taufkirchen, Germany). After 24 hours, primary cells grew out from isolated tubules.

RT-PCR. For RT-PCR total RNA from tissue or primary cells was isolated using NucleoSpin RNA II columns (Macherey-Nagel, Dueren, Germany). Total RNA (1 µg / 50 µl reaction) was reverse-transcribed using random primer (Promega, Mannheim, Germany) and M-MLV Reverse Transcriptase RNase H Minus (Promega). Each RT-PCR reaction contained sense (0.5 µM) and antisense primer (0.5 µM) (Supplemental Table 2), 0.5 µl cDNA and GoTaq Polymerase (Promega). After 2 min at 95°C cDNA was amplified (35 cycles for target sequence and 30 cycles for the reference GAPDH) for 30 s at 95°C, 30 s at 56°C and 1 min at 72°C. PCR products were visualized by loading on peqGREEN (Peqlab; Duesseldorf, Germany) containing agarose gels and analysed using ImageJ.

Western Blotting. *Isolated medullary renal primary cells:* Proteins were isolated using a sample buffer containing 25 mM Tris-HCl, 150 mM NaCl, 100 mM dithiothreitol, 5.5% Nonidet P-40, 5% glycerol, 1 mM EDTA and 1% protease inhibitor mixture (Roche, cOmplete, EDTA-free, Mannheim, Germany). Proteins were separated by 8.5 % sodium dodecyl sulfate (SDS) polyacrylamide gel and transferred to a polyvinylidene difluoride membrane (GE Healthcare Europe GmbH, Munich, Germany) or 4-20% Mini-PROTEAN TGX Stain-Free (Bio-Rad) using a semi-dry transfer unit (Bio-Rad, Hercules, CA, USA). Membranes were incubated with primary anti-TMEM16A rabbit polyclonal antibody (Davids Biotech, Regensburg, Germany; 1:1000), anti-CFTR (alomone labs, Jerusalem, Israel, 1:1000) or anti-PKD1 (Polycystin-1 (7E12), Santa Cruz; 1:500) mouse antibody overnight at 4 °C. Proteins were visualized using horseradish peroxidase-conjugated secondary antibody and ECL detection. Beta-Actin was

used as a loading control. *Whole kidneys:* Proteins were isolated using a sample buffer containing 50 mM Tris-HCl, 150 mM NaCl, 10 mM EDTA, 1% sodium deoxycholate, 0.1% SDS and 1% protease inhibitor mixture (Roche, cOmplete, EDTA-free) and 1% Triton X-100. Proteins were seperated using 8% SDS polyacrylamide gels for TMEM16A and NuPAGE 3-8% Tris-Acetate Protein Gels for CFTR (Life Technologies/Gibco). For detection of TMEM16A the proteins were blotted via iBlot 2 Dry Blotting System (Thermo Fisher Scientific) to a polyvinylidene difluoride membrane (GE Healthcare Europe GmbH, Munich, Germany). For detection of CFTR the proteins were blotted using a semi-dry transfer unit (Bio-Rad) for 3 h. The membranes were incubated with primary antibody anti-TMEM16A DOG-1 ploYclonal (Thermo Fisher, 1:1000) and anti-CFTR (Alomone labs, Jerusalem, Israel 1:500) overnight at 4 °C. Proteins were visualized using horseradish peroxidase-conjugated secondary antibody and ECL detection. Beta-Actin was used as loading control.

Immunohistochemistry and antibodies. Affinity purified polyclonal antiserum against mouse TMEM16A was produced in rabbits immunized with DPDAECKYGLYFRDGKRKVD (aa 44-63, N-terminus) or NHSPTTHPEAGDGSPVPSYE (aa 957-976, C-terminus), coupled to keyhole limpet hemocyanin (Davids Biotechnologie, Regensburg, Germany) as described previously.[18] Mouse kidneys were fixed by perfusion with 4% (v/v) paraformaldehyde and post-fixed in 0.5 mol/L sucrose and 4% paraformaldehyde solution. Paraffin sections of 2 µm were blocked with 5% bovine serum albumin (BSA) and 0.04% Triton X-100 in PBS for 30min. For co-staining of CFTR and TMEM16A, anti-CFTR (rabbit; 1:100; Alomone labs) and anti-TMEM16A (rabbit; 1:200, P80, described previously[19]) antibodies were used in 0.5% BSA and 0.04% Triton X-100 overnight at 4 ºC. As secondary antibodies, anti-rabbit IgG Alexa Fluor 555 and 488 antibodies (1:1000; Thermo Fisher Scientific) were used. Ki-67 staining was performed using a monoclonal anti-ki-67 antibody (rabbit; 1:100, Linaris, Dossenheim, Germany). Sections were counterstained with Hoe33342 (1:200, Sigma-Aldrich). Signals were amplified by the use of the Vectastain Elite ABC Kit (Vector Laboratories, Burlingame, CA) according to the manufacturer's instructions. Signals were analyzed with a DM6000B fluorescence microscope (Leica, Wetzlar, Germany), and photographs were taken with a Leica DFC 450C camera.

Quantification of immunohistochemistry and fluorescent signals. Four random photographs were taken from the cortex of each kidney (n = 5 per condition) at a magnification of X200. Immunofluorescence (TMEM16A and CFTR) was analyzed as described previously [177]. Briefly, fluorescent signals were turned into 8-bit images after subtracting background (ImageJ) and a predefined threshold was used for all images to capture signals. For quantification of ki67, the color deconvolution algorithm (ImageJ) was applied to dissect the different signals, followed by binarization and particle analysis to obtain the ratio of the number of positive cells and cortex area (normalized to mm^2 cortex tissue).

Morphological analyses. Photographs from hematoxylin and eosin–stained kidney sections were taken at a magnification of X25 and stitched to obtain single photographs of the whole transverse kidney sections using a Leica DM6000B microscope and a Leica DFC 450C camera. We used an algorithm that separates normal tubule space from cystic area by defining diameters of non-cystic tubules <50 µm (ImageJ) as described previously [182]. The whole cyst area was divided by the whole cortex area and defined as cystic index.

YFP-quenching assay. For YFP-quenching assays, primary renal cells were infected with lentiviral vectors to express halide-sensitive YFP_{I152L}, as previously described [183]. Cells were isolated from 4 different mice per condition and for each mouse 40 cells were measured. Quenching of the intracellular fluorescence generated by the iodide sensitive Enhanced Yellow Fluorescent Protein (EYFP-I152L) was used to measure anion conductance. YFP-I152L fluorescence was excited at 500 nm using a polychromatic illumination system for microscopic fluorescence measurement (Visitron Systems, Puchheim, Germany) and the emitted light measured at 535±15 nm with a Coolsnap HQ CCD camera (Roper Scientific). Cells were grown on cover slips and mounted in a thermostatically controlled imaging chamber maintained at 37°C. Cells were continuously perfused at 8 ml/min with Ringer solution (mmol/l: NaCl 145; KH_2PO_4 0,4; K_2HPO_4 1,6; Glucose 5; $MgCl_2$ 1; Ca^{2+}-gluconate 1.3) and quenching of YFP-I152L fluorescence by I^- influx was induced by replacing 5 mM extracellular Cl^- with I^-. and exposed to I^- concentration of 5 mM by replacing same amount of NaCl with equimolar NaI. Background fluorescence was subtracted, while auto-fluorescence was negligible. Changes in fluorescence induced by I^- are expressed as initial rates of maximal fluorescence decrease ($\Delta F/\Delta t$). For quantitative analysis, cells with low or excessively high fluorescence were discarded.

Patch clamping. Patch-clamp experiments were performed in the fast whole-cell configuration. Patch pipettes had an input resistance of 2–4 MΩ, when filled with a solution containing (mM) KCl 30, K^+-gluconate 95, NaH_2PO_4 1.2, Na_2HPO_4 4.8, EGTA 1, Ca^{2+}-gluconate 0.758, $MgCl_2$ 1.034, D-glucose 5, ATP 3. pH was 7.2, the Ca^{2+} activity was 0.1 µM. The access conductance was measured continuously and was 30–140 nS. Currents (voltage clamp) and voltages (current clamp) were recorded using a patch-clamp amplifier (EPC 7, List Medical Electronics, Darmstadt, Germany), the LIH1600 interface and PULSE software (HEKA, Lambrecht, Germany) as well as Chart software (AD-Instruments, Spechbach, Germany). Data were stored continuously on a computer hard disc and were analyzed using PULSE software. In regular intervals, membrane voltages (V_c) were clamped in steps of 20 mV from -100 to +100 mV relative to resting potential. Membrane conductance G_m was calculated from the measured current (I) and V_c values according to Ohm's law**.**

Statistics. Data are reported as mean ± SEM. Student's t-test for unpaired samples and

ANOVA were used for statistical analysis. A p value of < 0.05 was accepted as significant difference. Data are expressed as mean ± SEM. Differences among groups were analyzed using one-way ANOVA, followed by a Bonferroni test for multiple comparisons. An unpaired or paired t-test was applied to compare the differences between two groups. $P<0.05$ was considered statistically significant.

Results

Knockout of Cftr does not inhibit cyst development in ADPKD mice.

Pkd1 knockout was achieved by tamoxifen-treatment at postnatal day 20-22 of KspCreER^{T2};Pkd1$^{lox;lox}$ and KspCreER^{T2};Pkd1$^{lox;lox}$/Cftr$^{lox;lox}$ animals to generate either single tubule-specific Pkd1$^{-/-}$ knockout or double Pkd1$^{-/-}$/Cftr$^{-/-}$ knockout animals (Figure 1A,B). Knockout of Pkd1 led to a significant polycystic kidney phenotype 10 weeks after induction (Figure 1C,D). Remarkably, additional knockout of Cftr had no impact on cyst formation (Figure 1C,D). As reported previously, knockout of Pkd1 enhanced renal cell proliferation significantly (Figure 1E,F).[19] This increase in cell proliferation was unaffected by additional knockout of Cftr (Figure 1E,F). These data indicate that CFTR is not required for upregulation of proliferation and cyst growth in adult ADPKD mice.

TMEM16A is upregulated in Pkd1$^{-/-}$ mice, independent of CFTR.

Knockout of Pkd1 causes upregulation of TMEM16A in kidneys of mouse and human [177,184]. Upregulation of TMEM16A expression and ATP-activated whole cell currents persist throughout disease development and increase over time (Supplemental Figure 1). In kidneys from Pkd1$^{-/-}$ mice, enhanced expression of TMEM16A is detected in the apical membrane of the cyst epithelium, along with upregulation of CFTR (Figure 2). Due to the relationship of CFTR and TMEM16A reported earlier [177,185], we wondered whether deletion of CFTR would affect expression of TMEM16A. However, in the absence of CFTR, TMEM16A-expression was still found to be enhanced by deletion of Pkd1 (Figure 2). Western blots from whole kidney lysates indicate that loss of CFTR expression in Pkd1$^{-/-}$/Cftr$^{-/-}$ kidneys does not affect expression of TMEM16A (Supplemental Figure 2).

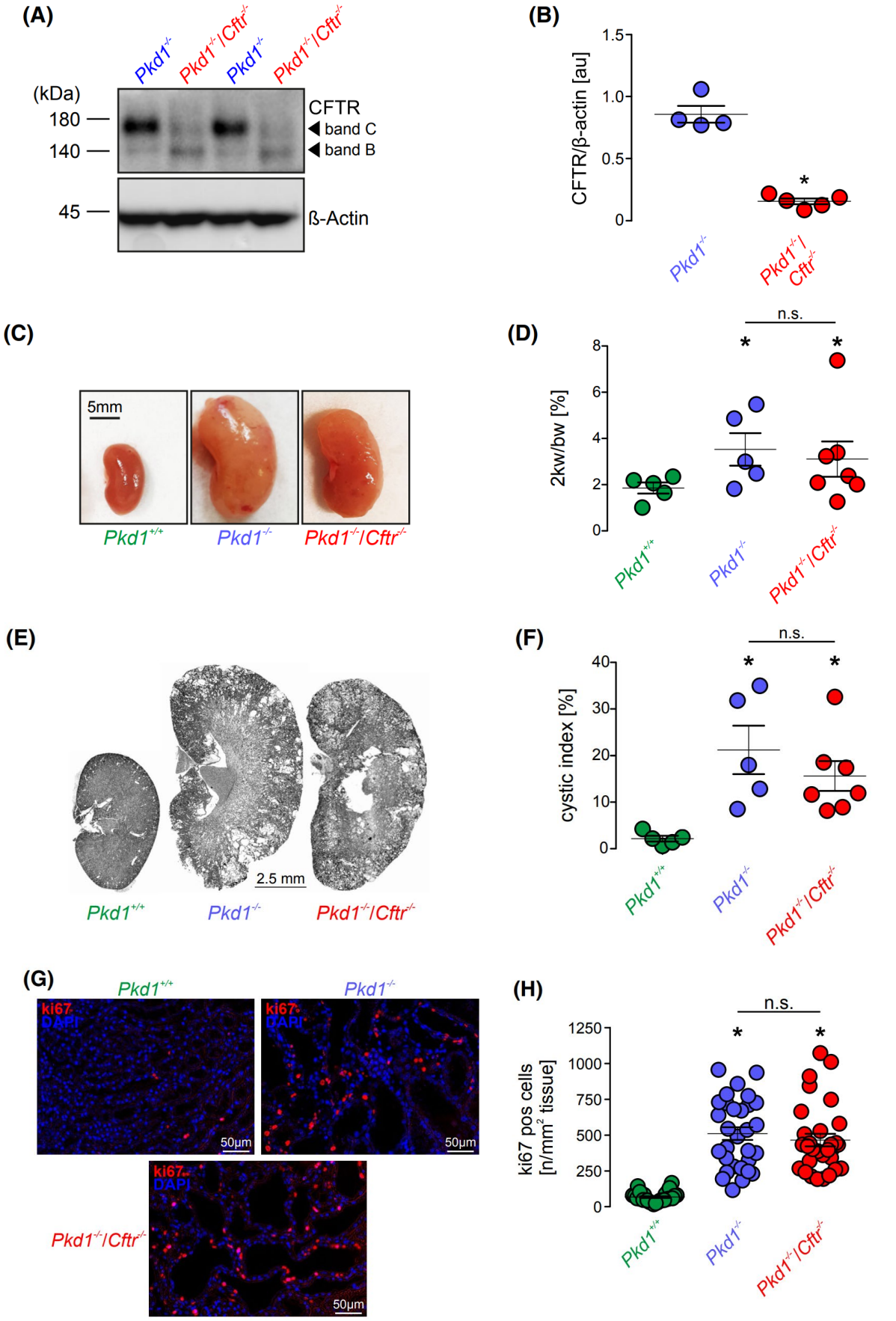

Figure 3.1 | *Knockout of Cftr does not inhibit cyst development in ADPKD.*

Tubule-specific knockout of Pkd1 (Pkd1$^{-/-}$) or double knockout of Pkd1 and Cftr (Pkd1$^{-/-}$/CFTR$^{-/-}$) was

induced by application of tamoxifen at postnatal day 20-22. Non-induced KspCreER^{T2};Pkd1$^{lox;lox}$ mice served as control (Pkd1$^{+/+}$). Analyses were performed 10 weeks after induction. (A) Western blotting from whole kidney lysates from Pkd1$^{-/-}$ (n=4), and Pkd1$^{-/-}$/Cftr$^{-/-}$ (n=5) mice detecting reduced expression of CFTR. The core glycosylated immature form of CFTR is designated as "band B". The complex glycosylated form of CFTR, representing transit through the Golgi, is termed "band C". (B) Quantification of expression of CFTR based on densitometric analysis with CFTR (band C) normalized to β-actin. * significant difference when compared to Pkd1$^{-/-}$, t-test. (C) Tubule-specific knockout of Pkd1 (Pkd1$^{-/-}$; n = 5 animals) induced polycystic kidney disease indicated by increased kidney weight. Additional knockout of Cftr (Pkd1$^{-/-}$/Cftr$^{-/-}$; n = 7 animals) did not prevent cyst formation and kidney weight. Non-induced KspCreER^{T2}; Pkd1$^{lox;lox}$ (Pkd1$^{+/+}$; n = 5 animals) served as controls. (D) Summary of 2 times kidney weight (2kw) to body weight (bw). * significant difference when compared to Pkd1$^{+/+}$, One-Way ANOVA, Posthoc test: Bonferroni-Holm. (E) Tubule-specific knockout of Pkd1 (Pkd1$^{-/-}$; n = 5 animals) induced cyst formation. Additional knockout of Cftr (Pkd1$^{-/-}$/Cftr$^{-/-}$; n = 7 animals) did not prevent cyst formation. Non-induced KspCreER^{T2}; Pkd1$^{lox;lox}$ (Pkd1$^{+/+}$; n = 5 animals) served as controls. (F) Corresponding cystic indices (defined as cortical cyst area normalized to whole cortex area). Mean ± SEM. * significant difference when compared to Pkd1$^{+/+}$, One-Way ANOVA, Posthoc test: Bonferroni-Holm. (G) Analysis of cell proliferation in Pkd1$^{+/+}$, Pkd1$^{-/-}$, and Pkd1$^{-/-}$/Cftr$^{-/-}$ tissues indicated by Ki67 expression. (H) Summary of Ki67 positive cells/mm^2 tissue area in Pkd1$^{+/+}$, Pkd1$^{-/-}$, and Pkd1$^{-/-}$/Cftr$^{-/-}$ kidneys. Mean ± SEM. * significant difference when compared to Pkd1$^{+/+}$, One-Way ANOVA, Posthoc test: Bonferroni-Holm.

Dominating TMEM16A currents in renal epithelial cells from Pkd1$^{-/-}$ mice.

The above-mentioned results ask for the contribution of CFTR to the chloride currents present in primary renal epithelial cells. Therefore, medullary renal primary cells were isolated and characterized 8 - 10 weeks after induction confirming distal tubular origin of the cells (Supplemental Figure 3). Of note, and in line with previous findings [182,186], Pkd1-knockout resulted in an increased expression of the purinergic receptor P2y2 (Supplemental Figure 3). Increase in intracellular cAMP by IBMX (100 µM) and forskolin (2 µM) (I/F) activated no CFTR-mediated whole cell currents in Pkd1-competent cells (Figure 3). We demonstrated earlier that loss of Pkd1 leads to upregulation of CFTR expression [177]. In fact, a small but significant I/F-activated CFTR current was observed in renal cells isolated from Pkd1$^{-/-}$ animals, which was abolished by additional knockout of Cftr (Figure 3). Expression of CFTR in Pkd1$^{-/-}$ mice as well as depletion of CFTR in Pkd1$^{-/-}$/Cftr$^{-/-}$ mice has been confirmed by Western blotting of whole kidney lysates (Supplemental Figure 2) and isolated primary epithelial cells (Supplemental Figure 4).

In contrast to the small CFTR-mediated whole cell current, the ATP-activated TMEM16A-dependent current was much more prominent in Pkd1$^{-/-}$ cells, and was not attenuated by additional knockout of Cftr (Figure 4).

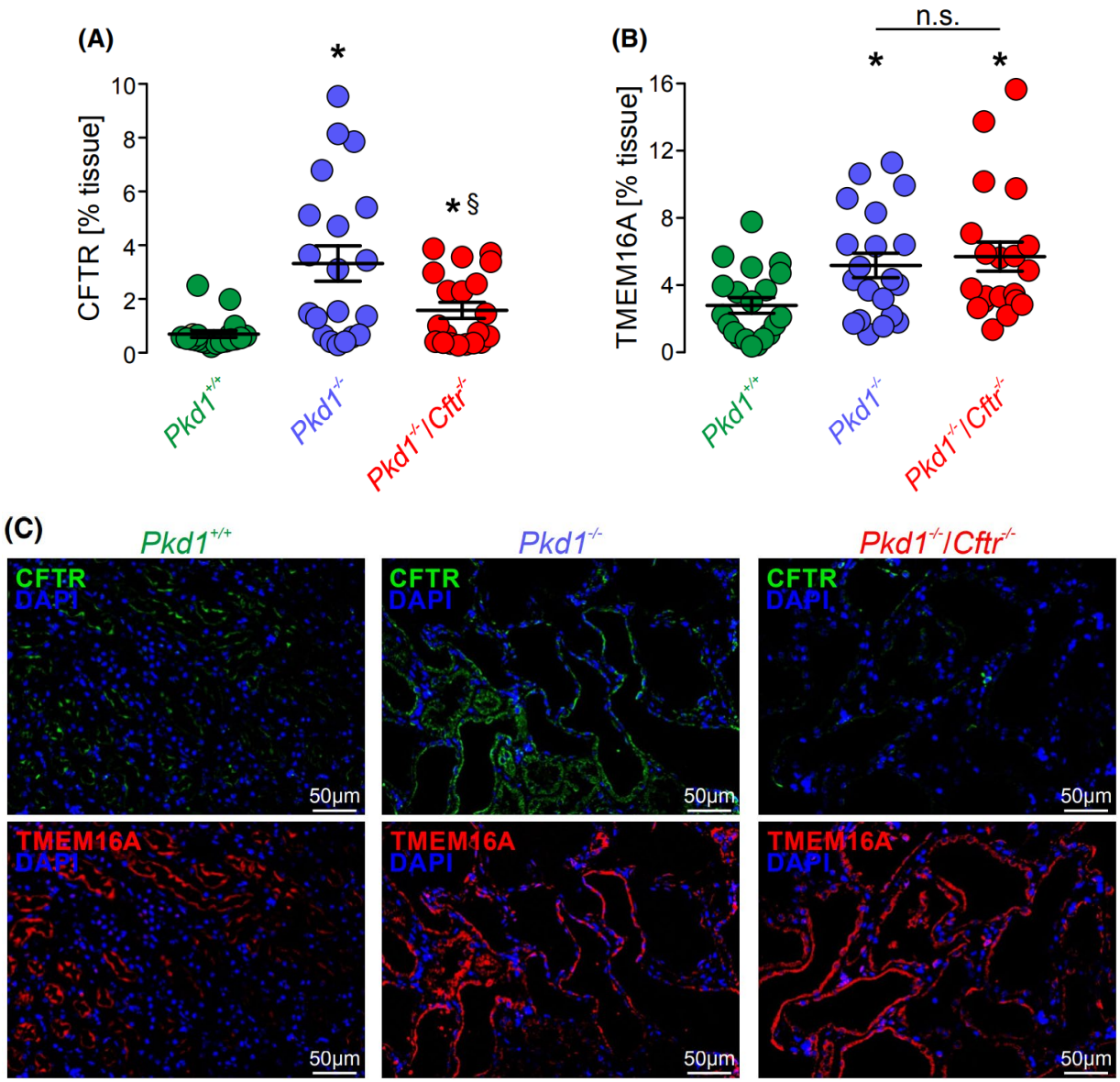

Figure 3.2 | *TMEM16A is upregulated in Pkd1$^{-/-}$ as well as in Pkd1$^{-/-}$/Cftr$^{-/-}$ double-knockout animals.* Kidney sections from Pkd1$^{+/+}$, Pkd1$^{-/-}$, Pkd1$^{-/-}$/CFTR$^{-/-}$ mice (each n = 5 animals with each a total of n = 20 photos) were stained for CFTR and TMEM16A. (A) analysis of CFTR–positive area in relation to the whole cortex area. (B) analysis of TMEM16A–positive area in relation to the whole cortex area. * significant difference when compared to Pkd1$^{+/+}$, unpaired t-test. § significant difference when compared to Pkd1$^{-/-}$, One-Way ANOVA, Posthoc test: Bonferroni-Holm. (C) Representative CFTR stainings (green) and nuclei (blue) in the upper panel and representative TMEM16A stainings (red) and nuclei (blue) in the lower panel.

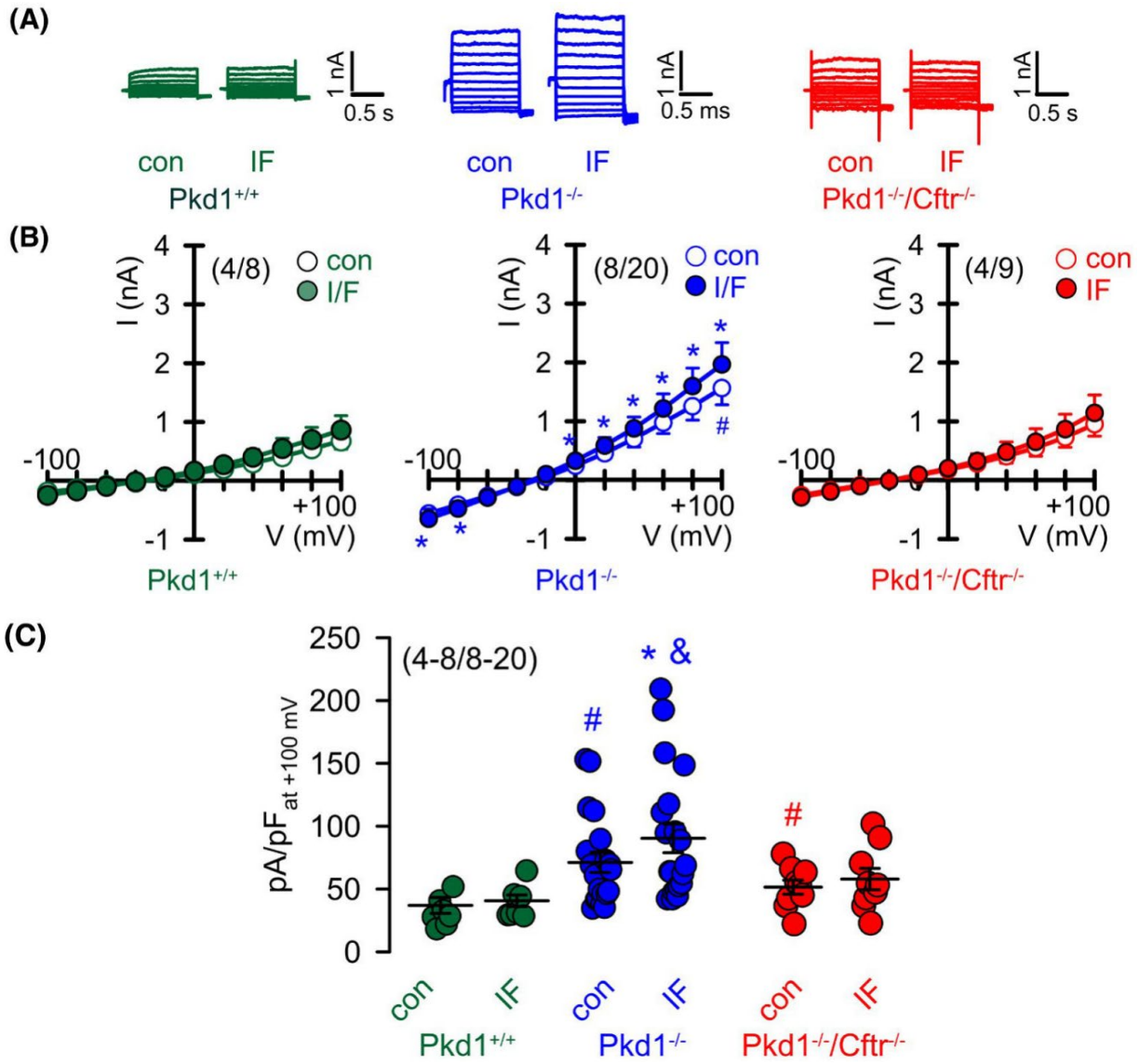

Figure 3.3 | *cAMP-activated CFTR currents make a minor contribution to the whole cell Cl- conductance in Pkd1-/- cells.*

Whole cell patch clamp recordings in primary epithelial cells from Pkd1$^{+/+}$, Pkd1$^{-/-}$, and Pkd1$^{-/-}$/Cftr$^{-/-}$ mice were performed. Currents were obtained under basal conditions (Con) and after stimulation with IBMX/Forskolin (IF, 100 µM/ 2 µM). **(A)** Original whole cell patch clamp recordings in primary epithelial cells from Pkd1$^{+/+}$, Pkd1$^{-/-}$, and Pkd1$^{-/-}$/Cftr$^{-/-}$ mice showing currents obtained under basal conditions and after stimulation with IF. **(B)** I/V curves for the currents shown in A. (C) Summaries of the current densities for the currents summarized in I/V curves shown in B. (number of mice/number of cells). * significant difference when compared to control, paired t-test. # significant difference when compared to Pkd1$^{+/+}$ con, & significant difference when compared to Pkd1$^{+/+}$ IF, One-Way ANOVA, Posthoc test: Bonferroni-Holm.

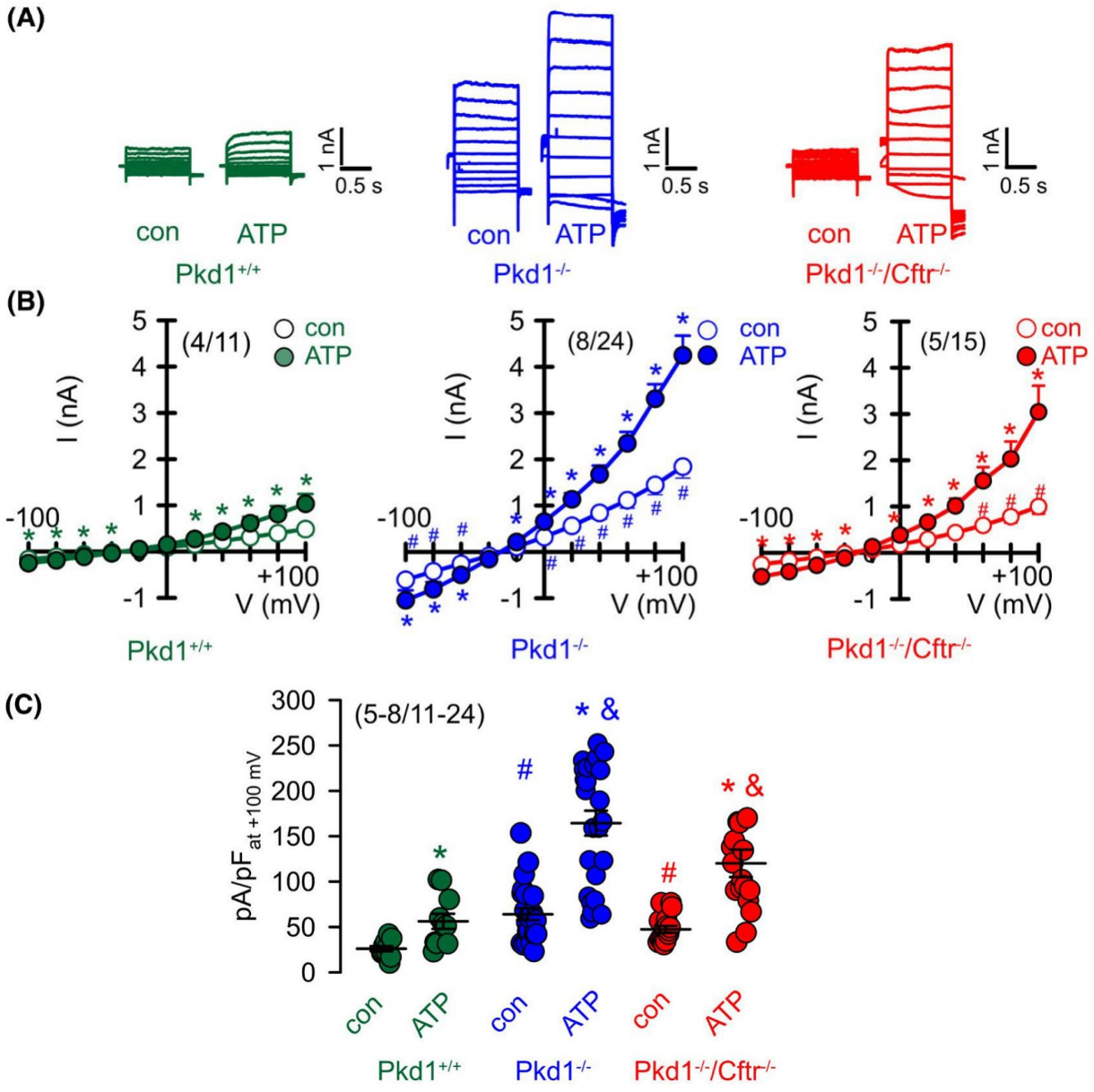

Figure 3.4 |*Ca^{2+}-activated Cl^- currents are upregulated in Pkd1$^{-/-}$ cells independent of CFTR expression.*

Whole cell patch clamp recordings in primary epithelial cells from Pkd1$^{+/+}$, Pkd1$^{-/-}$, and Pkd1$^{-/-}$/Cftr$^{-/-}$ mice were performed. Currents were obtained under basal conditions (Con) and after stimulation with ATP (50 µM). (A) Original whole cell patch clamp recordings in primary epithelial cells from Pkd1$^{+/+}$, Pkd1$^{-/-}$, and Pkd1$^{-/-}$/Cftr$^{-/-}$ mice illustrating currents obtained under basal conditions and after stimulation with ATP. (B) I/V curves for the currents shown in A. **(C)** Summaries of the current densities for the currents summarized in I/V curves shown in B. (number of mice/number of cells). * significant difference when compared to control, paired t-test. # significant difference when compared to Pkd1$^{+/+}$ con, & significant difference when compared to Pkd1$^{+/+}$ cells stimulated with ATP, One-Way ANOVA, Posthoc test: Bonferroni-Holm.

These results correspond well to previous findings reported in mouse primary medullary epithelial cells and M1 mouse collecting duct cells lacking expression of Pkd1 [177,187]. The present data also suggest enhanced basal membrane currents in PKD1$^{-/-}$ cells in the absence of ATP (Figure 4,5). Enhanced currents are not detectable when related to the membrane surface area (current density, pA/pF) presumably because of the larger cell size and capacitance of Pkd1$^{-/-}$ cells due to loss of polycystin-1 [188]. Removal of extracellular chloride or current-inhibition by the TMEM16A-inhibitor Ani9 indicated a basal activity of TMEM16A in PKD1$^{-/-}$ cells (Figure 5).

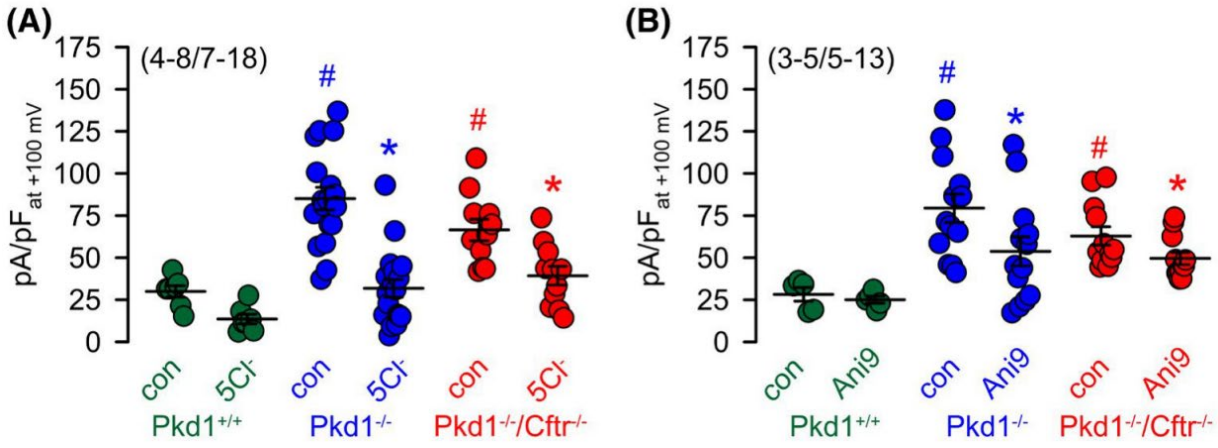

Figure 3.5 | *Ca^{2+}-activated Cl^- currents dominate in Pkd1$^{-/-}$ cells and are mediated by TMEM16A.* Whole cell patch clamp recordings in primary epithelial cells from Pkd1$^{+/+}$, Pkd1$^{-/-}$, and Pkd1$^{-/-}$/Cftr$^{-/-}$ mice were performed. Currents were obtained under basal conditions (Con), after removal of extracellular Cl^- by replacement with the impermeable gluconate ions (5Cl^-), or in the presence of 10 µM of the TMEM16A inhibitor Ani9. **(A)** Summaries for current densities under basal conditions (Con) and after Cl^- removal (5Cl^-). **(B)** Summaries for current densities under basal conditions and after application of the TMEM16A inhibitor Ani9. (number of mice/number of cells). *significant difference when compared to control, paired t-test. # significant difference when compared to Pkd1$^{+/+}$ con, One-Way ANOVA, Posthoc test: Bonferroni-Holm.

In order to validate enhanced ATP-activated chloride currents in Pkd1$^{-/-}$ and Pkd1$^{-/-}$/Cftr$^{-/-}$ cells, we used an independent technique to assess the anion permeability by measuring iodide-induced quenching of yellow fluorescent protein (YFP). In the presence of 5 mM iodide (5I^-) in the extracellular bath solution, stimulation with ATP (100 µM) caused a rapid YFP-fluorescence-quenching. ATP-induced quenching was enhanced in both Pkd1$^{-/-}$ and Pkd1$^{-/-}$/Cftr$^{-/-}$ cells, thus confirming the results obtained in patch clamp experiments (Figure 6). I/F (cAMP increase) activated a small but significant YFP-quenching in Pkd1$^{-/-}$ but not Pkd1$^{+/+}$ and Pkd1$^{-/-}$/Cftr$^{-/-}$ cells, which again shows a minimal contribution of CFTR to chloride secretion by renal epithelial cells from mice lacking PKD1.

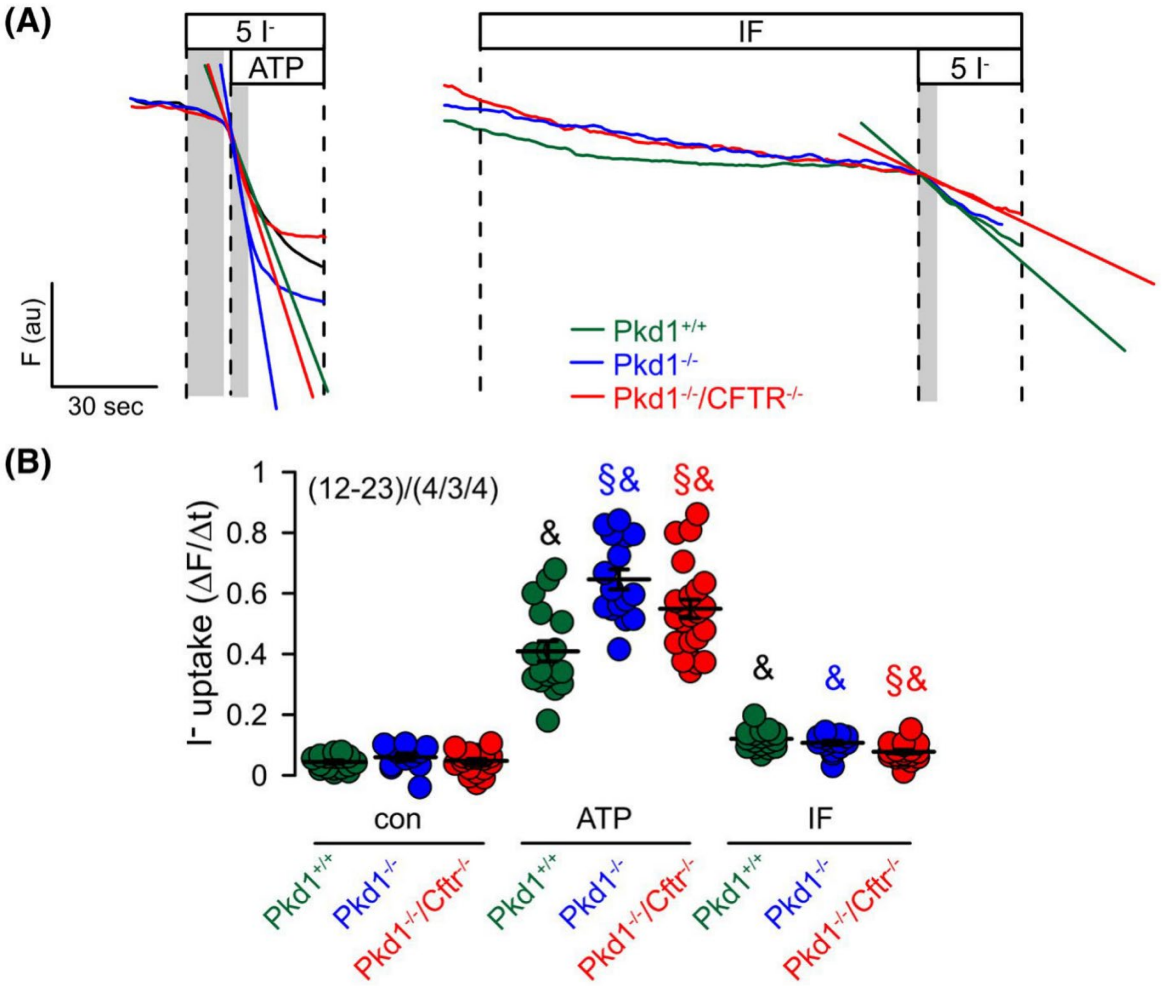

Figure 3.6 | *Halide permeability in Pkd1$^{-/-}$ cells largely depends on Ca^{2+}- but not cAMP-mediated signaling.*

Measurement of iodide-induced quenching of yellow fluorescent protein (YFP) in isolated primary renal epithelial cells from Pkd1$^{+/+}$, Pkd1$^{-/-}$, and Pkd1$^{-/-}$/Cftr$^{-/-}$ mice were performed in the presence of 5 mM extracellular iodide (5I^{-}) under basal conditions (Con), in the presence of ATP (100 µM), or in the presence of IBMX/Forskolin (IF, 100 µM/ 2 µM). **(A)** Original tracings for basal, Ca^{2+}- and IF- activated (100 µM ATP) anion conductances detected by YFP quenching in cells from Pkd1$^{+/+}$, Pkd1$^{-/-}$, and Pkd1$^{-/-}$/Cftr$^{-/-}$ mice. To measure the fast activation of iodide conductance by ATP, ATP was added in the presence of iodide. Whereas iodide was added after 2 min IF incubation when iodide conductance was maximal (determinate by patch clamp experiments). Initial slopes correlate with the size of anion conductance. **(B)** Summary of initial slopes (ΔFluorescence/s) for the experiments shown in A. (number of mice/number of measured cells). § significant difference when compared to Pkd1$^{+/+}$, One-Way ANOVA, Posthoc test: Bonferroni-Holm. & significant difference when compared to control (con), One-Way ANOVA, Posthoc test: Bonferroni-Holm, $ significant difference to Pkd1$^{+/+}$ IF and Pkd1$^{-/-}$ IF, One-Way ANOVA, Posthoc test: Bonferroni-Holm.

Our results demonstrate that renal cyst formation in an adult mouse ADPKD model is largely independent of CFTR. In connection with our previous report we conclude that inhibition of TMEM16A [85,177,187] rather than CFTR [172,189] will be effective to reduce cyst growth in ADPKD.

Discussion

Cyst growth in ADPKD is mediated by chloride secretion and fluid transport across the cyst epithelium into the cyst lumen. The chloride channel CFTR has been suggested to be largely involved in this process based on numerous findings in MDCK cells, human ADPKD cyst cells, cAMP-stimulated metanephric mouse kidneys and a neonatal, kidney-specific Pkd1 knockout mouse model (reviewed in [166]). In contrast, we show that knockout of Cftr in an adult Pkd1 orthologous mouse model does not inhibit cyst formation. CFTR currents activated by cAMP (I/F) only slightly contributed to whole cell currents in primary renal epithelial cells isolated from Pkd1$^{-/-}$knockout mice. Instead, we found that knockout of Pkd1 resulted in enhanced expression of TMEM16A, causing pronounced ATP- dependent, i.e. calcium-activated chloride currents in Pkd1$^{-/-}$ cells, and, importantly, also in Pkd1$^{-/-}$/Cftr$^{-/-}$ cells. This is seemingly in contradiction with earlier *in vitro* studies [62,167]. In other studies with primary cells from ADPKD patients, ATP-dependent chloride transport strongly assisted cAMP-dependent chloride currents [190,191]. These data are in line with our own studies showing a pronounced crosstalk between cAMP- and calcium-dependent signaling pathways: (i) purinergic receptors such as P2Y2R increase intracellular calcium. (ii) intracellular calcium affects the activity of enzymes that control intracellular cAMP like adenylate cyclases [151,185]. (iii) intracellular cAMP and PKA affect proteins like SERCA which in contrast affects intracellular calcium levels. (iv) Most importantly, membrane expression of CFTR requires the presence of TMEM16A [185,192]. Tubular deletion of TMEM16A in our Pkd1 orthologous model was accompanied by significant reduction of CFTR expression [177]. *In vivo* renal cyst development largely depends on enhanced cell proliferation and on TMEM16A-mediated fluid secretion, apart from additional reported factors [177,187]. For both, cell proliferation and fluid secretion, upregulation of TMEM16A expression is largely responsible, while CFTR does not contribute to augmented cell proliferation in Pkd1$^{-/-}$ kidneys. Upregulation of TMEM16A enhances cyclin D1 and the MAPK kinase pathway [193]. Moreover, cyclin kinase D1 (CDK1) was found to be dysregulated in Pkd1 orthologous mouse models [144]. Conditional co-deletion of Cdk1 significantly improved progression of the disease [144].

Appearance of TMEM16A currents and a small but significant CFTR current in renal primary cells, required the knockout of Pkd1. It was not observed in control cells, making a culture artifact unlikely. Moreover, the role of TMEM16A for chloride transport has now been demonstrated by patch clamping, YFP-quenching, and Ussing chamber measurements. We chose a mouse model with a time-course of 10 weeks resulting in polycystic kidneys, which however still was not lethal and did not result in decline of renal function as shown previously [182]. This model, although being still rather rapid compared to the course of the disease in humans, may better reflect disease progression found in humans than embryonic *ex vivo* or neonatal *in vivo* cyst development occurring within a few days. Of note, CFTR may play a more

prominent role in neonatal or embryonic tubule cells which would explain the significant impact of CFTR in early onset and rapid progressive PKD models [172,173]. Kidneys in our mouse model experience hypoxia upon expanding cyst enlargement, which leads to induction of the hypoxia-inducible transcription factor (HIF)-1α [182]. This further promotes calcium-activated chloride secretion, e.g. by transcriptional induction of P2Y2R [182,186,194]. Activation of HIF-1α might vary between the different models, which may determine the contribution of CFTR and TMEM16A.

After all, we did find a small but significant CFTR-mediated chloride secretion. Such an ongoing secretion that takes place over years in human disease, may have an impact on disease progression in patients. At last it should be mentioned that the contribution of CFTR to epithelial chloride secretion is variable in the mouse, with lower activity in the airways but pronounced contribution in the intestine [195-197]. Apart from a few findings, loss of CFTR function does not lead to an overt phenotype in human and mouse. A more recent report shows that in healthy mice it is only expressed in ß-intercalated cells, where it controls bicarbonate secretion [198].

Taken together the present data together with previous reports [85,177,187] identify TMEM16A rather than CFTR as a promising pharmacological target to inhibit cyst growth in ADPKD.

Acknowledgements

BB was supported by the Deutsche Forschungsgemeinschaft (DFG, German Research Foundation), project number 387509280, SFB 1350 (project A2 and B3). KK and RS were supported by the Deutsche Forschungsgemeinschaft (DFG, German Research Foundation), project number 387509280, SFB 1350 (project A3). AK was supported by the Interdisciplinary Center for Clinical Research Erlangen (project J71). We are grateful to Prof. Dr. Dorien J.M. Peters (Department of Human Genetics, Leiden University Medical Center, Leiden, The Netherlands) for providing us with the ADPKD mouse model. The mice with a floxed CFTR allele were kindly provided by Dr. Mitchell Drumm and Dr. Craig Hodges (Case Western Reserve University, 10900 Euclid Avenue, Cleveland, Ohio 44106-7219). This work was performed by KS in fulfillment of the requirements for obtaining the degree Dr. rer. Nat.

Supplementary material

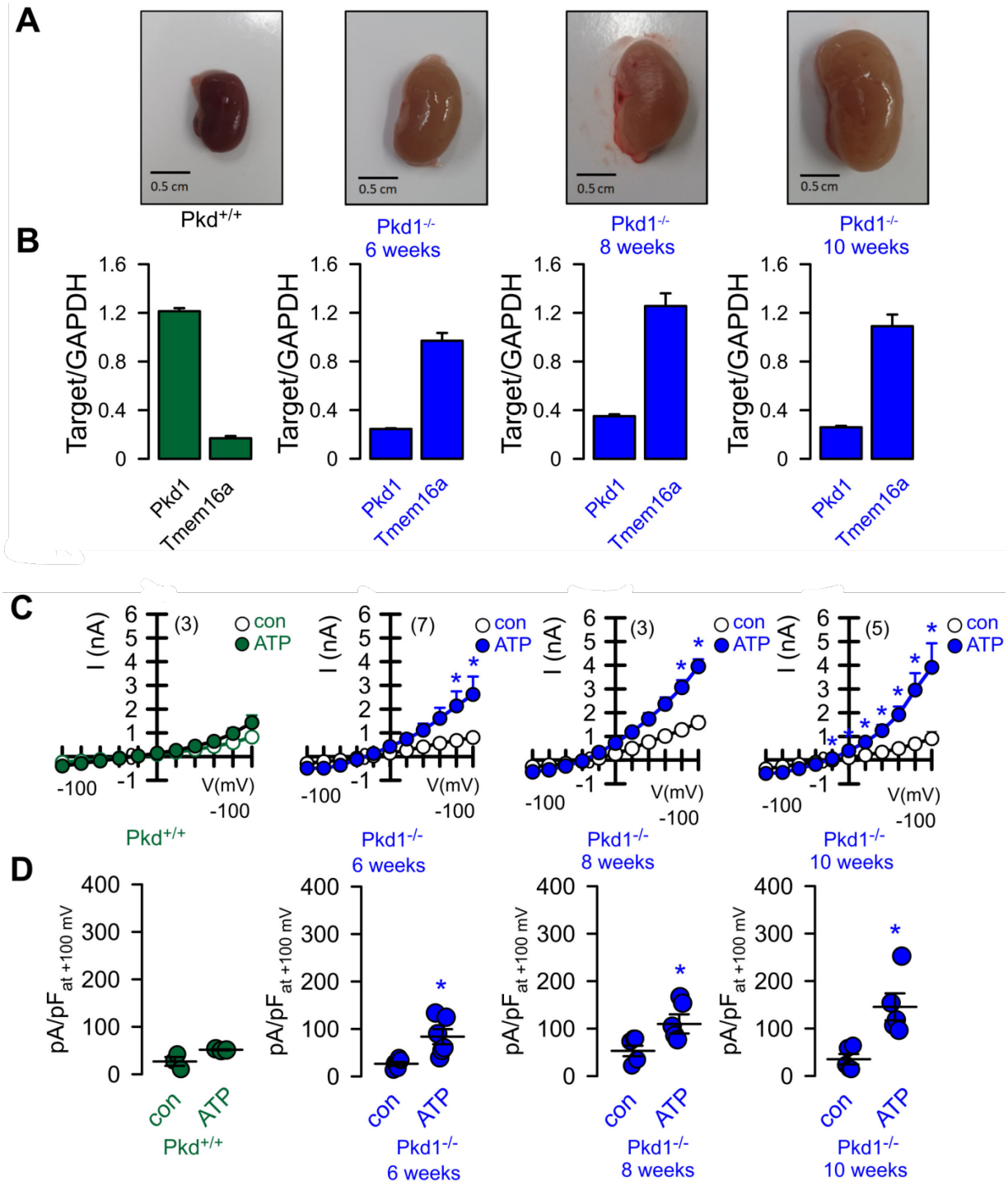

Supplemental figure 3.1 | *Renal cyst development is associated with an increase in Ca^{2+} activated Cl- currents.*

(A) Macroscopic pictures of kidneys from wild type (WT) and $Pkd1^{-/-}$ mice isolated at 6 weeks, 8 weeks and 10 weeks after tamoxifen injection. **(B)** RT-PCR summary of mRNA expression of Pkd1 and Tmem16a relative to Glyceraldehyde 3-phosphate dehydrogenase (Gapdh) in primary epithelial cells from kidneys shown in A. **(C)** I/V curves of whole cell current Patch clamp in primary epithelial cells from kidneys shown in A under basal conditions (Con) and after ATP stimulation, (number of cells). **(D)**

Summaries of current densities for the currents summarized in I/V curves shown in C. * significant difference when compared to WT-Pkd1. § significant difference when compared to WT-Tmem16a.

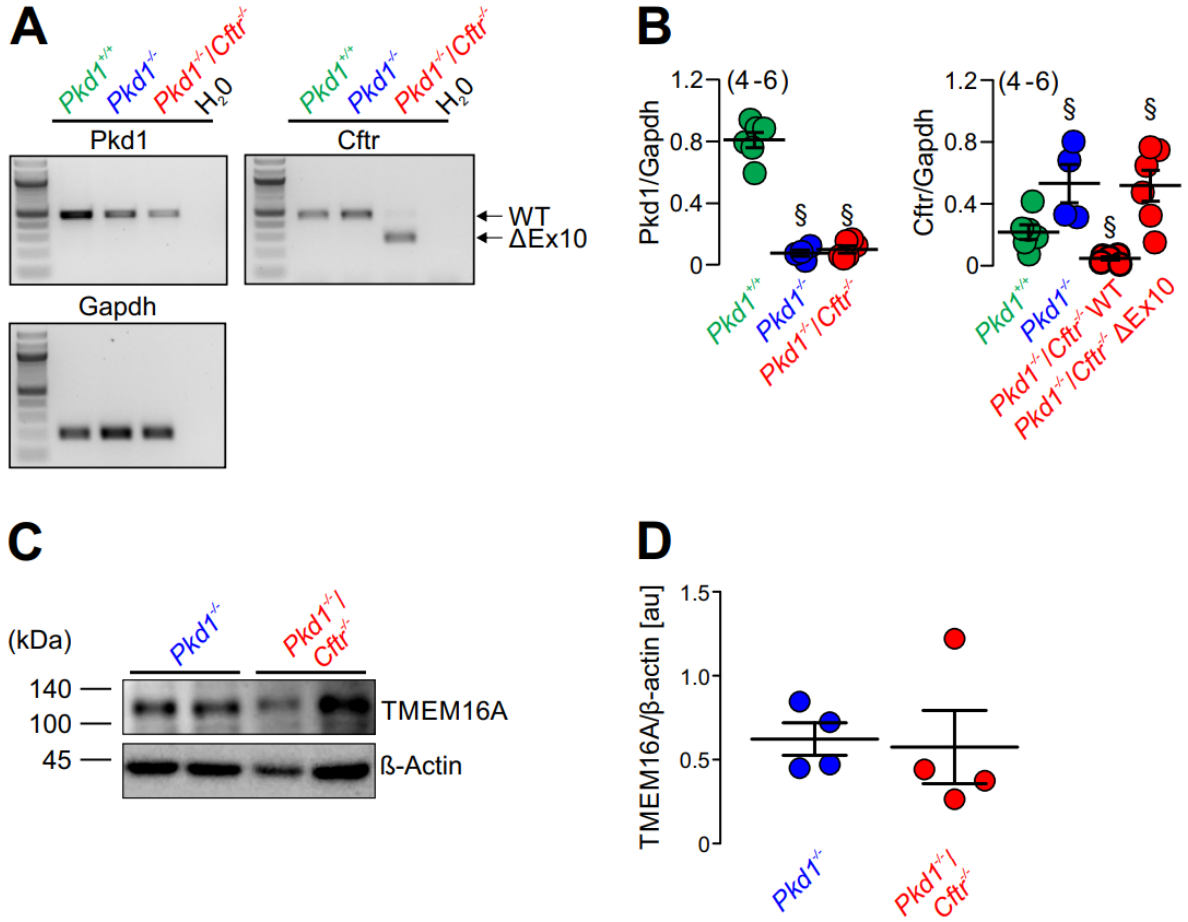

Supplemental figure 3.2 | *TMEM16a and CFTR expression in whole kidney lysates.*

(A) Expression and confirmation of knockout of Pkd1 and Cftr in Pkd1$^{+/+}$, Pkd1$^{-/-}$, and Pkd1$^{-/-}$/Cftr$^{-/-}$ tubular epithelial cells as indicated by RT-PCR. Deletion of Exon 10 (ΔEx10) of Cftr produces a shorter band (293 bp) compared to wildtype Cftr (WT, 476 bp). **(B)** Summary of mRNA expression of Pkd1 and Cftr relative to Glyceraldehyde 3-phosphate dehydrogenase (Gapdh). (number of mice). § significant difference when compared to Pkd1$^{+/+}$, One-Way ANOVA, Posthoc test: Bonferroni-Holm. **(C)** Western blotting from whole kidney lysates (each n = 4) from Pkd1$^{-/-}$, and Pkd1$^{-/-}$/Cftr$^{-/-}$ mice detecting equal expression of TMEM16A. **(D)** Quantification of expression of TMEM16A based on densitometric analysis with TMEM16A normalized to β-actin.

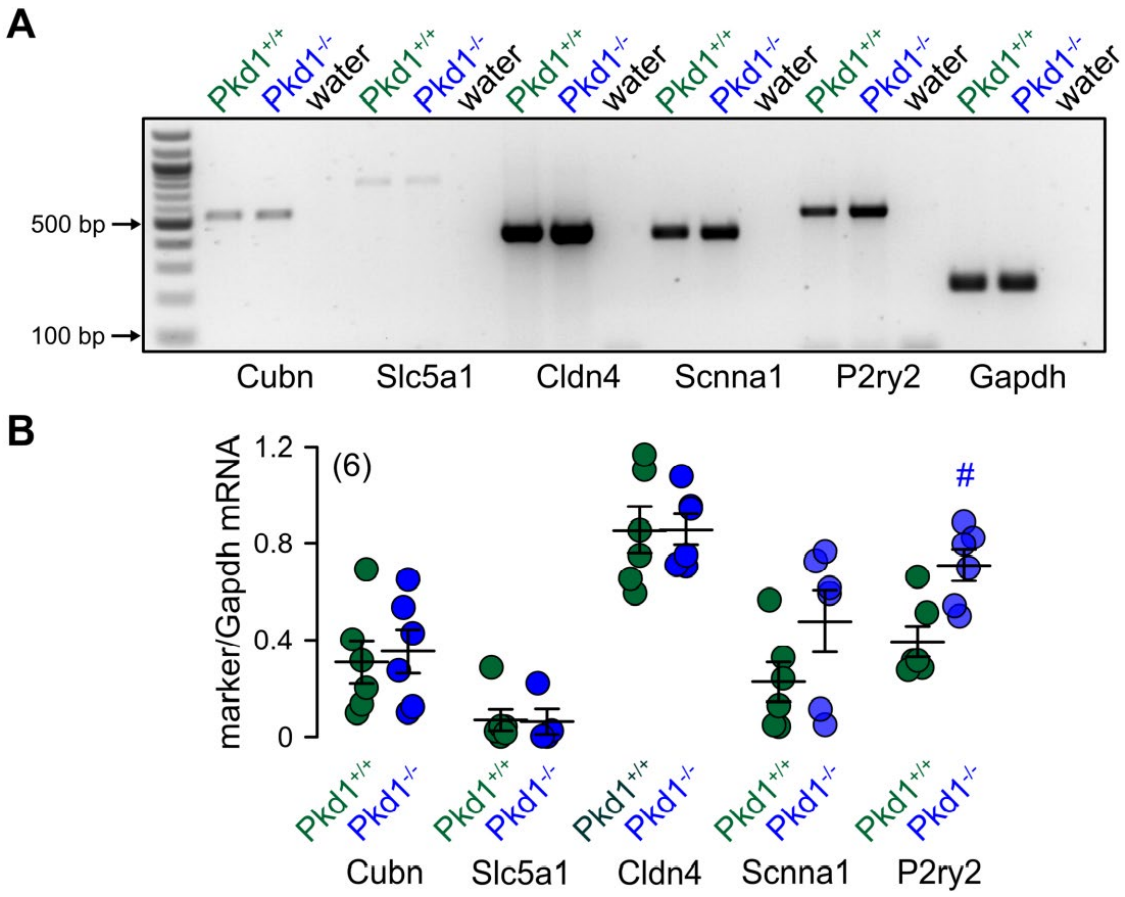

Supplemental figure 3.3 | *Characterization of primary cells isolated from mouse kidneys.*
Isolated cells (each from n=6 kidneys) were tested for the proximal tubular epithelial markers cubilin (Cubn) and sodium glucose cotransporter 1 as well as the distal markers claudin 4 (Cldn4) and epithelial sodium channel (αENAC) and the purinergic receptor P2y2r (P2ry2) by RT-PCR. **(A)** Representative blot of RT-PCR products. **(B)** Summary of mRNA expression of all markers relative to Glyceraldehyde 3-phosphate dehydrogenase (Gapdh). # significant compared to Pkd1$^{+/+}$ P2ry2.

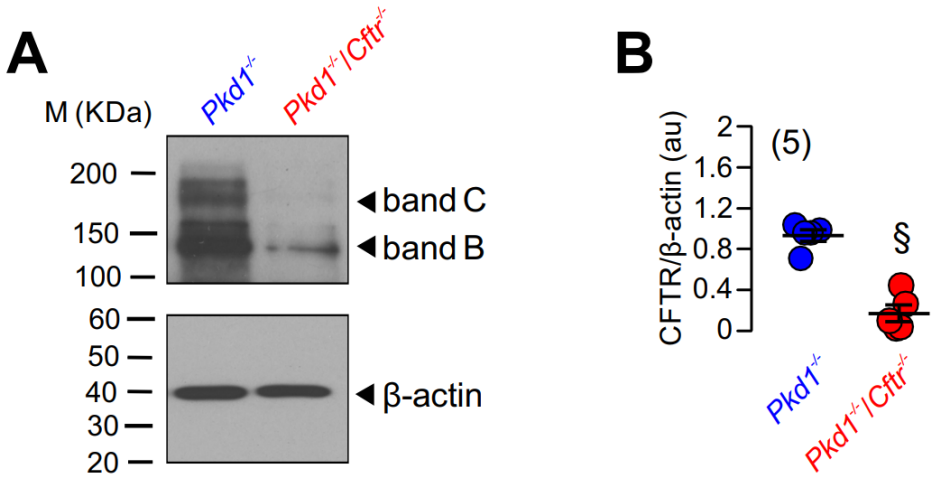

Supplemental figure 3.4 | *CFTR expression in primary isolated tubular epithelial cells.*
(A) Protein expression and tubular epithelial-specific knockout of Cftr in isolated tubular epithelial cells from Pkd1$^{-/-}$, and Pkd1$^{-/-}$/Cftr$^{-/-}$ mice was analysed by Western blotting. The core glycosylated immature

form of CFTR is designated as "band B". The complex glycosylated form of CFTR, representing transit through the Golgi, is termed "band C". **(B)** Summary of CFTR protein expression (band C) relative to β-actin.

Supplemental Table 3.1 | *Genotyping primer sequences*

Primer	**Gene**	**Sequence 5‘- 3‘**
mPKD1 loxPF	Pkd1	ACCCTTCCCTGAGCCTCCAC
mPKD1 loxPR	Pkd1	CCACAGGGGAAGCCATCATA
F427 Va	Ksp	CATTCTCTCCCACTGAATGGA
F427 Vb	Ksp	ACAGAGTGGGGTTTGTGTCTG
inv	Ksp	AACTGTCCCCTTGTCATACCC
CFTR_FP	Cftr E 10	CCACAGGCATAATCATGGAA
CFTR_RP	Cftr E 10	TGTGACTCCACCTTCTCCAA

Supplemental Table 3.2 | *RT-PCR Primer*

Gene	**Sequence 5‘- 3‘**	**Size (bp)**
Pkd1 NM_013630.2	for: CTTCTACTTTGCCCATGAGG rev: CTTCTACTTGCACCTCTGTC	473
Cftr NM_021050.2	for: GAATCCCCAGCTTATCCACG rev: CTTCACCATCATCTTCCCTAG	544
Tmem16a NM_178642.6	for: GTGACAAGACCTGCAGCTAC rev: GCTGCAGCTGTGGAGATTC	406
Cubn (Cubilin) NM_001081084.2	for: GCCATCCAGATGCAACCT rev: CATGAATCTGAAGGTACTCCC	536
Slc5a1 (Sglt1) NM_019810.4	for: GACAGTAGCACCTTGAGCC rev: CTTCCTTGGCGGTAAAATTTC	757
Cldn4 (Claudin 4) NM_009903.2	for: GAATCTCCTTGGCAGTCCTG rev: CATAGGGTTGTAGAAGTCGCG	425
Scnna1 (aEnaC) NM_011324.2	for: CCTTGACCTAGACCTTGACG rev: CGAATTGAGGTTGATGTTGAG	409
P2ry2 ($P2Y_2$) NM_008773.4	for: GGAACCCTGGAATAGCACC rev: CTGGTGGTGACGAAGTAGAG	510
Gapdh NM_001289726	for: GTATTGGGCGCCTGGTCAC rev: CTCCTGGAAGATGGTGATGG	200

CHAPTER 4 | GENDER-DEPENDENT PHENOTYPE IN POLYCYSTIC KIDNEY DISEASE IS DETERMINED BY DIFFERENTIAL INTRACELLULAR Ca^{2+} SIGNALS

Abstract

Autosomal dominant polycystic kidney disease (ADPKD) is caused by loss of function of PKD1 (polycystin 1) or PKD2 (polycystin 2). The Ca^{2+}-activated Cl^- channel TMEM16A has a central role in ADPKD. Expression and function of TMEM16A is upregulated in ADPKD which causes enhanced intracellular Ca^{2+} signaling, cell proliferation, and ion secretion. We analyzed kidneys from Pkd1 knockout mice and found a more pronounced phenotype in males compared to females, despite similar levels of expression for renal tubular TMEM16A. Cell proliferation, which is known to be enhanced with loss of $Pkd1^{-/-}$, was larger in male when compared to female $Pkd1^{-/-}$ cells. This was paralleled by higher basal intracellular Ca^{2+} concentrations in primary renal epithelial cells isolated from $Pkd1^{-/-}$ males. The results suggest enhanced intracellular Ca^{2+} levels contributing to augmented cell proliferation and cyst development in male kidneys. Enhanced resting Ca^{2+} also caused larger basal chloride currents in male primary cells, as detected in patch clamp recordings. Incubation of mouse primary cells, mCCDcl1 collecting duct cells or M1 collecting duct cells with dihydrotestosterone (DHT) enhanced basal Ca^{2+} levels and increased basal and ATP-stimulated TMEM16A chloride currents. Taken together, the more severe cystic phenotype in males is likely to be caused by enhanced cell proliferation, possibly due to enhanced basal and ATP-induced intracellular Ca^{2+} levels, leading to enhanced TMEM16A currents. Augmented Ca^{2+} signaling is possibly due to enhanced expression of Ca^{2+} transporting/regulating proteins.

Keywords: TMEM16A; ADPKD; polycystic kidneys; androgen; estrogen; CFTR

Published in: Talbi, K., Cabrita, I., Schreiber, R., & Kunzelmann, K. (2021). Gender-Dependent Phenotype in Polycystic Kidney Disease Is Determined by Differential Intracellular Ca^{2+} Signals. *International journal of molecular sciences*, *22*(11), 6019.

Own experimental contribution: Animal treatment, kidney perfusion, paraffin-embedding**,** histological analysis, renal medullary primary cells isolation, immunohistochemistry, whole cell patch clamp, intracellular Ca^{2+} measurements.
Own written contribution: Original draft preparation.
Other contributions: Designed experiments and analysed data.

Introduction

Male gender is a risk factor for progression of autosomal-dominant polycystic kidney disease (ADPKD) [2,5]. Affected men demonstrate faster loss of renal function and earlier onset of end stage renal disease, when compared to women [4]. Orchiectomy led to reduced renal size and cyst volume density, indicating attenuation of renal disease. In contrast, testosterone substitution was shown to antagonize the protective effect of gonadal ablation [14]. Also, in females, testosterone increased kidney size and cyst growth, clearly identifying androgens as a progression factor. On the other hand, estrogens have been proposed as protective hormones [199]. These results have been confirmed in additional experiments with rats [13,200]. Thus both, androgens and estrogens have an impact on cyst growth and disease progression in ADPKD.

Evidence has been provided for a crucial role of two chloride ion channels in the pathology of ADPKD, namely protein kinase A-regulated cystic fibrosis transmembrane conductance regulator (CFTR) and the Ca^{2+}-activated Cl^- channel transmembrane 16A (TMEM16A). Support for a pro-secretory role of CFTR in ADPKD came from a number of *in vitro* studies [68,75,167,201], *ex vivo* experiments in embryonic renal cysts in metanephric organ culture [77,202], and observations *in vivo* in animals and humans [77,79,203]. In contrast, another *in vivo* study could not confirm a protective effect of missing CFTR-function in cystic fibrosis for ADPKD [80].

Subsequent work identified a contribution of purinergic Ca^{2+} signaling to ADPKD [83,152,178]. In a series of studies *in vitro*, in metanephric renal organ cultures, and in mice *in vivo*, we demonstrated the essential contribution of TMEM16A to renal cyst formation in ADPKD [67,86,137,204,205]. We showed that knockout of Tmem16a or inhibition of TMEM16A *in vivo* by the FDA-approved drugs such as niclosamide, benzbromarone, and the TMEM16A-specific inhibitor Ani9 largely reduced cyst enlargement and abnormal cyst cell proliferation. Based on these results, we proposed a novel therapeutic concept for the treatment of ADPKD, based on inhibition of TMEM16A.

In the present study we asked whether enhanced expression or function of TMEM16A, and/or hormonal regulation may account for the more severe phenotype in male ADPKD. Typically, loss of PKD1 leads to a more severe phenotype than loss of PKD2 and accounts for about 85% of all ADPKD. We therefore examined *Pkd1-/-* animals in the present study. While loss of PKD1 does not affect expression of PKD2, loss of either PKD1 or PKD2 leads to similar changes in intracellular Ca^{2+} signalling [86,206].

In a previous study, androgen-response elements were found in the TMEM16A promoter region, and were shown to be relevant for testosterone-dependent induction of TMEM16A [207]. Moreover, TMEM16A expression was found to be enhanced in male when compared to female sympathetic ganglia [208], but lower levels were detected in male than in female urethral smooth

muscle [209]. Apart from the differences in TMEM16A-expression, CFTR might be expressed at lower levels in female ADPKD individuals, which could contribute to reduced renal cyst growth in females. In fact, a so-called cystic fibrosis (CF) gender gap describes the higher mortality in females with CF, due to lower expression of CFTR [210]. Lower CFTR-expression may be caused by estrogen-dependent regulation of CFTR [211,212].

In ADPKD, cysts occur in different renal tubular segments, yet it is assumed that most cysts are derived from the collecting duct [138]. In the present study we analysed primary epithelial cells isolated from renal medulla and mouse mCCDcl1 collecting duct cells. We compared properties of primary cells isolated from male and female mice, and examined whether gender differences can be reproduced in the mCCDcl1 cell line by treatment with male (dihydrotestosterone) and female (estrogen) hormones. We detected enhanced renal cyst growth and cell proliferation in male mice lacking expression of the polycystic kidney disease gene Pkd1 (polcycystin 1), when compared to female Pkd1-/- mice. The data suggest enhanced proliferation, increased basal Ca^{2+} levels, and larger secretory chloride currents in cells derived from male Pkd1-/- kidneys, which is likely to contribute to enhanced progression in male ADPKD patients.

Results

Male Mice Lacking Expression of Pkd1 Show a Larger Number of Renal Cysts, but Similar Levels of Expression of TMEM16A.

The KspCreERT2;Pkd1lox;lox system was used to obtain a tamoxifen inducible tubule-specific knockout of Pkd1, as described previously [67,213]. Knockdown of Pkd1 in male and female mice was validated by RT-PCR (Fig. 1A,B). 10 weeks old Pkd1-/- mice demonstrated multiple renal cysts, which were more pronounced in males when compared to females (Fig. 1C,D).

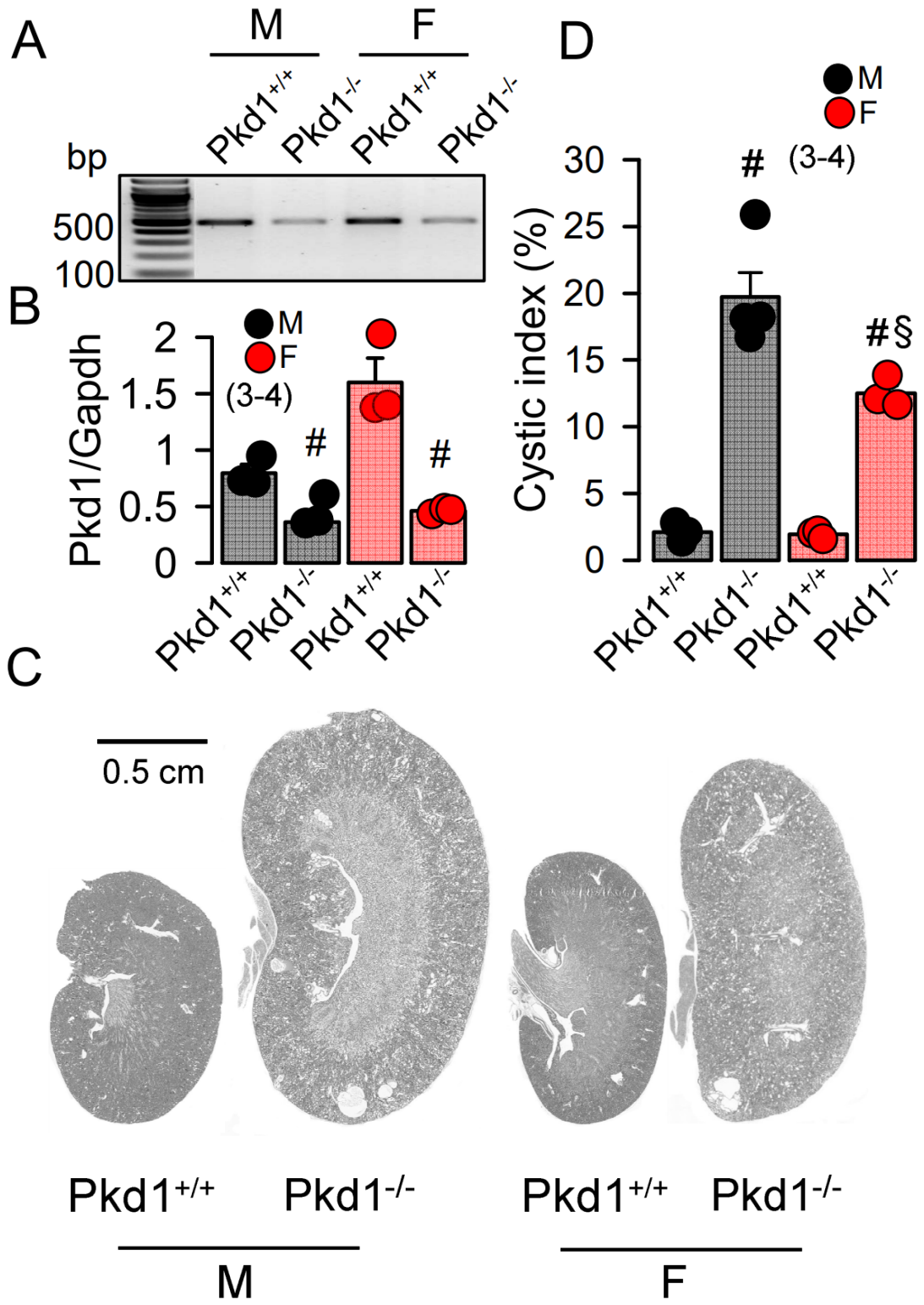

Figure 3.1 | ***Renal cysts in male and female PKD1-knockout mice.***

(**A,B**) RT-PCR of Pkd1 in renal primary epithelial cells from male (M) and female (F) $Pkd1^{+/+}$ and $Pkd1^{-/-}$ mice, and semiquantitative analysis of expression. (**C**) HE staining of whole kidneys and analysis of renal cysts by stitching microscopy. Male $Pkd1^{-/-}$ kidneys had larger sizes when compared to kidneys from female $Pkd1^{-/-}$ mice. (**D**) Cystic index in male and female $Pkd1^{+/+}$ and Pkd1-/- kidneys. Mean ± SEM (number of animals in each series). #Significant difference when compared to $Pkd1^{+/+}$ ($p < 0.05$; unpaired t-test). §significant difference when compared to male ($p < 0.05$; ANOVA with Tukey's post-hoc test).

In our previous study we reported a crucial role of the Ca^{2+} activated Cl^- channel TMEM16A for development of polycystic kidneys in Pkd1-/- mice and in additional *in vitro* models for ADPKD [67,86,137]. We therefore expected to find higher levels of TMEM16A-expression in kidneys from male Pkd1-/- mice. However, both Western blotting of TMEM16A from renal lysates, as well as immunohistochemistry suggested similar levels of TMEM16A-expression in kidneys from male and female Pkd1-/- mice (Fig. 2). Similarly, mRNA-expression for the epithelial Cl^- channel cystic fibrosis transmembrane conductance regulator (CFTR) was not different between males and females (Fig. S1).

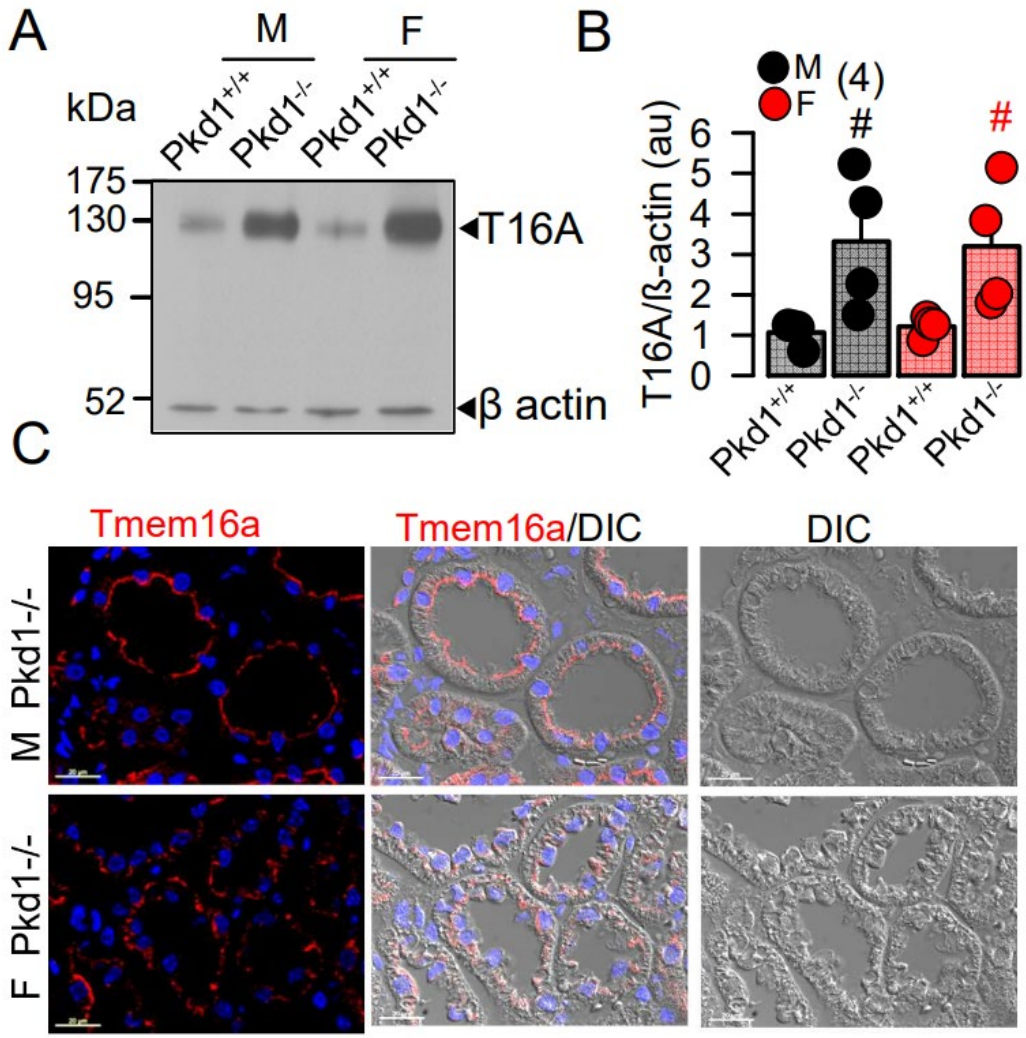

Figure 4.2 | *Expression of TMEM16A in male and female PKD1$^{-/-}$ mice.*

(**A,B**) Western blotting of TMEM16A-expression in primary renal epithelial cells from kidneys of male and female Pkd1$^{+/+}$ and Pkd1$^{-/-}$ mice. (**C**) Immunocytochemistry of Tmem16a in kidneys from male and female Pkd1$^{-/-}$ mice. Bar = 20 µm. Representative images from three mice each. Mean ± SEM (number of animals in each series). #Significant difference when compared to Pkd1$^{+/+}$ ($p < 0.05$; unpaired t-test).

Cell Proliferation and Basal Ca^{2+} Levels Are More Enhanced in Renal Epithelial Cells from Pkd1$^{-/-}$ Males than Pkd1$^{-/-}$ Females.

Cell proliferation is enhanced in kidneys from Pkd1-/- mice [67]. We compared cell proliferation in males and females using ki-67 staining. The results show that cell proliferation is enhanced

in kidneys from both male and female Pkd1-/- mice, however, proliferation was more enhanced in males (Fig. 3A,B).

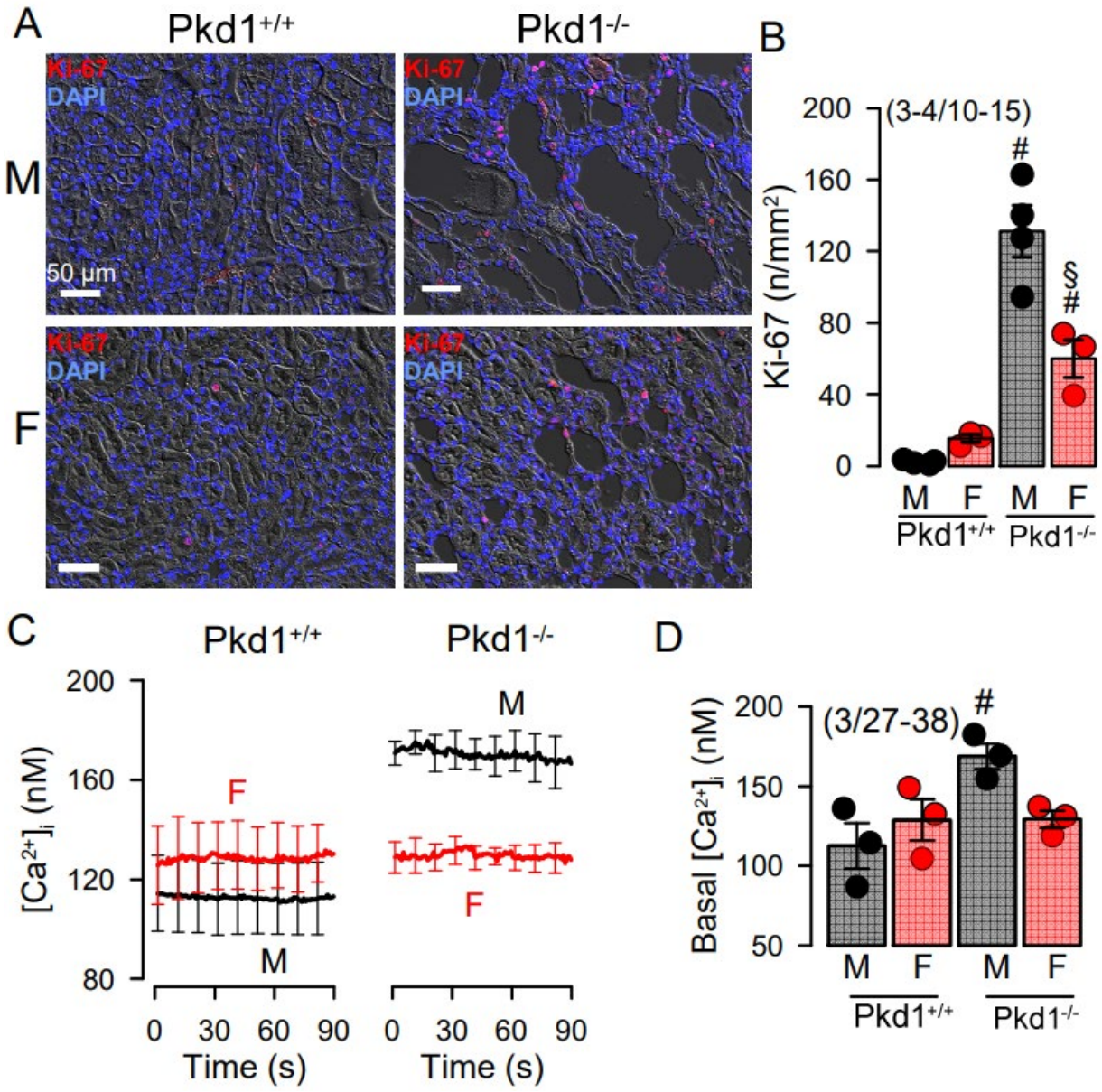

Figure 4.3 | ***Cell proliferation and intracellular Ca^{2+} concentrations in renal epithelial cells from Pkd1$^{+/+}$ and Pkd1$^{-/-}$ mice.***

(A) Analysis of tubular epithelial cell proliferation in kidney sections from male and female Pkd1$^{+/+}$ and Pkd1$^{-/-}$ mice as indicates by Ki-67 staining. Bars = 50 µm. (**B**) Summary of Ki-67 positive cells/mm^2 tissue area in kidneys from male and female Pkd1$^{+/+}$ and Pkd1$^{-/-}$ mice. Bars = 50 µm. (**C,D**) Intracellular basal Ca^{2+} concentrations ($[Ca^{2+}]_i$) as assessed by Fura2 indicates higher basal $[Ca^{2+}]_i$ in male Pkd1$^{-/-}$ mice. Mean ± SEM (number of animals/number of experiments in each series). #Significant difference when compared to Pkd1$^{+/+}$ ($p < 0.05$; unpaired t-test). §Significant difference when compared to male ($p < 0.05$; ANOVA and Tukey's post-hoc test).

Cellular Ca^{2+} levels are intimately related with cell proliferation, and have been shown to be

augmented in renal epithelial cells from mice lacking expression of Pkd1, which leads to enhanced expression of TMEM16A [67,86,206]. We therefore compared basal Ca^{2+} levels in primary renal epithelial cells from male and female mice. Remarkably, knockout of Pkd1 caused higher basal Ca^{2+} levels in renal epithelial cells from males, but not in cells from female kidneys (Fig. 3C,D). These results suggest a contribution of enhanced intracellular Ca^{2+} levels to augmented cell proliferation and cyst development in male kidneys.

We further compared whole cell currents measured in primary renal epithelial cells isolated from male and female kidneys. Primary cells were isolated from male and female Pkd1+/+ and Pkd1-/- mice. As reported previously, in cells isolated from male or female Pkd1+/+ animals, we found little activation of TMEM16A currents by increase of intracellular Ca^{2+}, using the purinergic ligand ATP (Fig. 4A,B, left panels). In contrast, cells isolated from Pkd1-/- animals showed large ATP-activated whole cell currents. We noticed that the basal current in male Pkd1-/- cells was significantly larger than that in measured in female Pkd1-/- cells (Fig. 4A,B, right panels). This may be explained by the fact that male Pkd1-/- cells showed a higher basal intracellular Ca^{2+} concentration (Fig. 3C,D). We also examined whole cell currents activated by IBMX and forskolin (IF), which both increase intracellular cAMP. No activation of whole cell currents was observed in Pkd1+/+ cells, while a small but significant current was activated in male Pkd1-/- cells (Fig. 4C,D). Patch clamp ion current data were supported by additional iodide quenching data, which also indicated a larger halide permeability in male when compared to female Pkd1-/- cells (Fig. S2). Taken together, higher basal Ca^{2+} concentrations, enhanced proliferation and larger basal Cl^- currents may explain the more pronounced cystic phenotype in male Pkd1-/- kidneys.

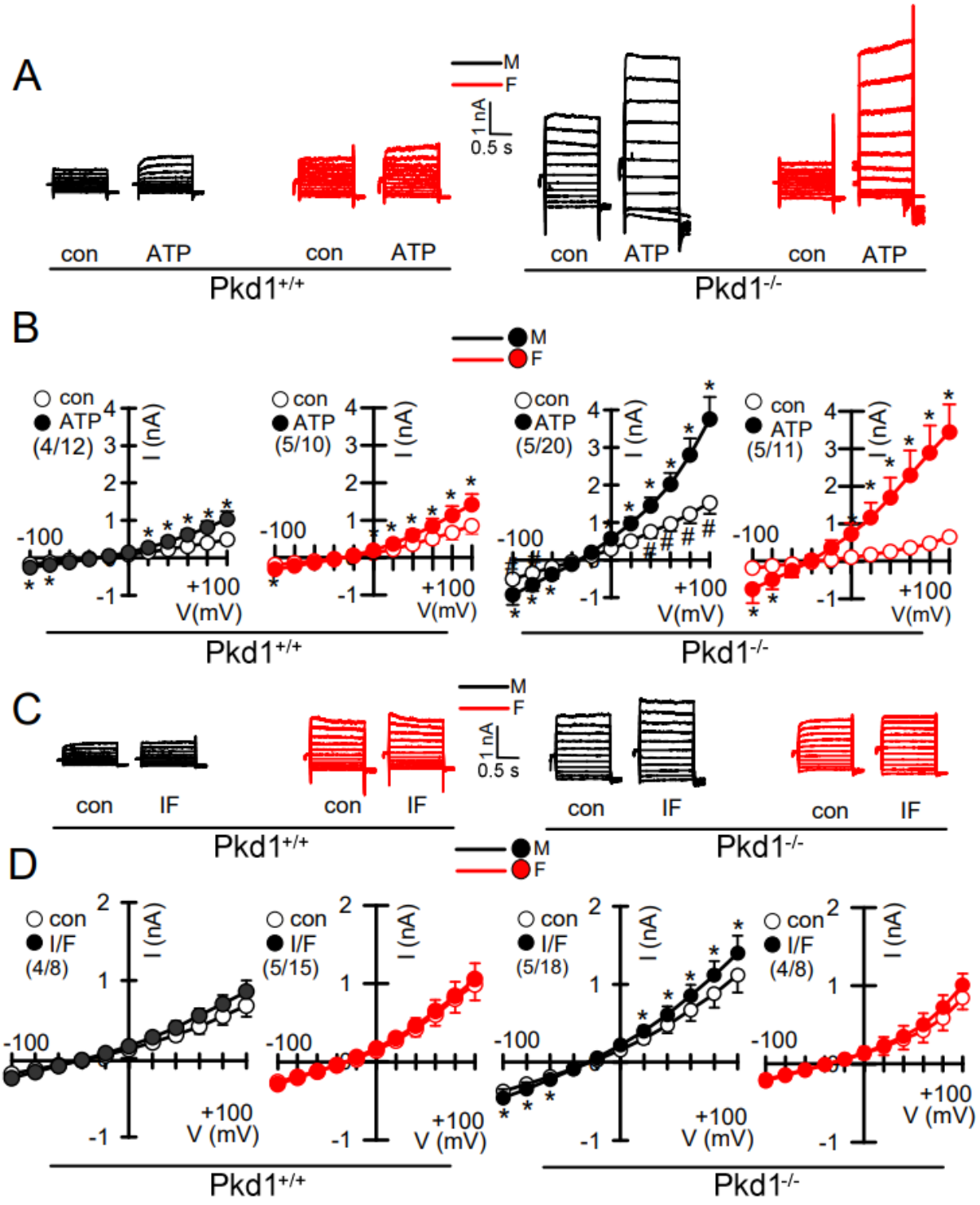

Figure 4.4 | *Whole cell patch clamp experiments in primary renal epithelial cells from male and female Pkd1$^{+/+}$ and Pkd1$^{-/-}$ mice.*

(A) Original whole cell overlay currents of basal and ATP (50 µM) - activated currents in male and female Pkd1$^{+/+}$ and Pkd1$^{-/-}$ mice. (**B**) Summary i/v curves of basal and ATP-activated currents indicating larger ATP-activated currents in Pkd1$^{-/-}$ mice and larger basal currents in male Pkd1$^{-/-}$ mice. **(C)** Original overlay currents of basal and IF (100 µM IBMX and 2 µM forskolin)-activated currents in male and female Pkd1$^{+/+}$ and Pkd1$^{-/-}$ mice. **(D)** Summary i/v curves of basal and IF-activated currents indicating small but significant IF-activated currents in male Pkd1$^{-/-}$ mice. Mean ± SEM (number of animals/number of

experiments in each series). *Significant activation by ATP and IF, respectively ($p < 0.05$; paired t-test). #Significant difference compared to other basal currents ($p < 0.05$; ANOVA and Tukey's post-hoc test).

Testosterone augments ATP-induced whole cell currents in female Pkd1+/+ cells.

Androgens have been implicated in the severity of the disease phenotype in ADPKD [214]. We therefore examined the impact of dihydrotestosterone (DHT) on ion currents in primary renal epithelial cells, isolated from female Pkd+/+ mice. Expression of androgen receptors in primary renal epithelial cells was determined by RT-PCR (Fig. 5A,B). Also different types of estrogen receptors were found to be expressed in these cell (Fig. 5C). As expected, ATP-activated whole cell currents were moderate in control cells, but were significantly enhanced in cells treated with DHT. In contrast, in cells treated with the inhibitor of androgen receptors, cyproterone acetate (CA), no whole cell currents could be activated by ATP (Fig. 5D,E).

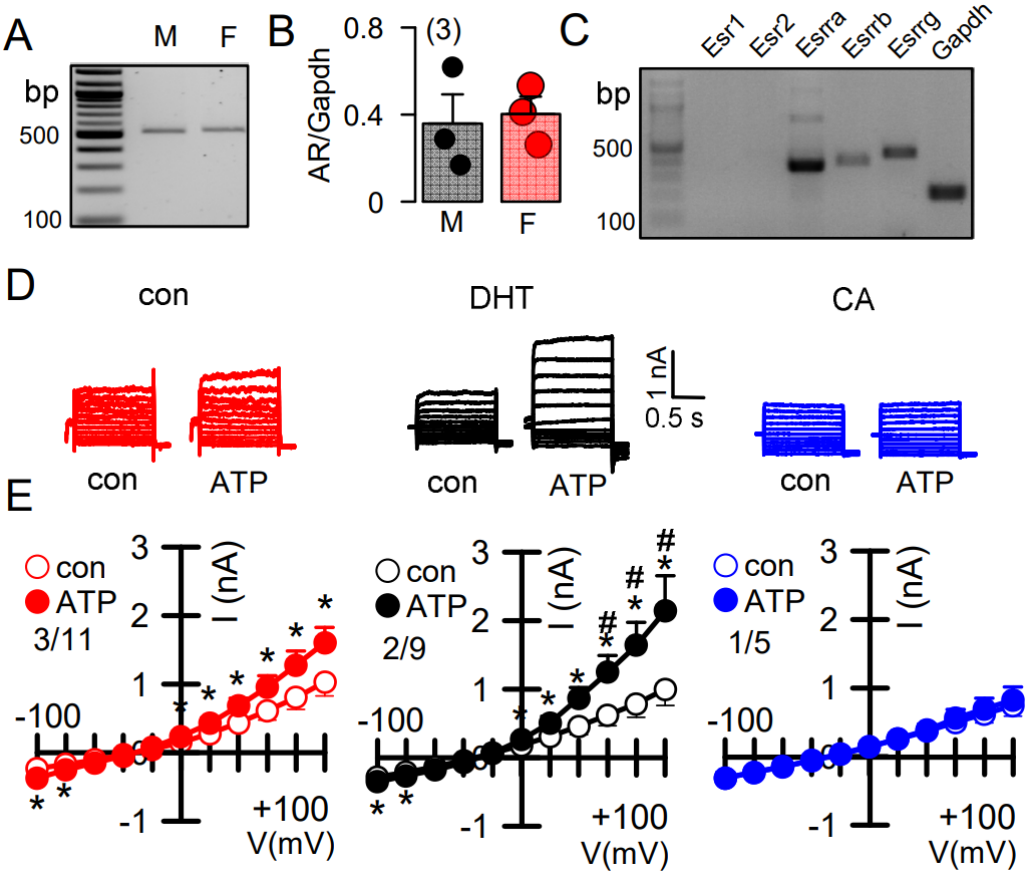

Figure 4.5 | ***Effect of dihydrotestosterone on whole cell currents in primary renal epithelial cells from female Pkd1+/+ mice.***

(**A,B**) RT-PCR analysis of expression of the androgen receptor (AR) in primary renal epithelial cells from male and female kidneys.(**C**) Expression of estrogen receptors in primary renal epithelial cells from female Pkd1+/+ mice. (**D,E**) Whole cell current overlays and corresponding I/V-curves from primary renal epithelial cells of female Pkd1+/+ mice. ATP (50 µM) -activated currents were augmented in cells-incubated ON with dihydrotestosterone (DHT; 10 µM, 24 hrs), but were absent in cyproterone acetate (CA, 10 µM, 24 hrs) incubated cells. Mean ± SEM (number of animals/number of experiments in each

series). *Significant activation by ATP ($p < 0.05$; paired t-test). #Significant difference when compared to con (no DHT) ($p < 0.05$; ANOVA and Tukey's post-hoc test).

DHT-dependent regulation of Ca^{2+} activated Cl^- currents was further examined in mCCDcl1 mouse renal cortical collecting duct cells [215]. These cells express TMEM16A, CFTR and receptors for testosterone and estrogen (Fig. 6A,B). However, the main estrogene receptors Esr1 and Esr2 are not expressed in renal epithelial cells, suggesting that estrogen-dependent regulation of protein expression is not dominating in the kidney.

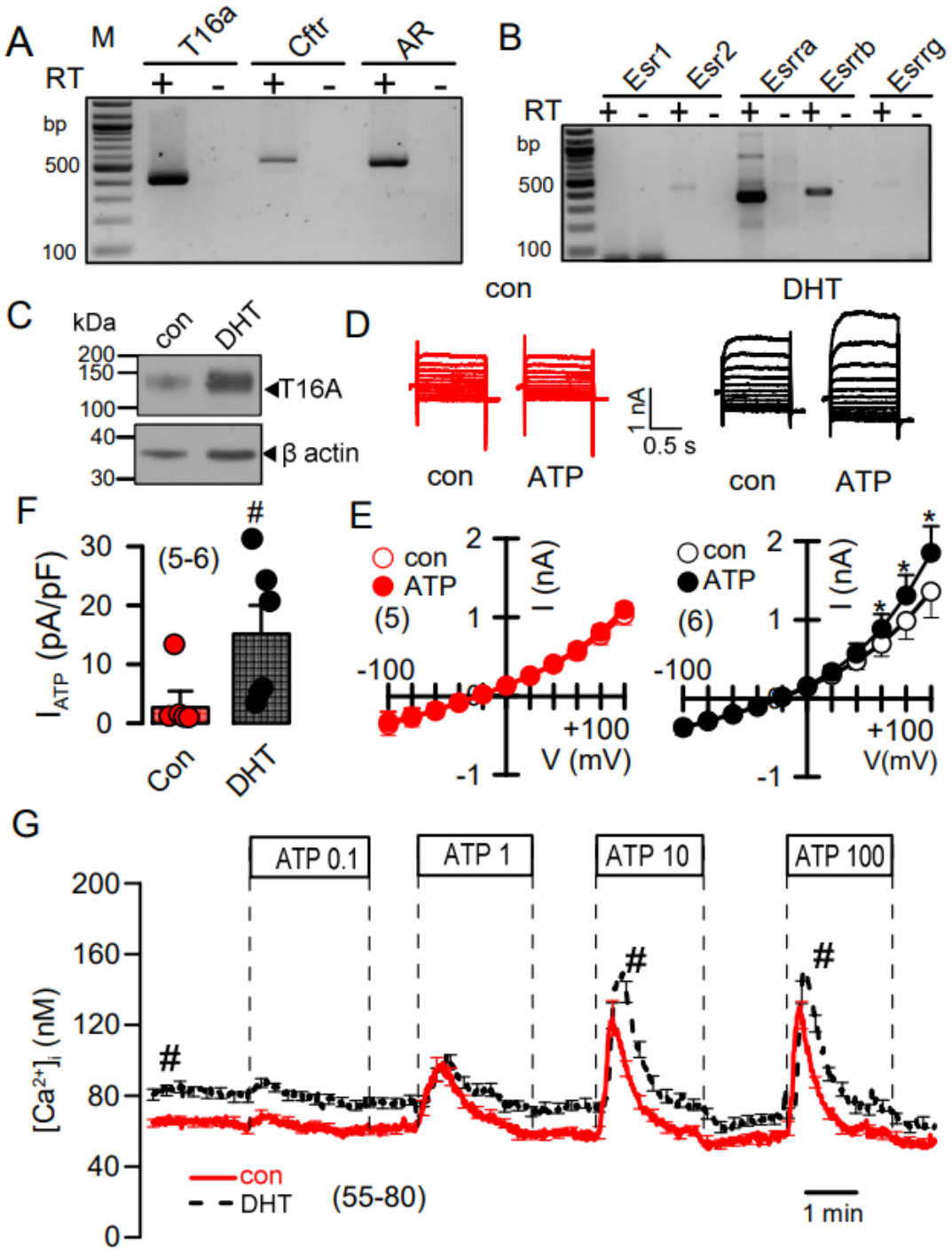

Figure 4.6 | ***Effect of dihydrotestosterone on whole cell currents and intracellular Ca^{2+} concentrations in mouse mCCDcl1 cortical collecting duct cells.***

(A,B) RT-PCR analysis of expression of Tmem16a, Cftr, androgen receptors **(A)**, and estrogen receptors **(B)** in $Pkd1^{+/+}$ mCCDcl1 mouse collecting duct cells. **(C)** Western blot from mCCDcl1 cells, indicating upregulation of Tmem16a-expression by DHT. **D–E)** Whole cell current overlays **(D)**, corresponding I/V-curves **(E)**, and summary of ATP (0.1 µM) -activated whole cell currents **(F)** from mCCDcl1 cells, indicating larger basal and ATP-activated currents in DHT (10 µM; 24 hrs) treated cells. Current densities (pA/pF) were assessed at the clamp voltage of +100 mV. **(G)** Basal and ATP (0.1–100 µM)–induced increase in intracellular Ca^{2+} concentration in control (con) and DHT-incubated mCCDcl1 cells. Mean ± SEM (number of experiments). *Significant activation by ATP ($p < 0.05$; paired t-test). #Significant difference compared to con ($p < 0.05$; unpaired t-test).

Treatment with DHT enhanced expression of TMEM16A in mCCDcl1 cells (Fig. 6C). In these cells, ATP concentrations as low as 0.1 µM stimulated a whole cell current that was not observed in the absence of DHT (Fig. 6D-F). Upregulation of ATP-activated whole cell currents by DHT was also observed in mouse M1 collecting duct cells, which also showed a slight but detectable increase in cAMP-activated currents upon DHT treatment (Fig. S3). No whole Cl^- currents could be activated in cells incubated with estrogen.

Testosterone enhances intracellular Ca^{2+} signals.

DHT increased expression of TMEM16A and enhanced ATP-activated whole cell currents, which may be due to enhanced intracellular Ca^{2+} signaling. We measured intracellular Ca^{2+} concentrations in control mCCDcl1 cells, and in cells treated with DHT. Cells were stimulated by different concentrations of ATP, which caused a concentration-dependent increase in intracellular the Ca^{2+} concentration (Fig. 6G). Notably, DHT did not further enhance transient Ca^{2+} increase induced by ATP, but shifted the basal Ca^{2+} concentration to higher values. This suggests a Ca^{2+} leakage out of the endoplasmic reticulum (ER) Ca^{2+} store, or enhanced Ca^{2+} influx through plasma membrane Ca^{2+} channels (Fig. 6G).

We applied a Ca^{2+} store release protocol to empty the ER Ca^{2+} store by inhibiting the sarcoplasmic endoplasmic reticulum ATPase (SERCA), using cyclopiazonic acid (CPA). Remarkably, removal of extracellular Ca^{2+} lead to a more pronounced decrease in basal cytosolic Ca^{2+} in DHT, but not in EST-treated cells (Fig. 7A, left and middle panel). Subsequent addition of CPA induced a more pronounced Ca^{2+} store release in DHT-treated cells, and a largely augmented Ca^{2+} influx upon re-addition of extracellular Ca^{2+} (Fig. 7A, left and right panel). Thus, Ca^{2+} store release and store operated Ca^{2+} influx were augmented in DHT-treated cells. We analyzed the expression of a number of Ca^{2+} transporting proteins such as inositol trisphosphate receptors (IP3R1-3), the Ca^{2+} influx channels Orai1, TRPC1, TRPV4, and the ER Ca^{2+} sensor stromal interaction molecule 1 (Stim1). Notably, expression of a number of Ca^{2+} channels and Stim1 were augmented by both DHT and EST incubated cells. As shown in Fig. 6C, DHT enhanced expression of TMEM16A, while EST had no significant effect on TMEM16A-expression (data not shown). By comparing Ca^{2+} signals obtained from male and female

primary renal epithelial cells, we also found higher basal Ca^{2+} levels in male cells, along with larger ATP-induced Ca^{2+} transients (Fig. S4). Taken together, the more severe cystic phenotype found in males is likely to be caused by enhanced cell proliferation possibly due to enhanced basal intracellular Ca^{2+} levels, which is probably due to enhanced expression of Ca^{2+} transporting/regulating proteins.

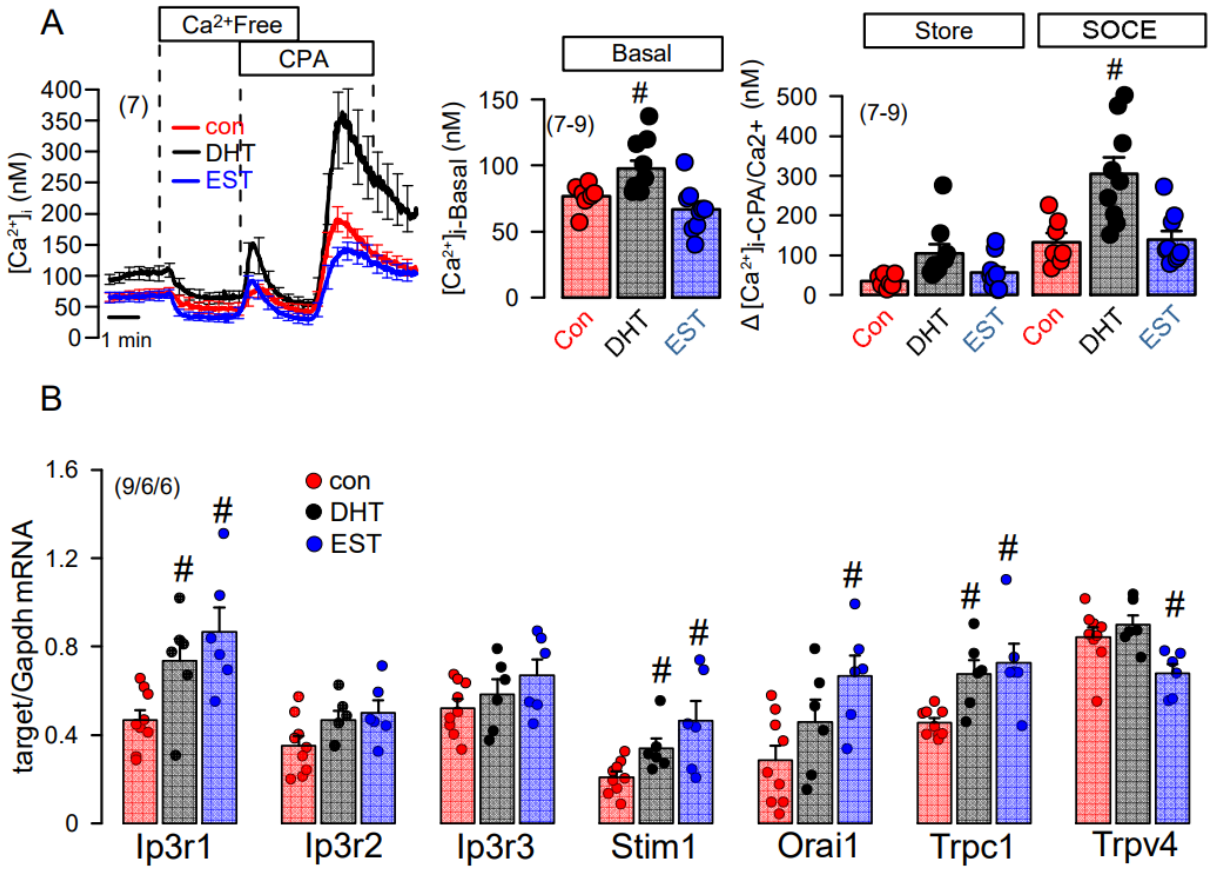

Figure 4.7 | ***Effect of dihydrotestosterone and estrogen on intracellular Ca^{2+} concentrations and expression of Ca^{2+}-regulating proteins in mouse mCCDcl1 cortical collecting duct cells.***

(A) Summary time course of the effects of extracellular Ca^{2+}-free buffer and cyclopiazonic acid (10 µM) on intracellular Ca^{2+} concentrations in control mCCDcl1 cells and mCCDcl1 cells treated with dihydrotestosterone (DHT; 10 µM, 24 hrs) and estrogen (EST, 10 µM; 24 hrs). Summary of basal intracellular Ca^{2+} concentration and changes in intracellular Ca^{2+} induced by CPA (Ca^{2+} store release through leakage channels; Store) and re-addition of Ca^{2+} to the extracellular buffer (store operated Ca^{2+} entry; SOCE). **(B)** RT-PCR analysis of the expression of Ca^{2+}-regulating proteins and effects of DHT and EST. Mean ± SEM (number of experiments in each series). #Significant increase when compared with con ($p < 0.05$; ANOVA).

Discussion

In the present study we analysed primary epithelial cells isolated from renal medulla and mouse mCCDcl1 collecting duct cells. We compared properties of primary cells isolated from male and female mice, and examined whether gender differences can be reproduced in the mCCDcl1 cell line by treatment with DHT and EST. We asked whether enhanced expression or function of TMEM16A, and/or hormonal regulation may account for the more severe ADPKD phenotype caused by knockout of Pkd1. As shown previously, loss of PKD1 or PKD2 lead to similar changes in intracellular Ca^{2+} signalling which could be reproduced in the present study [86,206]. The present data show a higher cystic index in kidneys from male Pkd1-/- mice. Although expression of the disease-associated Ca^{2+} activated Cl^- channel TMEM16A was not different between male and female Pkd1-/- kidneys, cell proliferation, basal cytosolic Ca^{2+} levels and basal Cl^- currents were larger in renal epithelial cells derived from males (Fig. 1-4).

Proliferation of renal tubular epithelial cells is enhanced in both male and female kidneys from Pkd1-/- knockout mice, however, the effect is more pronounced in male kidneys. Proliferation is predominantly due to upregulation of TMEM16A-expression as demonstrated in our recent study [67]. TMEM16A is well known to enhance proliferation in different types of cells including cancer cells. This is due to upregulation of Ca^{2+} (ATP-) activated chloride currents and upregulated ATP-induced Ca^{2+} store release [67]. Enhanced Ca^{2+} signalling is also demonstrated by augmented store release triggered by cyclopiazonic acid with consecutive increase in store-operated Ca^{2+} entry. These changes are observed in both primary renal epithelial cells from male and female Pkd1-/- mice, however, upregulation of these Ca^{2+} signals is more pronounced in epithelial cells from males (Fig. S5). Also, a small cAMP-regulated CFTR current was detected in cells from male Pkd1-/- kidneys, but was not found in cells from female kidneys. Expression levels for CFTR were not different between male and female kidneys as detected by semiquantitative RT-PCR or Western blotting.

Higher TMEM16A currents and small but detectable CFTR currents were also found in renal epithelial cells upon exposure to dihydrotestosterone, which also enhanced expression of TMEM16A. Importantly, Cha et al reported three androgen-response elements in the TMEM16A promoter region, which are relevant for the DHT-dependent induction of TMEM16A [207]. Comparable to our previous report showing inhibition of cell proliferation and renal cyst growth [67], Cha et al reported inhibition of prostate hyperplasia by siRNA-knockdown of TMEM16A [207]. In contrast, androgens potentiated renal cell proliferation and cyst enlargement through ERK1/2-dependent and ERK1/2-independent signaling in another study [214]. However, in our study we were unable to detect different levels for TMEM16A-expression in male and female kidneys (Fig. 2). A likely explanation might be that knockout of Pkd1 induced already a strong upregulation of TMEM16A-expression [67], thereby overrunning androgen-dependent regulation of expression. Notably, in cultured mCCDcl1 collecting duct cells, where Pkd1 is not

knocked out, androgen-dependent upregulation of TMEM16A is detected (Fig. 6).

Enhanced basal (Fig. 3,6,7) and ATP-activated (Fig. 6, S4) Ca^{2+} levels were clearly detectable in male primary renal epithelial cells and androgen treated mCCDcl1 cells. Androgens also caused increased intracellular Ca^{2+} levels in prostate and skeletal muscle cells [216,217]. A number of previous studies examined the effects of androgens on cytosolic Ca^{2+} signaling, and expression of proteins that regulate intracellular Ca^{2+} levels. Thus androgens upregulated the Ca^{2+} influx channel Orai1 in MCF-7 breast tumor cells [218], while in LNCaP cells, androgens were shown to increase cytosolic Ca^{2+} by enhancing Ca^{2+} influx through L-type channels [219], and via G-protein coupled receptors [220,221]. Moreover, expression of the Ca^{2+} sensor in the endoplasmic reticulum, stromal interaction molecule 1 (STIM1), was shown to be regulated by androgens [222]. Conversely, estradiol was shown to inhibit phosphorylation of STIM1 which attenuated SOCE [223].

We found lower expression of TRPV4 upon treatment with estradiol, which may suggest a role of TRPV4 in differential Ca^{2+} signaling in male vs. female renal epithelial cells. Enhanced expression of TRPV4 was also found in male hypertensive rats when compared to female animals [224]. However, given the number of Ca^{2+} transporting proteins that differ between cells derived from males and females, enhanced basal Ca^{2+} levels in males is likely due to a combination of differentially expressed Ca^{2+} transporting proteins. We believe that the differences in basal Ca^{2+} concentrations could be sufficient to explain different basal activity of TMEM16A in male and female cells. Activation of TMEM16A depends largely on the membrane voltage [225]. Activation of inward currents at hyperpolarized (physiological) voltages require higher $[Ca^{2+}]_i$ than outward currents and are in the range of 1 µM and higher. However, Ca^{2+} concentrations related to channel activity are typically obtained by Ca^{2+} sensing dyes, which measure global cytosolic Ca^{2+} concentrations, such as Fura-2. These global $[Ca^{2+}]_i$ do not reflect the true Ca^{2+} levels in the TMEM16A-containing subapical compartment. We now know that TMEM16A is a membrane tether that binds the receptor for inositol trisphosphate (IP3) and thereby enhances local Ca^{2+} levels in close proximity to TMEM16A [117]. Using membrane bound Ca^{2+} sensors, remarkably higher Ca^{2+} concentrations were found in TMEM16A-containing compartments underneath the cell membrane, causing more pronounced activation of TMEM16A [116]. Finally, differential expression of splice variants for TMEM16A could be an additional reason for the larger basal Cl^- currents detected in male renal epithelial cells. For example, Ferrera and collaborators reported differential Ca^{2+} sensitivity for the isoforms TMEM16A(a,b,c), and TMEM16A(a,c) [226]. Differential expression of TMEM16A isoforms should be therefore examined in subsequent studies.

The results of the present study may be summarized as follows: i) Renal cysts found in ADPKD caused by knockout of Pkd1, are associated with enhanced basal intracellular Ca^{2+} levels and enhanced agonist (ATP)- and CPA-induced Ca^{2+} store release and SOCE. ii) The more severe phenotype in males is related to larger store release and SOCE detected in cells

derived from males when compared to females (Fig. S5). iii) Stimulation of the androgen receptor by DHT in cells derived from primary female cells and in the mCCDcl1 cell line reproduces the findings obtained in primary male tissues. iv) Gender-dependent phenotype differences are not explained by different levels of expression of the ADPKD-relevant ion channel TMEM16A. v) Differential Ca^{2+} homeostasis in kidneys of male and female ADPKD patients is suggested. vi) Higher Ca^{2+} levels not only enhance TMEM16A- activity, but may also contribute to higher activity of CFTR [151]. vii) Additional work will be required to identify the molecular mechanisms underlying the gender-dependent differences of Ca^{2+} signalling in ADPKD.

Materials and Methods

RT-PCR. For semi-quantitative RT-PCR total RNA from primary medullary kidney epithelial cells were isolated using NucleoSpin RNA II columns (Macherey-Nagel, Düren, Germany). Total RNA (0.5 µg / 25 µl reaction) was reverse-transcribed using random primer (Promega, Mannheim, Germany) and M-MLV Reverse Transcriptase RNase H Minus (Promega, Mannheim, Germany). Each RT-PCR reaction contained sense (0.5 µM) and antisense primer (0.5 µM) (table 1), 0.5 µl cDNA and GoTaq Polymerase (Promega, Mannheim, Germany).

Table 3.1 | *Primers used for PCR-analysis.*

Gene Accession Number	Primer	Size (bp)
Tmem16a NM_001242349.2	s: 5′-GTGACAAGACCTGCAGCTAC as: 5′-GCTGCAGCTGTGGAGATTC	406
Cftr NM_021050.2	s: 5′-GAATCCCCAGCTTATCCACG as: 5′-CTTCACCATCATCTTCCCTAG	544
Pkd1 NM_013630.2	s: 5′-CTTCTACTTTGCCCATGAGG as: 5′-CTTCTACTTGCACCTCTGTC	473
AR NM_013476.4	..s: 5´-GAAATGGGACCTTGGATGGAG as: 5′- GGTTGGTTGTTGTCATGTCCG	518
Esr1 NM_007956.5	s: 5′-CTCAAGATGCCCATGGAGAG as: 5′-GTTTCCTTTCTCGTTACTGCTG	441
Esr2 NM_207707.1	s: 5′-GACCTACGCAAGACATGGAG as: 5′-CTTGGACTAGTAACAGGGCTG	436
Esrra NM_007953.2	s: 5′-CAGGGCAGTGGGAAGCTAG as: 5′-GCTACTGCCAGAGGTCCAG	362
Esrrb NM_011934.4	s: 5′-GTGGTATCATGGAGGACTCC as: 5′-GTCAATGGCTTTTTAGCAGGTG	388

Esrrg NM_011935.3	s: 5′-CAGCACCATCGTAGAGGATC as: 5′-CATGGCATAGATCTTCTCTGG	442
Gapdh NM_001289726	s: 5′-GTATTGGGCGCCTGGTCAC as: 5′-CTCCTGGAAGATGGTGATGG	200

After 2 min at 95 °C cDNA was amplified (targets 30 cycles, reference Gapdh 25 cycles) for 30 s at 95 °C, 30 s at 56 °C, and 1 min at 72 °C. PCR products were visualized by loading on Midori Green Xtra (Nippon Genetics Europe) containing agarose gels and analyzed using Image J 1.52r (NIH, Bethesda, Maryland, USA).

Cell culture. The mouse collecting duct cell line mCCDcl1 was kindly provided by Prof. Dr. Johannes Loffing (Institute of Anatomy, University of Zurich, Zurich, Switzerland) and were grown as described previously [215]. M1 mouse collecting duct cells were grown as outlined in an earlier publication [227].

Renal medullary primary cells isolation. Mice were sacrificed through Co2 inhalation and cervical dislocation and kidneys were kept in ice-cold DMEM/F12 medium (Thermo Fisher Scientific, Darmstadt, Germany). The renal capsule was removed under sterile conditions. The medulla was separated from the cortex and chopped into smaller pieces of tissue using a sharp razor blade (Heinz Herenz, Hamburg, Germany). Tissues were incubated in Hanks balanced salt solution/DMEM/F12 (Life Technologies/Gibco®, Karlsruhe, Germany) containing 1 mg/ml collagenase type 2 (Worthington, Lakewood, USA) for 20 min at 37 °C. The digested tissue was passed through a 100 µm cell strainer (Merck KGaA, Darmstadt, Germany), transferred to a 50 ml falcon tube and washed with ice-cold PBS. After centrifugation at 1880 rpm for 4 min/4 °C, cells were resuspended and centrifuged 3X at 2260 rpm for 4 min at 4 °C. After washing with ice-cold PBS, tubular preparations were cultured at 37 °C/5% CO_2 in DMEM/F12 supplemented with 1% FBS, 1% Pen/Strep, 1% L-Glutamine (200 mM), 1% ITS (100×), 50 nM hydrocortisone, 5 nM triiodothyronine, and 5 nM Epidermal Growth Factor (Sigma Taufkirchen, Germany). After washing with ice-cold PBS, tubular preparations were maintained at 37 °C/5% CO_2 in DMEM/F12 supplemented with 1% FBS, 1% Pen/Strep, 1% L-Glutamine (200 mM), 1% ITS (100×), 50 nM hydrocortisone, 5 nM triiodothyronine, and 5 nM Epidermal Growth Factor (Sigma Taufkirchen, Germany). After 24 h, primary cells grew out from isolated tubules.

Animals and treatments. Animal experiments were approved by the local institutional review board and all animal experiments complied with the with the United Kingdom Animals Act, 1986, and associated guidelines, EU Directive 2010/63/EU for animal experiments. Experiments were approved by the local Ethics Committee of the Government of Unterfranken/Wuerzburg (AZ: 55.2-2532-2-328). Mice with a floxed *PKD1* allele were generously provided by Prof. Dr. Dorien

J.M. Peters (Department of Human Genetics, Leiden University Medical Center, Leiden, The Netherlands) [23]. Animals were hosted on a 12:12 h light:dark cycle under constant temperature (24 ± 1 °C) in standard cages. They were fed a standard diet with free access to tap water. Generation of mice with a tamoxifen inducible, kidney epithelium-specific *Pkd1*-deletion was done as previously described [67]. Mice carrying loxP-flanked conditional alleles of *Pkd1* were crossed with KSP-Cre mice in a C57BL/6 background (KspCreER^{T2};*Pkd1*$^{lox;lox}$; abbreviated as *Pkd1*$^{-/-}$). Mice in the age of 8–10 weeks were used in the experiments.

Histologic analysis, Cystic index. Photographs from hematoxylin and eosin–stained kidney sections were taken at a magnification of ×23 and stitched to obtain single photograph of the whole transverse kidney sections using a Axiovert 200 microscope (Zeiss, Germany). The whole kidney cortex was defined as region of interest using ImageJ (version 1.48). Next, we used an algorithm (ImageJ software version 1.48) that separates normal tubule space from cystic area by defining diameters of noncystic tubules < 50 mm[138]. The whole cortex cyst area was divided by the whole cortex area and defined as the cystic index.

Immunohistochemistry. Five-micron thick transverse kidney sections were stained. Anti-TMEM16A (rabbit; 1:100; Abcam, Berlin, Germany) antibody was used as described previously [137]. As secondary antibodies, anti-rabbit IgG Alexa Fluor 546 (1:300; Thermo Fisher Scientific, Inc., Erlangen, Germany) was used. Immunofluorescence was detected using an Axiovert 200 microscope equipped with ApoTome and AxioVision (Zeiss, Germany).

Western blotting. Proteins were isolated from perfused whole kidneys and from mCCDcl1 cells using a sample buffer containing 25 mM Tris–HCl, 150 mM NaCl, 1% Nonidet P-40, 5% glycerol, 1 mM EDTA, and 1% protease inhibitor mixture (Roche, Mannheim, Germany). Equal amounts of protein were separated using 8,5% sodium dodecyl sulfate (SDS) polyacrylamide gel. Proteins were transferred to a polyvinylidene difluoride membrane (GE Healthcare Europe GmbH, Munich, Germany) using a semi-dry transfer unit (Bio-Rad). Membranes were incubated with primary anti-TMEM16A (rabbit 1:500; Alomone, Jerusalem, Israel) mouse antibody overnight at 4 °C. Proteins were visualized using horseradish peroxidase-conjugated secondary antibody and ECL detection. Beta-Actin was used as a loading control.

Ki-67 assay. Ki-67 staining was performed using a monoclonal anti-ki-67 antibody (rabbit; 1:100, Linaris, Dossenheim, Germany). Signals were amplified by the use of the Vectastain Elite ABC Kit (Vector Laboratories, Burlingame, CA) according to the manufacturer's instructions. Signals were analyzed with a Axiovert 200 microscope (Zeiss, Germany).

Patch Clamp. Patch-clamp experiments were performed in the fast whole-cell configuration.

Patch pipettes had an input resistance of 4–6 MΩ, when filled with a cytosolic-like" pipette filling solution [228] containing (mM) KCl 30, K-gluconate 95, NaH_2PO_4 1.2, Na_2HPO_4 4.8, EGTA 1, Ca-gluconate 0.758, $MgCl_2$ 1.034, D-glucose 5, ATP 3. pH was 7.2, the Ca^{2+} activity was 0.1 µM. The extracellular bath perfusion was a Ringer solution containing (mmol/l) NaCl 145; KH_2PO_4 0.4; K_2HPO_4 1.6; Glucose 5; $MgCl_2$ 1; Ca^{2+}-Gluconat 1.3. The access conductance was measured continuously and was 30–140 nS. Currents (voltage clamp) and voltages (current clamp) were recorded using a patch-clamp amplifier (EPC 9, List Medical Electronics, Darmstadt, Germany) and PULSE software (HEKA, Lambrecht, Germany) as well as Chart software (AD-Instruments, Spechbach, Germany). In intervals, membrane capacitance was measured using the EPC9 device. Data were stored continuously on a computer hard disc and were analyzed using PULSE software. In regular intervals, membrane voltages (V_c) were clamped in steps of 20 mV from −100 to +100 mV relative to resting potential. Current densities (pA/pF) were assessed at the clamp voltage of +100 mV.

Iodide quenching experiments. For YFP-quenching assays, primary renal cells were infected with lentiviral vectors to express halide-sensitive YFP_{I152L}, as previously described [229]. Primary renal cells were isolated and cultured and for each mouse 40 cells were measured. Quenching of the intracellular fluorescence generated by the iodide sensitive Enhanced Yellow Fluorescent Protein (EYFP-I152L) was used to measure anion conductance. YFP-I152L fluorescence was excited at 500 nm using a polychromatic illumination system for microscopic fluorescence measurement (Visitron Systems, Puchheim, Germany) and the emitted light measured at 535 ± 15 nm with a Coolsnap HQ CCD camera (Roper Scientific). Quenching of YFP-I152L fluorescence by I^- influx was induced by replacing 5 mM extracellular Cl^- with I^-. Cells were grown on coverslips and mounted in a thermostatically controlled imaging chamber maintained at 37 °C. Cells were continuously perfused at 8 ml/min with Ringer solution and exposed to I^- concentration of 5 mM by replacing same amount of NaCl with equimolar NaI. Background fluorescence was subtracted, while auto-fluorescence was negligible. Changes in fluorescence induced by I^- are expressed as initial rates of maximal fluorescence decrease ($\Delta F/\Delta t$). For quantitative analysis, cells with low or excessively high fluorescence were discarded.

Measurement of $[Ca^{2+}]_i$. Cells were loaded with 2 µM Fura-2/AM and 0.02% Pluronic F-127 (Invitrogen, Darmstadt, Germany) in Ringer solution (mmol/l: NaCl 145; KH_2PO_4 0.4; K_2HPO_4 1.6; Glucose 5; $MgCl_2$ 1; Ca^{2+}-Gluconat 1.3) for 1 h in the dark at room temperature. Cells were perfused with Ringer solution at 37 °C and fluorescence was detected using an inverted microscope (Axiovert S100, Zeiss, Germany) and a high speed polychromator system (VisiChrome, Puchheim, Germany). Fura-2 was excited at 340/380 nm, and emission was recorded between 470 and 550 nm using a CoolSnap camera (CoolSnap HQ, Visitron). $[Ca^{2+}]_i$ was calculated from the 340/380 nm fluorescence ratio after background subtraction. The

formula used to calculate $[Ca^{2+}]_i$ was $[Ca^{2+}]_i = Kd \times (R - R_{min})/(R_{max} - R) \times (S_{f2}/S_{b2})$, where R is the observed fluorescence ratio. The values R_{max} and R_{min} (maximum and minimum ratios) and the constant S_{f2}/S_{b2} (fluorescence of free and Ca^{2+}-bound Fura-2 at 380 nm) were calculated using 1 µmol/l ionomycin (Calbiochem), 5 µmol/l nigericin, 10 µmol/l monensin (Sigma), and 5 mmol/l EGTA to equilibrate intracellular and extracellular Ca^{2+} in intact Fura-2-loaded cells. The dissociation constant for the Fura-2•Ca^{2+} complex was taken as 224 nmol/l.

Materials and statistical analysis. All compounds used were of highest available grade of purity. Data are reported as mean ± SEM. Student's *t* test for unpaired samples and ANOVA were used for statistical analysis. $P < 0.05$ was accepted as significant difference. Data are expressed as mean ± SEM. Differences among groups were analyzed using one-way ANOVA, followed by a Bonferroni test for multiple comparisons. An unpaired *t* test was applied to compare the differences between two groups.

Acknowledgments

Supported by the Deutsche Forschungsgemeinschaft (DFG, German Research Foundation), project number 387509280, SFB 1350 (project A3). We are grateful to Dorien J.M. Peters (Department of Human Genetics, Leiden University Medical Center, Leiden, The Netherlands) for providing us with the ADPKD mouse model and Johannes Loffing (Institute of Anatomy, University of Zurich, Zurich, Switzerland) for providing the mouse renal cortical collecting duct cell line mCCDcl1. We thank Sascha Hofmann, Helena Lowak, and Patricia Seeberger for experimental and technical assistance.

Supplementary Materials

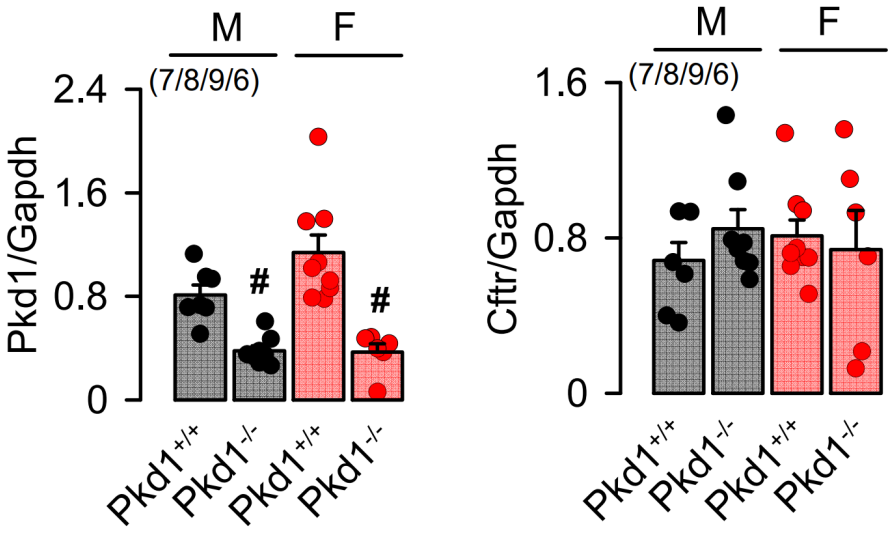

Supplemental figure 4.1 | *CFTR mRNA expression in primary renal epithelial cells.*
Semiquantitative RT-PCR analysis of CFTR mRNA expression in primary medullary renal epithelial cells from male (M) and female (F) Pkd1+/+ and Pkd1-/- mice. Mean ± SEM (number of animals). # Indicates significant knockdown of Pkd1 ($p<0.05$; unpaired t-test).

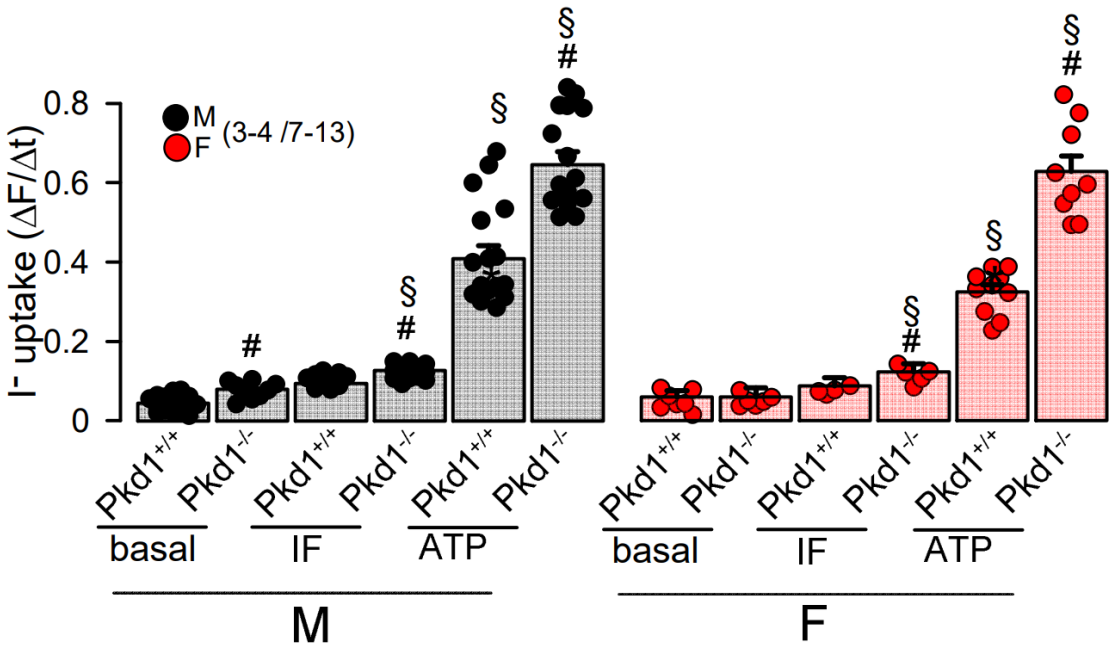

Supplemental figure 4.2 | *YFP-quenching to assess anion permeability.*
Summaries of single cell yellow fluorescence protein (YFP) iodide quenching (I- uptake) experiments in primary renal epithelial cells from male and female Pkd1+/+ and Pkd1-/-mice. I- uptake was assessed under basal conditions and after stimulation with IF (100 µM/2 µM) or ATP (50 µM). Mean ± SEM (number of animals/number of experiments in each series). #Significant difference compared to Pkd1+/+ ($p<0.05$;

unpaired ttest). §Significant difference compared to basal (p<0.05; ANOVA and Tukey's post-hoc test).

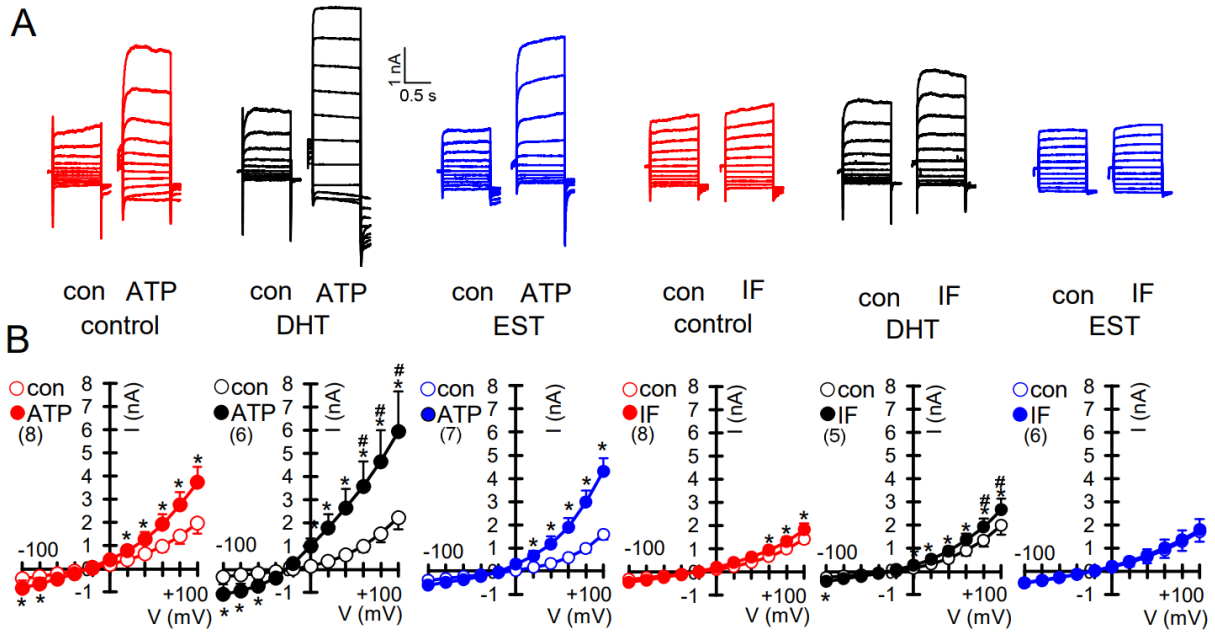

Supplemental figure 4.3 | *Ion currents in M1 mouse collecting duct cells.*

A) Overlay currents for ATP (100 µM) and IBMX/forskolin (IF; 100 µM/2 µM) - activated whole cell currents in untreated cells (control) and cells treated with dihydrotestosterone (DHT; 10 µM, 24 hrs) or estrogen (EST; 10 µM, 24 hrs). **B)** Summary current / voltage relationships corresponding to overlay currents shown in A. Mean ± SEM (number of experiments). *Significant increase by ATP or IF (p<0.05; paired t-test). #Significant difference compared to control (p<0.05; ANOVA and Tukey's post-hoc test).

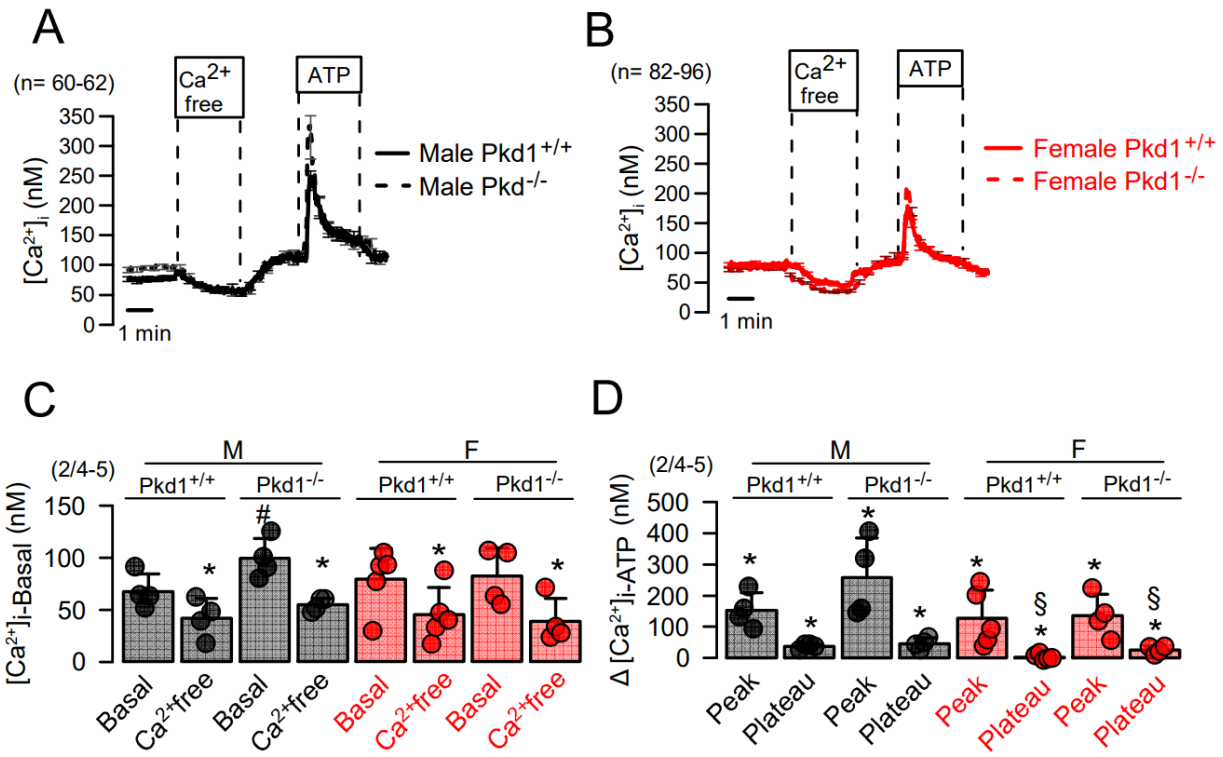

Supplemental figure 4.4 | *Basal and ATP-induced intracellular Ca^{2+} in primary renal epithelial cells.*

A,B) Summary time course for basal and ATP (100 µM) -induced intracellular Ca2+ concentrations in male (A) and female (B) Pkd1+/+ and Pkd1-/- mice. **C,D)** Summary of basal (C) and ATP-induced (D) intracellular Ca2+ concentrations in male and female PKD1+/+ and PKD1-/- mice. Mean ± SEM (number of experiments). *Significant effect by extracellular Ca2+ free and ATP ($p < 0.05$; paired ttest). #Significant difference when compared to Pkd1+/+ ($p < 0.05$;ANOVA). § Significant difference compared to male ($p < 0.05$; ANOVA).

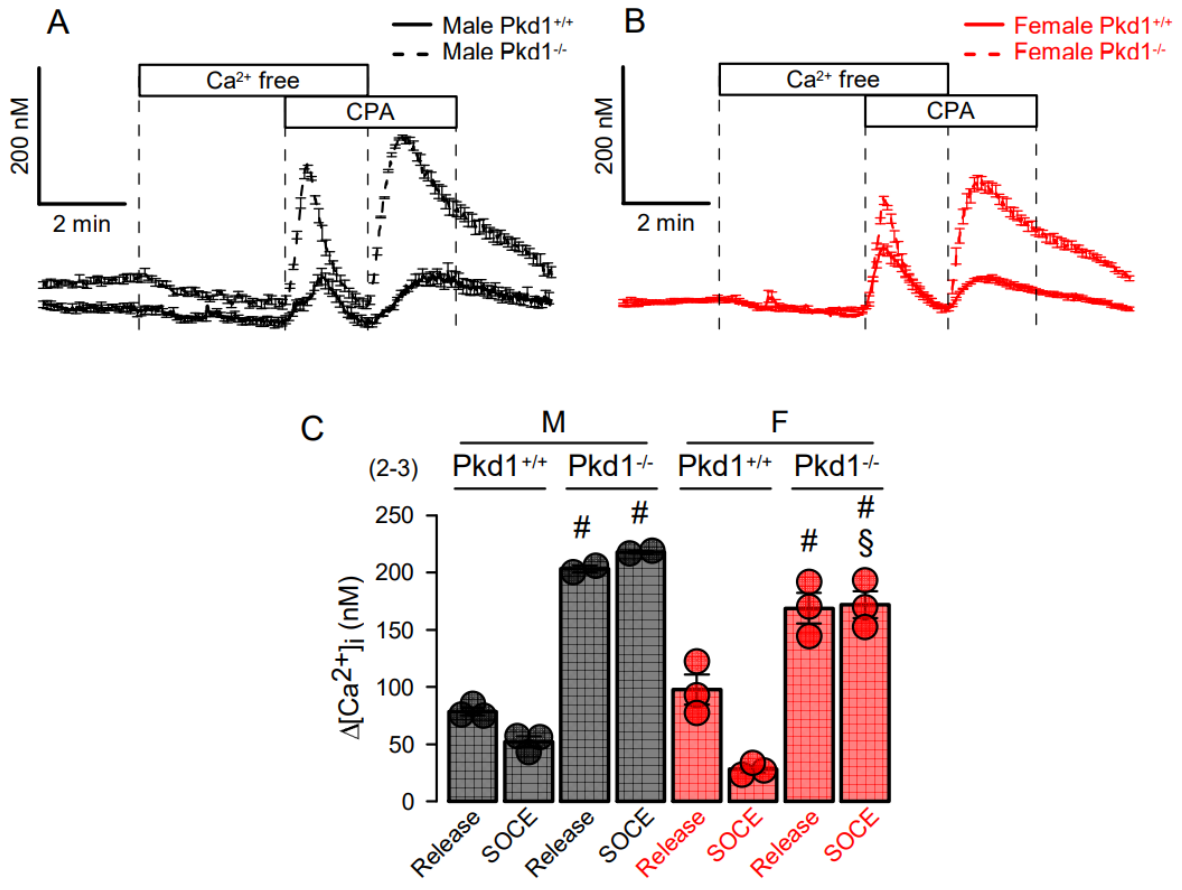

Supplemental figure 4.5 | *CPA-induced store release in male and female primary renal epithelial cells.*

CPA-induced Ca2+ store release in primary renal epithelial cells from male **(A)** and female **(B)** Pkd1+/+ and Pkd1-/- mice. **C)** Summary of store release Ca2+ and store operated Ca2+ entry (SOCE) shown in A and B. Mean ± SEM (number of experiments). #Significant difference when compared to Pkd1+/+ ($p < 0.05$; unpaired ttest). §Significant difference compared to male ($p < 0.05$; ANOVA and Tuckey's posthoc test).

CHAPTER 5 | CALMODULIN-DEPENDENT REGULATION OF OVEREXPRESSED BUT NOT ENDOGENOUS TMEM16A EXPRESSED IN AIRWAY EPITHELIAL CELLS

Abstract

Regulation of the Ca^{2+}-activated Cl^- channel TMEM16A by Ca^{2+}/calmodulin (CAM) is discussed controversially. In the present study, we compared regulation of TMEM16A by Ca^{2+}/calmodulin (holo-CAM), CAM-dependent kinase (CAMKII), and CAM-dependent phosphatase calcineurin in TMEM16A-overexpressing HEK293 cells and TMEM16A expressed endogenously in airway and colonic epithelial cells. The activator of the Ca^{2+}/CAM-regulated K^+ channel KCNN4, 1-EBIO, activated TMEM16A in overexpressing cells, but not in cells with endogenous expression of TMEM16A. Evidence is provided that CAM-interaction with TMEM16A modulates the Ca^{2+} sensitivity of the Cl^- channel. Enhanced Ca^{2+} sensitivity of overexpressed TMEM16A explains its activity at basal (non-elevated) intracellular Ca^{2+} levels. The present results correspond well to a recent report that demonstrates a Ca^{2+}-unbound form of CAM (apo-CAM) that is pre-associated with TMEM16A and mediates a Ca^{2+}-dependent sensitization of activation (and inactivation). However, when using activators or inhibitors for holo-CAM, CAMKII, or calcineurin, we were unable to detect a significant impact of CAM, and limit evidence for regulation by CAM-dependent regulatory proteins on receptor-mediated activation of endogenous TMEM16A in airway or colonic epithelial cells. We propose that regulatory properties of TMEM16A and other members of the TMEM16 family as detected in overexpression studies, should be validated for endogenous TMEM16A and physiological stimuli such as activation of phospholipase C (PLC)-coupled receptors.

Keywords: TMEM16A; calmodulin; CAMKII; calcineurin; Ca^{2+}-activated Cl^- channel; anoctamin 1; CAM

Published in: Talbi, K., Ousingsawat, J., Centeio, R., Schreiber, R., & Kunzelmann, K. (2021). Calmodulin-Dependent Regulation of Overexpressed but Not Endogenous TMEM16A Expressed in Airway Epithelial Cells. *Membranes*, *11*(9), 723.

Own experimental contribution: Whole cell patch clamp.

Own written contribution: Original draft preparation.

Other contributions: Designed experiments and analysed data.

Introduction

In our earlier study we analyzed the regulation of the Ca^{2+} activated Cl^- channel (CaCC) TMEM16A. We found that the channel can be activated by activators of Ca^{2+}/calmodulin (CAM)-regulated KCNN4 K^+ channels, such as 1-EBIO and riluzole [100]. In addition, we demonstrated that TMEM16A physically interacts with CAM. A subsequent report indicated that the anion selectivity of TMEM16A is dynamically regulated by the Ca^{2+}/CAM complex [230]. The team demonstrated that CAM reversibly increases the permeability ratio P_{HCO3-}/P_{Cl-}. Further support for a CAM-dependent regulation of TMEM16A came from an interesting study by the Colecraft-team [105]. They described a Ca^{2+}-unbound form of CAM (apo-CAM), which is pre-associated with TMEM16A or the paralogue TMEM16B channel complexes. Apo-CAM mediates a Ca^{2+} dependent sensitization of activation and Ca^{2+} dependent inactivation of TMEM16 channels [104,105]. Moreover, CAM-dependent activation and inactivation of TMEM16A had also been found in an earlier study [231]. In contrast to these studies, others did not find evidence for regulation of TMEM16A by CAM or alteration of the bicarbonate permeability of TMEM16A by CAM [102,232].
While direct CAM-regulation of TMEM16A is discussed controversially, several studies demonstrate that CAM-dependent kinase II (CAMKII) regulates CaCC/TMEM16A. However, CAMKII was found to activate [233-237] and to inhibit [238-242] CaCC and TMEM16A, respectively. Greenwood and Leblanc found a cell type-dependent activation/inhibition of CaCC by CAMKII [243], while Ko et al found differential regulation of TMEM16A by CAMKII, depending on the splice variant [244,245]. One study showed modulation of TMEM16A Cl^- currents by CaMKIIγ phosphorylation at serine residues in TMEM16A. Serine525 and Serine727 in TMEM16A were mutated to alanine, but only mutation at Ser727 (S727A) reversed the CaMKIIγ inhibition of the TMEM16A Cl^- current [240].

Earlier studies describe a cross-talk between Ca^{2+}/CAMKII-dependent regulation and inositol (3,4,5,6)-phosphate dependent regulation of CaCC, which also appears to be cell type dependent, possibly explaining some of the controversial findings outlined above [246,247]. In our earlier study, we observed that regulation of TMEM16A by INO-4995, a lipid inositol phosphate, differs depending on whether the channel is overexpressed in mammalian cells such as HEK293, or whether regulation of endogenous TMEM16A is examined [248]. While overexpressed TMEM16A was potently activated by the inositolphosphate INO-4995, endogenous TMEM16A expressed in airway and colonic epithelial cells was not. Activation of endogenous TMEM16A by purinergic receptor stimulation was augmented by INO-4995 [248]. Along the same line, the membrane permeable dioctanoyl-PIP_2 phosphatidylinositol 4,5-bisphosphate-diC8 activated overexpressed TMEM16A, but did not touch endogenous TMEM16A [249]. Also other previously reported activators of TMEM16A such as melittin or cinnamaldehyde failed to activate endogenous TMEM16A. These differences prompted us to

compare the role of CAM for acute receptor-mediated activation of TMEM16A in overexpressing cells and epithelial cells with endogenous expression of TMEM16A. Here we made use of 4 different cell lines. HEK293 cells were used to study regulation of overexpressed TMEM16A, while airway epithelial cells (BCi_NS1, CFBE) and colonic HT_{29} cells were used to study regulation of endogenous TMEM16A. We demonstrate the absence of a significant CAM-dependent regulation for endogenous TMEM16A, solidifying the conclusion that control by CAM and other regulatory properties are indeed different for endogenous and overexpressed TMEM16A. Moreover, we made use of independent techniques (patch clamp, Ussing chamber, YFP-quenching) to reduce the chance for misinterpretations due to methodological artefacts.

The data suggest no significant role of CAM and the CAM-dependent proteins CAMKII and calcineurin for activation of endogenous TMEM16A, while CAM is likely to enhance Ca^{2+} sensitivity of overexpressed TMEM16A.

Materials and Methods

Cell culture. All cells were grown at 37°C in a humidified atmosphere with 5% (v/v) CO_2. Culture conditions for CFBE and HT_{29} cells have been described earlier [250]. In brief, airway epithelial cells were grown in DMEM/Ham's F-12 with L-Glutamine medium supplemented with 10% (v/v) fetal bovine serum (FBS), 1% (v/v) L-glutamine 200mM and 1% (v/v) HEPES 1M (all from Capricorn Scientific, Ebsdorfergrund, Germany). CFBE parental cells were grown in MEM with Earle's Salts with L-Glutamine medium (Capricorn Scientific, Ebsdorfergrund, Germany) supplemented with 10% FBS. The airway epithelial cell line H441 was grown in RPMI and DMEM media. The immortalized human airway basal cell line BCi-NS1 (kindly provided by Prof. Ron Crystal, Weill Cornell Medical College, NY, USA) was maintained in Bronchial Epithelial Growth Media (Lonza). Cells were differentiated by growing on permeable supports in an air-liquid interface (ALI) for up to 30 days in Pneumacult-Ex medium supplemented with Pneumacult-Ex 50X supplement (#05008; STEMCELL Technologies), 96 µg/ml hydrocortisone (H0888; Sigma-Aldrich), and 1% penicillin–streptomycin (10,000 U/ml) (15140-148; Gibco).

cDNA, siRNA-TMEM16A, RT-PCR. Construction of pcDNA31 human TMEM16A (abc) has been described previously [229]. Cells were transfected using standard protocols for Lipofectamine 3000. Knockdown of TMEM16A in CFBE parental cells was performed by transfecting siTMEM16A (5-CCUGUACGAAGAGUGGGCACGCUAU-3, Invitrogen, Carlsbad, California, USA) using standard protocols for Lipofectamine 3000 (Invitrogen, Carlsbad, California, USA). Scrambled siRNA (Silencer® Select Negative Control siRNA #1, Ambion, Austin, Texas, USA) was transfected as negative control. All experiments were performed 72h after transfection. For RT-PCR total RNA from HT29 and CFBE cells were isolated using NucleoSpin RNA II columns (Macherey-Nagel, Düren, Germany). Total RNA (0.5 µg / 25 µl

reaction) was reverse-transcribed using random primer (Promega, Mannheim, Germany) and M-MLV Reverse Transcriptase RNase H Minus (Promega, Mannheim, Germany). Each RT-PCR reaction contained sense (0.5 µM) and antisense primer (0.5 µM) (table 1), 0.5 µl cDNA and GoTaq Polymerase (Promega, Mannheim, Germany). After 2 min at 95°C cDNA was amplified (targets 35 cycles, reference Gapdh 25 cycles) for 30 s at 95°C, 30 s at 56°C and 1 min at 72°C. PCR products were visualized by loading on Midori Green Xtra (Nippon Genetics Europe) containing agarose.

Table 5.1 | *Primers for PCR.*

Gene Accession Number	**Primer**	**Size (bp)**
TMEM16A (abcd) NM_001378092.1		
Splice variant a	s: 5'- GGACCCTGATGCCGAGTGC as: 5'- GGAGAAGGGATAGGAGAGTC	547
Splice variant b	s: 5'- ACAGCAAAACCCGGAGC as: 5'- TCTCTGGTCACACATCTCC	462
Splice variant c	s: 5'- ACAGCAAAACCCGGAGC as: 5'- GGATGATCCTTGACAGCCTC	703
Splice variant d	s: 5'- GAAGAAAGAGTCCAGAAAC as: 5'- CCGATCTCTCCATGTCAGC	136
KCNN4 NM_002250.3	s: 5'- GATTTAGGGGCGCCGCTGAC as: 5'- CTTGCCCCACATGGTGCCC	405
Gapdh NM_001289726	s: 5'- GTATTGGGCGCCTGGTCAC as: 5'- CTCCTGGAAGATGGTGATGG	200

Patch Clamping. Cells were patch clamped after growing on coated glass coverslips for 2-3 days. Whole cell patch clamp techniques and data analysis have been described earlier [151]. In brief, patch pipettes were filled with a cytosolic-like solution containing (in mM): KCl 30, K-Gluconate 95, NaH_2PO_4 1.2, Na_2HPO_4 4.8, EGTA 1, Ca-Gluconate 0.758, $MgCl_2$ 1.03, D-Glucose 5, ATP 3; pH 7.2. The intracellular (pipette) Ca^{2+} activity was 0.1 µM. Fast whole cell current recordings were performed as described recently [251]. The bath was perfused continuously with standard bicarbonate-free Ringer's solution (in mM: NaCl 145, KH_2PO_4 0.4, K_2HPO_4 • 3 H_20 1.6, Glucose 5, $MgCl_2$ • 6 H_20 1, Ca-Gluconate • 1 H_20 1.3) at a rate of 8 mL/min.

Patch pipettes had an input resistance of 2–4 MΩ and whole cell currents were corrected for serial resistance. Currents were recorded using a patch clamp amplifier (EPC 7, List Medical Electronics, Darmstadt, Germany), the LIH1600 interface and PULSE software (HEKA, Lambrecht, Germany) as well as Chart software (AD Instruments, Spechbach, Germany). Cells were stimulated with 1, 10 or 100 µM ATP in standard bicarbonate-free Ringer's solution. Cells were current clamped for most of the time. In regular intervals, membrane voltage (*Vc*) was clamped in steps of 20 mV from -100 to +100 mV. The inhibitor of Ca^{2+}-activated KCNN4 K^+ channels, If indicated TRAM-34 (100 nM), was present in the patch clamp and other experiments to avoid contributions of Ca^{2+} activated K^+ channels.

Ussing chamber. Short circuit Ussing chamber measurements were performed on filter grown BCi-NS1 cells. To that end BCi-NS1 were grown for up to 30 days on permeable supports (Snapwell, Corning) and differentiated in Pneumacult-Ex medium supplemented with Pneumacult-Ex 50X supplement (#05008; STEMCELL Technologies), 96 µg/ml hydrocortisone (H0888; Sigma-Aldrich), and 1% penicillin–streptomycin (10,000 U/ml) (15140-148; Gibco). Experiments were performed under short circuit Ussing chamber conditions (Physiological instruments) in the presence of 5% CO_2 and 25 mM HCO_3^- at 37 °C as described earlier [252].
YFP quenching. Cells stably transfected with iodide-sensitive YFP were plated in transparent, 96-well plates (Sarstedt, Nümbrecht, Germany), cultured 24–72 h to 80–90% confluence, washed with gluconate substituted-Ringer solution (mmol/L: NaCl 100–120; Na+-gluconate 20–40; KCl 5; MgCl2 1; CaCl2 2; D-Glucose 10; HEPES 10), and incubated with or without test compounds in this solution. Total intracellular YFP fluorescence intensity in each well was measured in a fluorescence microplate reader (NOVOstar, BMG Labtech, Ortenberg, Germany) kept at 37 ◦C, using an excitation wavelength of 485 nm and emission detection at 520 nm. Fluorescence was read continuously during injection of an iodide (I−)-substituted Ringer solution (mmol/L: NaCl 100–120; NaI 20–40; KCl 5; MgCl2 1; CaCl2 2; D-Glucose 10; HEPES 10) by a syringe pump and following injections of a symmetrical Ringer solution (in mmol/L: NaCl 100–120; Na+-Gluconate 10–20; NaI 10–20; KCl 5; MgCl2 1; CaCl2 2; D-Glucose 10; HEPES 10) carrying test compounds. Original data were collected, background fluorescence was subtracted, and the initial rate of maximal fluorescence decay caused by I- influx/YFP fluorescence-quenching upon acute injection (or pre-incubation) of test compounds was measured to determine anion conductance/activity of TMEM16A.

Materials and statistical analysis. All compounds used were of highest available grade of purity and were obtained from Sigma-Aldrich (St. Louis, Missouri, USA), unless indicated otherwise. Data are shown as individual traces/representative images and/or as summaries with mean values ± SEM, with the respective number of experiments given in each figure's

legend. The population-effective sizes for the experiments were typically around 0.87-0.94. As we did not want to rely on results obtained in one cell line only, we compared results obtaiend in overexpressing HEK293 cells with those obtained in cell expressing endogenous TMEM16A channels (CFBE, BCi-NS1, HT_{29} cells). For statistical analysis, paired or unpaired Student's t-test or ANOVA were used where appropriate. A *p*-value of < 0.05 was accepted as a statistically significant difference.

Results

Overexpressed TMEM16A is spontaneously active due to enhanced Ca^{2+} sensitivity.

We observed in earlier studies that TMEM16A, when overexpressed in HEK293 cells, produces whole cell currents in the presence of basal cytosolic Ca^{2+} concentrations of 0.1 µM and with physiological concentrations of K^+, Na^+ and Cl^- in the patch pipette filling solution [253,254] (Fig. 1C,D). Such basal currents were not observed in cells expressing TMEM16A endogenously, such as HT_{29} colonic epithelial or CFBE airway epithelial cells [254] (Fig. 1A,B). Here, TMEM16A was activated only after increase in the intracellular Ca^{2+} concentration, e.g. by application of the purinergic agonist ATP [254] (Fig. 1A,B, Fig. 6). In overexpressing cells, application of ATP, activated whole cells currents in addition to the already enhanced basal currents. Enhanced and activated currents were inhibited by different blockers of TMEM16A such as CaCCinhAO1 (AO1) or niflumic acid [100,253]. Also enhanced basal currents were inhibited by application of AO1 or in the absence of pipette (cytosolic) Ca^{2+}, indicating that TMEM16A is in charge of both enhanced basal and ATP-activated currents (Fig. 1E-H). These data strongly suggest a higher Ca^{2+} sensitivity of overexpressed TMEM16A when compared with endogenous TMEM16A.

To further demonstrate enhanced Ca^{2+} sensitivity of overexpressed TMEM16A, we performed patch clamp experiments in which we loaded the patch pipette with pipette filling solution containing different free Ca^{2+} concentrations. At 0 µM pipette Ca^{2+} no TMEM16A whole cell currents were observed in overexpressing HEK293 cells or CFBE cells expressing endogenous TMEM16A. Whole cell currents were activated in overexpressing HEK293 cells at Ca^{2+} concentrations as low as 0.01 µM (10^{-8} M), while TMEM16A currents in CFBE cells were only observed at 1 µM (10^{-6} M) Ca^{2+}, again strongly suggesting a higher Ca^{2+} sensitivity for overexpressed TMEM16A (Fig. 2). At 10 µM Ca^{2+}, whole cell currents were smaller due to the well-known Ca^{2+} dependent inactivation of TMEM16A [248]. No whole cell currents were activated in mock-transfected HEK293 cells.

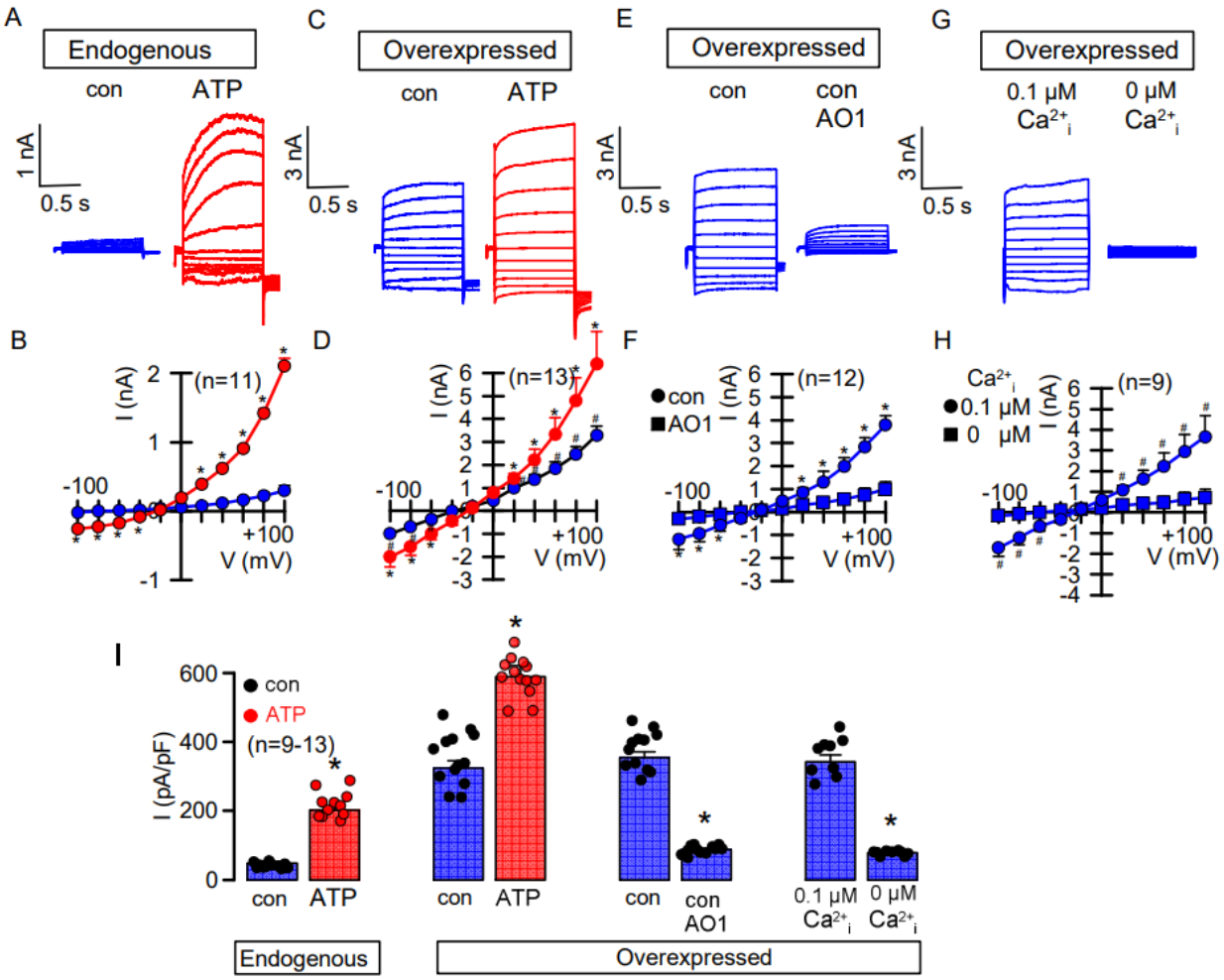

Figure 5.1 | *Overexpressed TMEM16A is spontaneously active due to enhanced Ca^{2+} sensitivity.* TMEM16A whole cell currents were activated by 100 µM ATP in CFBE airway epithelial cells expressing TMEM16A endogenously (A,B) and in HEK293 cells overexpressing TMEM16A (C,D). A,B) TMEM16A is closed under control conditions ([Ca2+]i = 0.1 µM) and is opened by ATP-induced increase in [Ca2+]i. C,D) Whole cell currents were detected in TMEM16A-overexpressing cells under control conditions, with additional activation by ATP. E,F) Whole cell currents detected under basal conditions were inhibited by the TMEM16A-blocker CaCCinhAO1 (AO1, 20 µM). G,H) Whole cell currents detected under control conditions ([Ca2+]i = 0.1 µM) were not detected in the absence of Ca2+ in the pipette filling solution. I) Summary of the current densities. Mean ± SEM (n = number of experiments). *Significant activation by ATP and inhibition by AO1, respectively ($p < 0.05$; paired t-test). #Significant difference when compared to endogenous currents or in presence of 0 µM [Ca2+]i, respectively ($p < 0.05$; unpaired t-test).

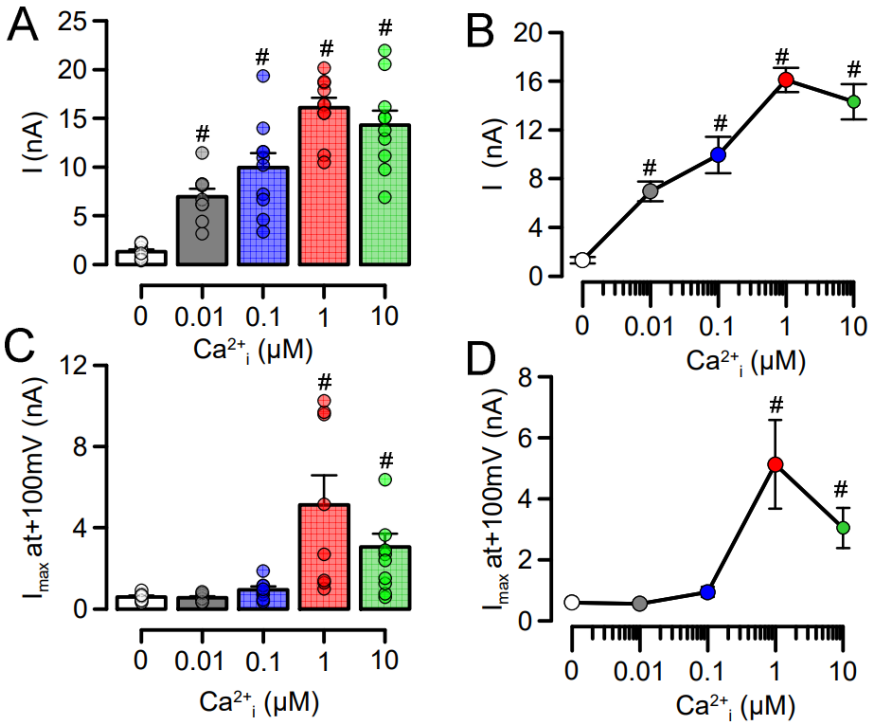

Figure 5.2 | *Enhanced Ca^{2+} sensitivity of overexpressed TMEM16A.*

Patch pipettes were filled with solutions containing different free Ca^{2+} concentrations (0–10 μM). At 0 μM pipette Ca^{2+} no TMEM16A, whole cell currents were observed in overexpressing HEK293 cells or CFBE cells expressing endogenous TMEM16A. (**A**,**B**) Whole cell currents were activated in overexpressing HEK293 cells at Ca^{2+} concentrations as low as 0.01 μM. (**C**,**D**) TMEM16A currents in CFBE cells were only observed at 1 μM Ca^{2+}. Mean ± SEM (n = number of experiments). #Significant activation when compared to 0 μM Ca^{2+} ($p < 0.05$; ANOVA).

Enhanced Ca^{2+} sensitivity of overexpressed TMEM16A is modulated by CAM.

We previously reported regulation of TMEM16A by CAM [100], which, however, has been discussed controversially (c.f. Introduction). Here we examined activation of overexpressed TMEM16A by the activator of the CAM/KCNN4 complex, 1-EBIO. No effects were seen for 1-EBIO in mock-transfected HEK293 cells. In contrast, TMEM16A-overexpressing cells showed enhanced basal currents, which were further augmented by 1-EBIO, clearly suggesting CAM-regulation of TMEM16A. Application of the CAM-inhibitor trifluoperazine (TFP) inhibited enhanced basal currents and attenuated activation by 1-EBIO. Moreover, the TMEM16A-inhibitor CaCCinhAO1 (AO1) [255] strongly inhibited enhanced basal currents and abolished the effect of 1-EBIO (Fig. 3A-E). Finally, activation by 1-EBIO was examined in overexpressing HEK293 cells treated with scrambled RNA or with siRNA for CAM. Activation by 1-EBIO was attenuated in cells in which expression of CAM was knocked down (Fig. 3F,G). Knockdown of CAM was assessed by semiquantitative RT-PCR and was 94 ± 2 % (n=5). activation of TMEM16A in CFBE cells. These results suggest that enhanced basal TMEM16A currents are due to enhanced Ca^{2+} sensitivity, probably modulated by association of CAM with TMEM16A.

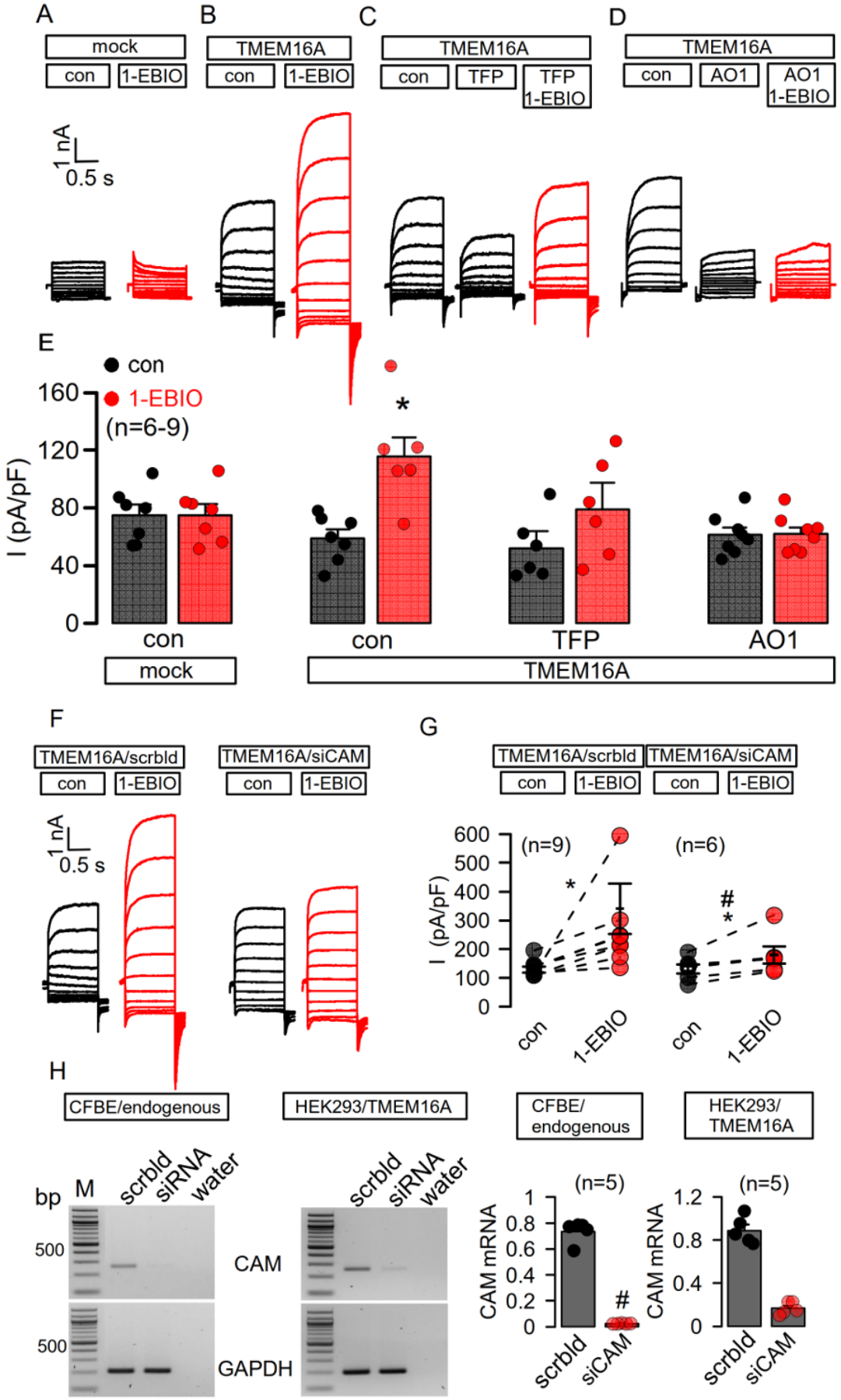

Figure 5.3 | ***Enhanced Ca^{2+} sensitivity of overexpressed TMEM16A is mediated by CAM.***

*(***A**–**D**) No effect of 1-EBIO (1 mM) on whole cell currents in mock-transfected HEK293 cells. Basal activity of TMEM16A and further activation by 1-EBIO in TMEM16A-overexpressing HEK293 cells. Inhibition of basal TMEM16A-activity and attenuation of the effect of 1-EBIO by the CAM-inhibitor trifluoperazine (TFP, 10 µM). Inhibition of basal TMEM16A-activity and inhibition of TMEM16A-activation by 1-EBIO using CaCC-inhAO1 (AO1, 20 µM). (**E**) Summary of the current densities. (**F**,**G**) Basal activity of TMEM16A and further activation by 1-EBIO in overexpressing HEK cells treated with scrambled RNA (scrbld) or with siRNA for CAM (siCAM). (**H**) Knockdown of CAM was assessed by semiquantitative RT-PCR in both CFBE cells expressing endogenous TMEM16A and in HEK293 cells overexpressing TMEM16A. Similar number of CAM-transcripts are expressed in CFBE and HEK293 cells. Mean ± SEM (n = number of experiments). *Significant activation by 1-EBIO and inhibition by AO1 or TFP, respectively ($p < 0.05$; paired t-test). #Significant difference when compared to activation in the absence of AO1, TFP, or siCAM, respectively ($p < 0.05$; unpaired t-test).

Similar number of CAM-transcripts are expressed in CFBE and HEK293 cells (Fig. 3H). Notably, in contrast to TMEM16A-overexpressing HEK293 cells, no effect of siRNA-CAM was observed on the

No activation of endogenous TMEM16A by 1-EBIO and no CAMKII-dependent regulation of TMEM16A in airway epithelial cells.

We examined whether CAM-dependent regulation can also be detected for TMEM16A expressed endogenously in CFBE airway epithelial cells. Expression of TMEM16A in CFBE cells has been shown previously [151,250]. We also found expression of Ca^{2+} activated KCNN4 channels in CFBE (and H441) airway epithelial cells, but not in HEK293 cells (Fig. 4A). Both CFBE and HT_{29} colon epithelial cells express the splice variant TMEM16Aa,b,c (Fig. 4B). Patch clamp experiments were performed in the absence or presence of TRAM-34, a potent inhibitor of Ca^{2+} activated KCNN4 K^+ channels. In the absence of TRAM-34, 1-EBIO activated a whole cell current and hyperpolarized the membrane voltage (Fig. 4C,D). In contrast, in the presence of TRAM-34, no hyperpolarization was observed and 1-EBIO did not activate whole cell currents (Fig. 4E,F). Under both conditions ATP activated whole cell currents. The data suggest that in airway epithelial cells with endogenous TMEM16A, 1-EBIO activates KCNN4 but not TMEM16A.

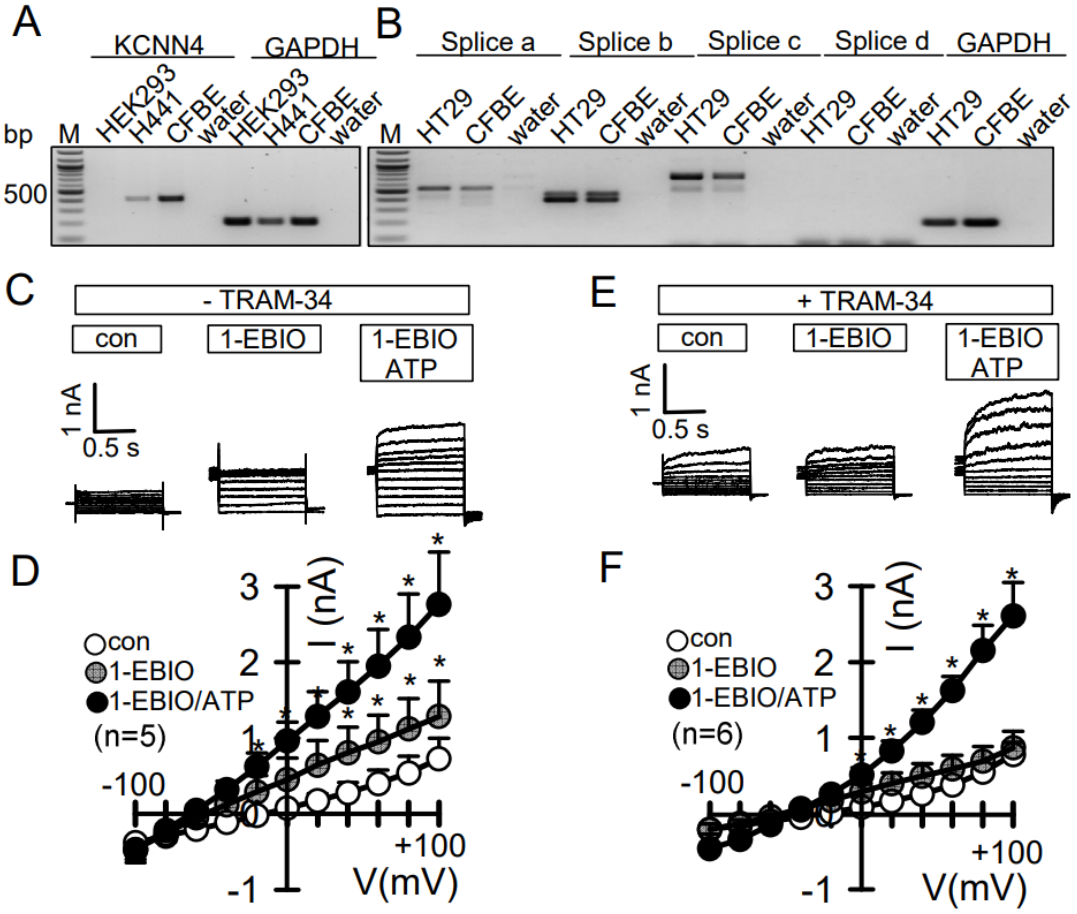

Figure 5.4 | ***No activation of endogenous TMEM16A by 1-EBIO in CFBE airway epithelial cells.*** *(***A**) RT-PCR analysis indicating expression of Ca^{2+}-activated KCNN4 channels in H441 and CFBE airway epithelial cells but not in HEK293 cells. (**B**) RT-PCR analysis indicating expression of the splice variant TMEM16Aa,b,c in HT_{29} colonic epithelial and CFBE airway epithelial cells. (**C**,**D**) Whole cell currents and current/voltage relationships demonstrating current activation and hyperpolarization by 1-EBIO (1 mM) and additional activation by ATP (100 µM). (**E**,**F**) Activation of whole cell currents and hyperpolarization by 1-EBIO is inhibited by the KCNN4 blocker TRAM-34 (100 nM). Mean ± SEM (n = number of experiments). *Significant activation by 1-EBIO and additional activation by ATP ($p < 0.05$; paired t-test).

Because CAM-dependent kinase (CAMKII) and the serine/threonine-phosphatase calcineurin require CAM to operate, we examined the effects of other CAM-activators (DCEBIO, riluzole), CAMKII-inhibitors (KN-62, KN-93), and the calcineurin-inhibitor tacrolimus (FK-506) on basal and ATP-activated endogenous currents in airway epithelial cells. Notably DCEBIO enhanced basal currents and both DCEBIO and riluzole somewhat augmented ATP-activated currents but failed to reach significance (Fig. 5A,B). Tacrolimus, and inhibition of CAMKII attenuated ATP-activated currents. Taken together, apart from CAMKII-dependent activation there is no clear evidence for CAM, or calcineurin-dependent regulation of endogenous TMEM16A in CFBE airway epithelial cells.

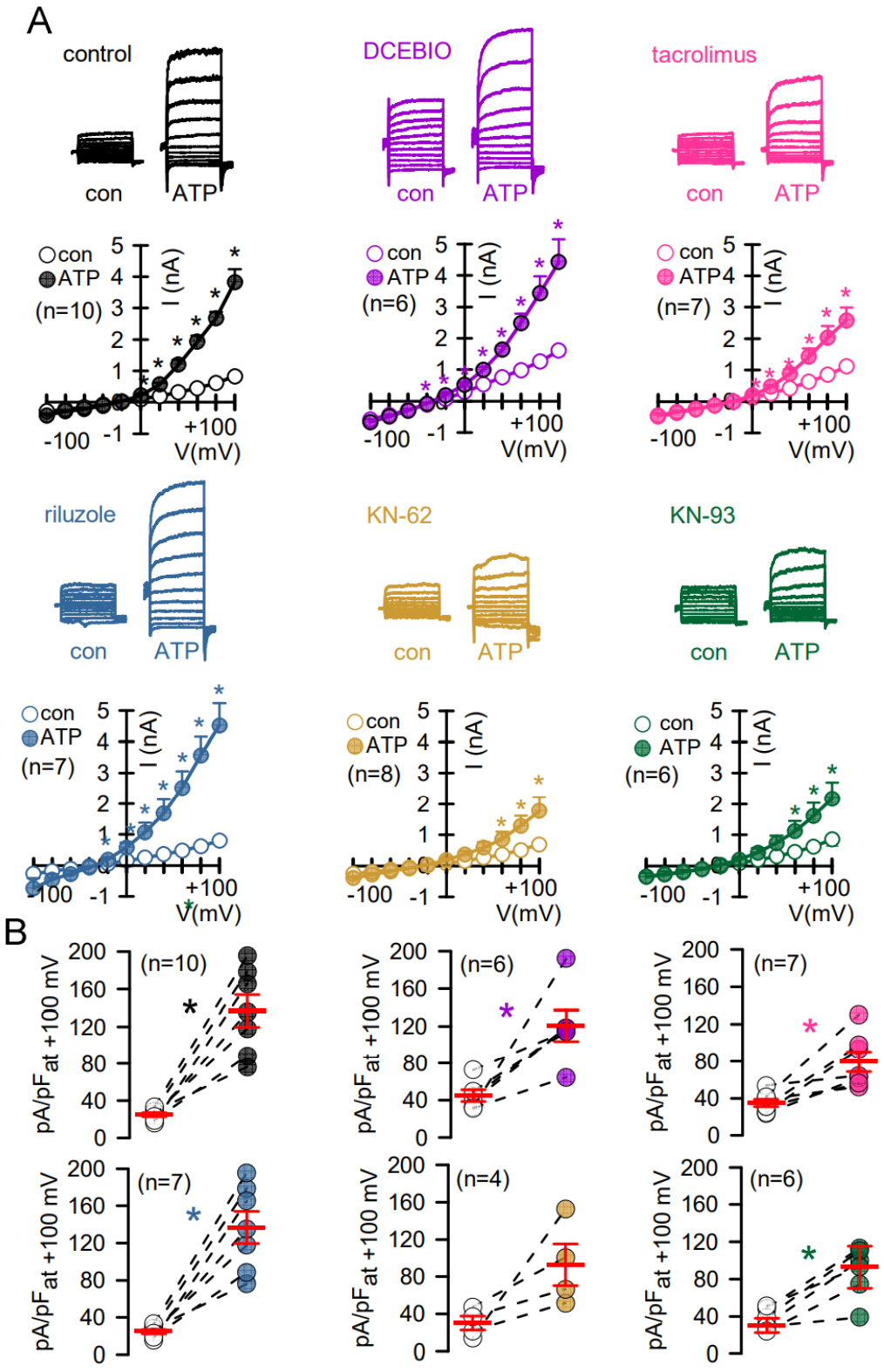

Figure 5.5 | ***Evidence for CAMKII-dependent activation of TMEM16A but not for CAM- or calcineurin-dependent regulation of endogenous TMEM16A in CFBE airway epithelial cells.***

A) Whole cell patch clamp analysis of ATP (100 µM)-activated TMEM16A currents and effects of the 1-EBIO analogues DCEBIO and riluzole (both 10 µM), the CAMKII-inhibitors KN-62 and KN-93 (both 10 µM) and the calcineurin inhibitor tacrolimus (10 µM). Cells were pre-incubated with the compounds, which were also present during the experiment. Under all conditions, significant activation of whole cell

currents by ATP was observed. While the KCNN4 activators DCEBIO and riluzole enhanced ATP-activated currents, KN-62, KN-93, and tacrolimus reduced current activation. The time course for ATP-activation of TMEM16A remained unchanged by the drugs. (**B**) Calculated current densities. All experiments were performed in the presence of the KCNN4-inhibitor TRAM-34. Mean ± SEM (n = number of experiments). *Significant activation by ATP ($p < 0.05$; paired t-test).

No evidence for CAM, CAMKII, or calcineurin-dependent regulation of endogenous TMEM16A expressed in BCi-NS1 airway epithelial cells.

In order to exclude cell specific or methodological factors, we re-examined CAM, CAMKII, or calcineurin-dependent regulation in Ussing chamber recordings with human BCi-NS1 airway epithelial cells. When grown on permeable supports these cells differentiate into a polarized epithelium with airway epithelial typical properties [250,256]. Cells were measured under control conditions or after exposure to KN-93, DCEBIO, or tacrolimus. Compounds were added subsequently to luminal or basolateral sides of the epithelium, and the effects of TRAM-34 (T-34), the epithelial Na^+ channel inhibitor amiloride (amil), the inhibitor of the cystic fibrosis transmembrane conductance regulator Cl^- channel CFTRinh172 (Inh172), and ATP on short circuit currents (Isc) were examined. Neither Na^+ absorption by ENaC, nor basal Cl^- currents by CFTR or ATP-activated TMEM16A/CFTR currents were significantly affected by any of the inhibitors (Fig. 6).

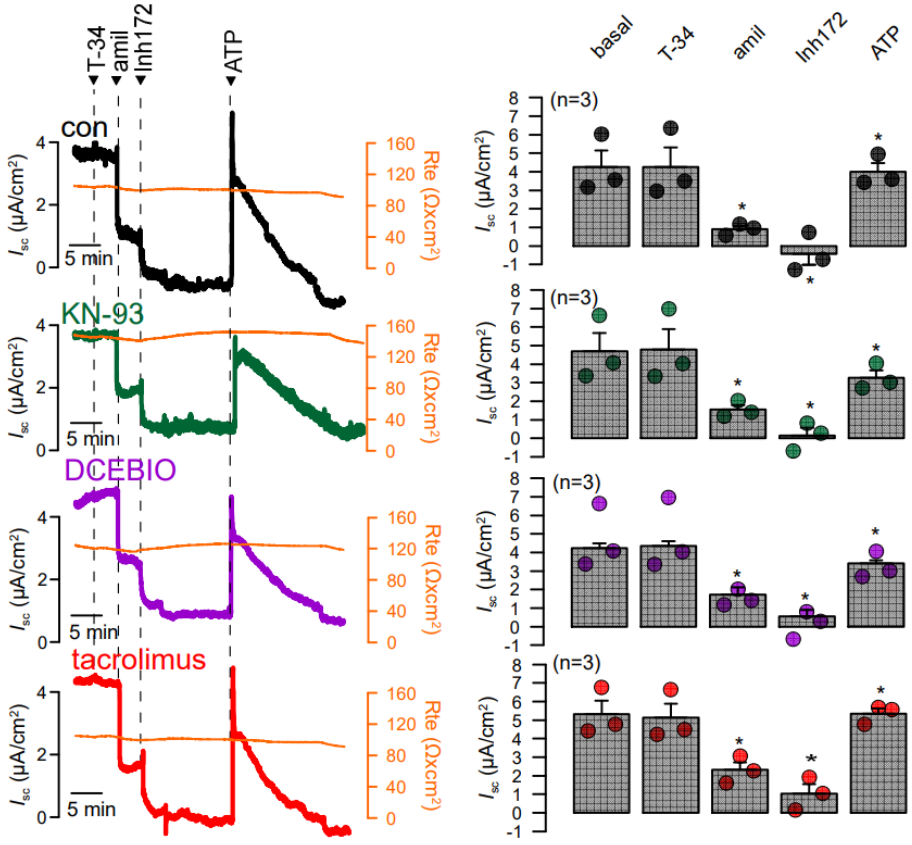

Figure 5.6 | ***No evidence for CAM, CAMKII, or calcineurin-dependent regulation of endogenous TMEM16A in BCi-NS1 airway epithelial cells.***

Left panels: Ussing chamber recordings from human BCi-NS1 airway epithelial cells, assessing the ion transport by continuously measuring the transepithelial short circuit current Isc. Original continuous recordings of the short circuit currents Isc in the absence or presence of different inhibitors. The transepithelial resistance was continuously monitored in parallel. Cells were measured under control conditions or after exposure to KN-93 (10 µM), DCEBIO (10 µM), or tacrolimus (100 nM). Right panels: Summaries for the short circuit currents corresponding to continuous Isc recordings shown in the left panels. The effects of TRAM-34 (T-34, 100 nM), amiloride (amil, 10 µM), CFTRinh172 (Inh172, 20 µM), and ATP (5 µM) on Isc are summarized. Mean ± SEM (n = number of experiments). *Significant effects of amil, Inh172, and ATP ($p < 0.05$; paired t-test).

No evidence for CAM, CAMKII, or calcineurin-dependent regulation of endogenous TMEM16A in HT_{29} colonic epithelial cells.

We finally examined if any of the inhibitors affects ATP-activated TMEM16A whole cell currents in HT_{29} colonic epithelial cells. Here we used iodide quenching of halide-sensitive yellow-fluorescent protein (YFP), stably expressed in HT_{29} cells. ATP-induced quenching in HT_{29} cells transfected with scrambled RNA was impressive (Fig. 7A) and was completely abolished by siRNA-knockdown of TMEM16A (Fig. 7B), indicating that TMEM16A if fully in charge of ATP, i.e. Ca^{2+} activated whole cell currents in HT_{29} cells. None of the inhibitors DCEBIO, KN-62, KN-93, riluzole or tacrolimus, applied at different concentrations, affected current activation by ATP (Fig. 7C,D). Taken together, the results suggest that CAM-dependent regulation of TMEM16A is present in overexpressing HEK293 cells, but show little effects on TMEM16A expressed endogenously in airway and colonic epithelial cells.

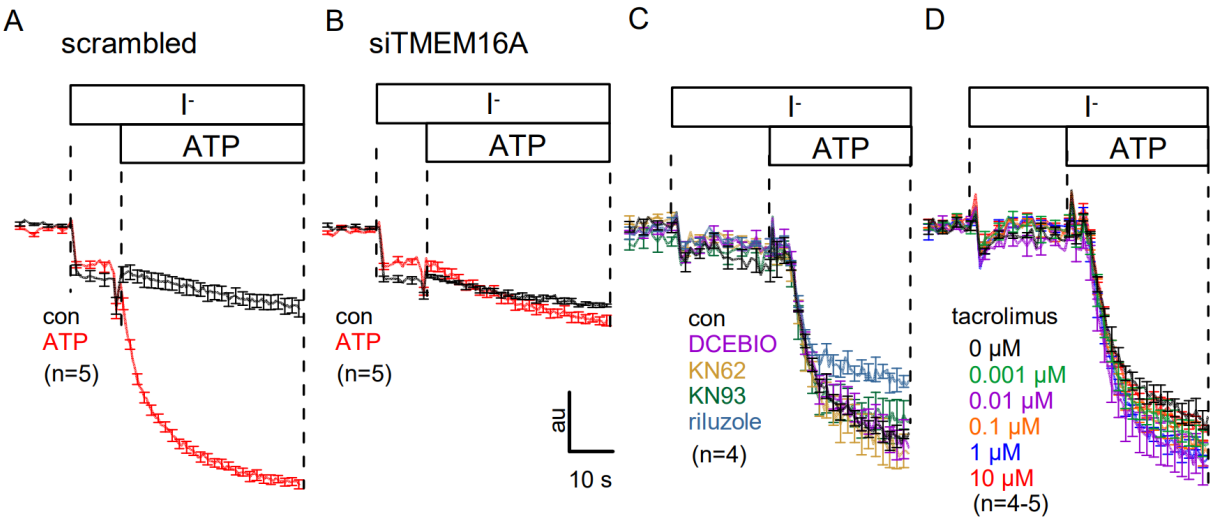

Figure 5.7 | ***No evidence for CAM, CAMKII, or calcineurin-dependent regulation of endogenous TMEM16A in HT_{29} colonic epithelial cells.***

Iodide quenching of YFP stably expressed in HT_{29} colonic epithelial cells was used to assess 5µM ATP-activated halide permeability by activation of TMEM16A. (**A**) ATP-induced quenching in mock transfected HT_{29} cells. (**B**) ATP-induced quenching in HT_{29} cells with siRNA-knockdown of TMEM16A. **(C)**

Preincubation of the cells with DCEBIO, KN-62, KN-93, and riluzole (all 10 µM) did not affect ATP-induced quenching. (**D**) Incubation with different concentrations of tacrolimus did not affect ATP-induced quenching. All experiments were performed in the presence of TRAM-34. Mean ± SEM (n = number of experiments). au = arbitrary units for fluorescence quenching.

Discussion

Regulation of the Ca^{2+} activated Cl^- channel TMEM16A has been studied extensively. In most patch clamp studies, the channel is examined as overexpressed protein activated by high pipette Ca^{2+}, in the presence of unphysiological salt concentrations at 20 °C [257,258]. Our previous work showed that activation of TMEM16A by phosphatidylinositol 4,5-bisphosphate or inositol 3,4,5,6-tetrakisphosphate is well detected for overexpressed TMEM16A but not for endogenous TMEM16A [248,249]. Also other activators or inhibitors show differential effects between overexpressed and endogenous channels [249]. The overexpressed channel is already active at basal intracellular (pipette) Ca^{2+} as low as 0.01 µM. This enhanced basal current is reduced at temperatures lower than 37 °C [253,254]. Notably, similar is observed for TMEM16F, which is a phospholipid scramblase and a nonselective ion channel [254]. Interestingly, the calcium-hypersensitive aspartic acid 408-to-glycine 408 (D408G) TMEM16F mutant showed spontaneous scrambling and ion channel activity when overexpressed in HEK293 cells, but both scrambling and ion currents were not enhanced in macrophages isolated from mice with the corresponding knockin mutation [254,259](data not shown). For both TMEM16A and TMEM16F we proposed a role of lipid-dependent regulation modulating their Ca^{2+} sensitivity and activity at basal Ca^{2+} activity. Lipid-dependent regulation may depend on the ambient temperature and other factors such as temperature-sensitive phospholipase A2, reactive oxygen species and the cytosolic (pipette) ion composition [254,260]. Moreover, we speculated earlier that i) massively overexpressed TMEM16A may end up in non-raft compartments which are more accessible to other cellular Ca^{2+} sources, ii) overexpressed TMEM16A may translocate its activating Ca^{2+} source, i.e. the endoplasmic reticulum, by membrane tethering, and iii) unknown antagonistic accessory proteins may be stoichiometrically underrepresented overexpressing cells [116,118,248,249]. It is also entirely possible that temperature-sensitive Ca^{2+} permeable transient receptor potential (TRP) channels are involved in the temperature-sensitive activation of TMEM16A [261-263]. Notably, TRP channels have also been shown the be regulated by PIP_2 and CAM [264,265]. Alternatively, other accessory proteins may interact differentially under overexpressed or endogenous conditions [249].

Pre-association of Ca^{2+}-free CAM (apoCAM) may preferentially occur with overexpressed TMEM16A and thus sensitize the channel for intracellular Ca^{2+} [104,105]. Accordingly, the benzimidazolone 1-EBIO may then promote the association between apoCAM and TMEM16A. 1-EBIO is a known activator of Ca^{2+} sensitive SK-channels [266,267]. SK channels, e.g. KCNN4,

consist of a α-subunit that requires CAM as ß-subunit to gate the channel upon binding of Ca^{2+} to CAM. 1-EBIO enhances the interaction between the α-subunit and CAM and thereby shifts the $[Ca^{2+}]_i$/channel activity-relationship to lower $[Ca^{2+}]_i$ [268]. Notably, 1-EBIO did not activate any SK currents in the absence of $[Ca^{2+}]_i$ [268] and similarly TMEM16A was not spontaneously active and was not activated by 1-EBIO in the absence of cytosolic (pipette) Ca^{2+} (Fig. 1).

Association of a ß-subunit such as holoCAM or apoCAM with TMEM16A may no longer be surprising, given the recent findings of an association of the KCNQ1-K^+ channel ß-subunit KCNE1 with TMEM16A [269]. Nevertheless, activation of TMEM16A by benzimidazolone compounds and effects of CAM-regulated CAMKII or calcineurin were very moderate in epithelial cells with endogenous expression of TMEM16A.

Taken together, it appears indispensable to examine whether activation by CAM and other accessory proteins/ß-subunits [269], phosphatidylinositols, temperature or small molecule activators, respectively, does exist for endogenous channels expressed in non-cultured cells and tissues under physiological conditions.

Acknowledgments

This research was supported by the Deutsche Forschungsgemeinschaft (DFG, German Research Foundation), project number 387509280, SFB 1350 (project A3), UK CF Trust SRC013, DFG KU756/14-1, and Gilead Stiftung. We thank Prof. Dr. Luis Galietta (Telethon Institute of Genetics and Medicine, Pozzuoli, Italy) for providing the HT_{29}/YFP cells and Prof. Dr. Ron Chrystal (Weill Cornell Medical College, New York, New York) for providing the BCi-NS1 cell line. We thank Dr. Yuemin Tian for experimental assistance.

CHAPTER 6 | A TMEM16J VARIANT LEADS TO DYSREGULATED CYTOSOLIC CALCIUM CAUSING CHRONIC RENAL DISEASE

Abstract

SIGIRR (single immunoglobulin IL-1 related receptor), PKP3 (plakophilin 3), and TMEM16J, a putative calcium-activated ion channel or phospholipid scramblase, control immune response and the extend of inflammation. Variants of SIGIRR/PKP3/TMEM16J lead to severe inflammatory diseases such as pneumonia, enterocolitis and kidney graft rejection. Meta-analysis of genome-wide association studies identified TMEM16J-T604A as a strong promotor for chronic kidney disease (CDK), but the disease mechanism and function of TMEM16J remains unknown. We demonstrate TMEM16J as calcium-activated calcium permeable leak channel in the endoplasmic reticulum. (ER) that controls intracellular distribution of calcium, receptor-mediated intracellular Ca^{2+} signals and transcription of pro-inflammatory cytokines. Renal epithelial cells that express the variant TMEM16J-T604A show enhanced calcium signals and interleukin release. This study identifies TMEM16J as a major regulator of intracellular Ca2+ signaling, ion channel activity and inflammation, and suggests a pronounced impact of TMEM16J in the immune response by T-lymphocytes.

Keywords: TMEM16J; anoctamin 9; ANO9; chronic renal failure; renal transplant; Ca^{2+} signaling

Published in: Schreiber, R., **Talbi, K.**, Ousingsawat, J., & Kunzelmann, K. (2023). A TMEM16J variant leads to dysregulated cytosolic calcium which may lead to renal disease. *FASEB J*, *37*(1), e22683.

Own experimental contribution: Isolation of primary proximal tubule cells, kidney perfusion, paraffin-embedding, intracellular Ca^{2+} measurements.

Own written contribution: Original draft preparation.

Other contributions: Designed experiments and analysed data**.**

Introduction

Exaggerated immune response is inhibited by extra- and intracellular mechanisms [124]. A genetic region encoding single immunoglobulin interleukin-1 related receptor (SIGIRR), plakophilin 3 (PKP3) and transmembrane 16 protein member J, (TMEM16J, anoctamin 9) was identified as essential negative regulator of immune response [125,270]. Common single nucleotide polymorphisms (SNPs) in the SIGIRR-PKP3-TMEM16J gene region are associated with tuberculosis, and studies of SIGIRR-deficient mice suggest a central role of SIGIRR for negative regulation of innate immune pathways and adaptive immune response [125,271-273]. Thus, SIGIRR is known to control colonic epithelial homeostasis, inflammation, and tumorigenesis [273], and negatively regulates adaptive immunity against kidney grafts [274]. Importantly, dendritic cells lacking expression of SIGIRR release more IL-6 upon stimulation with toll-like receptor 4 (TLR4) ligands or TNF-α, which contributes to rejection of renal grafts [274]. Dendritic cells and T-cells are key players in allograft rejection and renal diseases, and thus modulation of their function represents a therapeutic strategy [275]. Dendritic cells can be derived from monocytes exposed to GM-CSF and IL-4 and subsequently mature by LPS-binding to TLR4, a process that is strongly supported by vitamin D [276]. Remarkably, low VitD levels in people carrying SIGIRR-PKP3-TMEM16J host variants are associated with tuberculosis and death of HIV-Infected infants [277].

Members of the TLR/IL-1R superfamily mediate ischemia/reperfusion injury and initiate immune response in transplanted kidneys, a process that is modulated by SIGIRR [274]. Stanzick and collaborators demonstrated a role of SIGIRR and TMEM16J for chronic renal failure, which is characterized by reduction in glomerular filtration and increased urinary albumin excretion [120,278]. A large GWAS meta-analysis of creatinine-based estimated glomerular filtration rates (eGFR) in chronic kidney disease (CKD) patients was performed by a genetics consortium and the UK Biobank. Prioritization revealed several compelling CKD-related genes, among them were SIGIRR and TMEM16J [120]. The TMEM16J variant T604A was one of the top hits related to CKD. We speculated that loss of function of either SIGIRR, PKP3 or TMEM16J predisposes to hyperinflammation and renal failure. An impaired SIGIRR-PKP3-TMEM16J cascade may no longer prevent tissue injury due to overshooting initiate immune responses in transplanted kidneys and during postischemic activation of intrarenal myeloid cells [279].

The immunomodulatory role of SIGIRR at the level of IL-1 and Toll-like receptors, and its role in inflammatory diseases are well described [218,280,281]. However. it remains puzzling how TMEM16J dampens initiate immune responses. Our previous work demonstrated a role of TMEM16 proteins in intracellular Ca^{2+} signaling and for the release of cytokines [116]. Here we examined whether TMEM16J controls intracellular Ca^{2+} signals and thereby affects renal cellular immune responses and inflammation. The results provide a molecular mechanism by which the TMEM16J variant TMEM16J-T604A may lead to CKD and renal failure.

Materials and Methods

Cell culture and transfection. Human Embryonic Kidney (HEK) 293T were cultured in DMEM (Dulbecco's Modified Eagle Medium, Thermo Fisher Scientific, Darmstadt, Germany) with 10% FBS, without antibiotics. HEK293 cells were transfected with siRNA against TMEM16J (Stealth RNAi, Invitrogen, Thermo Fisher, Scientific, Waltham, MA 02451, USA) or scrambled siRNA (Stealth RNAi, Invitrogen, Thermo Fisher, Scientific, Waltham, MA 02451, USA) using standard protocols for Lipofectamine 3000 (Thermo Fisher Scientific, Darmstadt, Germany). All experiments were performed 48-72h after transfection. Successful knockdown of anoctamins was demonstrated by real time RT-PCR. IHKE-1 cells were cultured with HAM's F12 (Life Technologies/Gibco®, Karlsruhe, Germany) and Dulbecco's modified Eagle's medium (Life Technologies/Gibco®, Karlsruhe, Germany) 1:1, supplemented with 15 mM HEPES (Life Technologies/Gibco®, Karlsruhe, Germany), 100,000 U/l penicillin and 100 mg/l streptomycin (Life Technologies/Gibco®, Karlsruhe, Germany), 10 µg/l epidermal growth factor (Calbiochem, Bad Soden, Germany), 36 µg/l hydrocortisone (Sigma-Aldrich, Merck KGaA, Darmstadt, Germany), 1% fetal calf serum (Life Technologies/Gibco®, Karlsruhe, Germany), 912 mg/l $NaHCO_3$ (Merck, Darmstadt, Germany), 5 mg/l insulin (Sigma-Aldrich, Merck KGaA, Darmstadt, Germany), 5 mg/l transferrin (SigmaAldrich, Merck KGaA, Darmstadt, Germany), 5 µg/l Na^+ selenite (Sigma-Aldrich, Merck KGaA, Darmstadt, Germany), 55 mg/l Na^+ pyruvate (Sigma-Aldrich, Merck KGaA, Darmstadt, Germa) and 2 mM L-glutamine (Life Technologies/Gibco®, Karlsruhe, Germany). Cells were incubated with LPS 100 ng/ml (L9143, Sigma-Aldrich, Merck KGaA, Darmstadt, Germa) for 24h. All cells were cultured at 37°C in a humidified atmosphere of 5% (v/v) CO_2.

Isolation of cortical primary cells. Mice were killed by cervical dislocation after exposure to CO_2. Kidneys were removed and kept in ice-cold DMEM/F12 medium (Thermo Fisher Scientific, Darmstadt, Germany). The renal capsule was removed under germ-free conditions. Cortex and medulla were separated and chopped into smaller pieces of tissue using a sharp razor blade (Heinz Herenz, Hamburg, Germany). Tissues were incubated in Hanks balanced salt solution/DMEM/F12 (Life Technologies/Gibco®, Karlsruhe, Germany) containing 1 mg/ml collagenase type 2 (Worthington, Lakewood, USA) for 20 min at 37° C. The digested tissue was passed through a 100 µm cell strainer (Merck KGaA, Darmstadt, Germany), transferred to a 50 ml falcon tube and washed with ice cold PBS. After centrifugation at 5100 rpm for 4 min / 4° C, cells were resuspended. After resuspension, the cortical cell pellet was centrifuged at 17500 rpm for 30 min at 4° C through a 45 % Percoll (Ge Healthcare GmbH, Munich, Germany) 55 % 2X PBS-Glucose gradient. After washing with ice-cold PBS, tubular preparations were maintained at 37 °C / 5 % CO_2 in DMEM/F12 supplemented with 1 % FBS, 1 % Pen/Strep, 1 % L-Glutamine (200 mM), 1 % ITS (100x), 50 nM hydrocortisone, 5 nM triiodothyronine, and 5 nM

Epidermal Growth Factor (Sigma Taufkirchen, Germany). After 24 hours, primary cells grew out from isolated tubules.

Immunohistochemistry, Immunofluorescence. Mouse kidneys were fixed by perfusion with 4% paraformaldehyde and post-fixed in 0.5 mol/l sucrose and 4% paraformaldehyde solution. The paraffin-embedded tissues were cut at 5 µm on a rotary microtome (Leica Mikrotom RM 2165, Wetzlar, Germany). The sections were de-waxed and re-hydrated. For immunohistochemistry section were cooked in citrate buffer (pH 6) for 15 min and permeabilized and blocked with 0.04% Triton X-100 and 5% BSA for 30 min at 37°C. Sections were incubated with primary antibodies against TMEM16J (DPAB23788, Lot: LLE290412, Creative Diagnostics, Shirley, NY 11967, USA), megalin (sc-515750, Lot: F2821, Santa Cruz, Dallas, Texas 75220, USA), calbindin (#300, Lot: 07, Swant, PO Box 327, 1723 Marly 1, Switzerland) and AQP2 (sc-9882, Lot: D2910,Santa Cruz, Dallas, Texas 75220, USA) in 0.5% BSA and 0.04% Triton X-100 overnight at 4 °C and subsequent with a secondary donkey anti-rabbit Alexa 555 (for TMEM16J, ab150074, Lot: GR3241278-7, Abcam, Berlin, Germany), donkey anti goat Alexa 488 (for AQP2; A11055, Lot: 1087906), donkey anti mouse Alexa 488 (A21202, Lot: 1915874, for calbindin) or donkey anti mouse Alexa 660 (A21055, Lot: 1495928, for megalin) IgG (Invitrogen, Thermo Fisher, Scientific, Waltham, MA 02451, USA) for 1h at 37°C. Sections were counterstained with Hoe33342 (Sigma-Aldrich, Merck KGaA, Darmstadt, Germany). For cellular localisation HEK293T cells were transfected with TMEM16J tagged with mcherry or GFP in pcDNA31 or SIGIRR tagged with CFP in pcDNA31. Endoplasmic reticulum (ER) was visualised using ER-Tracker (BlueWhite DPX, E12353, Lot: 1177457, Invitrogen, Thermo Fisher, Scientific, Waltham, MA 02451, USA). Plasma membrane was stained with FM 4-64 (T13320, Lot: 1702510, molecular probes, Invitrogen, Thermo Fisher, Scientific, Waltham, MA 02451, USA). Immunofluorescence was detected using an Axiovert Observer microscope equipped with ApoTome2 and ZEN 2.6 (blue edition) Software (Carl Zeiss Microscopy Deutschland GmbH, Oberkochen, Germany).

RT-PCR. For semi-quantitative RT-PCR total RNA from tracheal epithelial cells, lung tissue, Calu3 or 6CFSMEo$^-$ cells was isolated using NucleoSpin RNA II columns (Macherey-Nagel, Düren, Germany). Total RNA (0.5 µg / 25 µl reaction) was reverse-transcribed using random primers (Promega, Mannheim, Germany) and M-MLV Reverse Transcriptase RNase H Minus (Promega, Mannheim, Germany). Each RT-PCR reaction contained sense (0.5 µM) and antisense primers (0.5 µM) (table 1), 0.5 µl cDNA and GoTaq Polymerase (Promega, Mannheim, Germany). After 2 min at 95°C, cDNA was amplified (targets 30-35 cycles, reference Gapdh 25 cycles) for 30 s at 95°C, 30 s at 56°C and 1 min at 72°C. PCR products were visualized by loading on Midori Green Xtra (Nippon Genetics Europe) containing agarose gels and analysed using Image J 1.52r (NIH, USA).

Measurement of $[Ca^{2+}]i$. Measurement of cytosolic Ca^{2+} changes were performed as described recently [86]. In brief, HEK293T, IHKE and cortical primary cells were loaded with 2 µM Fura-2, AM (BIOZOL, Eching, Germany) in OptiMEM (Gibco, Thermo Fisher, Scientific, Waltham, MA 02451, USA) with 0.02% Pluronic F-127 (Invitrogen, Thermo Fisher, Scientific, Waltham, MA 02451, USA) in ringer solution (mmol/l: NaCl 145; KH_2PO_4 0,4; K_2HPO_4 1,6; Glucose 5; $MgCl_2$ 1; Ca^{2+}-Gluconat 1,3) for 1h at room temperature. Fluorescence was detected in cells perfused with Ringer's solution at 37 °C using an inverted microscope (Axiovert S100, Zeiss, Germany) and a high speed polychromator system (VisiChrome, Puchheim, Germany). Fura-2 was excited at 340/380 nm, and the emission was recorded between 470 and 550 nm using a CCD-camera (CoolSnap HQ, Visitron Systems, Germany). $[Ca^{2+}]_i$ was calculated from the 340/380 nm fluorescence ratio after background subtraction. The formula used to calculate $[Ca^{2+}]_i$ was $[Ca^{2+}]_i = Kd \times (R-R_{min})/(R_{max}-R) \times (S_{f2}/S_{b2})$, where R is the observed fluorescence ratio. The values R_{max} and R_{min} (maximum and minimum ratios) and the constant S_{f2}/S_{b2} (fluorescence of free and Ca^{2+}-bound Fura-2 at 380 nm) were calculated using 2 µmol/liter ionomycin (Biomol GmbH, Hamburg, Germany) and 5 mmol/liter EGTA to equilibrate intracellular and extracellular Ca^{2+} in intact Fura-2-loaded cells. The dissociation constant for the Fura-2•Ca^{2+} complex was taken as 224 nmol/liter [282]. ER Ca^{2+} signals were detected in Ca^{2+} sensor ER-LAR-GECO1 (Addgene, Cambridge, MA, USA, [283]) expressing cells. Cells were excited at 560 nm and emission was recorded between 620±30 nm. Control of experiment, imaging acquisition, and data analysis were done with the software package Meta-Fluor (Universal imaging, USA).

Measurement of IL-6 and IL-8 release. IL-6 and IL-8 secretion were detected by using quantikine colorimetric sandwich ELISA kits (R&D systems, Wiesbaden-Nordenstadt, Germany). IHKE1 cells overexpressing TMEM16J and silencing TMEM16J were treated with 100 ng/ml lipopolysaccharides (LPS, Sigma, Taufkirchen, Germany). The supernatants were collected after 24 hrs of LPS treatment. Particulates were removed by centrifugation and assay immediately according to the protocol for the company. The signal was detected by using microplate reader NOVOstar (BMG Labtech, Offenburg, Germany).

Patch Clamp. Cells were patch clamped when grown on coated glass coverslips. Coverslips were mounted in a perfused bath chamber on the stage of an inverted microscope (IM35, Zeiss) and kept at 37 °C. Patch pipettes were filled with a cytosolic-like solution containing (in mM): KCl 30, K-Gluconate 95, NaH_2PO_4 1.2, Na_2HPO_4 4.8, EGTA 1, Ca-Gluconate 0.758, $MgCl_2$ 1.03, D-Glucose 5, ATP 3; pH 7.2. The intracellular (pipette) Ca^{2+} activity was 0.1 µM. The bath was perfused continuously with standard bicarbonate-free Ringer's solution (in mM: NaCl 145, KH_2PO_4 0.4, K_2HPO_4 1.6, Glucose 5, $MgCl_2$ 1, Ca-Gluconate 1.3) at a rate of 8 ml/min. Patch pipettes had an input resistance of 2–5 MΩ and whole cell currents were corrected for serial

resistance. Currents were recorded using a patch clamp amplifier EPC9, and PULSE software (HEKA, Lambrecht, Germany) as well as Chart software (AD Instruments, Spechbach, Germany). Cells were stimulated with 1 µM ATP in the absence and presence of TRAM34. In regular intervals, membrane voltage (*V*c) was clamped in steps of 20 mV from -100 to +100 mV from a holding voltage of -100 mV. Current density was calculated by dividing whole cell currents by cell capacitance.

Materials and statistical analysis. All compounds used were of highest available grade of purity and were bought from Sigma-Aldrich (Merck KGaA, Darmstadt, Germany), unless indicated otherwise. Data are shown as individual traces/representative images and/or as summaries with mean values ± SEM, with the respective number of experiments given in each figure legend. For statistical analysis, paired or unpaired Student's t-test or ANOVA were used as appropriate. A *p*-value of < 0.05 was accepted as a statistically significant difference.

Results

TMEM16J is expressed in the endoplasmic reticulum of mouse proximal tubular epithelial cells.

SIGIRR, TMEM16J and PKP3 limit immune response and dampen inflammation in various organs including kidney [125,271-273,284]. The genetically linked immunosuppressive proteins SIGIRR and TMEM16J are strongly expressed in the human kidney (Supplementary Fig. 1). Renal epithelial SIGGIR expression and function has been demonstrated previously, however, the role of TMEM16J in the kidney is entirely unknown. Immunocytochemistry of TMEM16J in mouse kidney identified expression in cortex and medulla as indicated by co-staining with the marker proteins megalin (proximal tubule), calbindin (distal tubule) and aquaporin 2 (AQP2; collecting duct). Most prominent expression was found in the proximal tubule (Fig. 1a). In isolated mouse primary proximal tubular epithelial (MPTE) cells TMEM16J was found to be expressed in the endoplasmic reticulum (ER) but not in the plasma membrane (Fig. 1b). Similar, overexpressed of TMEM16J in HEK293 cells was also localized in the ER, while SIGIRR was expressed in the plasma membrane (Fig. 1c).

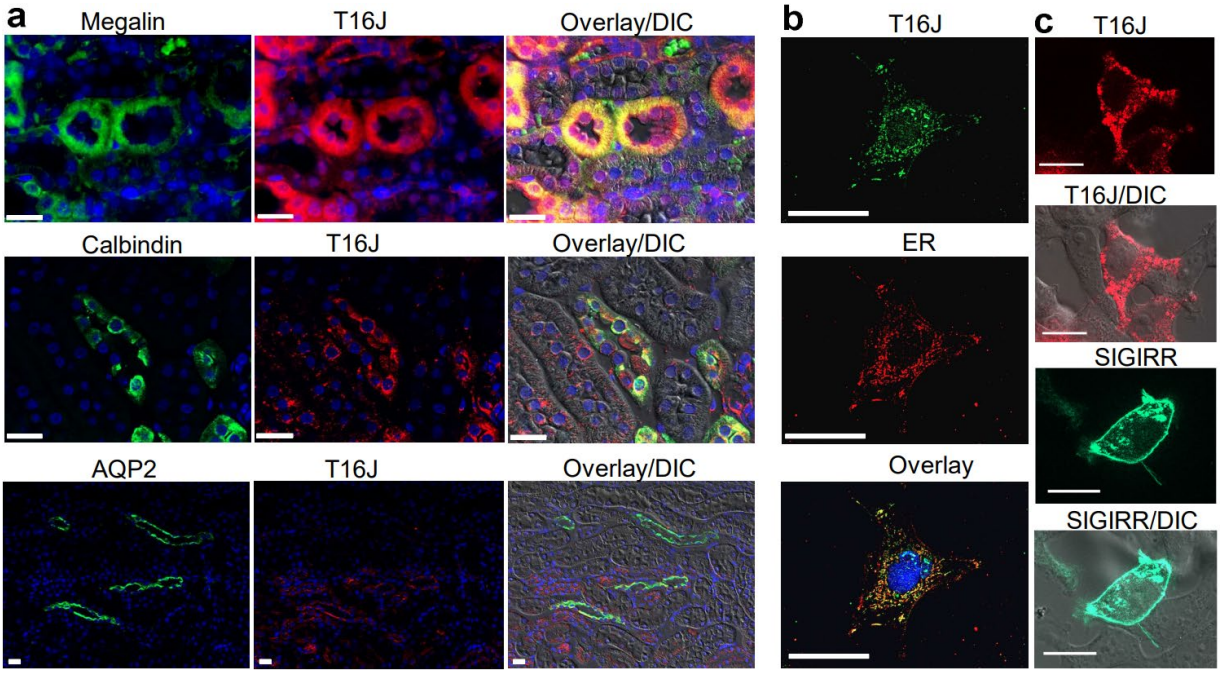

Figure 6.1 | *Expression of TMEM16J in the endoplasmic reticulum of renal epithelial cells.*

a) Preferential Expression of TMEM16J (red) in proximal tubular epithelial cells of mouse kidney. Co-staining with markers of proximal tubules (megalin), distal tubule (calbindin) and collecting duct (aquaporin 2; AQP2). TMEM16J was located in intracellular compartments. **b)** Co-staining of TMEM16J (green) with calreticulin (red) identifies preferential location in the endoplasmic reticulum (ER) of mouse primary proximal tubular epithelial cells. **c)** Overexpression of TMEM16J and SIGIRR in HEK293 cells indicates expression of TMEM16J in the ER, while SIGIRR is expressed in the plasma membrane.

TMEM16J may operate as an ER-localized Ca^{2+}-leak channel.

Like in renal epithelial cells, TMEM16J overexpressed in HEK293 cells is located in the ER, but not in the plasma membrane, as reported in a previous study (Fig. 2a) [285]. ER-location was identical for both wild type TMEM16J (T16J) and for the TMEM16J variant TMEM16J-T604A (T16J-T604A) that was found to be associated with chronic kidney disease [120]. We previously described a strong modulation of receptor-mediated Ca^{2+} signaling by TMEM16 proteins [116] and therefore compared the potential effects of T16J and T16J-T604A on intracellular Ca^{2+}. Basal intracellular Ca^{2+} levels ($[Ca^{2+}]_i$) were enhanced by both T16J and T16J-T604A (Fig. 2b). Receptor-mediated increase in cytosolic Ca^{2+} by purinergic stimulation with ATP was strongly reduced in cells expressing T16J. This inhibitory effect on $[Ca^{2+}]_i$ was attenuated in T16J-T604A expressing cells (Fig. 2c,d). Importantly, inhibition of ER-Ca^{2+} store release (peak) and store operated Ca^{2+} influx (SOCE; plateau) was attenuated for T16J-T604A. The results indicate inhibition of Ca^{2+} release and/or attenuated ER-store filling in the presence of T16J, with both effects being reduced for T16J-T604A. This was further analyzed by emptying the ER Ca^{2+} store with the SERCA-inhibitor cyclopiazonic acid (CPA). Notably, Ca^{2+} release by CPA and store operated Ca^{2+} entry (SOCE) were reduced in T16J-T604A expressing cells (Fig. 2e-g).

We compared directly the intra-ER Ca^{2+} concentrations ($[Ca^{2+}]_{ER}$) using the Ca^{2+} sensor ER-

LAR-GECO1. The data indicated a clearly reduced basal $[Ca^{2+}]_{ER}$ for both T16J and T16J-T604A expressing cells. The relatively low Ca^{2+} sensitivity of ER-LAR-GECO1 did not allow to resolve further differences, but did indicate attenuated ATP-induced Ca^{2+} release for both T16J and T16J-T604A, while subsequent CPA-induced release was not different to mock-transfected cells (Fig. 2h-j). The data suggest that T16J operates as an ER Ca^{2+} leak channel that lowers $[Ca^{2+}]_{ER}$.

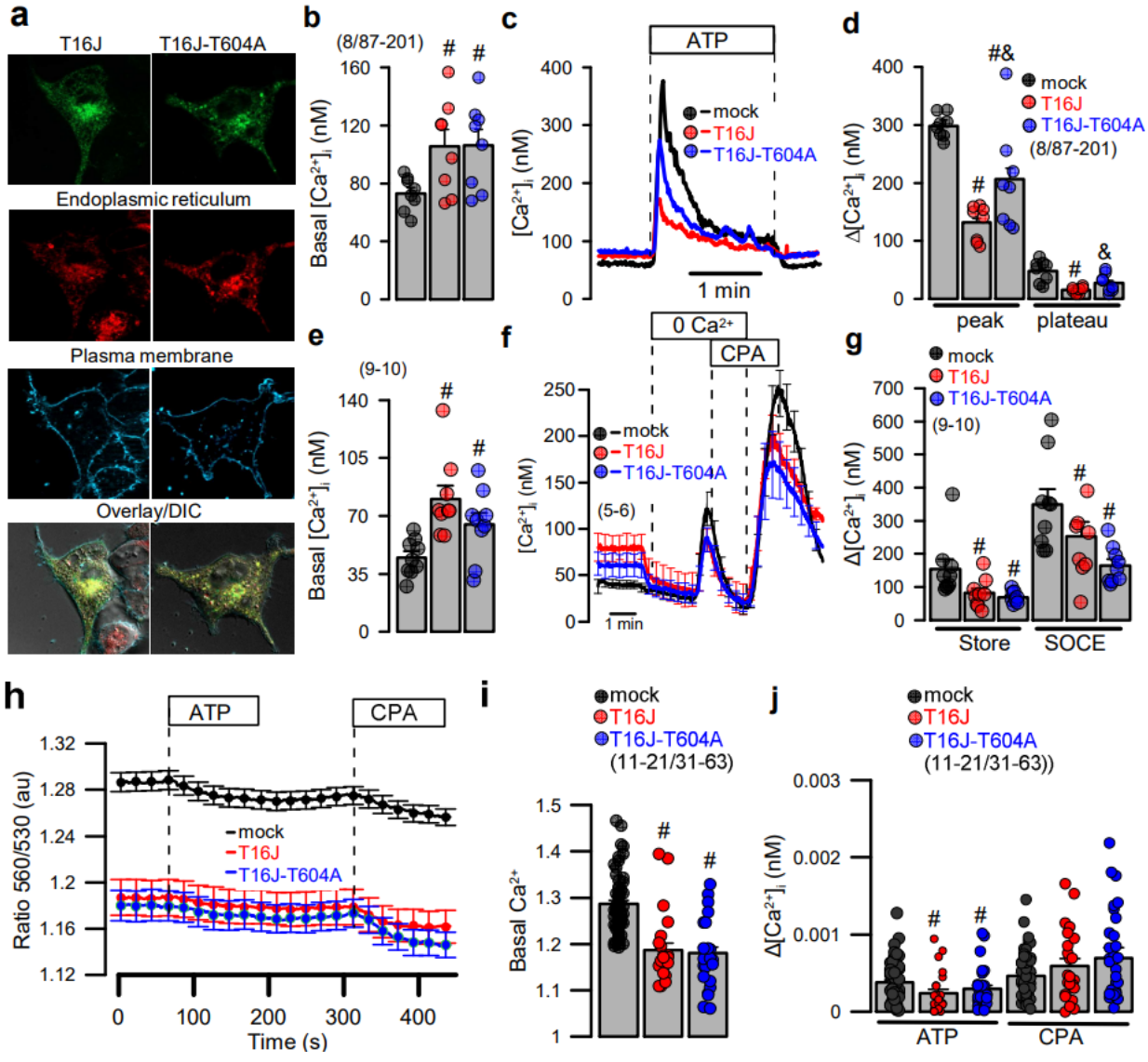

Figure 6.2 | ***TMEM16J and the variant TMEM16J-T604A attenuate intracellular Ca^{2+} signals by lowering ER-Ca^{2+} load.***

a) Life co-staining of the ER (red, ER-tracker) and the plasma membrane marker (cyan FM4-64; Molecular Probes) identifies expression (green, GFP) of TMEM16J (left) and TMEM16J-T604A (right) predominantly in the ER, but not in the plasma membrane of overexpressing HEK293 cells. **b**) Fura2 Ca^{2+}-measurements indicate higher basal intracellular Ca^{2+} levels of HEK293 cells expressing TMEM16J or TMEM16J-T604A, when compared to mock transfected cells. **c,d**) ATP (100 µM) induced ER Ca^{2+} store release is attenuated by TMEM16J and to a lesser extent by TMEM16J-T604A. **e-g**) Basal Ca^{2+}

levels are inhibited significantly by removal of extracellular Ca^{2+} (0 Ca^{2+}) in TMEM16J and TMEM16J-T604A expressing cells, but not in mock transfected cells. ER store release induced by the SERCA-inhibitor CPA (10 µM) and store-operated Ca^{2+} influx (SOCE) upon re-addition of extracellular Ca^{2+} is attenuated in TMEM16J and TMEM16J-T604A expressing cells. **h-j**) ER-Ca^{2+} measured with the dye ER-LAR-GECO1, indicates lower ER-Ca^{2+} levels and attenuated ATP-induced Ca^{2+} release for both TMEM16J and TMEM16J-T604A expressing cells. Mean ± SEM (number of cover slips analyzed/number of individual experiments). #significant difference when compared to mock ($p<0.05$; ANOVA).

Enhanced activity of PMCA in the presence of TMEM16J curtails intracellular Ca^{2+} signals.

T16J interacts with the scaffold protein DLG1, which controls the activity of the plasma membrane Ca^{2+}-ATPase (PMCA) (http://www.interactome-atlas.org). PMCA is ubiquitously expressed and plays a key role in fine tuning the magnitude and duration of intracellular Ca^{2+} signals following activation of G-protein-coupled receptors (GPCRs) [286]. PMCA is also expressed in HEK293, immortalized human proximal kidney epithelial (IHKE-1) and MPTE cells (Supplementary Fig. 2). A signal compartment close to the plasma membrane containing T16J, DLG1 and PMCA could lead to activation of PMCA and curtailed Ca^{2+} signals as observed in T16J expressing cells. In fact, HEK293 cells expressing T16J or T16J-T604 showed short-lived Ca^{2+} signals upon stimulation of GPCRs, by reducing the duration of the Ca^{2+} plateau (Fig. 3a-c). We found that vanadate, an inhibitor of PMCA, enhanced plateau-Ca^{2+} and prolonged Ca^{2+} signals to Ca^{2+} plateau durations found in the absence of T16J (Fig. 3d-f). It should be mentioned that experiments with the more specific PMCA-inhibitor caloxin 1B1 also prolonged Ca^{2+} signals in cells expressing TMEM16J (data not shown). Taken together, the data suggest upregulation of PMCA-function in the presence of TMEM16J, possibly by relocating local intracellular $[Ca^{2+}]_i$, and activation of calmodulin, which disinhibits PMCA [286].

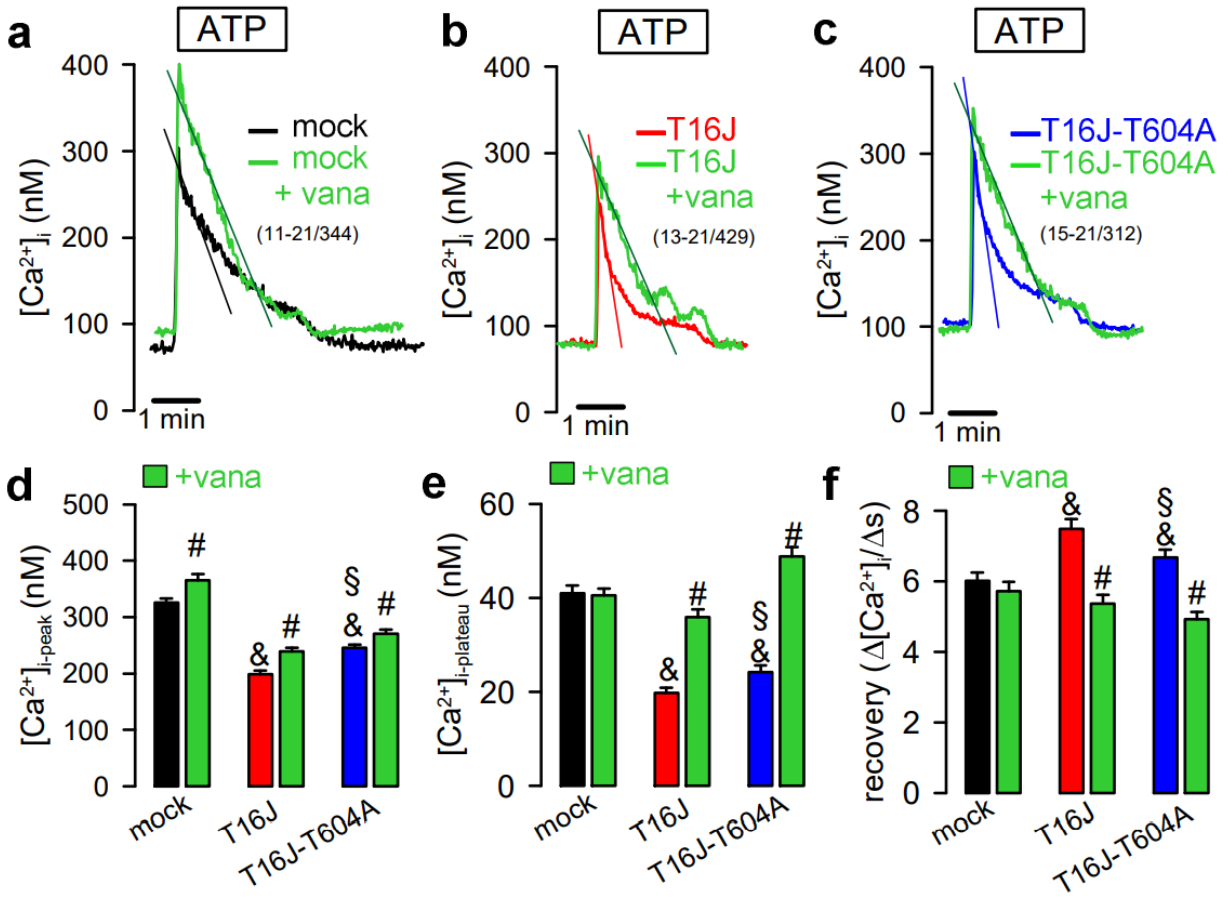

Figure 6.3 | *Enhanced PMCA-activity in cells expressing TMEM16J and TMEM16J-T604A.*
a-c) Original recordings of the intracellular Ca2+ concentrations measured by Fura2 in mock-transfected and TMEM16J or TMEM16J-T604A expressing HEK293 cells in the absence or presence of the PMCA-inhibitor vanadate (vana; 200 µM). **d-f**) Vanadate enhanced the ATP-induced plateau and prolonged the recovery from ATP-induced Ca2+ increase in TMEM16J or TMEM16J-T604A expressing cells but not in mock transfected cells. Because of the large number of individual observations, the scatter blot has been omitted. Mean ± SEM (number of cover slips analyzed/number of individual experiments). #significant difference when compared to mock ($p<0.05$; ANOVA).

Ca^{2+}-dependent activation of whole cell currents by TMEM16J which is compromised in the variant TMEM16J-T604A.

Endogenous TMEM16J in MPTE cells and overexpressed TMEM16J in HEK293 cells is located in the ER. In fact, using patch clamp recordings we did not measure additional whole cell membrane currents in HEK293 cells overexpressing T16J or T16J-T604A (Fig. 4). However, targeting of intracellular transmembrane proteins to the plasma membrane can be enhanced by C-terminal fusion to a CAAX (cysteine, two aliphatic amino acids plus methionin, serine, alanin, cystein or glutamin) motif [287]. Despite fusion to CAAX, a substantial portion of overexpressed CAAX-T16J still remained intracellular, but some CAAX-T16J escaped to the plasma membrane [287]. We detected membrane expression of CAAX-T16J using combined GFP-fluorescence and patch clamp (CAAX-T16J-CFP) and found activation of whole cell

currents by increase in intracellular Ca^{2+} upon stimulation with the purinergic agonist ATP or with the Ca^{2+} ionophore ionomycin [287] (Fig. 4a,b). In contrast, ATP did not activate the variant CAAX-T16J-T604A (CAAX-T16J-T604A-CFP), indicating a defect in Ca^{2+}-dependent activation of T16J-T604A. However, a closer inspection of the calculated current densities revealed enhanced constitutive (basal) currents in cells expressing T16J or T16J-T604A and independent of CAAX (Fig. 4c). Higher basal currents correspond to higher basal Ca^{2+} levels found in cells expressing T16J or T16J-T604A (Fig. 2b,e). The results suggest that both T16J or T16J-T604A produce a ER-Ca^{2+} leak that activates TMEM16F (T16F) expressed endogenously in the plasma membrane of HEK293 cells [253]. Activation of endogenous T16F by the ER-localized T16J-paralog T16D (TMEM16D, ANO4) has been shown previously [116]. T16D was also described as bona fide Ca $^{2+}$-dependent non-selective cation channel [288]. In summary, the data suggest that both T16J and the variant T16J-T604A form ER-localized Ca^{2+} permeable ion channels providing a basal ER Ca^{2+} leak. While T16J is further activated by increase in cytosolic Ca^{2+}, T16J-T604 has lost its Ca^{2+} regulation or the Ca^{2+} response curve was shifted to higher cytosolic Ca^{2+} concentrations Ca^{2+}.

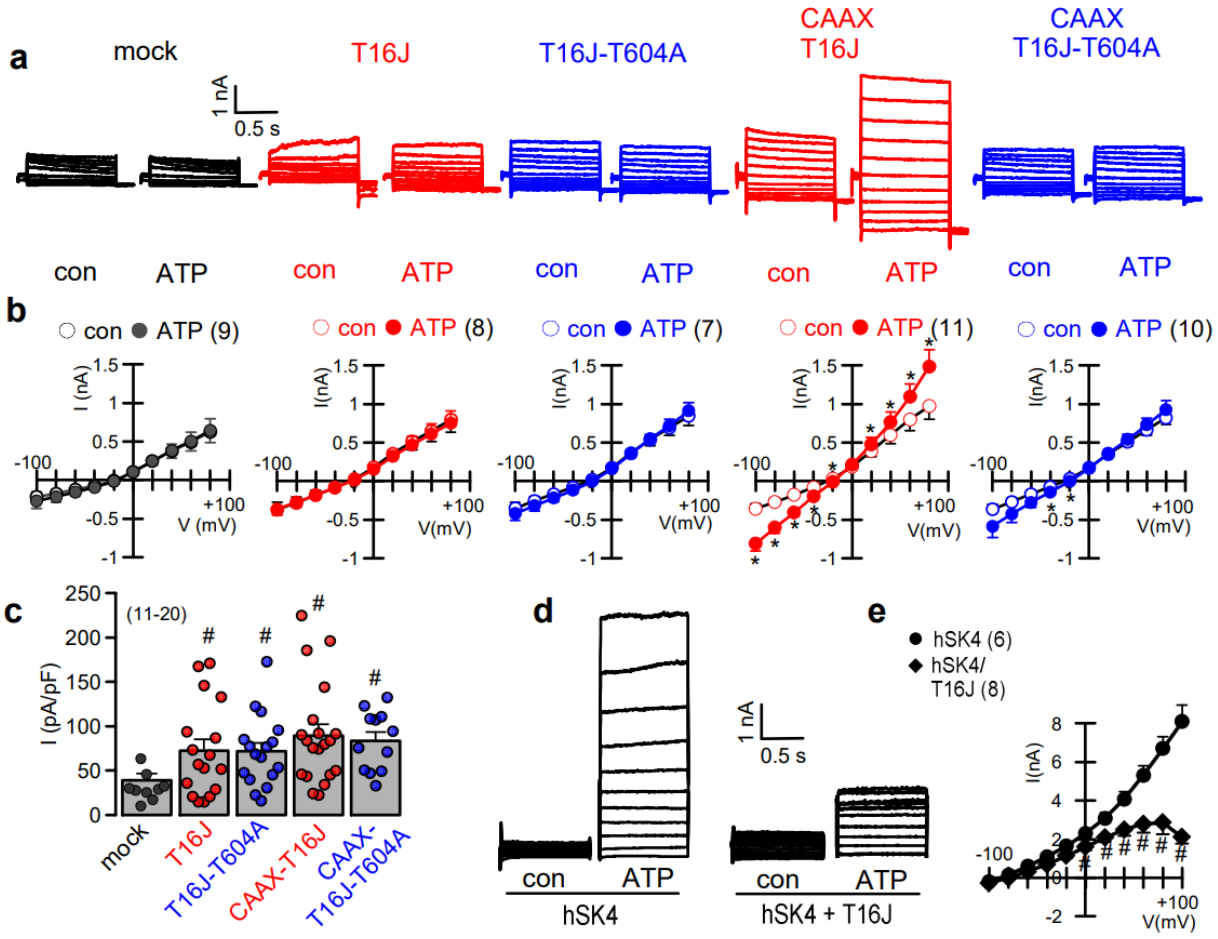

Figure 6.4 | ***TMEM16J is forming a Ca^{2+} permeable ion channel in the endoplasmic reticulum that is impaired in the variant TMEM16J-T604A.***

a,b) Whole cell current overlays of ion currents and corresponding current/voltage relationships before

and after stimulation with ATP (100 mM). TMEM16J and TMEM16J-T604A without or with C-terminal CAAX motif (KKKKSKTKCVIM) were expressed in HEK293 cells and compared with mock-transfected cells. Whole cell currents could be activated by ATP only in TMEM16J-T604A expressing cells. c) Basal current densities (at clamp voltages of +100 mV) indicated enhanced basal currents in TMEM16J, CAAX-TMEM16J and TMEM16J-T604A, CAAX-TMEM16J-T604A expressing cells. **d,e**) Whole cells currents and corresponding I/V curves in cells expressing hSK4 or coexpressing hSK4 and TMEM16J. Ca2+-dependent activation of hSK4 by purinergic stimulation (100 µM ATP) was strongly attenuated by coexpression of TMEM16J. Mean ± SEM (number of cells). *significant activation ATP (paired t-test). # significantly different from mock and hSK4 ($p<0.05$; ANOVA and unpaired t-test, respectively).

We further examined the effect of attenuated ER Ca^{2+}-store filling in the presence of T16J. The Ca^{2+}-activated K^+ channel KCa3.1 (KCNN4; SK4) is activated by stimulation of GPCRs and IP3-mediated Ca^{2+} store release and has an obvious role in innate and adaptive immunity [289,290]. We examined activation of overexpressed hSK4 channels by purinergic stimulation with ATP (Fig. 4d,e). Large hSK4 whole cell currents were activated by ATP, which strongly hyperpolarized the membrane voltage. In contrast, when coexpressed with T16J, activation of hSK4 was strongly attenuated due to reduced ER-store filling and consecutive reduced IP3-mediated Ca^{2+} store release. Thus, T16J attenuates receptor-mediated Ca^{2+} signaling and inhibits activation of Ca^{2+} regulated K^+ channels and TMEM16A Cl^- channels (data not shown).

Renal epithelial cells expressing TMEM16J-T604A present compromised Ca^{2+} signaling leading to constitutive transcription and release of cytokines.

We examined whether regulation of intracellular Ca^{2+} signals by endogenous TMEM16J is present in IHKE-1 renal epithelial cells. IHKE-1 cells express T16J and SIGIRR along with Toll-like receptor 4 (TLR4) (Fig. 5a, Fig. S3). Similar to MPTE cells, T16J is also expressed in the ER membrane of IHKE-1 cells (Fig. 5b). Expression of T16J was potently downregulated by siRNA (Fig. 5c). When stimulated with ATP, increase in intracellular Ca^{2+} was clearly detectable and was even enhanced after knockdown of T16J (Fig. 5d-f). In contrast, additional overexpression of T16J augmented basal Ca^{2+} concentrations and strongly attenuated ATP-induced Ca^{2+} increase, which was somewhat surprising. We therefore sequenced T16J and found homozygous endogenous expression of T16J-T604A instead of T16J, although the A-variant at position 604 of T16J has a frequency of only 3.6 % (Fig. 5g) [120]. Even more surprising, sequencing of two other proximal tubular epithelial cell lines, HK-2 and SA7K, also showed homozygosity for T604A (not shown). We speculated that T604A might provide a selection/growth advantage, but did not detect a change in cell proliferation or cell survival upon knockdown of T16J-T604A (Fig. S4).

Because expression of TMEM16J correlates inversely immune response and inflammation [125,270], we examined whether transcription and/or release of interleukins is affected by expression of T16J-T604A in IHKE-1 cells. mRNA-analysis of IL-6 and IL-8 revealed

constitutive high levels for both pro-inflammatory cytokines, which was hardly further enhanced by stimulation of TLR-4 receptors with lipopolysaccharides (LPS) (Fig. 5i,j). Remarkably, knockdown of T16A-T604A strongly attenuated expression of IL-6 and IL-8 (Fig. 5h-j). Corresponding to high constitutive transcription of IL-6 and IL-8, IHKE-1 cells demonstrated high basal release of IL-6 and IL-8, which, again, was not further enhanced by LPS (Fig. 5k,l). Remarkably, siRNA-knockdown of T16J-T604A strongly inhibited release of both cytokines. Thus, the presence of T16J-T604A induces transcription and release of pro-inflammatory cytokines in IHKE-1 cells.

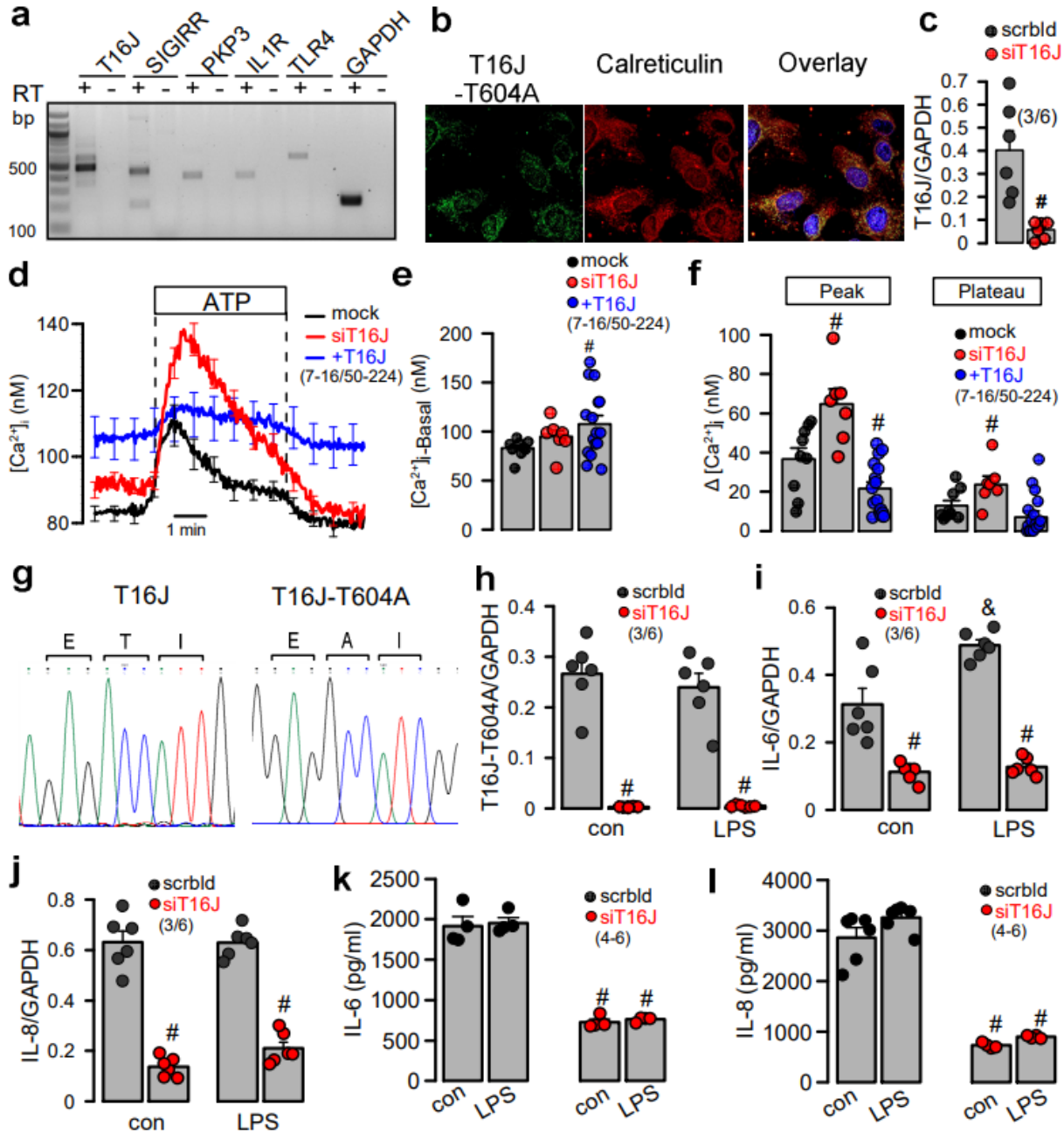

Figure 6.5 | ***Renal epithelial cells expressing T604A-TMEM16J present attenuated Ca^{2+} signaling with constitutive transcription and release of cytokines.***

a) RT-PCR indicating expression of TMEM16J, SIGIRR and PKP3 as well as IL-1R and TLR4 in IHKE1

renal proximal-tubular epithelial cells. **b**) Immunocytochemistry indicate expression of endogenous TMEM16J-T604A in the ER (stained by calreticulin) of IHKE1 cells. **c**) Semiquantitative RT-PCR indicating suppression of TMEM16J-T604A expression by siRNA. **d**) ATP (100 µM) induced increase of intracellular Ca^{2+} in mock-transfected IHKE1 cells (black), and cells treated with siRNA-TMEM16J (red) or overexpressing TMEM16J (blue). **e**) Basal Ca^{2+} levels in IHKE1 cells transfected with siRNA-TMEM16J or TMEM16J. **f**) ATP-induced store release (peak) and SOCE (plateau) in siRNA-TMEM16J or TMEM16J transfected cells. **g**) Sequencing identifying homozygous expression of TMEM16J-T604A in IHKE1 cells. **h**) Semiquantitative RT-PCR indicating suppression of TMEM16J-T604A expression by siRNA in IHKE1 cells, under control conditions and in the presence of LPS. **i,j**) Expression of endogenous IL-6 and IL-8 in the presence or absence (si-T16J) of TMEM16J-T604A. **k,l**) Release of IL-6 and IL-8 by IHKE1 cells in the presence or absence (siT16J) of TMEM16J-T604A. Mean ± SEM (number of coverslips/cells or number of assays). *significant activation ATP (paired t-test). #significant difference to scrambled (scrbld) or mock ($p<0.05$; ANOVA and unpaired t-test, respectively).

Primary renal epithelial cells expressing TMEM16J show no constitutive release of cytokines and LPS-induced release is not inhibited by knockdown of TMEM16J.

Constitutive high release of IL-6 and IL-8 by T16J-T604A expressing IHKE-1 cells asks for comparison with proximal renal epithelial cells expressing T16J. As mentioned, all proximal tubular cell lines (IHKE-1, HK-2, and SA7K) express the variant T604A. We therefore examined MPTE cells, which express mouse wild type T16J (mouse T595 corresponding to human T604). MPTE cells express the proteins of the Tmem16j-Sigirr-Pkp3 gene region along with Tlr4 (Fig. 6a).

T16j could be successfully downregulated by siRNA in both control MPTE cells and cells exposed to LPS (Fig. 6b). In sharp contrast to T16J-T604A expressing IHKE-1 cells, MPTE cells did not show a constitutive transcription of IL-6 or Cxcl1 (corresponding to human IL-8), and cytokine release was negligible under control conditions (Fig. 6c-f). LPS markedly increased transcription and cellular release of IL-6 and CXCL1, independent of expression of T16j. Taken together, the present results demonstrate a role of TMEM16J for ER-Ca^{2+} store filling and intracellular Ca^{2+} signaling which affects gene transcription and release of pro-inflammatory cytokines (Fig. 7). Abnormal intracellular Ca^{2+} signaling in people carrying the T16J-T604A variant may lead to chronic renal disease [120].

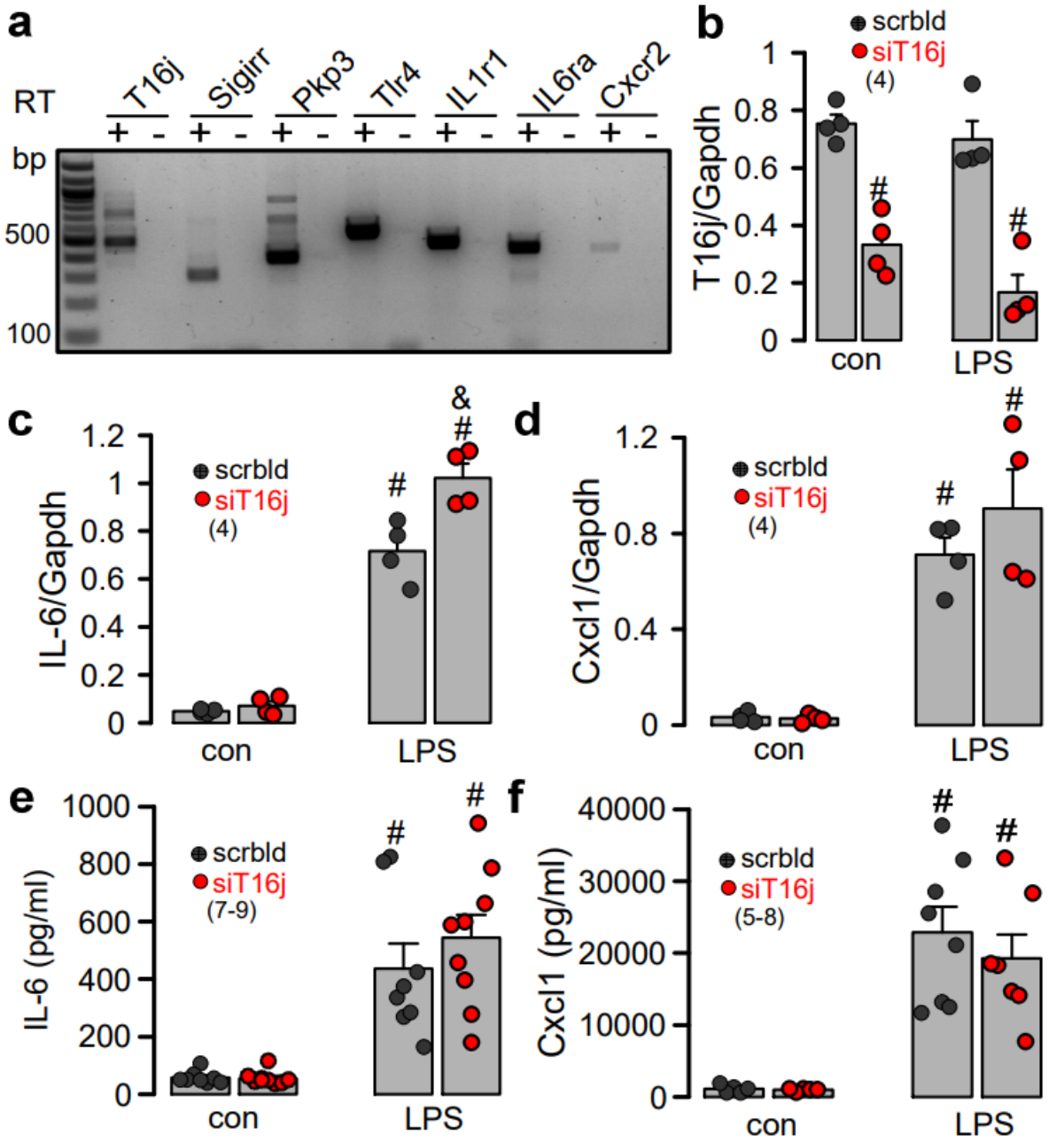

Figure 6.6 | *LPS is required for interleukin release in primary renal epithelial cells which is not inhibited by knockdown of TMEM16J.*

a) RT-PCR indicating expression of TMEM16J, SIGIRR and PKP3 and cytokine receptors / TLR4 in mouse primary renal tubular epithelial (MPTE) cells. **b**) Semiquantitative RT-PCR indicating suppression of TMEM16J-expression by siRNA. **c,d**) Expression of endogenous IL-6 and Cxcl1 in MTPE cells in the presence or absence of TMEM16J, and before and after stimulation with LPS. **e,f**) Release of IL-6 and Cxcl1 by MPTE cells in the presence or absence of TMEM16J, and before and after stimulation with LPS. Mean ± SEM (number of assays). #significant difference compared to control ($p<0.05$; unpaired t-test). &significant difference compared to scrbld ($p<0.05$; unpaired t-test).

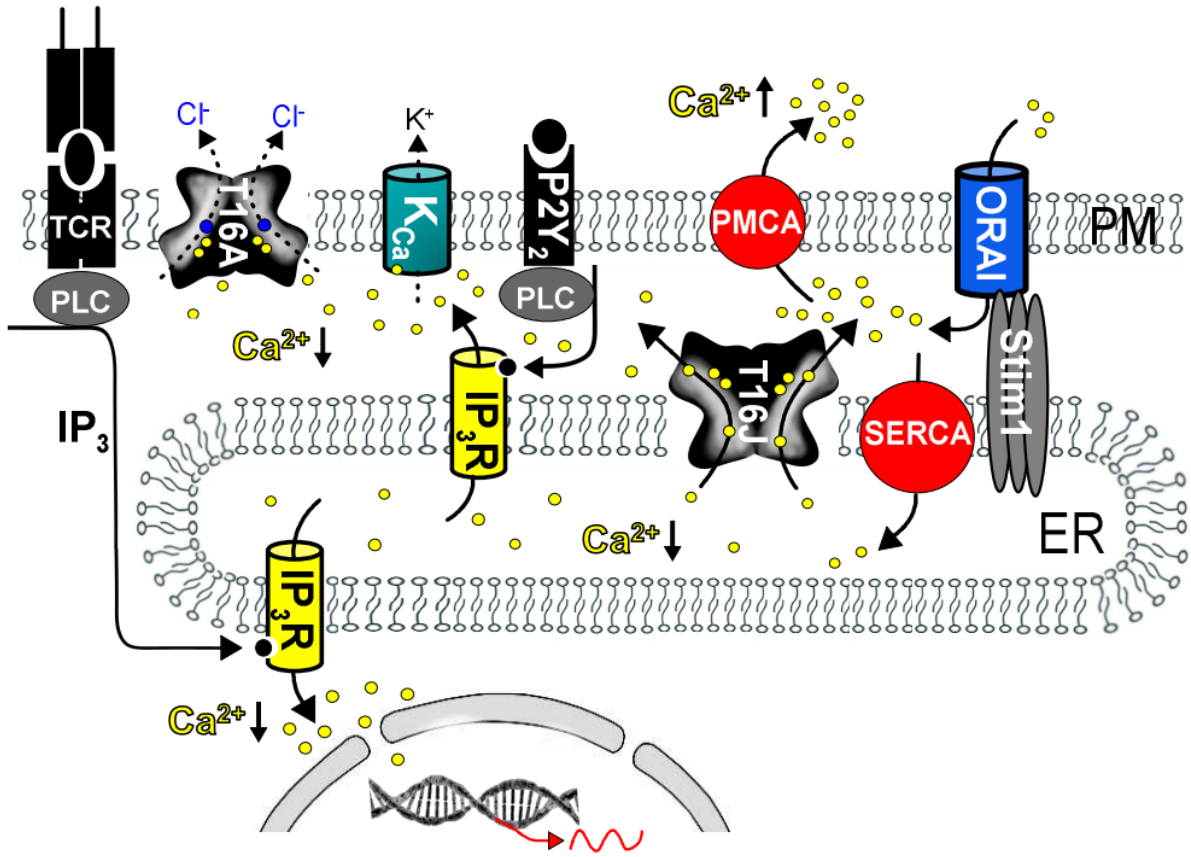

Figure 6.7 | Model for attenuated Ca^{2+} signaling and suppression of immune response by TMEM16J.

TMEM16J (T16J) is a Ca^{2+} activated Ca^{2+} leak channel in the endoplasmic reticulum (ER) which lowers loading of the ER Ca^{2+} store. Ca2+ outward transport by the plasma membrane Ca^{2+} -ATPase (PMCA) is enhanced, thereby further attenuating Orai/Stim1 and SERCA -mediated refill of the store. Lower store filling leads to attenuated IP3 induced Ca^{2+} release. This GPCR-mediated activation of Ca^{2+} dependent ion channels such as SK4 (KCa) and TMEM16A (T16A) is inhibited, and transcription of inflammatory mediators is attenuated. In T-cells, T-cell receptor mediated Ca^{2+} signaling is also inhibited with the consequence of reduced Ca^{2+} at the immune synapse, lower cytokine production and less proliferation and differentiation. Immune response and inflammation are attenuated.

Discussion

TMEM16J is an ER-localized Ca^{2+}-permeable ion channel that has reduced activity when expressed as T604A variant.

SIGIRR is highly expressed in epithelial cells from kidney, gut and liver, as well as in immune cells such as dendritic cells and T-cells [124]. TMEM16J, a putative ion channel or phospholipid scramblase [257], is located in the same genetic region. Common polymorphisms in the PKP3-SIGIRR-TMEM16J gene region are associated with susceptibility to diverse inflammatory diseases like tuberculosis, pneumonia, enterocolitis, psoriasis, chronic renal disease and many other inflammatory conditions [120,125,272,291]. This suggests that similar to

SIGIRR, also TMEM16J acts as a negative regulator of inflammation and immunity [292]. The present study presents a molecular mechanism by which TMEM16J dampens tissue inflammation elicited by activation of Toll-like or interleukin-1 receptors. A previous study proposed TMEM16J as cAMP-activated Ca^{2+} permeable nonselective ion channel [285]. Here we show that TMEM16J is an intracellular, ER-localized ion channel with negligible expression in the plasma membrane. It was possible to push plasma membrane expression of TMEM16J, by attaching a CAAX motif [287]. CAAX-TMEM16J was activated by GPCR-mediated Ca^{2+} increase, while CAAX-TMEM16J-T604A could not be activated. Homology modelling of TMEM16J suggests a location of T604 in the transmembrane domain 9, near the putative Ca^{2+} binding site, which may possibly affect Ca^{2+} binding and opening of the channel (Fig. S5). It has been demonstrated that binding of the compound canthaxanthin to TMD9 activates the TMEM16J paralogue TMEM16A, probably by changing its Ca^{2+} sensitivity [293]. We therefore speculate that TMD9 in TMEM16J may similarly affect Ca^{2+} sensitivity of TMEM16J. In contrast, we did not detect activation by increase of intracellular cAMP using 3-Isobutyl-1-methylxanthine (IBMX; 100 µM) and forskolin (2 µM) (Fig. S6).

TMEM16J controls intracellular Ca^{2+} signaling.

The data highlight the effect of TMEM16J on intracellular Ca^{2+} signals. Ca^{2+} loading of the ER Ca^{2+} store is lowered in the presence of TMEM16J. While TMEM16J can be further activated by increase in intracellular Ca^{2+}, this was not observed for TMEM16J-T604A (Fig. 4). Direct measurement of $[Ca^{2+}]_{ER}$ using the Ca^{2+} sensor ER-LAR-GECO1 exhibited lower ER-Ca^{2+} for both TMEM16J and TMEM16J-T604A. ER-LAR-GECO1 measurements could not resolve differences between cells expressing TMEM16J and TMEM16J-T604A, probably due to the low Ca^{2+} sensitivity of ER-LAR-GECO1 for Ca^{2+} [116]. According to the present data TMEM16J (and possibly also TMEM16D and TMEM16H) may operate as Ca^{2+}-activated ER Ca^{2+}-leak channels [162,288,294]. Lower ER Ca^{2+} load with TMEM16J and TMEM16J-T604A results in enhanced Ca^{2+} influx under control (non-stimulated) conditions, as shown by removal of extracellular Ca^{2+} (Fig. 2f,g). Unexpectedly, store operated Ca^{2+} entry after ER store emptying by CPA was also attenuated in the presence of TMEM16J or TMEM16J-T604A. Notably, Jha et al demonstrated that the TMEM16J-paralogue TMEM16H tethers the ER to a phosphatidylinositol-4,5-bisphosphate ($PI_{(4,5)}P_2$) rich compartment that contains Orai/Stim1 and the Ca^{2+}-pump PMCA [162]. This compartment allows tight communication of Ca^{2+} transporting proteins to control the intensity of Ca^{2+} signaling. Because TMEM16H, TMEM16J and TMEM16D similarly attenuate receptor-mediated Ca^{2+} signals [116], we could speculate that TMEM16J and TMEM16D have a similar function as TMEM16H. Moreover, homologous proteins such as yeast TMEM16A-paralogue Ist2 and the Ca^{2+} activated Cl^- channel TMEM16A also operate as ER-PM tethers [118]. TMEM16J (and possibly TMEM16D) may therefore also operates as ER-PM tethers, although a search for potential PIP_2/membrane interaction sides

did not reveal a cluster of positively charged amino acids in either C- or N- terminus of TMEM16J (Fig. S8) [295]. Compartmentalized organization of Ca^{2+} transporting proteins by TMEM16J may shorten Ca^{2+} signals due to activation of PMCA, suggesting translocation by TMEM16J of the ER to ER-PM junctions that contains PMCA, similar to TMEM16H (Fig 3). This is further supported by the interaction of TMEM16J with the PDZ-domain protein discs large homolog 1 (Dlg1), a protein that is required for immune cell polarity and regulation of PMCA [286,296-299]. As suggested for TMEM16H [162], absence or compromised function of TMEM16J and failure to build ER/PM compartments may result in runaway Ca^{2+} responses and renal pathology.

Loss of function mutations in TMEM16J cause exaggerated Ca^{2+} signals and organ disease.

The present data show that TMEM16J dampens receptor mediated Ca^{2+} signals and that attenuated TMEM16J-function upsets regulation and probably compartmentalization of intracellular Ca^{2+}. Compromised organ function is also seen for the paralogue TMEM16D [116,162,300]. In the zona glomerulosa of adrenal glands, TMEM16D is one of the most common proteins and limits aldosterone secretion and cell proliferation [300]. Organ disease that occurs through variant-expression of SIGIRR or TMEM16J leads to hyperinflammatory responses by tissue malfunction and/or abnormal T-cell response [271]. Interestingly, decreased numbers of SIGIRR-positive CD4+ T-helper cells is found in patients with systemic lupus erythematosus [301]. Intracellular Ca^{2+} is central to T-cell response and formation of the immunological synapse [302,303]. It is therefore interesting to note, that TMEM16J is expressed at particular high levels in T-helper cells and other specialized T-cells (https://www.proteinatlas.org/ENSG00000185101-ANO9/immune+cell). Modulation of TMEM16J-activity by small molecules may therefore provide a novel toolbox to control T-cell response and inflammation.

Acknowledgements

Supported by the Deutsche Forschungsgemeinschaft (DFG, German Research Foundation), project number 387509280, SFB 1350 (project A3).

Supplementary Materials

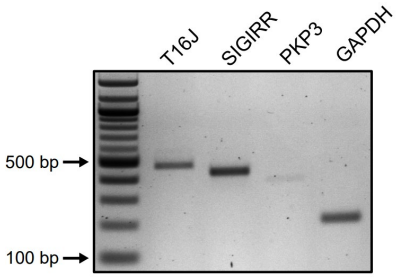

Supplementary figure 6.1 | *Expression of TMEM16J, SIGIRR and PKP3 in human kidney.*
Expression of TMEM16J (T16J), single immunoglobulin interleukin-1 related receptor (SIGIRR), and plakophilin 3 (PKP3) in human kidney, as detected by RT-PCR.

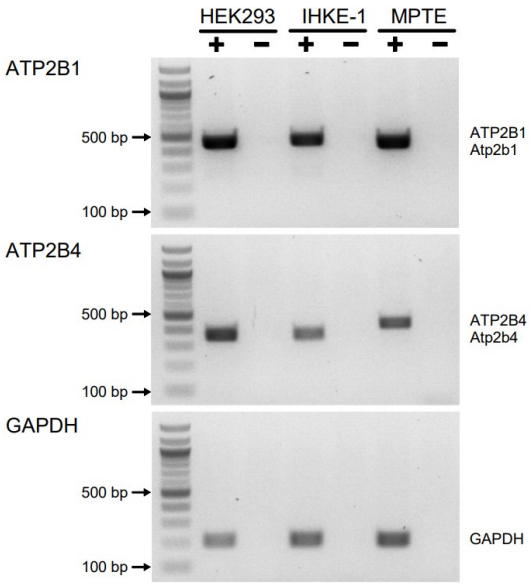

Supplementary figure 6.2 | *Expression of PMCAs.*
Expression of plasma membrane Ca2+-ATPases (PMCA; ATP2B1, ATP2B2) in HEK293 cells, immortalized human kidney epithelial (IHKE-1) cells, and primary proximal tubular epithelial (MPTE) cells, as detected by RT-PCR.

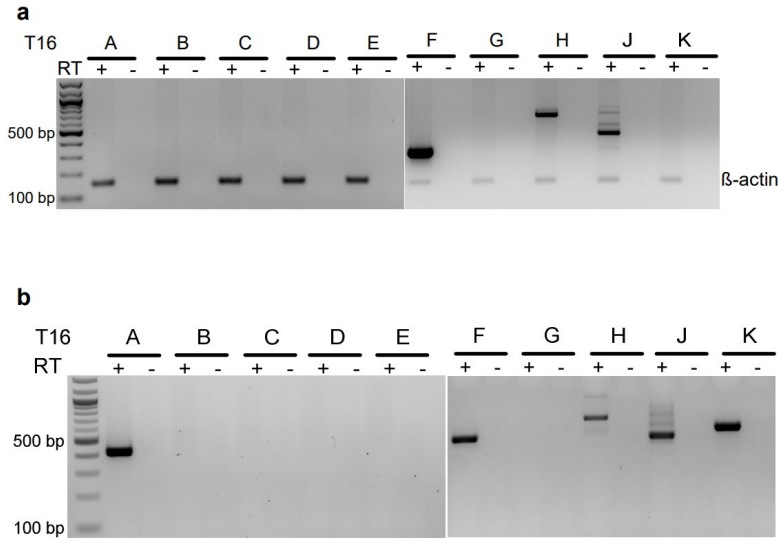

Supplementary figure 6.3 | *Expression of TMEM16 proteins in IHKE-1 and MPTE cells.*

Expression of TMEM16 (T16A) A-K in a) immortalized human kidney epithelial (IHKE-1) and b) mouse primary proximal tubular epithelial (MPTE) cells as detected by RT-PCR.

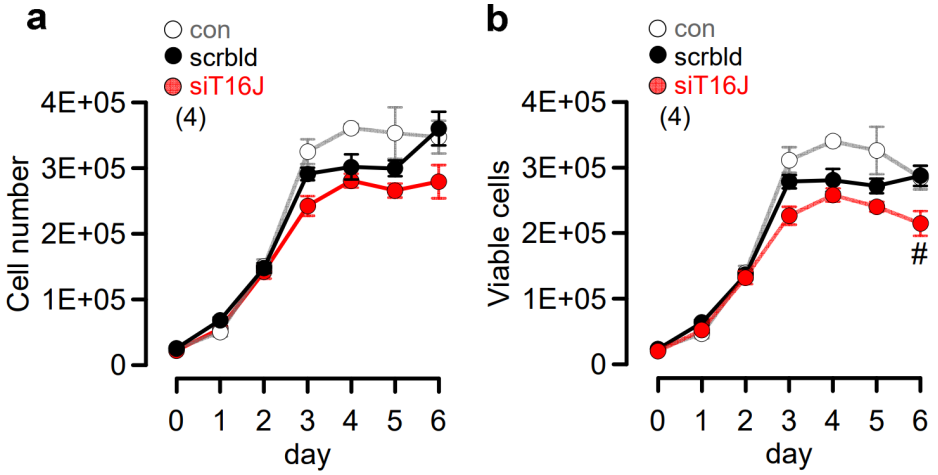

Supplementary figure 6.4 | *Expression of TMEM16 proteins in IHKE-1 and MPTE cells.*

Supplementary Figure 4. Cell proliferation and cell death is not affected by expression of TMEM16J in IHKE-1 cells. **a)** Cell proliferation assed by cell counting of non-transfected (con) cells, and cells treated with scrambled RNA (scrbld) or siRNA for TMEM16J (siT16J). **b)** Number of viable cells. Mean ± SEM (number of experiments).

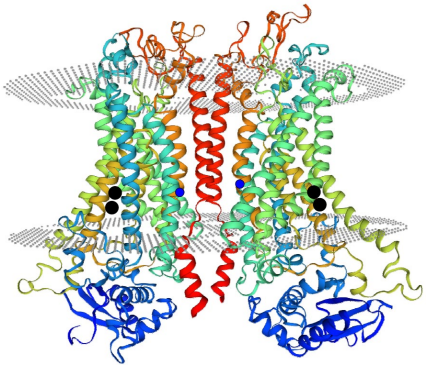

Supplementary figure 6.5 | *Putative structure of TMEM16J.*

Supplementary Figure 5. Putative structure of TMEM16J based on mouseTMEM16F. Sequence identity 35.43% (Waterhouse, A., Bertoni, M., Bienert, S., Studer, G., Tauriello, G., Gumienny, R., Heer, F.T., de Beer, T.A.P., Rempfer, C., Bordoli, L., Lepore, R., Schwede, T. SWISS-MODEL: homology modelling of protein structures and complexes. Nucleic Acids Res. 46(W1), W296-W303 (2018). Black filled circles: Approximate location of Ca2+ binding sites in each subunit. Blue filled circles: Approximate location of T604 in TMD9 (orange helix).

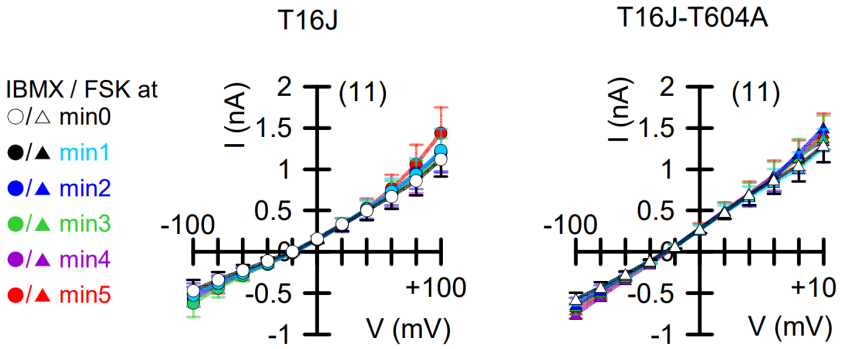

Supplementary figure 6.6 | *No activation of TMEM16J by increase in intracellular cAMP.*

TMEM16J (T16J) and the variant TMEM16JT604A (T16J-T604A) were expressed in HEK293 cells. Over a time period of 5 min intracellular cAMP was enhanced by stimulation with 3-Isobutyl-1-methylxanthine (IBMX; 100 µM) and forskolin (2 µM), which did not activate additional whole cell currents. Current/voltage relationships with mean ± SEM (number of experiments).

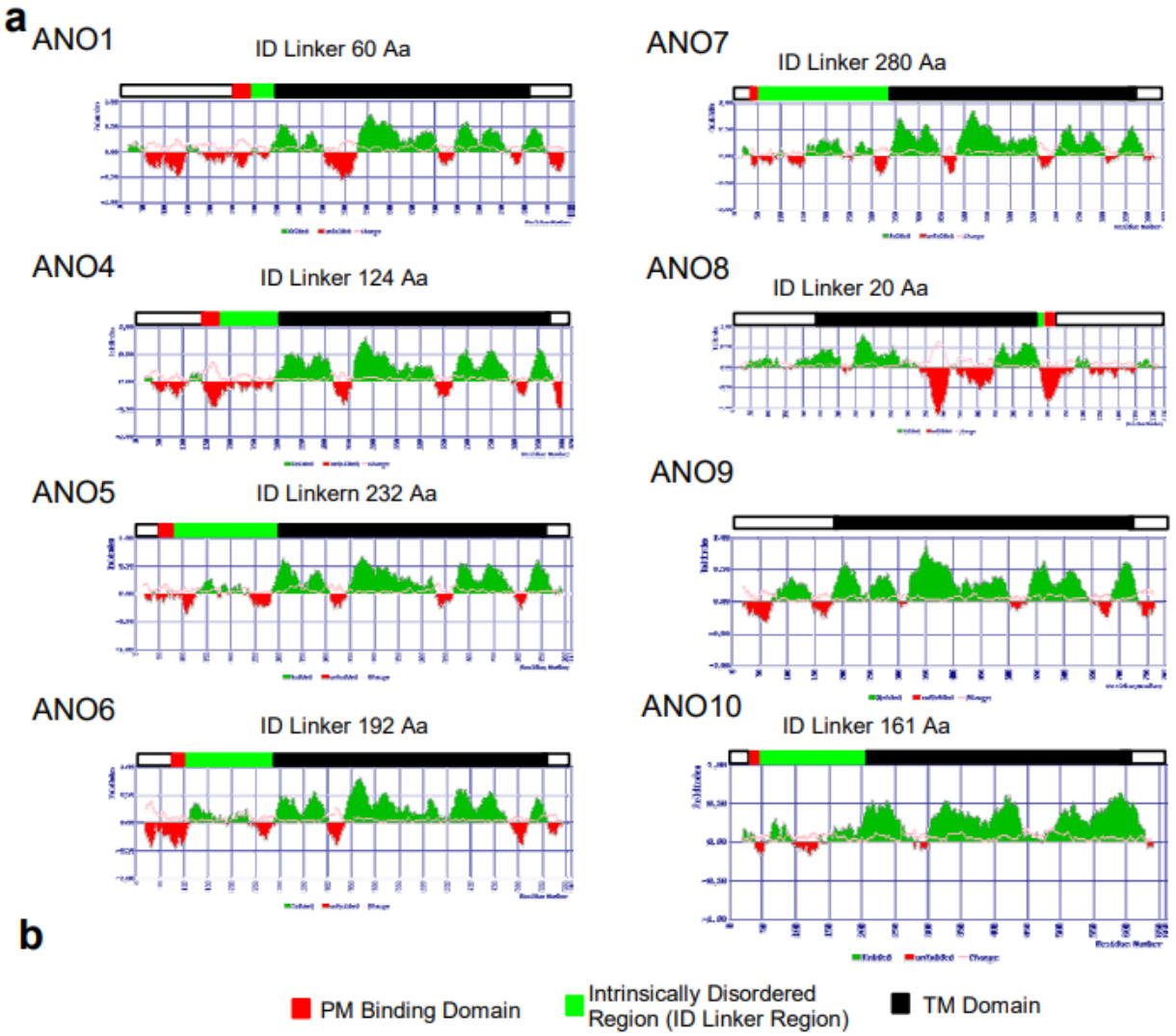

Supplementary figure 6.7 | *TMEM16J does not contain a cluster of positively charged amino acids in either N- or C terminus.*

a) Comparison of potential plasma membrane (PM) binding domains, intrinsically disordered regions and

transmembrane (TM) domain in different TMEM16 (anoctamin; ANO) paralogs. **b)** Amino acid sequence of human TMEM16J (ANO9).

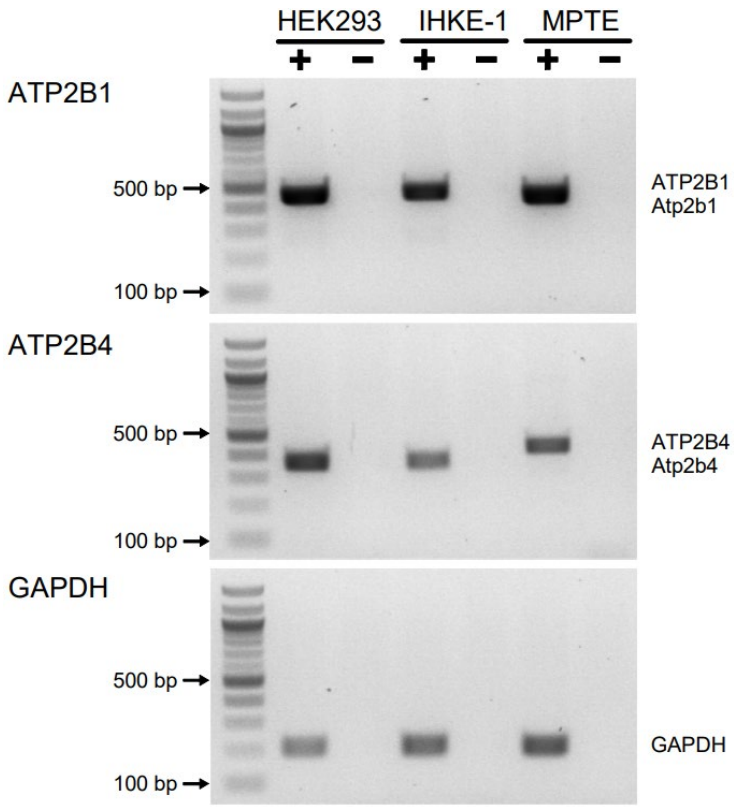

Supplementary figure 6.8 | ***Uncropped blots.***

DISCUSSION

LOSS OF PKD1 AND PKD2 SHARE COMMON EFFECTS ON INTRACELLULAR Ca^{2+} SIGNALING

Disrupted intracellular Ca^{2+} signaling is a central player in ADPKD pathology, driving increased proliferation and Cl^- secretion. The PKD1 and PKD2 genes, mutations of which lead to ADPKD, encode polycystins which are widely involved in calcium homeostasis. Polycystin-1 (PC-1) is a large transmembrane protein usually found in complex with the Ca^{2+} permeable channel PC-2 and is known to regulate its function. In epithelial cells, the PC1/PC-2 complex operates to regulate Ca^{2+} at three locations: at the ER, the PM, and the primary cilium [304]. Dysregulated polycystin function has been linked to abnormal Ca^{2+} signaling and cyst growth in ADPKD. How Ca^{2+} signaling is dysregulated in type-1 or in type-2 ADPKD is, however, controversial. Some studies have reported that a decreased Ca^{2+} signaling and an increased cAMP concentration lead to cyst growth [57], while others have demonstrated that Ca^{2+} was elevated in ADPKD [67]. PC-2 is a non-selective cation channel expressed mainly in the ER. Pkd2 knockout by shRNA reduced cyclopiazonic acid (CPA) -induced ER-Ca^{2+} store release, increased purinergic ER- Ca^{2+} store release and reduced basal cytoplasmic Ca^{2+}. Additional knockout of TMEM16A reduced ATP-stimulated Ca^{2+} store release but had no effect on the reduced basal Ca^{2+}. Our team has previously shown, in contrast to other reports [155], that Ca^{2+} signaling is enhanced in a $Pkd1^{-/-}$ mouse model [67]. We additionally demonstrate that the knockdown of Pkd1 increases basal Ca^{2+} and purinergic ER-Ca^{2+} store release in a TMEM16A-dependent manner in medullary and cortical primary cells (Chapter 2, Fig.1e-g).

These results can be interpreted as such: at the ER, PC-2 functions as an ER-Ca^{2+} leakage channel, leaking Ca^{2+} into the cytoplasm. At the PM, PC-2 plays the role of an influx channel regulating Ca^{2+} entry from the extracellular milieu into the cytoplasm. Absence of functional PC-2 leads to a decrease in leakage activity and Ca^{2+} influx, a consequent decrease in basal cytoplasmic Ca^{2+} and an increase in ER-Ca^{2+} store. TMEM16A tethers the ER to the plasma membrane, and its upregulation in ADPKD enhances the efficacy of purinergic signaling, hence the increase in IP3R-mediated Ca^{2+} signals in cells from both $Pkd1^{-/-}$ and $Pkd2^{-/-}$ mice (Fig 7.1). In $Pkd1^{-/-}$, PC-2 leakage channel activity at the ER and Ca^{2+} influx channel activity at the PM are further enhanced due to the absence of PC-1 inhibitory effects, resulting in increased Ca^{2+} leak into the cytoplasm together with an increase in Ca^{2+} influx. Additional TMEM16A-knockout, however, reduced basal Ca^{2+} in $PKD1^{-/-}$ cells indicating that TMEM16A contributes to increased basal cytoplasmic Ca^{2+}. Consistently, ER-Ca^{2+} store release induced by Ca^{2+} modulating agents, including ATP and CPA, has been shown to increase PC-2 PM expression and PM Ca^{2+} permeability in rat proximal tubule cells [305].

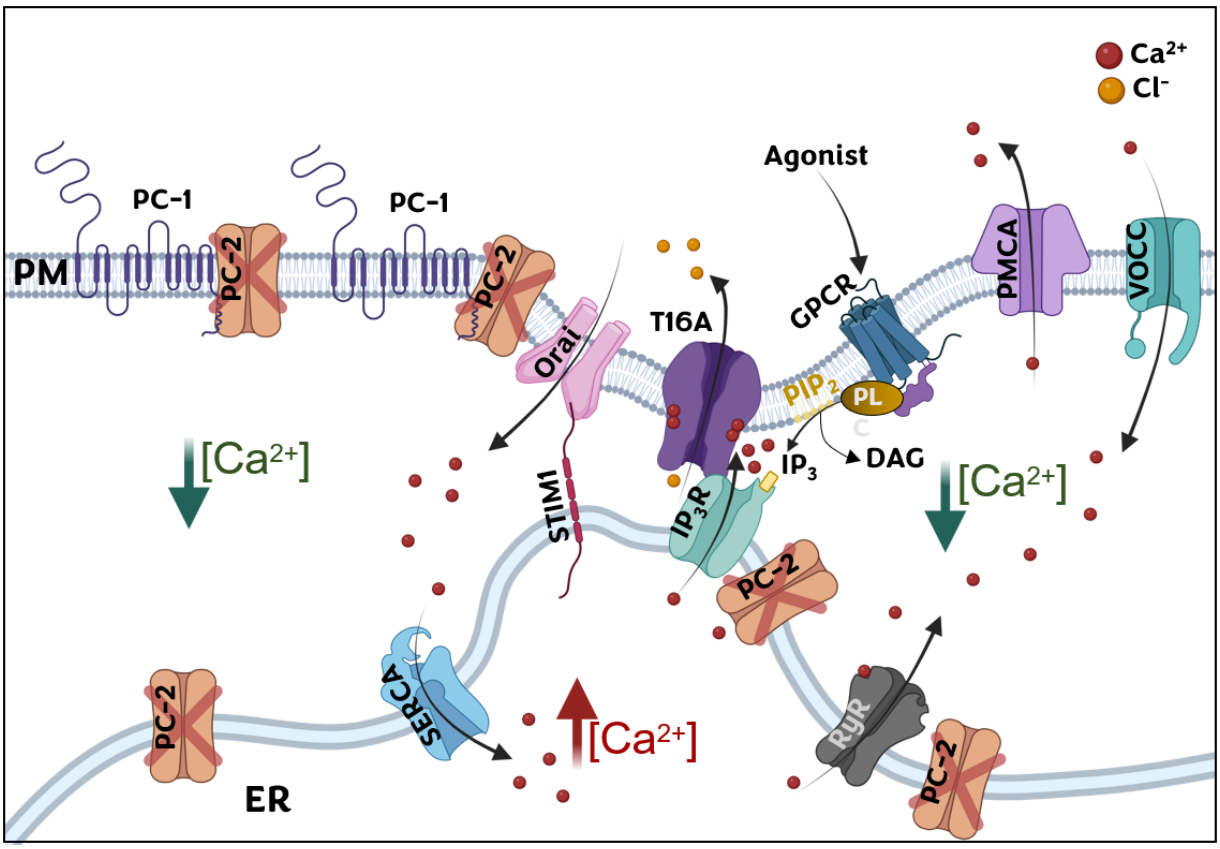

Figure 7.1 | *Disrupted calcium signaling induced by mutations to PKD2.*
Scheme illustrating proposed mechanisms leading to Ca^{2+} signaling disruption in absence of PC-2 function. Increased ER-Ca^{2+} store concentration and decreased cytoplasmic Ca^{2+} concentration are due to the abolished PC-2 ER-leakage channel function and absence of PC-2 stimulation of IP3R. TMEM16A tethers the ER to the PM by interacting with the IP3R, and its upregulation in ADPKD further enhances purinergic Ca^{2+} signaling. Created with BioRender.com

In ADPKD, the expression of both $P2Y_2$ receptors and TMEM16A is increased [152].Thus, increased luminal ATP concentration and increased receptor-mediated Ca^{2+} signaling might consequently enhance PC-2 PM expression and Ca^{2+} influx. At the PM, PC-2 can also interact with other PM Ca^{2+} channels and modulate their activity [306], inducing an additional increase in cytoplasmic Ca^{2+}. Furthermore, PC-2 functionally interacts with the IP3R, prolonging the half-decay time (t1/2) of IP3-induced Ca^{2+} transients [44] and thus contributes to the formation of signaling microdomains required for Ca^{2+}-stimulated Ca^{2+} release by ryanodine receptors [307]. This PC-2/IP3R complex is inhibited by PC-1, which instead promotes the interaction between IP3R and STIM1 [45]. Absence of functional PC-1 might then lift the negative regulation on the IP3R/PC-2 complex, which enhances IP3R-induced Ca^{2+} release from the ER store, in addition to increased TMEM16A expression which further enhances purinergic Ca^{2+} signaling (Fig 7.2). In line with our findings, Yanda et al., had shown that proximal tubular epithelial cells from PC-1 null mice had higher intracellular Ca^{2+} and SOCE, and that these cells had an increased expression of IP3R and STIM1. Importantly, we also demonstrate a TMEM16A-dependent

increase in SOCE in Pkd1$^{-/-}$, while enhanced SOCE in Pkd2$^{-/-}$ was not related to TMEM16A. P2Y$_2$/TMEM16A induced an increase in PM-expression of PC-2 which may also contribute to a TMEM16A-dependent increase in SOCE in Pkd1$^{-/-}$ but not in Pkd2$^{-/-}$ cells. An alternative hypothesis to explain our results may be the existence of different Ca^{2+} stores [156], where TMEM16A might regulate Ca^{2+} stores stimulated by purinergic signaling, whereas TMEM16A-independent Ca^{2+} stores are regulated by PC-1 and PC-2.

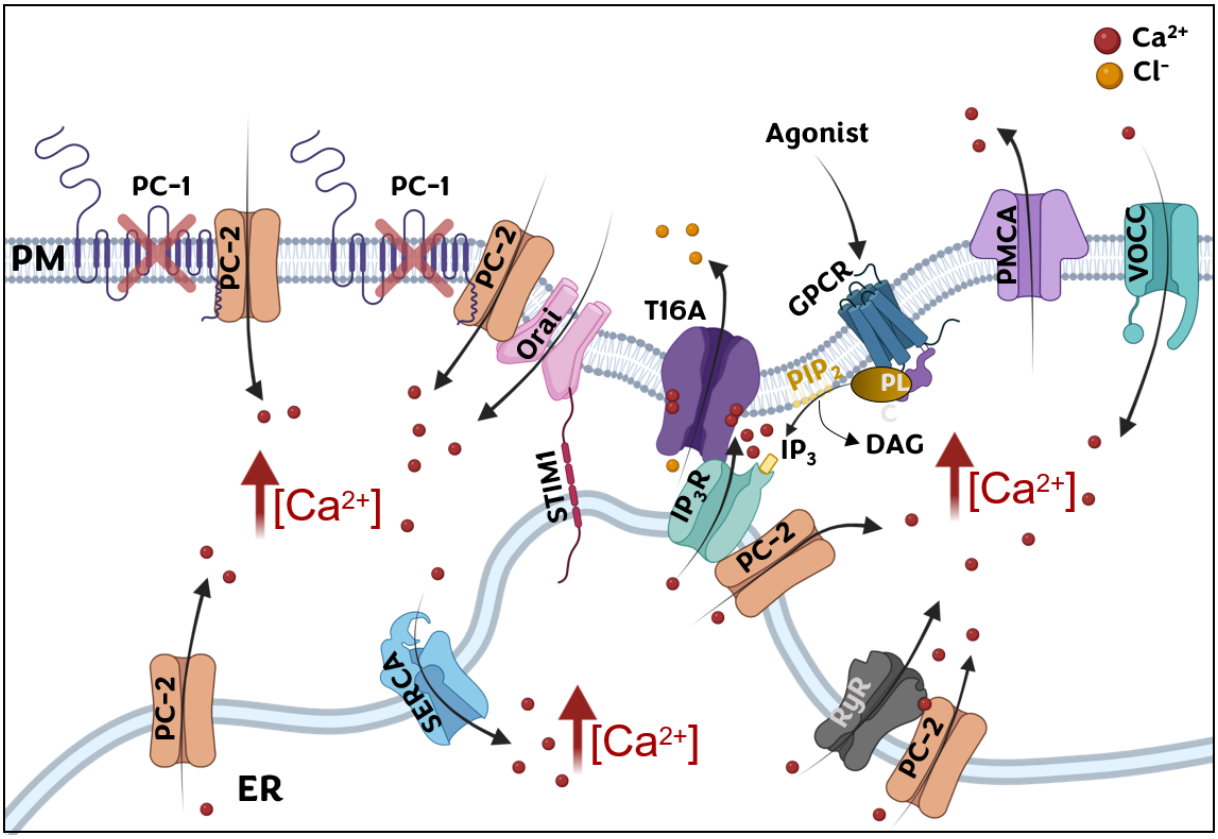

Figure 7.2 | *Disrupted calcium signaling induced by mutations to PKD1.*
Scheme illustrating proposed mechanisms leading to Ca^{2+} signaling disruption in absence of PC-1. PC-2, expressed at the ER, leaks Ca^{2+} into the cytosol and enhances IP3R activity, inducing an increase in cytosolic Ca^{2+}. At the PM, PC-1-dependent regulation of PC-2 channels is lifted, PC-2 mediates Ca^{2+} influx to the cytosol and interacts with TRP channels leading to a further increase in the cytoplasmic Ca^{2+} concentration. SERCA pump activity is stimulated following Ca^{2+} influx through TRP channels, leading to increased loading of the ER Ca^{2+} store. TMEM16A tethers the ER to the plasma membrane by interacting with the IP3R, and upregulation in ADPKD further enhances purinergic Ca^{2+} signaling. Created with BioRender.com

In brief, we report disrupted Ca^{2+} signaling by Pkd1- and Pkd2-knockdown. Absence of PC-1 induces a basal Ca^{2+} increase, while the absence of PC-2 decreases Ca^{2+} in resting cells. In contrast, disease-causing purinergic ER-Ca^{2+} signaling is increased with downregulation of either Pkd1 or Pkd2, in a TMEM16A-dependent manner.

CFTR IS NOT REQUIRED FOR CYST GROWTH IN AN ADPKD MOUSE MODEL

Cyst growth is the hallmark of ADPKD and is mediated by enhanced cell proliferation and upregulation of transepithelial Cl^- secretion into the cyst lumen. These cysts mainly originate from the proximal tubules or collecting ducts where, in human and mouse kidneys, the chloride channels TMEM16A and CFTR are mainly expressed [110]. TMEM16A was localised to cyst-lining epithelia and was shown to induce Ca^{2+}-activated Cl^- secretion and proliferation in cyst models from embryonic kidney and Madin-Darby canine kidney (MDCK) cells [137]. Our team has previously demonstrated that TMEM16A expression is upregulated in ADPKD models using MDCK and M1 cells, as well as primary tubular epithelial cells from Pkd1-knockout mice. TMEM16A-knockdown or inhibition reduced Ca^{2+} signaling, proliferation and chloride secretion [86]. Furthermore, Cabrita et al., showed that the knockout of TMEM16A, or its pharmacological inhibition *in vivo,* remarkably reduced abnormal proliferation and kidney cysts development [67]. These data suggest a critical role for TMEM16A in enhanced proliferation and secretion in ADPKD.

Numerous *in vitro* studies also put forward an essential role for the cAMP-activated channel CFTR. Increased synthesis of cAMP was reported to stimulate proliferation, fluid secretion and cyst expansion in cultured renal epithelial ADPKD cells [308]. Cl^- secretion stimulated by forskolin, which activates adenylate cyclase, was inhibited by antisense oligonucleotides against CFTR [75]. In the present work, we have investigated the role of CFTR in cyst formation *in vivo* using tubule-specific Pkd1-knockout ($Pkd1^{-/-}$) and $Pkd1^{-/-}/Cftr^{-/-}$ double-knockout mouse models. As expected, Pkd1-knockdown induced kidney enlargement and cyst development in our mouse model. However, additional Cftr-knockdown had surprisingly little to no effect on cyst development and kidney size (Chapter 3, Fig 3.1a-e). To understand why, we investigated the CFTR role in Cl^- secretion and cell proliferation. Using the patch clamp technique, we have found that cAMP activated only a minimal Cl^- current in cultured primary renal epithelial cells from $Pkd1^{-/-}$ mice (Chapter 3, Fig 3.3a-c), while ATP induced large Cl^- currents, which were TMEM16A-mediated and not abolished by the absence of CFTR (Chapter 3, Fig 3.4a-c). These results demonstrate that CFTR is not the main mediator of Cl^- secretion driving cysts development. One should also consider that Cl^- secretion into the cyst lumen may not even be that relevant for cyst formation, but rather the enhanced proliferation seen in renal cells affected by ADPKD.

In line with previous reports, we have found that TMEM16A expression is increased in $Pkd1^{-/-}$ mice and that Cftr-knockdown did not affect TMEME16A expression, which remained enhanced in $Pkd1^{-/-}/Cftr^{-/-}$ mice (Chapter 3, Fig 3. 2a-c). CFTR expression was also increased in $Pkd1^{-/-}$ mice, however, TMEM16A knockout in $Pkd1^{-/-}$ mice significantly decreased enhanced expression [67], which means that enhanced expression of TMEM16A is required for enhanced CFTR expression in kidney tubules. Notably, our team reported earlier that epithelial Cl^-

transport by CFTR in airways and intestine requires TMEM16A [135]. Taken together, these results suggest that TMEM16A is essential for proper expression and function of CFTR across multiple secretory epithelia including the kidney. Along this line, in ß-intercalated cells of the collecting duct CFTR supports HCO_3^- excretion by pendrin [74].

Hypoxia and hypoxia-inducible factor-1α (HIF-1α) enhances $P2Y_2$ receptor expression and Cl^- secretion [152,204]. Similar to a previous report [137], we have also found that $P2Y_2$ expression is enhanced in our Pkd1-knockout mice. $P2Y_2$ receptors mediate purinergic Ca^{2+} signaling, and their expression is enhanced by HIF-1α along with enhanced expression of TMEM16A. This explains the importance of ATP-activated currents we measured in our cultured primary tubular epithelial cells. *In vivo*, these purinergic receptors are expressed apically in cyst-lining epithelial cells, where luminal ATP concentrations can reach up to 10μM [82]. We speculate that this ATP/$P2Y_2$/TMEM16A-rich environment translates into an enhanced $P2Y_2$ receptor activation, subsequent increase in purinergic Ca^{2+} signaling and activation of the Ca^{2+} dependent Cl^- secretion through TMEM16A.

Increased expression of $P2Y_2$ receptors and activity had been reported in several types of cancer, where it enhances cell proliferation through diverse mechanisms, including modulation of the cytoskeleton dynamics and activation of PLC, Ca^{2+} signaling and NF-κB pathways [309]. Increased proliferation was not attenuated by Cftr-knockdown (Chapter 3, Fig 3.1g-h) despite the fact that CFTR expression was enhanced in Pkd1$^{-/-}$ mice (Chapter 3, Fig 3. 2a,c). A similar observation was made in a MDCK cells cyst model, where pharmacological inhibition of CFTR with CFTR blockers such as CFTR-inh-172 and GlyH-101 did not affect proliferation [77]. Conversely, TMEM16A-knockdown dramatically attenuated proliferation in kidney tissue of Pkd1$^{-/-}$ mice [67], proving that TMEM16A mediates intensified proliferation in ADPKD. These are evidence that argue for the importance of proliferation in the overall pathology of ADPKD.

In ADPKD renal epithelium, a cyst originates from a single cell which undergoes an abnormal proliferative event following dysregulated Ca^{2+} signaling due to defective PC-1/PC-2 complex activity. Initially, cysts are open to the parent tubule lumen and are filled with unabsorbed glomerular filtrate. Chloride and fluid secretion contribution to cyst development becomes relevant only once the cyst reaches a certain size and disengages from the parent tubule to form an anatomically-independent sac. Up until then, cyst formation and growth seem to depend mainly on proliferation. Transepithelial fluid secretion, together with ceaseless proliferation, drives growth and expansion of already existing autonomous cysts [310]. Taking this into account, the fact that CFTR has no impact on cell proliferation perhaps explains why its knockdown in our Pkd1$^{-/-}$ mouse model had little effect on cyst formation. We speculate that, when Cftr is knocked out, proliferation is not affected, early cysts are still able to form, and Cl^- secretion can still be mediated through TMEM16A for later cyst expansion. However, when TMEM16A is absent, abnormal proliferation, which is the earliest cellular event in cytogenesis,

is averted, and consequent cyst formation is nipped in the bud. CFTR, considering its channel characteristics, might mediate a small but continuous basal Cl^- secretion, which we, after all, were able to detect (Chapter 3, Fig 3. 3a-c). These currents were by no mean essential for 10 weeks of cyst development in our mouse model. In humans however, where cysts grow over decades, CFTR mediated Cl^- secretion may contribute at least to a faster disease progression. In fact, although cystic fibrosis (CF) is not entirely protective against ADPKD, the coexistence of both diseases in humans can limit the severity of ADPKD phenotype. Patients with both CF and ADPKD displayed smaller and fewer renal cysts and lower blood pressure in comparison to their family members who have ADPKD only [79]. Importantly, while human patients suffer from a severe CF phenotype, Cftr-knockdown did not induce airway disease in mice [311]. Therefore, when interpreting CFTR-related data from mice, it is very important to note that human physiology seems to depend more on CFTR function.

In conclusion, these findings, in addition to previous reports, highlight a predominant role of TMEM16A and not CFTR in ADPKD pathology.

SEX-DEPENDENT PHENOTYPE IN ADPKD IS MEDIATED BY DIFFERENTIAL INTRACELLULAR CA^{2+} SIGNALING

Sex differences in kidney structure and function have been described in several species and include the renin-angiotensin-aldosterone (RAAS) system, expression of transporters and inflammation [312]. Male ADPKD patients have an earlier onset of ESRD compared to women [4,5]. Multiple studies have demonstrated that ADPKD progression and severity is influenced by sex hormones in different experimental models [12-14]. Along the fourth chapter, we investigated potential hormonal mechanisms driving these sex differences as well as the role of TMEM16A, considering its importance in the overall ADPKD pathology.

Tubule specific-knockdown of Pkd1 induced a more pronounced cyst formation in male mice compared to female (Chapter 4, Fig 4.1) despite similar levels of TMEM16A expression (Chapter 3, Fig 4.2). ATP-induced currents were also not increased in primary medullary cells from male mice (Chapter 4, Fig 4.4 a-b). Interestingly, proliferation in $Pkd1^{-/-}$ mice was significantly higher in male kidney tissue (Fig4.A-B). Increased proliferation and Ca^{2+} signaling in ADPKD are tightly linked to TMEM16A. We show in chapter one that downregulation of Pkd1 triggers an increase in Ca^{2+} signaling which is TMEM16A-dependent. Remarkably, basal cytoplasmic Ca^{2+} levels were increased in cultured primary medullary cells from $Pkd1^{-/-}$ male but not female mice (Chapter 4, Fig 4.3c-d), which translated into a higher basal current in male $Pkd1^{-/-}$ cells (Chapter 4, Fig 4.4a-b). These results indicate that higher basal Ca^{2+} requires both TMEM16A and sex-dependent effects. Although we could not detect differential protein expression in $Pkd1^{-/-}$ male and female mice, a role of TMEM16A cannot per se be excluded, as the channel activity might be different in male and female. Moreover, dihydrotestosterone (DHT)

treatment increased TMEM16A expression and ATP-induced currents in mouse cortical collecting duct (mCCDcl1) cells (Chapter 4, Fig 4.6c-f). Finally an androgen-response element is present in the TMEM16A promotor region [207]. In our ADPKD model, where the increase in TMEM16A expression is already quite dramatic, detecting a sex difference in expression profile might be challenging. Cytosolic Ca^{2+} measurements showed that the ER-Ca^{2+}store release and SOCE were increased in renal primary epithelial cells from Pkd1$^{-/-}$ mice, and that this increase was more pronounced in male mice (Chapter 4. Fig 4.S5). Again, we know from chapter two that Pkd1$^{-/-}$ increase in ER-Ca^{2+} store release and SOCE are TMEM16A-dependent. Treatment with DHT in mCCDcl1 cells resulted in a similar increase in Ca^{2+} signaling, while estradiol (EST) had a negligible effect (Chapter 4, Fig 4.7 a). Taken together, the above results suggest that TMEM16A mediates enhanced Ca^{2+} signaling in Pkd1$^{-/-}$, and that sex-related effects, possibly through androgens, further aggravates it.

Androgens exert their effect via a 'slow' AR-dependent mechanism which results in the regulation of target gene expression, or via a 'fast' nongenomic AR-independent mechanism which modulates cell-surface proteins activity [313]. Androgens were reported to rapidly modulate intracellular Ca^{2+} in several cell types, including male rat osteoblasts, macrophages, mouse T cells, rabbit kidney cells and skeletal muscle cells, and are thought to do so through an AR-independent pathway. Couchourel et al., have showed that testosterone enhanced Ca^{2+} transport in distal tubule luminal membranes by activating T-type Ca^{2+} channel via MEK kinase- or tyrosine kinase-dependent mechanisms [314]. In isolated testicular cells (Sertoli cells), testosterone increased cytoplasmic Ca^{2+} by activating extracellular Ca^{2+} influx into the cytosol while progesterone had no effect. Rapid Ca^{2+} increase suggested a nongenomic effect of testosterone in addition to the slower genomic pathway [315]. Similarly, in LNCaP prostate cancer cells, DHT induced an increase in cytosolic Ca^{2+} following Ca^{2+} influx via L-type Ca^{2+} channels [220]. A chemical library screening using Pkd1$^{-/-}$ zebra fish model identified androstandione, a precursor of androgens, as a potent modulator of cyst growth through AR-independent signaling. Androgen effect was confirmed in an *in vitro* 3D Pkd1$^{-/-}$ cyst model [316]. These results revealed a strong 'fast' impact of testosterone on Ca^{2+} signaling which might be relevant for secretion in *in vivo* scenarios, considering the enhanced TMEM16A expression in ADPKD. Hence, androgens might worsen ADPKD progression in males through enhanced activation of TMEM16A-mediated Cl^- secretion, possibly by increasing the activity of Ca^{2+} influx channels. *In vitro* stimulation of isolated primary kidney cells with ATP did not show any sex difference in TMEM16A-mediated Cl^- currents (Chapter 3, Fig 3.4), which can be due to the fact that these cells in culture were deprived from the nongenomic effect of hormones.

Remarkably, these isolated primary kidney cells from male and female mice presented gene expression, basal current and Ca^{2+} signaling differences in absence of all hormonal stimulation and after several days in culture. Such differences can be due a late receptor-mediated effect of sex hormones on gene expression, or more likely through other more

permanent pathways. In fact, the sex of the individual cell affects its function independently of sex hormones [317]. Genes on the Y chromosome for example, play an essential role in the regulation of gene expression and protein stability [318]. When primary cells are isolated and cultured, potential sex differences can stem from the autonomous effect of sex chromosomes, or from permanent epigenetic modifications induced by perinatal androgens [6].

Interestingly, we found that the expression of the PM Ca^{2+}-permeable nonselective cation channel TRPV4 was downregulated in mCCDcl1 cells following 24h incubation with EST (Chapter 4, Fig 4.7b). In mouse kidney, TRPV4 was shown to be abundant in the collecting ducts, with a dominant apical expression [319]. Importantly, these channels physically and functionally interact with TMEM16A. In fact, CaCCs activators, such as Eact, were shown to be activators of TRPV1 and TRPV4, indicating physiological association between TMEM16A and TRPV function [320,321]. A similar interaction in the kidney might therefore explain the enhanced basal Ca^{2+} and basal Cl^- current in $Pkd1^{-/-}$ cells from male mice where we also found TRPV4 expression to be higher compared to females. EST treatment lowered TRPV4 expression, which means that reduced SOCE and basal Ca^{2+} in $Pkd1^{-/-}$ female mice is possibly due to a protective effect of estrogens, mediated by a decreased Ca^{2+} influx channels expression.

Taken together, the sex-dependent difference in ADPKD phenotype severity is mediated by differential Ca^{2+} signaling which is possibly sensitive to sex hormones and their potential effect on TMEM16A activity. Additional studies are required to fully understand the mechanism through which biological sex affects Ca^{2+} signaling and ADPKD progression.

CALMODULIN REGULATES OVEREXPRESSED BUT NOT ENDOGENOUS TMEM16A

TMEM16A, as a member of the CaCCs family, requires intracellular Ca^{2+} binding for activation. Compared to its paralogue TMEM16B, TMEM16A is highly sensitive to Ca^{2+} especially at positive membrane potentials. In addition to the primary Ca^{2+} binding sites, a third Ca^{2+} binding site with a high Ca^{2+} affinity, phosphatidylinositol-(4,5)-bisphosphate (PIP2), and calmodulin (CAM) may regulate TMEM16A channel activity [94]. In earlier studies, our team showed that overexpressed and endogenous TMEM16A react differently to several agents. For example, the lipid inositol phosphate INO-4995 and the membrane permeable dioctanoyl-PIP2-phosphatidylinositol-4,5-bisphosphate-diC8 activated overexpressed but not endogenous TMEM16A [248,249]. In the current study, we examined how TMEM16A overexpression modifies the channel behaviour and interaction with CAM as well.

Using whole cell patch clamp, we found TMEM16A to be spontaneously active when overexpressed (Chapter 5, Fig 5.1c-d, i) due to increased Ca^{2+} sensitivity (Chapter 5 Fig 5.2), when compared to endogenous TMEME16A (Chapter 5, Fig 5.1a-b,i). In TMEM16A-overexpressing HEK293T cells, CAM/KCNN4 K^+ channel activator 1-EBIO activated TMEM16A current in the presence but not in the absence of Ca^{2+}. This activation was abolished by CAM

inhibitor trifluoperazine and siRNA against CAM (Chapter 5, Fig 5.3). However, in CFBE airway epithelial cells which express TMEM16A endogenously, 1-EBIO activated KCNN4 but not a TMEM16A current (chapter 5, Fig5 .4). Tien et al, similarly showed that CAM did not modulate endogenous TMEM16A Ca^{2+} sensitivity in *Xenopus* oocytes [322]. These results indicate that CAM can modulate Ca^{2+} sensitivity of overexpressed but not endogenous TMEM16A.

TMEM16A is expressed in cholesterol-rich lipid rafts [323,324] and is preferentially activated by IP3R-mediated ER-Ca^{2+}store release. These Ca^{2+} signals are compartmentalized by TMEM16A tethering of the ER to PM lipid rafts, which creates membrane-ER microdomains that mediate localized Ca^{2+} signaling. TMEM6A expression within these confined signaling compartments makes the channel insensitive to distant Ca^{2+} elevation, such as Ca^{2+} influx through VGCC [118]. The disruption of lipid rafts using the cholesterol depleting agent methyl-β-cyclodextrin was shown to disrupt IP3R/TMEM16A interaction in cultured dorsal root ganglion neurons and to sensitize TMEM16A to Ca^{2+} signals generated by VGCC [117]. In addition, in vascular smooth muscle cells, cholesterol depletion increased TMEM16A-mediated chloride currents [323], while cholesterol addition had an inhibitory effect on TMEM16A current in human aortic endothelial cells and in heterologous HEK293 cells [325], which suggests that cholesterol can negatively regulate TMEM16A activity. Finally, Kawata et al.,[326] reported in a recent study that caveolin-1 knockout mice display an increase in TMEM16A currents. Caveolin-1 is a structural protein required for the formation of a subset of lipid rafts known as caveolae.

Based on these results, TMEM16A can be exposed to other Ca^{2+} sources and other regulating proteins in the absence of these lipid rafts. We hypothesize that overexpressed TMEM16A might be localized outside of lipid rafts across the PM and, when no longer shielded in cholesterol microdomains, interactions with other proteins including CAM might become possible. Likewise, it is possible that the Ca^{2+}-free form of CAM, apoCAM, which pre-associates with TMEM16A, preferentially does so in overexpression conditions. In fact, apoCaM was shown to interact with both TMEM16A and TMEM16B at resting Ca^{2+} concentration and to increase TMEME16A Ca^{2+} sensitivity in overexpressing HEK293 cells [105]. 1-EBIO activates KCNN4 channel by promoting CAM binding as a β-subunit, which induces a shift in channel-activating $[Ca^{2+}]_i$ towards lower values. It is possible therefore that 1-EBIO promotes apoCAM binding to overexpressed TMEM16A. However, in a native environment, such interaction might be hindered by TMEM16A localization in the PM within confined lipid rafts, or, alternatively, by TMEM16A regulatory proteins, which might be underexpressed in relation to TMEM16A in overexpressing cells.

Several studies advocate for the exclusive activation of TMEM16A by direct Ca^{2+} binding and rule out CAM implication in TMEM16A regulation [101,102,322] . We showed through the present work that CAM regulates overexpressed but not endogenous TMEM16A, which indicates that TMEM16A interaction with CAM or other regulatory proteins can only be validated in an endogenous expression system under physiological conditions.

TMEM16J REGULATES Ca^{2+} SIGNALLING AND THE IMMUNE RESPONSE

The PKP3-SIGIRR-TMEM16J genomic region is a negative regulator of the immune response [125]. SIGIRR and PKP3 involvement in immunity have been previously addressed [128,273], while the role of TMEM16J remained elusive. A genome wide association study identified the TMEM16J variant, TMEM16J-T604A, as a risk factor for CKD [120]. TMEM16 proteins are deeply involved in the regulation of Ca^{2+} signalling [118] and earlier work from our team had shown that TMEM16J expression dampens Ca^{2+} signals [116]. Therefore, in the sixth chapter, we explored the mechanisms by which TMEM16J and TMEM16J-T604A modulate Ca^{2+} signaling and pro-inflammatory cytokines production, and how TMEM16J-T604A may predispose to chronic inflammation and CKD.

Our results revealed, for the first time, the presence of TMEM16J in mouse kidney tubules, mainly in proximal tubule cells (Chapter 6, Fig.6.1a). Unlike what was previously reported [285], we demonstrated that TMEM16J is expressed intracellularly at the level of the ER, and not at the PM (Chapter 6, Fig.6.1b). Endogenous TMEM16J or TMEM16J-T604A presented a similar subcellular localization in human kidney cell lines (Chapter 6, Fig.6.2a, Fig.6 5b). TMEM16J expression lowered ER-Ca^{2+} content, enhanced basal $[Ca^{2+}]_i$ and dampened CPA and ATP-induced ER-Ca^{2+} store release. TMEM16J-T604A had similar, but significantly less intense effects (Chapter 6, Fig.6.2b-j). Both TMEM16J and its variant induced an increase in basal whole cell currents in HEK293 cells (Chapter 6, Fig.6.4c). These currents are most likely mediated by the endogenously expressed TMEM16F in HEK293T following the increase in basal $[Ca^{2+}]_i$. TMEM16F is similarly activated by the TMEM16J ER-localized paralogue, TMEM16D [116]. When targeted to the PM, ATP activated a whole cell current in TMEM16J, but not in TMEM16J-T604A overexpressing cells (Chapter 6, Fig.6.4a-c), indicating a defect in its Ca^{2+}-dependent activation. Indeed, the T604A mutation is located in TMD 9 in close proximity to the Ca^{2+} binding sites (Chapter 6, S.fig.6.5) which might disrupt Ca^{2+} binding and lower or even abolish Ca^{2+} sensitivity, hence compromising channel activity. These results suggest that TMEM16J might function as a Ca^{2+} permeable channel leaking Ca^{2+} from the ER to the cytosol, and that this ER-Ca^{2+} store depletion function is compromised in TMEM16J-T604A.

Expression of TMEM16J and the TMEM16J variant caused a reduction in SOCE (Chapter 6, Fig.6.2f-g). Additionally, we found that TMEM16J shortens the duration of GPCR-mediated Ca^{2+} signals, making the decrease in $[Ca^{2+}]_i$ following release from the ER significantly faster. This effect was abolished by the PMCA inhibitors vanadate (Chapter 6, Fig.6.3) and caloxin 1B1, which implies that TMEM16J regulates Ca^{2+} signaling duration through the modulation of PMCA activity. Ca^{2+} efflux via PMCA is known to play an important role in controlling the magnitude and duration of Ca^{2+} signals following GPCR activation. The local increase in Ca^{2+} through Ca^{2+} release from the ER, and the consequent Ca^{2+} influx through SOCE are transient. In fact, once the signaling is achieved, the resting cytoplasmic $[Ca^{2+}]_I$ is re-established through

ER store re-filling by SERCA and Ca^{2+} efflux via PMCA and the Na^{+}/Ca^{2+} exchanger. Therefore, PMCA is central to the fine tuning of Ca^{2+} signals [298]. Interestingly, TMEM16J interacts with DLG1, which is a binding partner of PMCA. We propose therefore that TMEM16J might shorten Ca^{2+} signals duration by interacting with DLG1 to activate PMCA and Ca^{2+} efflux following local $[Ca^{2+}]_i$ increase.

Spatial segregation of Ca^{2+} signaling proteins within distinct PM microdomains is also an important factor for the regulation of Ca^{2+} signals, and TMEM16 proteins are no strangers to this concept. The Ca^{2+}-activated Cl^- channel TMEM16A tethers the ER to the plasma membrane through its interaction with the IP3R. In addition, TMEM16H attenuates GPCR mediated Ca^{2+} signals and tethers the ER to PIP2-rich plasma membrane compartments containing PMCA and Orai1. It is entirely possible therefore that TMEM16J also tethers the ER to PM regions which includes PMCA and components of the SOCE and enhances PMCA activity through DLG1 to negatively regulate Ca^{2+} signaling (Fig 7.3). DLG1 is a scaffolding protein which participates in several cellular functions, including proliferation, cell migration and immunity. In regulatory T cells, accumulation of DLG1 at the immunological synapse is important for triggering its immunosuppressive activity. Altered DLG1 function has been reported in multiple autoimmune and inflammatory diseases [297]. DLG1 might then additionally couple the TMEM16J effect on Ca^{2+} signaling to the immune response process.

We surprisingly found that unlike primary renal cells expressing TMEM16J (Chapter 6, Fig.6.6c-f), IHKE-1 cells which express TMEM16J-T604A constitutively transcribe and release pro-inflammatory cytokines even in the absence of TLR stimulation (Chapter 6, Fig.6.5h-i), indicating a state of spontaneous and persistent inflammation. Furthermore, downregulation of TMEM16J in primary proximal tubule cells induced an enhanced cytokine transcription and release following TLR activation (Chapter 6, Fig.6.6c-f). Conversely, downregulation of TMEM16J-T604A reduced constitutive and LPS-induced cytokine release (Chapter 6, Fig.6.5h-i). These results suggest that TMEM16J negatively controls inflammation, and that this function is compromised in TMEM16J-T604A.

In conclusion, we showed that TMEM16J controls Ca^{2+} signaling through two different mechanisms: i) TMEM16J directly controls the magnitude of Ca^{2+} signals by regulating ER Ca^{2+} store filling via its ER Ca^{2+} leakage channel function, and ii) TMEM16J indirectly regulates the duration of GPCR stimulated Ca^{2+} signals via activation of PMCA. We additionally demonstrate that TMEM16J negatively regulates pro-inflammatory cytokine transcription and release and speculate that this anoctamin does so through dampening of Ca^{2+} signals responsible for the stimulation of cytokine transcription. TMEM16J-T604A has the functions mentioned above compromised, which may explain the increase in inflammation in presence of this variant and therefore provide the link to CKD.

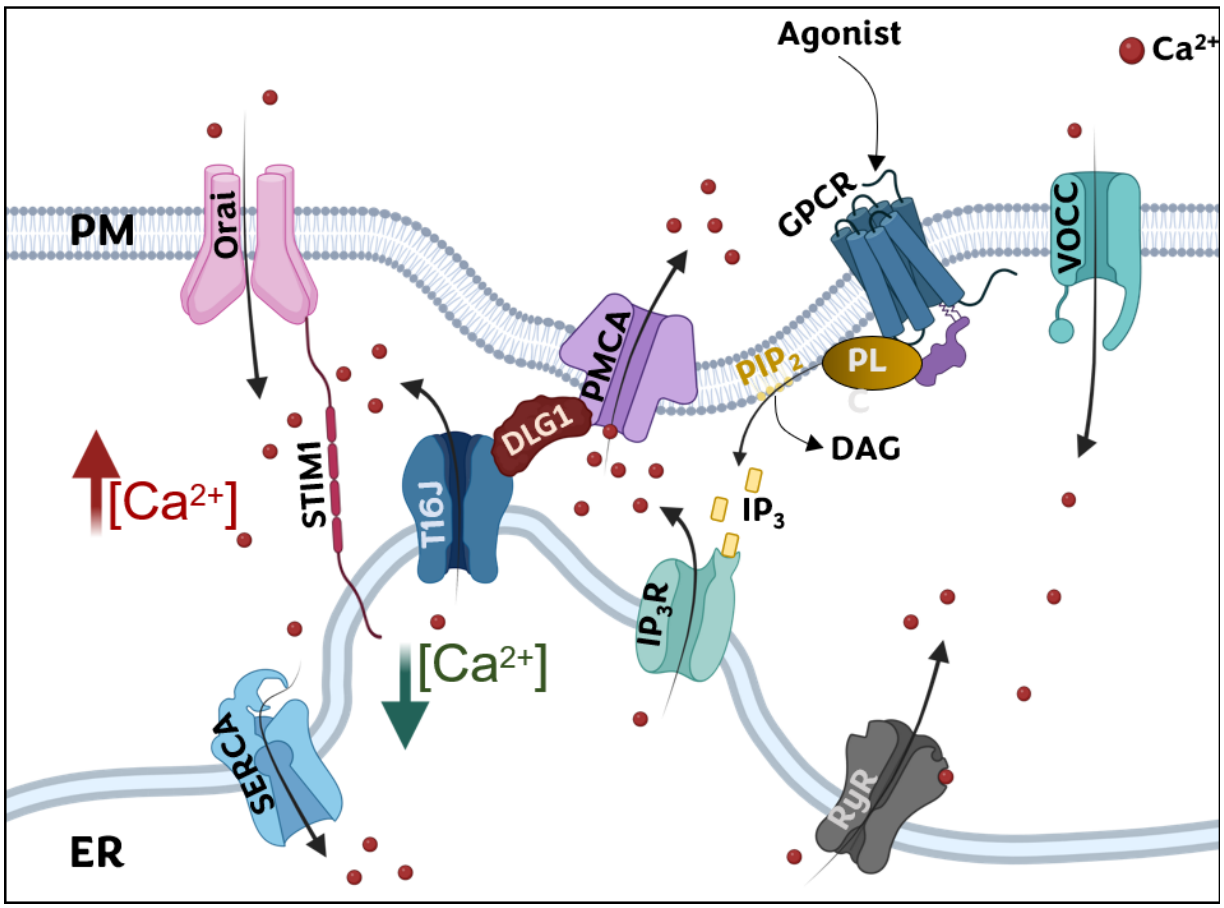

Figure 7.3 | *Calcium signaling is modulated by TMEM16J.*

Scheme illustrating the proposed TMEM16J (T16J) function as a regulator of Ca^{2+} signaling. TMEM16J is an ER localized Ca^{2+} permeable ion channel which leaks Ca^{2+} to the cytosol, leading to an increase in the cytoplasmic Ca^{2+} concentration and a decrease in the ER Ca^{2+} store. Following purinergic signaling and local Ca^{2+} increase, T16J stimulates PMCA activity and Ca^{2+} efflux through the interaction with the partner protein DLG1. Similar to many TMEM16 protein family members, T16J might function as an ER-PM tether and create a localized Ca^{2+} signaling microdomain. Created with BioRender.com.

CONCLUSIONS AND FUTURE PERSPECTIVES

Through the present work, we have demonstrated that the loss of both Pkd1 or Pkd2 induces an increase in ER Ca^{2+} store release dependent on TMEM16A. Furthermore, we have reported remarkable data proving that CFTR is not essential for cyst formation in an ADPKD mouse model *in vivo.* We have additionally provided further evidence for a predominant role of TMEM16A in proliferation and chloride section in ADPKD, and hence put forward TMEM16A rather than CFTR as a promising pharmacological target for cyst growth inhibition. Endogenous and overexpressed TMEM16A differ in a number of ways, including their sensitivity to regulatory molecules [248,249]. We have shown that calmodulin increases the Ca^{2+} sensitivity of overexpressed but not endogenous TMEM16A. Moreover, we have found evidence for sex-dependent differential Ca^{2+} signaling leading to a more severe ADPKD phenotype in males. Additional work is required for a better understanding of the underlying mechanisms.

We also reported for the first time that TMEM16J negatively regulates pro-inflammatory cytokine release *in vitro*, potentially via regulating Ca^{2+} signaling. The generation of tissue specific TMEM16J knockout and TMEM16J-T595A (corresponding to human T604A) knock-in mice will be a suitable approach to confirm and further investigate the role of TMEM16J and TMEM16J-T604A in CKD. This experimental model will allow the assessment of the impact of the TMEM16J absence and the TMEM16J variant presence *in vivo.* In addition, it would be interesting to study Ca^{2+} signaling and the immunological function of TMEM16J in isolated mouse primary kidney cells, which we know express mRNAs of TMEM16J, SIGIRR and PKP3, in addition to TLR4 and IL1R1. TMEM16J expression in human kidney should also be addressed, and human cell lines can be used to validate the results from murine cells. Depending on the results, identifying activators or inhibitors of TMEM16J among FDA-approved drugs libraries may hold a lot of potential for chronic inflammation and CKD treatment.

ACKNOWLEDGEMENTS

First and foremost, I would like to extend my sincerest gratitude to my mentor Prof. Karl Kunzelmann, for believing in me and giving me the opportunity to join his team. His unwavering support, insightful guidance and expertise in the field have made this journey a truly enriching experience for me. Thank you, Karl, for imparting so much knowledge.
This work would not have been possible without the invaluable assistance and guidance of my mentor Prof. Rainer Schreiber, who generously shared his knowledge and expertise. I am deeply grateful to you, Rainer, for your time and patience.
I am very grateful to Dr. Jiraporn Ousingsawat from whom I have learned so much and who was always there to offer help and advice, both for work and in daily life as well. I would also like to extend my gratitude to Dr. Inês Cabrita for her treasured support during the early stages of my PhD journey.
I express my heartfelt gratitude to Dr. Björn Buchholz for his invaluable mentorship and for the collaborative work included in this thesis.
My appreciation goes out also to our wonderful technical assistants, Patricia Seeberger and Helena Lowack, for being always available to offer support with lab work.

I would like to express my appreciation to the funders of this work; the Deutsche Forschungsgemeinschaft (DFG) and the SFB 1350.

A very special thank you to my dear friend and colleague Raquel Centeio, with whom I shared my ups and downs throughout the last 3 years. Without you, Centeio, this journey would have never been the same. I will always remember our time together in the lab, and all the jokes and laughter.
To all the friends that I have made here in Regensburg, thank you for all the moral support you have given me and for making me feel at home.

À la fin de ce parcours, je tiens à remercier toutes celles et ceux qui sont chers à mon coeur et à qui j'ai consacré peu de temps ces dernières années. Je suis profondément reconnaissante envers mes chers parents, Salma et Bechir, pour leur soutien moral et materiel. Leur amour et comprehension ont contribué à faire de moi la personne que je suis aujourd'hui. Je remercie également mon frère Imed qui m'a toujours encouragé. Mes remerciements s'étendent aussi à toute ma famille et mes amis en Tunisie.

ERKLÄRUNGEN

Hiermit erkläre ich, gem. § 6 Abs. 2, Nr. 6 der Promotionsordnung der Math.-Nat.-Fachbereiche zur Erlangung des Dr. rer. nat., dass ich die vorliegende Dissertation selbständig verfasst und mich keiner anderen als der angegebenen Hilfsmittel bedient habe.

Regensburg, den

KHAOULA TALBI

DETAILS

ADDRESS

Regensburg
Germany

EMAIL

talbikhawla34@gmail.com /
Khaoula.Talbi@ur.de

PROFILE

Motivated biomedical researcher with a focus on kidney diseases and ion channels. Skilled in conducting experiments and analyzing data. Strong background in cellular biology and electrophysiology.

EDUCATION

PhD in Biomedicine, Faculty of Biology and Pre-clinical Medicine, University of Regensburg Title: Ion channels and calcium signaling in kidney disease.
Regensburg, Germany

Oct 2019 –January 2023)

Masters in Molecular and cell Biology, Faculty of Sciences, University of Tunis El Manar / Pasteur institute of Tunis
Tunis, Tunisia

Sep 2015 – Feb 2018

Bachelors in Life sciences, Faculty of sciences, University of Tunis El Manar
Tunis, Tunis

Sep 2012 – Jun 2015

INTERNSHIPS

Laboratory of biomedical genomics and oncogenetics, Pasteur institute of Tunis
Tunis, Tunisia

Feb 2019 – Apr 2019

Laboratory of molecular and cellular hematology, Pasteur institute of Tunis
Tunis, Tunisia

Jan 2017 – Jan 2018

LANGUAGES

Arabic

French

English

Laboratory of biomedical genomics and oncogenetics, Pasteur institute of Tunis — Tunis, Tunisia

Jul 2016 – Aug 2016

Laboratory of hereditary and congenital diseases, Charles Nicolle hospital — Tunis, Tunisia

Mar 2015 — Apr 2015

CERTIFICATES

FELASA B, Humboldt university, Berlin

Aug 2022

CONFERENCES

Europhysiology 2022 (Poster) — Copenhagen, Denmark

Sep 2022

International SFB symposium (Poster) — Regensburg, Germany

May 2022

100th Meeting of the German Physiological Society (Poster) — Frankfurt am Main, Germany

Sep 2021

LAB SKILLS

Patch Clamp

Cell culture (primary cells and immortalized cell lines)

Mouse handling

Primary kidney cells isolationKidney

perfusion

Intracellular Calcium measurements

Immunohistochemistry

Viral transfection

PUBLICATIONS

1. Schreiber, R., **Talbi, K.**, Ousingsawat, J., & Kunzelmann, K. (2023). A TMEM16J variant leads to dysregulated cytosolic calcium which may lead to renal disease. *FASEB journal*: official publication of the Federation of American Societies for Experimental Biology, 37(1), e22683.

2. K. Jo, S., Centeio, R., Park, J., Ousingsawat, J., Jeon, D. K., **Talbi, K.**, Schreiber, R., Ryu, Kahlenberg, K., Somoza, V., Delpiano,, Gray, M. A., Amaral, M. D., Railean,V., Beekman, J. M., Rodenburg, L. W., Namkung, W., & Kunzelmann, K. (2022). The SLC26A9 inhibitor S9-A13 provides no evidence for a role of SLC26A9 in airway chloride secretion but suggests a contribution to regulation of ASL pH and gastric proton secretion. *FASEB journal*: official publication of the Federation of American Societies for Experimental Biology, 36(11), e22534.

3. K. Lin, J., Gettings, S. M., **Talbi, K.,** Schreiber, R., Taggart, M. J., Preller, M., Kunzelmann, K., Althaus, M., & Gray, A. (2022). Pharmacological inhibitors of the cystic fibrosis transmembrane conductance regulator exert off-target effects on epithelial cation channels. Pflugers Archiv: *European journal of physiology*, 10.1007/s00424-022-02758-9.

4. Ousingsawat, J., Centeio, R., Cabrita, I., **Talbi, K.**, Zimmer, O., Graf, M., Göpferich, A., Schreiber, R., & Kunzelmann, K. (2022). Airway Delivery of Hydrogel Encapsulated Niclosamide for the Treatment of Inflammatory Airway Disease. *International journal of molecular sciences*, 23(3), 1085.

4. Cabrita, I., **Talbi, K.**, Kunzelmann, K., Schreiber, R. (2021). Loss of PKD1 and PKD2 share common effects on intracellular Ca2+signaling. *Cell calcium*, 97, 102413.

5. Talbi, K., Cabrita, I., Schreiber, R., & Kunzelmann, K. (2021). Gender-Dependent Phenotype in Polycystic Kidney Disease Is Determined by Differential Intracellular Ca2+ Signals. *International journal of molecular sciences*, 22(11), 6019.

6. Centeio, R., Ousingsawat, J., Cabrita, I., Schreiber, R., **Talbi, K.,** Benedetto, R., Doušová, T., Verbeken, E. K., De Boeck, K., Cohen, I., & Kunzelmann, K. (2021). Mucus Release and Airway Constriction by TMEM16A May Worsen Pathology in Inflammatory Lung Disease. *International journal of molecular sciences*, 22(15), 7852.

7. Talbi, K., Ousingsawat, J., Centeio, R., Schreiber, R., & Kunzelmann, K. (2021). Calmodulin-Dependent Regulation of Overexpressed but Not Endogenous TMEM16A Expressed in Airway Epithelial Cells**.** *Membranes*, 11(9), 723.

8. Talbi, K., Cabrita, I., Kraus, A., Hofmann, S., Skoczynski, K., Kunzelmann, K., Buchholz, B., & Schreiber, R. (2021). The chloride channel CFTR is not required for cyst growth in an ADPKD mouse model. *FASEB journal*: official publication of the Federation of American Societies for Experimental Biology, 35(10), e21897.

9. Bouguerra, G., **Talbi, K.**, Trabelsi, N., Chaouachi, D., Boudriga, I., Abbès, S., & Menif, S. (2021). Enhanced Eryptosis in Glucose-6-Phosphate Dehydrogenase Deficiency. *Cellular*

physiology and biochemistry: international journal of experimental cellular physiology biochemistry, and pharmacology, 55(6), 761–772.

10. Centeio, R., Cabrita, I., Benedetto, R., **Talbi, K.**, Ousingsawat, J., Schreiber, R., Sullivan, J. K., & Kunzelmann, K. (2020**).** Pharmacological Inhibition and Activation of the Ca2+ Activated Cl- Channel TMEM16A. *International journal of molecular sciences*, 21(7), 2557

REFERENCE LIST

1. Lanktree, M.B.*, et al.* Prevalence Estimates of Polycystic Kidney and Liver Disease by Population Sequencing. *Journal of the American Society of Nephrology : JASN* **29**, 2593-2600 (2018).
2. Gabow, P.A.*, et al.* Factors affecting the progression of renal disease in autosomal-dominant polycystic kidney disease. *Kidney international* **41**, 1311-1319 (1992).
3. Cornec-Le Gall, E., Alam, A. & Perrone, R.D. Autosomal dominant polycystic kidney disease. *Lancet (London, England)* **393**, 919-935 (2019).
4. Johnson, A.M. & Gabow, P.A. Identification of patients with autosomal dominant polycystic kidney disease at highest risk for end-stage renal disease. *Journal of the American Society of Nephrology : JASN* **8**, 1560-1567 (1997).
5. Stewart, J.H. End-stage renal failure appears earlier in men than in women with polycystic kidney disease. *American journal of kidney diseases : the official journal of the National Kidney Foundation* **24**, 181-183 (1994).
6. Mauvais-Jarvis, F., Arnold, A.P. & Reue, K. A Guide for the Design of Pre-clinical Studies on Sex Differences in Metabolism. *Cell metabolism* **25**, 1216-1230 (2017).
7. Ho, C.K. & Habib, F.K. Estrogen and androgen signaling in the pathogenesis of BPH. *Nature reviews. Urology* **8**, 29-41 (2011).
8. De León-Nava, M.A.*, et al.* Immune sexual dimorphism: effect of gonadal steroids on the expression of cytokines, sex steroid receptors, and lymphocyte proliferation. *The Journal of steroid biochemistry and molecular biology* **113**, 57-64 (2009).
9. Ikeda, Y.*, et al.* Androgen receptor gene knockout male mice exhibit impaired cardiac growth and exacerbation of angiotensin II-induced cardiac fibrosis. *The Journal of biological chemistry* **280**, 29661-29666 (2005).
10. Luine, V.N. Sex steroids and cognitive function. *Journal of neuroendocrinology* **20**, 866-872 (2008).
11. Dubois, V.*, et al.* A satellite cell-specific knockout of the androgen receptor reveals myostatin as a direct androgen target in skeletal muscle. *FASEB journal : official publication of the Federation of American Societies for Experimental Biology* **28**, 2979-2994 (2014).
12. Cowley, B.D., Jr.*, et al.* Autosomal-dominant polycystic kidney disease in the rat. *Kidney international* **43**, 522-534 (1993).
13. Stringer, K.D.*, et al.* Gender hormones and the progression of experimental polycystic kidney disease. *Kidney international* **68**, 1729-1739 (2005).
14. Cowley, B.D., Jr., Rupp, J.C., Muessel, M.J. & Gattone, V.H., 2nd. Gender and the effect of gonadal hormones on the progression of inherited polycystic kidney disease in rats. *American journal of kidney diseases : the official journal of the National Kidney Foundation* **29**, 265-272 (1997).
15. Hughes, J.*, et al.* The polycystic kidney disease 1 (PKD1) gene encodes a novel protein with multiple cell recognition domains. *Nature genetics* **10**, 151-160 (1995).
16. Mochizuki, T.*, et al.* PKD2, a gene for polycystic kidney disease that encodes an integral membrane protein. *Science (New York, N.Y.)* **272**, 1339-1342 (1996).
17. Cornec-Le Gall, E.*, et al.* PKD2-Related Autosomal Dominant Polycystic Kidney Disease: Prevalence, Clinical Presentation, Mutation Spectrum, and Prognosis. *American journal of kidney diseases : the official journal of the National Kidney Foundation* **70**, 476-485 (2017).
18. Lu, W.*, et al.* Perinatal lethality with kidney and pancreas defects in mice with a targetted Pkd1 mutation. *Nature genetics* **17**, 179-181 (1997).
19. Wu, G.*, et al.* Cardiac defects and renal failure in mice with targeted mutations in Pkd2. *Nature genetics* **24**, 75-78 (2000).
20. Brasier, J.L. & Henske, E.P. Loss of the polycystic kidney disease (PKD1) region of chromosome 16p13 in renal cyst cells supports a loss-of-function model for cyst pathogenesis. *The Journal of clinical investigation* **99**, 194-199 (1997).
21. Qian, F., Watnick, T.J., Onuchic, L.F. & Germino, G.G. The molecular basis of focal cyst

formation in human autosomal dominant polycystic kidney disease type I. *Cell* **87**, 979-987 (1996).
22. Pei, Y.*, et al.* Somatic PKD2 mutations in individual kidney and liver cysts support a "two-hit" model of cystogenesis in type 2 autosomal dominant polycystic kidney disease. *Journal of the American Society of Nephrology : JASN* **10**, 1524-1529 (1999).
23. Lantinga-van Leeuwen, I.S.*, et al.* Kidney-specific inactivation of the Pkd1 gene induces rapid cyst formation in developing kidneys and a slow onset of disease in adult mice. *Human molecular genetics* **16**, 3188-3196 (2007).
24. Happé, H.*, et al.* Toxic tubular injury in kidneys from Pkd1-deletion mice accelerates cystogenesis accompanied by dysregulated planar cell polarity and canonical Wnt signaling pathways. *Human molecular genetics* **18**, 2532-2542 (2009).
25. Takakura, A.*, et al.* Renal injury is a third hit promoting rapid development of adult polycystic kidney disease. *Human molecular genetics* **18**, 2523-2531 (2009).
26. Nims, N., Vassmer, D. & Maser, R.L. Transmembrane domain analysis of polycystin-1, the product of the polycystic kidney disease-1 (PKD1) gene: evidence for 11 membrane-spanning domains. *Biochemistry* **42**, 13035-13048 (2003).
27. Brill, A.L. & Ehrlich, B.E. Polycystin 2: A calcium channel, channel partner, and regulator of calcium homeostasis in ADPKD. *Cellular signalling* **66**, 109490 (2020).
28. Ward, C.J.*, et al.* Polycystin, the polycystic kidney disease 1 protein, is expressed by epithelial cells in fetal, adult, and polycystic kidney. *Proceedings of the National Academy of Sciences of the United States of America* **93**, 1524-1528 (1996).
29. Ibraghimov-Beskrovnaya, O.*, et al.* Strong homophilic interactions of the Ig-like domains of polycystin-1, the protein product of an autosomal dominant polycystic kidney disease gene, PKD1. *Human molecular genetics* **9**, 1641-1649 (2000).
30. Ibraghimov-Beskrovnaya, O.*, et al.* Polycystin: in vitro synthesis, in vivo tissue expression, and subcellular localization identifies a large membrane-associated protein. *Proceedings of the National Academy of Sciences of the United States of America* **94**, 6397-6402 (1997).
31. Dell, K.M. The role of cilia in the pathogenesis of cystic kidney disease. *Current opinion in pediatrics* **27**, 212-218 (2015).
32. Babich, V.*, et al.* The N-terminal extracellular domain is required for polycystin-1-dependent channel activity. *The Journal of biological chemistry* **279**, 25582-25589 (2004).
33. Hanaoka, K.*, et al.* Co-assembly of polycystin-1 and -2 produces unique cation-permeable currents. *Nature* **408**, 990-994 (2000).
34. Liu, X.*, et al.* Polycystin-2 is an essential ion channel subunit in the primary cilium of the renal collecting duct epithelium. *eLife* **7**(2018).
35. Grieben, M.*, et al.* Structure of the polycystic kidney disease TRP channel Polycystin-2 (PC2). *Nature structural & molecular biology* **24**, 114-122 (2017).
36. Cai, Y.*, et al.* Calcium dependence of polycystin-2 channel activity is modulated by phosphorylation at Ser812. *The Journal of biological chemistry* **279**, 19987-19995 (2004).
37. Wilkes, M.*, et al.* Molecular insights into lipid-assisted Ca(2+) regulation of the TRP channel Polycystin-2. *Nature structural & molecular biology* **24**, 123-130 (2017).
38. Kuo, I.Y.*, et al.* The number and location of EF hand motifs dictates the calcium dependence of polycystin-2 function. *FASEB journal : official publication of the Federation of American Societies for Experimental Biology* **28**, 2332-2346 (2014).
39. Su, Q.*, et al.* Structure of the human PKD1-PKD2 complex. *Science (New York, N.Y.)* **361**(2018).
40. Nauli, S.M.*, et al.* Endothelial cilia are fluid shear sensors that regulate calcium signaling and nitric oxide production through polycystin-1. *Circulation* **117**, 1161-1171 (2008).
41. Delling, M., DeCaen, P.G., Doerner, J.F., Febvay, S. & Clapham, D.E. Primary cilia are specialized calcium signalling organelles. *Nature* **504**, 311-314 (2013).
42. AbouAlaiwi, W.A.*, et al.* Ciliary polycystin-2 is a mechanosensitive calcium channel involved in nitric oxide signaling cascades. *Circulation research* **104**, 860-869 (2009).
43. Delling, M.*, et al.* Primary cilia are not calcium-responsive mechanosensors. *Nature* **531**,

656-660 (2016).
44. Li, Y., Wright, J.M., Qian, F., Germino, G.G. & Guggino, W.B. Polycystin 2 interacts with type I inositol 1,4,5-trisphosphate receptor to modulate intracellular Ca2+ signaling. *The Journal of biological chemistry* **280**, 41298-41306 (2005).
45. Santoso, N.G., Cebotaru, L. & Guggino, W.B. Polycystin-1, 2, and STIM1 interact with IP(3)R to modulate ER Ca release through the PI3K/Akt pathway. *Cell Physiol Biochem* **27**, 715-726 (2011).
46. Anyatonwu, G.I., Estrada, M., Tian, X., Somlo, S. & Ehrlich, B.E. Regulation of ryanodine receptor-dependent calcium signaling by polycystin-2. *Proceedings of the National Academy of Sciences of the United States of America* **104**, 6454-6459 (2007).
47. Lemos, F.O. & Ehrlich, B.E. Polycystin and calcium signaling in cell death and survival. *Cell calcium* **69**, 37-45 (2018).
48. Terryn, S., Ho, A., Beauwens, R. & Devuyst, O. Fluid transport and cystogenesis in autosomal dominant polycystic kidney disease. *Biochim. Biophys. Acta* (2011).
49. Grantham, J.J*., et al.* Volume progression in polycystic kidney disease. *The New England journal of medicine* **354**, 2122-2130 (2006).
50. Mochizuki, T., Tsuchiya, K. & Nitta, K. Autosomal dominant polycystic kidney disease: recent advances in pathogenesis and potential therapies. *Clinical and experimental nephrology* **17**, 317-326 (2013).
51. Sun, Y*., et al.* Signaling pathway of MAPK/ERK in cell proliferation, differentiation, migration, senescence and apoptosis. *Journal of receptor and signal transduction research* **35**, 600-604 (2015).
52. Ibraghimov-Beskrovnaya, O. & Bukanov, N. Polycystic kidney diseases: from molecular discoveries to targeted therapeutic strategies. *Cellular and molecular life sciences : CMLS* **65**, 605-619 (2008).
53. Yamaguchi, T., Nagao, S., Kasahara, M., Takahashi, H. & Grantham, J.J. Renal accumulation and excretion of cyclic adenosine monophosphate in a murine model of slowly progressive polycystic kidney disease. *American journal of kidney diseases : the official journal of the National Kidney Foundation* **30**, 703-709 (1997).
54. Smith, L.A*., et al.* Development of polycystic kidney disease in juvenile cystic kidney mice: insights into pathogenesis, ciliary abnormalities, and common features with human disease. *Journal of the American Society of Nephrology : JASN* **17**, 2821-2831 (2006).
55. Belibi, F.A*., et al.* Cyclic AMP promotes growth and secretion in human polycystic kidney epithelial cells. *Kidney international* **66**, 964-973 (2004).
56. Yamaguchi, T*., et al.* Cyclic AMP activates B-Raf and ERK in cyst epithelial cells from autosomal-dominant polycystic kidneys. *Kidney international* **63**, 1983-1994 (2003).
57. Yamaguchi, T*., et al.* Calcium restriction allows cAMP activation of the B-Raf/ERK pathway, switching cells to a cAMP-dependent growth-stimulated phenotype. *The Journal of biological chemistry* **279**, 40419-40430 (2004).
58. Jouret, F. & Devuyst, O. Targeting chloride transport in autosomal dominant polycystic kidney disease. *Cellular signalling* **73**, 109703 (2020).
59. Capuano, I., Buonanno, P., Riccio, E., Amicone, M. & Pisani, A. Therapeutic advances in ADPKD: the future awaits. *Journal of nephrology* **35**, 397-415 (2022).
60. Tao, Y*., et al.* Pathways of caspase-mediated apoptosis in autosomal-dominant polycystic kidney disease (ADPKD). *Kidney international* **67**, 909-919 (2005).
61. Nowak, K.L. & Edelstein, C.L. Apoptosis and autophagy in polycystic kidney disease (PKD). *Cellular signalling* **68**, 109518 (2020).
62. Mangoo-Karim, R., Ye, M., Wallace, D.P., Grantham, J.J. & Sullivan, L.P. Anion secretion drives fluid secretion by monolayers of cultured human polycystic cells. *The American journal of physiology* **269**, F381-388 (1995).
63. Wallace, D.P., Grantham, J.J. & Sullivan, L.P. Chloride and fluid secretion by cultured human polycystic kidney cells. *Kidney international* **50**, 1327-1336 (1996).
64. Albaqumi, M*., et al.* KCa3.1 potassium channels are critical for cAMP-dependent chloride secretion and cyst growth in autosomal-dominant polycystic kidney disease. *Kidney international* **74**, 740-749 (2008).

65. Geering, K. Functional roles of Na,K-ATPase subunits. *Current opinion in nephrology and hypertension* **17**, 526-532 (2008).
66. Zatti, A.*, et al.* The C-terminal tail of the polycystin-1 protein interacts with the Na,K-ATPase alpha-subunit. *Molecular biology of the cell* **16**, 5087-5093 (2005).
67. Cabrita, I.*, et al.* Cyst growth in ADPKD is prevented by pharmacological and genetic inhibition of TMEM16A in vivo. *Nat Commun* **11**, 4320 (2020).
68. Hanaoka, K., Devuyst, O., Schwiebert, E.M., Wilson, P.D. & Guggino, W.B. A role for CFTR in human autosomal dominant polycystic kidney disease. *The American journal of physiology* **270**, C389-C399 (1996).
69. Thomson, R.B.*, et al.* Histopathological analysis of renal cystic epithelia in the Pkd2WS25/- mouse model of ADPKD. *American journal of physiology. Renal physiology* **285**, F870-880 (2003).
70. Zhang, Z., Liu, F. & Chen, J. Conformational Changes of CFTR upon Phosphorylation and ATP Binding. *Cell* **170**, 483-491.e488 (2017).
71. O'Riordan, C.R., Lachapelle, A.L., Marshall, J., Higgins, E.A. & Cheng, S.H. Characterization of the oligosaccharide structures associated with the cystic fibrosis transmembrane conductance regulator. *Glycobiology* **10**, 1225-1233 (2000).
72. Swahn, H. & Harris, A. Cell-Selective Regulation of CFTR Gene Expression: Relevance to Gene Editing Therapeutics. *Genes* **10**(2019).
73. Crawford, I.*, et al.* Immunocytochemical localization of the cystic fibrosis gene product CFTR. *Proc. Natl. Acad. Sci* **88**, 9262-9266 (1991).
74. Berg, P.*, et al.* The molecular mechanism of CFTR- and secretin-dependent renal bicarbonate excretion *J Physiol.* **599**, 3003-3011 (2021).
75. Davidow, C.J., Maser, R.L., Rome, L.A., Calvet, J.P. & Grantham, J.J. The cystic fibrosis transmembrane conductance regulator mediates transepithelial fluid secretion by human autosomal dominant polycystic kidney disease epithelium in vitro. *Kidney international* **50**, 208-218 (1996).
76. (!!! INVALID CITATION !!! {Li, 2004 #3652;Yang, 2008 #4474}).
77. Yang, B., Sonawane, N.D., Zhao, D., Somlo, S. & Verkman, A.S. Small-Molecule CFTR Inhibitors Slow Cyst Growth in Polycystic Kidney Disease. *J Am Soc. Nephrol* **19**, 1300-1310 (2008).
78. Shin, Y.B. & Park, J.H. Recent Trends in ADPKD Research. *Advances in experimental medicine and biology* **933**, 3-11 (2016).
79. O'Sullivan, D.A.*, et al.* Cystic fibrosis and the phenotypic expression of autosomal dominant polycystic kidney disease [see comments]. *American journal of kidney diseases : the official journal of the National Kidney Foundation* **32**, 976-983 (1998).
80. Persu, A.*, et al.* CF gene and cystic fibrosis transmembrane conductance regulator expression in autosomal dominant polycystic kidney disease. *Journal of the American Society of Nephrology : JASN* **11**, 2285-2296 (2000).
81. Rieg, T. & Vallon, V. ATP and adenosine in the local regulation of water transport and homeostasis by the kidney. *American journal of physiology. Regulatory, integrative and comparative physiology* **296**, R419-427 (2009).
82. Ilatovskaya, D.V., Palygin, O. & Staruschenko, A. Functional and therapeutic importance of purinergic signaling in polycystic kidney disease. *American journal of physiology. Renal physiology* **311**, F1135-f1139 (2016).
83. Schwiebert, E.M.*, et al.* Autocrine extracellular purinergic signaling in epithelial cells derived from polycystic kidneys. *Am. J Physiol Renal Physiol* **282**, F763-F775 (2002).
84. Hovater, M.B., Olteanu, D., Welty, E.A. & Schwiebert, E.M. Purinergic signaling in the lumen of a normal nephron and in remodeled PKD encapsulated cysts. *Purinergic. Signal* **4**, 109-124 (2008).
85. Buchholz, B.*, et al.* Anoctamin 1 induces calcium-activated chloride secretion and proliferation of renal cyst-forming epithelial cells. *Kidney international* **85**, 1058-1067 (2014).
86. Cabrita, I., Buchholz, B., Schreiber, R. & Kunzelmann, K. TMEM16A drives renal cyst growth by augmenting Ca(2+) signaling in M1 cells. *J Mol Med (Berl)* **98**, 659-671 (2020).
87. Hartzell, H.C., Putzier, I. & Arreola, J. Calcium-Activated Chloride Channels. *Annu. Rev.*

Physiol **67**, 719-758 (2005).
88. Caputo, A.*, et al.* TMEM16A, A Membrane Protein Associated With Calcium-Dependent Chloride Channel Activity. *Science (New York, N.Y.)* **322**, 590-594 (2008).
89. Schroeder, B.C., Cheng, T., Jan, Y.N. & Jan, L.Y. Expression cloning of TMEM16A as a calcium-activated chloride channel subunit. *Cell* **134**, 1019-1029 (2008).
90. Yang, Y.D.*, et al.* TMEM16A confers receptor-activated calcium-dependent chloride conductance. *Nature* **455**, 1210-1215 (2008).
91. Brunner, J.D., Lim, N.K., Schenck, S., Duerst, A. & Dutzler, R. X-ray structure of a calcium-activated TMEM16 lipid scramblase. *Nature* **516**, 207-212 (2014).
92. Paulino, C., Kalienkova, V., Lam, A.K.M., Neldner, Y. & Dutzler, R. Activation mechanism of the calcium-activated chloride channel TMEM16A revealed by cryo-EM. *Nature* **552**, 421-425 (2017).
93. Le, S.C., Liang, P., Lowry, A.J. & Yang, H. Gating and Regulatory Mechanisms of TMEM16 Ion Channels and Scramblases. *Front Physiol* **12**, 787773 (2021).
94. Ma, K., Wang, H., Yu, J., Wei, M. & Xiao, Q. New Insights on the Regulation of Ca2+ - Activated Chloride Channel TMEM16A. *J Cell Physiol* (2017).
95. Stevens, F.C. Calmodulin: an introduction. *Canadian journal of biochemistry and cell biology = Revue canadienne de biochimie et biologie cellulaire* **61**, 906-910 (1983).
96. Gnegy, M.E. Ca2+/calmodulin signaling in NMDA-induced synaptic plasticity. *Critical reviews in neurobiology* **14**, 91-129 (2000).
97. Walsh, M.P. Calmodulin and the regulation of smooth muscle contraction. *Molecular and cellular biochemistry* **135**, 21-41 (1994).
98. Berchtold, M.W. & Villalobo, A. The many faces of calmodulin in cell proliferation, programmed cell death, autophagy, and cancer. *Biochimica et biophysica acta* **1843**, 398-435 (2014).
99. Kaneko, H., Möhrlen, F. & Frings, S. Calmodulin contributes to gating control in olfactory calcium-activated chloride channels. *The Journal of general physiology* **127**, 737-748 (2006).
100. Tian, Y.*, et al.* Calmodulin-dependent activation of the epithelial calcium-dependent chloride channel TMEM16A. *FASEB journal : official publication of the Federation of American Societies for Experimental Biology* **25**, 1058-1068 (2011).
101. Terashima, H., Picollo, A. & Accardi, A. Purified TMEM16A is sufficient to form Ca2+-activated Cl- channels. *Proc. Natl. Acad. Sci. U. S A* **110**, 19354-19359 (2013).
102. Yu, K., Zhu, J., Qu, Z., Cui, Y.Y. & Hartzell, H.C. Activation of the Ano1 (TMEM16A) chloride channel by calcium is not mediated by calmodulin. *J Gen. Physiol* **143**, 253-267 (2014).
103. Perez-Cornejo, P.*, et al.* Anoctamin 1 (Tmem16A) Ca2+-activated chloride channel stoichiometrically interacts with an ezrin-radixin-moesin network. *Proc. Natl. Acad. Sci. U. S. A* **109**, 10376-10381 (2012).
104. Yang, T. & Colecraft, H.M. Calmodulin regulation of TMEM16A and 16B Ca-activated chloride channels. *Channels (Austin.)*, 0 (2015).
105. Yang, T., Hendrickson, W.A. & Colecraft, H.M. Preassociated apocalmodulin mediates Ca2+-dependent sensitization of activation and inactivation of TMEM16A/16B Ca2+-gated Cl- channels. *Proc. Natl. Acad. Sci. U. S. A* **111**, 18213-18218 (2014).
106. Duvvuri, U.*, et al.* TMEM16A, induces MAPK and contributes directly to tumorigenesis and cancer progression. *Cancer Res* **72**, 3270-3281 (2012).
107. Kunzelmann, K.*, et al.* Expression and function of epithelial anoctamins. *Exp. Physiol* **97**, 184-192 (2012).
108. Liu, Y., Liu, Z. & Wang, K. The Ca(2+)-activated chloride channel ANO1/TMEM16A: An emerging therapeutic target for epithelium-originated diseases? *Acta pharmaceutica Sinica. B* **11**, 1412-1433 (2021).
109. Leblanc, N. Targeting TMEM16A-encoded Ca(2+)-activated Cl(-) channels: a new paradigm for antihypertensive therapy? *Kidney international* **100**, 269-272 (2021).
110. Faria, D.*, et al.* The calcium activated chloride channel Anoctamin 1 contributes to the regulation of renal function. *Kindey Int* **85**, 1369-1381 (2014).
111. Schenk, L.K.*, et al.* Nephron-specific knockout of TMEM16A leads to reduced number

of glomeruli and albuminuria. *American journal of physiology. Renal physiology* **315**, F1777-F1786 (2018).
112. Ruppersburg, C.C. & Hartzell, H.C. The Ca2+-activated Cl- channel ANO1/TMEM16A regulates primary ciliogenesis. *Molecular biology of the cell* **25**, 1793-1807 (2014).
113. Urrutia, J.*, et al.* The Crossroad of Ion Channels and Calmodulin in Disease. *International journal of molecular sciences* **20**(2019).
114. Stefan, C.J., Manford, A.G. & Emr, S.D. ER-PM connections: sites of information transfer and inter-organelle communication. *Current opinion in cell biology* **25**, 434-442 (2013).
115. Wolf, W.*, et al.* Yeast Ist2 recruits the endoplasmic reticulum to the plasma membrane and creates a ribosome-free membrane microcompartment. *PLoS. ONE* **7**, e39703 (2012).
116. Cabrita, I.*, et al.* Differential effects of anoctamins on intracellular calcium signals. *FASEB journal : official publication of the Federation of American Societies for Experimental Biology* **31**, 2123-2134 (2017).
117. Jin, X.*, et al.* Activation of the Cl- Channel ANO1 by Localized Calcium Signals in Nociceptive Sensory Neurons Requires Coupling with the IP3 Receptor. *Sci. Signal* **6**, ra73 (2013).
118. Kunzelmann, K.*, et al.* Modulating Ca2+signals: a common theme for TMEM16, Ist2, and TMC. *Pflugers Archiv : European journal of physiology* **468**, 475-490 (2016).
119. Kunzelmann, K., Ousingsawat, J., Benedetto, R., Cabrita, I. & Schreiber, R. Contribution of Anoctamins to Cell Survival and Cell Death. *Cancers* **19**, E382 (2019).
120. Stanzick, K.J.*, et al.* Discovery and prioritization of variants and genes for kidney function in >1.2 million individuals. *Nat Commun* **12**, 4350 (2021).
121. Ammirati, A.L. Chronic Kidney Disease. *Revista da Associacao Medica Brasileira (1992)* **66Suppl 1**, s03-s09 (2020).
122. Germolec, D.R., Shipkowski, K.A., Frawley, R.P. & Evans, E. Markers of Inflammation. *Methods in molecular biology (Clifton, N.J.)* **1803**, 57-79 (2018).
123. Ebert, T.*, et al.* Inflammation and Premature Ageing in Chronic Kidney Disease. *Toxins* **12**(2020).
124. Lang, T. & Mansell, A. The negative regulation of Toll-like receptor and associated pathways. *Immunol Cell Biol* **85**, 425-434 (2007).
125. Horne, D.J.*, et al.* Common polymorphisms in the PKP3-SIGIRR-TMEM16J gene region are associated with susceptibility to tuberculosis. *J Infect. Dis* **205**, 586-594 (2012).
126. Roberts, B.J., Reddy, R. & Wahl, J.K., 3rd. Stratifin (14-3-3 σ) limits plakophilin-3 exchange with the desmosomal plaque. *PloS one* **8**, e77012 (2013).
127. Basu, S.*, et al.* Plakophilin3 loss leads to an increase in lipocalin2 expression, which is required for tumour formation. *Experimental cell research* **369**, 251-265 (2018).
128. Sklyarova, T.*, et al.* Hematopoietic plakophilin-3 regulates acute tissue-specific and systemic inflammation in mice. *European journal of immunology* **45**, 2898-2910 (2015).
129. Supino, D.*, et al.* Negative Regulation of the IL-1 System by IL-1R2 and IL-1R8: Relevance in Pathophysiology and Disease. *Frontiers in immunology* **13**, 804641 (2022).
130. Wiegert, J.S. & Bading, H. Activity-dependent calcium signaling and ERK-MAP kinases in neurons: a link to structural plasticity of the nucleus and gene transcription regulation. *Cell calcium* **49**, 296-305 (2011).
131. Park, Y.J., Yoo, S.A., Kim, M. & Kim, W.U. The Role of Calcium-Calcineurin-NFAT Signaling Pathway in Health and Autoimmune Diseases. *Frontiers in immunology* **11**, 195 (2020).
132. Chow, C.W., Rincón, M. & Davis, R.J. Requirement for transcription factor NFAT in interleukin-2 expression. *Mol Cell Biol* **19**, 2300-2307 (1999).
133. Harris, P.C. & Torres, V.E. Polycystic kidney disease. *Annu Rev Med* **60**, 321-337 (2009).
134. Schreiber, R., Faria, D., Skryabin, B.V., Rock, J.R. & Kunzelmann, K. Anoctamins support calcium-dependent chloride secretion by facilitating calcium signaling in adult mouse intestine. *Pflugers Archiv : European journal of physiology* **467**, 1203-1213 (2015).

135. Benedetto, R.*, et al.* Epithelial Chloride Transport by CFTR Requires TMEM16A. *Scientific reports* **7**, 12397 (2017).
136. Liu, Y.*, et al.* Volume-regulated Cl(-) current: contributions of distinct Cl(-) channel and localized Ca(2+) signals. *Am J Physiol Cell Physiol* **317**, C466-C480 (2019).
137. Buchholz, B.*, et al.* Anoctamin 1 induces calcium-activated chloride secretion and tissue proliferation in polycystic kidney disease. *Kidney international* **85**, 1058-1067 (2014).
138. Kraus, A.*, et al.* HIF-1alpha promotes cyst progression in a mouse model of autosomal dominant polycystic kidney disease. *Kidney international* **94**, 887-899 (2018).
139. Mendes, F.*, et al.* Establishment and Characterization of a novel polarized MDCK epithelial cellular model for CFTR studies. *Cell Physiol Biochemc* **16**, 281-290 (2005).
140. Kappes, J.C., Wu, X. & Wakefield, J.K. Production of trans-lentiviral vector with predictable safety. *Methods Mol Med* **76**, 449-465 (2003).
141. Wegierski, T.*, et al.* TRPP2 channels regulate apoptosis through the Ca2+ concentration in the endoplasmic reticulum. *EMBO J* **28**, 490-499 (2009).
142. Lee, E.J.*, et al.* TAZ/Wnt-β-catenin/c-MYC axis regulates cystogenesis in polycystic kidney disease. *Proceedings of the National Academy of Sciences of the United States of America* **117**, 29001-29012 (2020).
143. Xiao, Z.*, et al.* Polycystin-1 interacts with TAZ to stimulate osteoblastogenesis and inhibit adipogenesis. *The Journal of clinical investigation* **128**, 157-174 (2018).
144. Zhang, C.*, et al.* Cyclin-Dependent Kinase 1 Activity Is a Driver of Cyst Growth in Polycystic Kidney Disease. *Journal of the American Society of Nephrology : JASN* (2020).
145. Shen, A.W.*, et al.* SNX9 Inhibits Cell Proliferation and Cyst Development in Autosomal Dominant Polycystic Kidney Disease via Activation of the Hippo-YAP Signaling Pathway. *Front Cell Dev Biol* **8**, 811 (2020).
146. Fragiadaki, M.*, et al.* STAT5 drives abnormal proliferation in autosomal dominant polycystic kidney disease. *Kidney international* **91**, 575-586 (2017).
147. Song, X.*, et al.* Systems biology of autosomal dominant polycystic kidney disease (ADPKD): computational identification of gene expression pathways and integrated regulatory networks. *Human molecular genetics* **18**, 2328-2343 (2009).
148. Berg, P.*, et al.* Impaired Renal HCO(3) (-) Excretion in Cystic Fibrosis. *Journal of the American Society of Nephrology : JASN* **31**, 1711-1727 (2020).
149. Benedetto, R.*, et al.* Plasma membrane localized TMEM16 Proteins are Indispensable for expression of CFTR. *J Mol Med* **97**, 711-722 (2019).
150. Lerias, J.R.*, et al.* A novel microscopy-based assay identifies extended synaptotagmin-1 (ESYT1) as a positive regulator of anoctamin 1 traffic. *Biochimica et biophysica acta* **1865**, 421-431. (2018).
151. Lerias, J.*, et al.* Compartmentalized crosstalk of CFTR and TMEM16A (ANO1) through EPAC1 and ADCY1. *Cellular signalling* **44**, 10-19 (2018).
152. Kraus, A.*, et al.* P2Y2R is a direct target of HIF-1alpha and mediates secretion-dependent cyst growth of renal cyst-forming epithelial cells. *Purinergic Signal* **12**, 687-695 (2016).
153. Praetorius, H.A. & Leipziger, J. Primary cilium-dependent sensing of urinary flow and paracrine purinergic signaling. *Semin. Cell Dev. Biol* **24**, 3-10 (2013).
154. Mekahli, D., Parys, J.B., Bultynck, G., Missiaen, L. & De Smedt, H. Polycystins and cellular Ca2+ signaling. *Cellular and molecular life sciences : CMLS* **70**, 2697-2712 (2013).
155. Yamaguchi, T., Hempson, S.J., Reif, G.A., Hedge, A.M. & Wallace, D.P. Calcium restores a normal proliferation phenotype in human polycystic kidney disease epithelial cells. *Journal of the American Society of Nephrology : JASN* **17**, 178-187 (2006).
156. Himpens, B., De Smedt, H. & Casteels, R. Intracellular Ca2+ signaling induced by vasopressin, ATP, and epidermal growth factor in epithelial LLC-PK1 cells. *The American journal of physiology* **265**, C966-975 (1993).
157. Jin, X., Shah, S., Du, X., Zhang, H. & Gamper, N. Activation of Ca2+-activated Cl- channel ANO1 by localized Ca2+ signals. *J Physiol* **594**, 19-30 (2016).
158. Bill, A.*, et al.* Small molecule-facilitated degradation of ANO1 protein: a new targeting

approach for anticancer therapeutics. *The Journal of biological chemistry* **289**, 11029-11041 (2014).
159. Lüscher, B.P., Vachel, L., Ohana, E. & Muallem, S. Cl(-) as a bona fide signaling ion. *Am J Physiol Cell Physiol* **318**, C125-c136 (2020).
160. He, M.*, et al.* Chloride channels regulate differentiation and barrier functions of the mammalian airway. *eLife* **9**(2020).
161. He, M.*, et al.* Cytoplasmic Cl(-) couples membrane remodeling to epithelial morphogenesis. *Proceedings of the National Academy of Sciences of the United States of America* **114**, E11161-e11169 (2017).
162. Jha, A.*, et al.* Anoctamin 8 tethers endoplasmic reticulum and plasma membrane for assembly of Ca(2+) signaling complexes at the ER/PM compartment. *Embo j* **38**, e101452 (2020).
163. Muallem, S., Chung, W.Y., Jha, A. & Ahuja, M. Lipids at membrane contact sites: cell signaling and ion transport. *EMBO reports* **18**, 1893-1904 (2017).
164. Torres, V.E., Harris, P.C. & Pirson, Y. Autosomal dominant polycystic kidney disease. *Lancet (London, England)* **369**, 1287-1301 (2007).
165. Grantham, J.J., Mulamalla, S. & Swenson-Fields, K.I. Why kidneys fail in autosomal dominant polycystic kidney disease. *Nat Rev Nephrol* **7**, 556-566 (2011).
166. Terryn, S., Ho, A., Beauwens, R. & Devuyst, O. Fluid transport and cystogenesis in autosomal dominant polycystic kidney disease. *Biochimica et biophysica acta* **1812**, 1314-1321 (2011).
167. Grantham, J.J., Ye, M., Gattone, V.H., 2nd & Sullivan, L.P. In vitro fluid secretion by epithelium from polycystic kidneys. *The Journal of clinical investigation* **95**, 195-202 (1995).
168. Ye, M. & Grantham, J.J. The secretion of fluid by renal cysts from patients with autosomal dominant polycystic kidney disease. *The New England journal of medicine* **329**, 310-313 (1993).
169. Hanaoka, K., Devuyst, O., Schwiebert, E.M., Wilson, P.D. & Guggino, W.B. A role for CFTR in human autosomal dominant polycystic kidney disease. *The American journal of physiology* **270**, C389-399 (1996).
170. Gadsby, D.C., Vergani, P. & Csanády, L. The ABC protein turned chloride channel whose failure causes cystic fibrosis. *Nature* **440**, 477-483 (2006).
171. Ratjen, F. & Doring, G. Cystic fibrosis. *Lancet (London, England)* **361**, 681-689 (2003).
172. Yang, B., Sonawane, N.D., Zhao, D., Somlo, S. & Verkman, A.S. Small-molecule CFTR inhibitors slow cyst growth in polycystic kidney disease. *Journal of the American Society of Nephrology : JASN* **19**, 1300-1310 (2008).
173. Magenheimer, B.S.*, et al.* Early embryonic renal tubules of wild-type and polycystic kidney disease kidneys respond to cAMP stimulation with cystic fibrosis transmembrane conductance regulator/Na(+),K(+),2Cl(-) Co-transporter-dependent cystic dilation. *Journal of the American Society of Nephrology : JASN* **17**, 3424-3437 (2006).
174. Brill, S.R.*, et al.* Immunolocalization of ion transport proteins in human autosomal dominant polycystic kidney epithelial cells. *Proceedings of the National Academy of Sciences of the United States of America* **93**, 10206-10211 (1996).
175. O'Sullivan, D.A.*, et al.* Cystic fibrosis and the phenotypic expression of autosomal dominant polycystic kidney disease. *American journal of kidney diseases : the official journal of the National Kidney Foundation* **32**, 976-983 (1998).
176. Xu, N.*, et al.* Autosomal dominant polycystic kidney disease coexisting with cystic fibrosis. *Journal of nephrology* **19**, 529-534 (2006).
177. Cabrita, I.*, et al.* Cyst growth in ADPKD is prevented by pharmacological and genetic inhibition of TMEM16A in vivo. *Nature communications* **11**, 4320 (2020).
178. Wilson, P.D., Hovater, J.S., Casey, C.C., Fortenberry, J.A. & Schwiebert, E.M. ATP release mechanisms in primary cultures of epithelia derived from the cysts of polycystic kidneys. *Journal of the American Society of Nephrology : JASN* **10**, 218-229 (1999).
179. Praetorius, H.A. & Leipziger, J. ATP release from non-excitable cells. *Purinergic signalling* **5**, 433-446 (2009).
180. Chênevert, J.*, et al.* DOG1: a novel marker of salivary acinar and intercalated duct

differentiation. *Modern pathology : an official journal of the United States and Canadian Academy of Pathology, Inc* **25**, 919-929 (2012).
181. Ruiz, C.*, et al.* Enhanced expression of ANO1 in head and neck squamous cell carcinoma causes cell migration and correlates with poor prognosis. *PloS one* **7**, e43265 (2012).
182. Kraus, A.*, et al.* HIF-1alpha promotes cyst progression in a mouse model of autosomal dominant polycystic kidney disease. *Kidney international* **94**, 887-899 (2018).
183. Schreiber, R.*, et al.* Expression and function of epithelial anoctamins. *The Journal of biological chemistry* **285**, 7838-7845 (2010).
184. Magayr, T.A.*, et al.* Global microRNA profiling in human urinary exosomes reveals novel disease biomarkers and cellular pathways for autosomal dominant polycystic kidney disease. *Kidney international* (2020).
185. Benedetto, R.*, et al.* Epithelial Chloride Transport by CFTR Requires TMEM16A. *Scientific reports* **7**, 12397 (2017).
186. Kraus, A.*, et al.* P2Y2R is a direct target of HIF-1alpha and mediates secretion-dependent cyst growth of renal cyst-forming epithelial cells. *Purinergic Signal.* **12**, 687-695 (2016).
187. Cabrita, I., Buchholz, B., Schreiber, R. & Kunzelmann, K. TMEM16A drives renal cyst growth by augmenting Ca(2+) signaling in M1 cells. *Journal of molecular medicine (Berlin, Germany)* (2020).
188. Viau, A.*, et al.* Divergent function of polycystin 1 and polycystin 2 in cell size regulation. *Biochem Biophys Res Commun* **521**, 290-295 (2020).
189. Yanda, M.K., Cha, B., Cebotaru, C.V. & Cebotaru, L. Pharmacological reversal of renal cysts from secretion to absorption suggests a potential therapeutic strategy for managing autosomal dominant polycystic kidney disease. *The Journal of biological chemistry* **294**, 17090-17104 (2019).
190. Schwiebert, E.M.*, et al.* Autocrine extracellular purinergic signaling in epithelial cells derived from polycystic kidneys. *American journal of physiology. Renal physiology* **282**, F763-775 (2002).
191. Buchholz, B., Teschemacher, B., Schley, G., Schillers, H. & Eckardt, K.U. Formation of cysts by principal-like MDCK cells depends on the synergy of cAMP- and ATP-mediated fluid secretion. *J Mol Med* **89**, 251-261 (2011).
192. Benedetto, R.*, et al.* Plasma membrane-localized TMEM16 proteins are indispensable for expression of CFTR. *Journal of molecular medicine (Berlin, Germany)* **97**, 711-722 (2019).
193. Duvvuri, U.*, et al.* TMEM16A induces MAPK and contributes directly to tumorigenesis and cancer progression. *Cancer research* **72**, 3270-3281 (2012).
194. Buchholz, B.*, et al.* Hypoxia-inducible factor-1alpha causes renal cyst expansion through calcium-activated chloride secretion. *Journal of the American Society of Nephrology : JASN* **25**, 465-474 (2014).
195. Guilbault, C., Saeed, Z., Downey, G.P. & Radzioch, D. Cystic fibrosis mouse models. *American journal of respiratory cell and molecular biology* **36**, 1-7 (2007).
196. Snouwaert, J.N.*, et al.* An animal model for cystic fibrosis made by gene targeting. *Science* **257**, 1083-1088 (1992).
197. Clarke, L.L.*, et al.* Defective epithelial chloride transport in a gene-targeted mouse model of cystic fibrosis. *Science* **257**, 1125-1128 (1992).
198. Berg, P.*, et al.* Impaired Renal HCO(3) (-) Excretion in Cystic Fibrosis. *Journal of the American Society of Nephrology : JASN* (2020).
199. Dubey, R.K. & Jackson, E.K. Estrogen-induced cardiorenal protection: potential cellular, biochemical, and molecular mechanisms. *American journal of physiology. Renal physiology* **280**, F365-388 (2001).
200. Gretz, N.*, et al.* Gender-dependent disease severity in autosomal polycystic kidney disease of rats. *Kidney international* **48**, 496-500 (1995).
201. Buchholz, B., Teschemacher, B., Schley, G., Schillers, H. & Eckardt, K.U. Formation of cysts by principal-like MDCK cells depends on the synergy of cAMP- and ATP-mediated fluid secretion. *J Mol. Med* **89**, 251-261 (2011).

202. Magenheimer, B.S.*, et al.* Early embryonic renal tubules of wild-type and polycystic kidney disease kidneys respond to cAMP stimulation with cystic fibrosis transmembrane conductance regulator/Na(+),K(+),2Cl(-) Co-transporter-dependent cystic dilation. *Journal of the American Society of Nephrology : JASN* **17**, 3424-3437 (2006).
203. Xu, N.*, et al.* Autosomal dominant polycystic kidney disease coexisting with cystic fibrosis. *Journal of nephrology* **19**, 529-534 (2006).
204. Buchholz, B.*, et al.* Hypoxia-Inducible Factor-1α Causes Renal Cyst Expansion through Calcium-Activated Chloride Secretion. *Journal of the American Society of Nephrology : JASN* **25**, 465-474 (2014).
205. Schreiber, R.*, et al.* Lipid peroxidation drives renal cyst growth in vitro through activation of TMEM16A *Journal of the American Society of Nephrology : JASN* **30**, 228-242 (2019).
206. Cabrita, I., Talbi, K., Kunzelmann, K. & Schreiber, R. Loss of PKD1 and PKD2 share common effects on intracellular Ca2+ signaling *Cell Calcium (in press)* (2021).
207. Cha, J.Y.*, et al.* Anoctamin 1 (TMEM16A) is essential for testosterone-induced prostate hyperplasia. *Proc. Natl. Acad. Sci U. S A*, 201423827 (2015).
208. Martinez-Pinna, J., Soriano, S., Tudurí, E., Nadal, A. & de Castro, F. A Calcium-Dependent Chloride Current Increases Repetitive Firing in Mouse Sympathetic Neurons. *Front Physiol* **9**, 508 (2018).
209. Chen, D.*, et al.* ANO1 in urethral SMCs contributes to sex differences in urethral spontaneous tone. *American journal of physiology. Renal physiology* (2020).
210. Davis, P.B. The gender gap in cystic fibrosis survival. *J Gend Specif Med* **2**, 47-51 (1999).
211. Sweezey, N., Tchepichev, S., Gagnon, S., Fertuck, K. & O'Brodovich, H. Female gender hormones regulate mRNA levels and function of the rat lung epithelial Na channel [In Process Citation]. *Am. J. Physiol* **274**, C379-386 (1998).
212. Saint-Criq, V. & Harvey, B.J. Estrogen and the cystic fibrosis gender gap. *Steroids* **81**, 4-8 (2014).
213. Lantinga-van Leeuwen, I.S.*, et al.* Transgenic mice expressing tamoxifen-inducible Cre for somatic gene modification in renal epithelial cells. *Genesis* **44**, 225-232 (2006).
214. Nagao, S.*, et al.* Androgen receptor pathway in rats with autosomal dominant polycystic kidney disease. *Journal of the American Society of Nephrology : JASN* **16**, 2052-2062 (2005).
215. Gaeggeler, H.P.*, et al.* Mineralocorticoid versus glucocorticoid receptor occupancy mediating aldosterone-stimulated sodium transport in a novel renal cell line. *Journal of the American Society of Nephrology : JASN* **16**, 878-891 (2005).
216. Gong, Y., Blok, L.J., Perry, J.E., Lindzey, J.K. & Tindall, D.J. Calcium regulation of androgen receptor expression in the human prostate cancer cell line LNCaP. *Endocrinology* **136**, 2172-2178 (1995).
217. Estrada, M., Liberona, J.L., Miranda, M. & Jaimovich, E. Aldosterone- and testosterone-mediated intracellular calcium response in skeletal muscle cell cultures. *Am J Physiol Endocrinol Metab* **279**, E132-139 (2000).
218. Liu, G.*, et al.* Up-regulation of Orai1 expression and store operated Ca(2+) entry following activation of membrane androgen receptors in MCF-7 breast tumor cells. *BMC Cancer* **15**, 995 (2015).
219. Steinsapir, J., Socci, R. & Reinach, P. Effects of androgen on intracellular calcium of LNCaP cells. *Biochem Biophys Res Commun* **179**, 90-96 (1991).
220. Sun, Y.H., Gao, X., Tang, Y.J., Xu, C.L. & Wang, L.H. Androgens induce increases in intracellular calcium via a G protein-coupled receptor in LNCaP prostate cancer cells. *J Androl* **27**, 671-678 (2006).
221. Vicencio, J.M.*, et al.* Testosterone induces an intracellular calcium increase by a nongenomic mechanism in cultured rat cardiac myocytes. *Endocrinology* **147**, 1386-1395 (2006).
222. Berry, P.A., Birnie, R., Droop, A.P., Maitland, N.J. & Collins, A.T. The calcium sensor STIM1 is regulated by androgens in prostate stromal cells. *Prostate* **71**, 1646-1655 (2011).
223. Sheridan, J.T., Gilmore, R.C., Watson, M.J., Archer, C.B. & Tarran, R. 17β-Estradiol

inhibits phosphorylation of stromal interaction molecule 1 (STIM1) protein: implication for store-operated calcium entry and chronic lung diseases. *The Journal of biological chemistry* **288**, 33509-33518 (2013).
224. Onishi, M., Yamanaka, K., Miyamoto, Y., Waki, H. & Gouraud, S. Trpv4 involvement in the sex differences in blood pressure regulation in spontaneously hypertensive rats. *Physiol Genomics* **50**, 272-286 (2018).
225. Xiao, Q.*, et al.* Voltage- and calcium-dependent gating of TMEM16A/Ano1 chloride channels are physically coupled by the first intracellular loop. *Proc. Natl. Acad. Sci. U. S. A* **108**, 8891-8896 (2011).
226. Ferrera, L.*, et al.* Regulation of TMEM16A chloride channel properties by alternative splicing. *J. Biol. Chem* **284**, 33360-33368 (2009).
227. AlDehni, F.*, et al.* Role of bestrophin for proliferation and in epithelial to mesenchymal transition. *Journal of the American Society of Nephrology : JASN* **20**, 1556-1564 (2009).
228. Greger, R. & Kunzelmann, K. Simultaneous recording of the cell membrane potential and properties of the cell attached membrane of HT_{29} colon carcinoma and CF-PAC cells. *Pflugers Archiv : European journal of physiology* **419**, 209-211 (1991).
229. Schreiber, R.*, et al.* Expression and Function of Epithelial Anoctamins. *J. Biol. Chem* **285**, 7838-7845 (2010).
230. Jung, J.*, et al.* Dynamic modulation of ANO1/TMEM16A HCO3- permeability by Ca2+/calmodulin. *Proc. Natl. Acad. Sci U. S. A* (2013).
231. Vocke, K.*, et al.* Calmodulin-dependent activation and inactivation of anoctamin calcium-gated chloride channels. *J Gen. Physiol* **142**, 381-404 (2013).
232. Yu, Y. & Chen, T.Y. Purified human brain calmodulin does not alter the bicarbonate permeability of the ANO1/TMEM16A channel. *J Gen. Physiol* **145**, 79-81 (2015).
233. Wagner, J.A.*, et al.* Activation of chloride chanels in normal and cystic fibrosis airway epithelial cells by multifunctional calcium/calmodulin- dependent protein kinase. *Nature* **349**, 793-796 (1991).
234. Worrell, R.T. & Frizzell, R.A. CaMKII mediates stimulation of chloride conductance by calcium in T_{84}. *Am. J. Physiol* **260**, C877-C882 (1991).
235. McGill, J.M., Yen, M.S., Basavappa, S., Mangel, A.W. & Kwiatkowski, A.P. ATP-activated chloride permeability in biliary epithelial cells is regulated by calmodulin-dependent protein kinase II. *Biochem Biophys Res Commun* **208**, 457-462 (1995).
236. Xie, W.*, et al.* Inositol 3,4,5,6-tetrakisphosphate inhibits the calmodulin-dependent protein kinase II-activated chloride conductance in T84 colonic epithelial cells. *J. Biol. Chem* **271**, 14092-14097 (1996).
237. Schlenker, T. & Fitz, J.G. Ca(2+)-activated C1- channels in a human biliary cell line: regulation by Ca2+/calmodulin-dependent protein kinase. *The American journal of physiology* **271**, G304-310 (1996).
238. Wang, Y.X. & Kotlikoff, M.I. Inactivation of calcium-activated chloride channels in smooth muscle by calcium/calmodulin-dependent protein kinase. *Proc. Natl. Acad. Sci. U. S. A* **94**, 14918-14923 (1997).
239. He, X.D. & Goyal, R.K. CaMKII inhibition hyperpolarizes membrane and blocks nitrergic IJP by closing a Cl(-) conductance in intestinal smooth muscle. *Am J Physiol Gastrointest Liver Physiol* **303**, G240-246 (2012).
240. Lin, C.X.*, et al.* Ca(2+)/Calmodulin-Dependent Protein Kinase II gamma-Dependent Serine727 Phosphorylation Is Required for TMEM16A Ca(2+)-Activated Cl(-) Channel Regulation in Cerebrovascular Cells. *Circ J* **82**, 903-913 (2018).
241. Ayon, R.J.*, et al.* Molecular Mechanism of TMEM16A Regulation: Role of CaMKII and PP1/PP2A. *Am J Physiol Cell Physiol* (2019).
242. Sánchez-Solano, A.*, et al.* Regulation of the Ca(2+)-activated chloride channel Anoctamin-1 (TMEM16A) by Ca(2+)-induced interaction with FKBP12 and calcineurin. *Cell calcium* **89**, 102211 (2020).
243. Greenwood, I.A., Ledoux, J. & Leblanc, N. Differential regulation of Ca(2+)-activated Cl(-) currents in rabbit arterial and portal vein smooth muscle cells by Ca(2+)-calmodulin-dependent kinase. *J Physiol* **534**, 395-408 (2001).
244. Ko, W. & Suh, B.C. Differential Regulation of Ca(2+)-Activated Cl(-) Channel TMEM16A

Splice Variants by Membrane PI(4,5)P(2). *International journal of molecular sciences* **22**(2021).
245. Ko, W.*, et al.* Allosteric modulation of alternatively spliced Ca(2+)-activated Cl(-) channels TMEM16A by PI(4,5)P(2) and CaMKII. *Proceedings of the National Academy of Sciences of the United States of America* (2020).
246. Xie, W.*, et al.* Regulation of Ca2+-dependent Cl- conductance in a human colonic epithelial cell line (T84): cross-talk between Ins(3,4,5,6)P4 and protein phosphatases. *J Physiol* **510**, 661-673 (1998).
247. Ho, M.W., Kaetzel, M.A., Armstrong, D.L. & Shears, S.B. Regulation of a human chloride channel. a paradigm for integrating input from calcium, type ii calmodulin-dependent protein kinase, and inositol 3,4,5,6-tetrakisphosphate. *The Journal of biological chemistry* **276**, 18673-18680 (2001).
248. Tian, Y.*, et al.* Control of TMEM16A by INO-4995 and other inositolphosphates. *Br. J Pharmacol* **168**, 253-265 (2013).
249. Centeio, R.*, et al.* Pharmacological Inhibition and Activation of the Ca(2+) Activated Cl(-) Channel TMEM16A. *International journal of molecular sciences* **21**, 2557 (2020).
250. Cabrita, I.*, et al.* TMEM16A Mediated Mucus Production in Human Airway Epithelial Cells. *Am J Respir Cell Mol Biol* (2020).
251. Martins, J.R.*, et al.* Anoctamin 6 is an essential component of the outwardly rectifying chloride channel. *Proc. Natl. Acad. Sci. U. S. A* **108**, 18168-18172 (2011).
252. Benedetto, R.*, et al.* Transport properties in CFTR-/- knockout piglets suggest normal airway surface liquid pH and enhanced amiloride-sensitive Na(+) absorption. *Pflugers Archiv : European journal of physiology* **472**, 1507-1519 (2020).
253. Tian, Y., Schreiber, R. & Kunzelmann, K. Anoctamins are a family of Ca2+ activated Cl- channels. *J Cell Sci* **125**, 4991-4998 (2012).
254. Schreiber, R.*, et al.* Regulation of TMEM16A/ANO1 and TMEM16F/ANO6 ion currents and phospholipid scrambling by Ca2+ and plasma membrane lipid *J Physiology (London)* **596**, 217-229 (2018).
255. de la Fuente, R., Namkung, W., Mills, A. & Verkman, A.S. Small molecule screen identifies inhibitors of a human intestinal calcium activated chloride channel. *Mol Pharmacol* **73**, 758-768 (2008).
256. Centeio, R., Ousingsawat, J., schreiber, R. & Kunzelmann, K. CLCA1 Regulates Airway Mucus Production and Ion Secretion Through TMEM16A *Int ernational journal of molecular sciences* **22**, 5133 (2021).
257. Pedemonte, N. & Galietta, L.J. Structure and Function of TMEM16 Proteins (Anoctamins). *Physiol Rev* **94**, 419-459 (2014).
258. Whitlock, J.M. & Hartzell, H.C. Anoctamins/TMEM16 Proteins: Chloride Channels Flirting with Lipids and Extracellular Vesicles. *Annu Rev Physiol* (2017).
259. Suzuki, J., Umeda, M., Sims, P.J. & Nagata, S. Calcium-dependent phospholipid scrambling by TMEM16F. *Nature* **468**, 834-838 (2010).
260. Sirianant, L., Ousingsawat, J., Wanitchakool, P., Schreiber, R. & Kunzelmann, K. Cellular Volume regulation by Anoctamin 6:Ca2+, phospholipase A2,osmosensing. *Pflugers Archiv : European journal of physiology* **468**, 335-349 (2016).
261. Takayama, Y., Shibasaki, K., Suzuki, Y., Yamanaka, A. & Tominaga, M. Modulation of water efflux through functional interaction between TRPV4 and TMEM16A/anoctamin 1. *FASEB journal : official publication of the Federation of American Societies for Experimental Biology* **28**, 2238-2248 (2014).
262. Cho, H.*, et al.* The calcium-activated chloride channel anoctamin 1 acts as a heat sensor in nociceptive neurons. *Nat. Neurosci* **15**, 1015-1021 (2012).
263. Hawn, M.B., Akin, E., Hartzell, H.C., Greenwood, I.A. & Leblanc, N. Molecular Mechanisms of Activation and Regulation of ANO1-Encoded Ca2+-Activated Cl- Channels. *Channels (Austin)* (2021).
264. Hasan, R., Leeson-Payne, A.T., Jaggar, J.H. & Zhang, X. Calmodulin is responsible for Ca(2+)-dependent regulation of TRPA1 Channels. *Scientific reports* **7**, 45098 (2017).
265. Zheng, W.*, et al.* Direct Binding between Pre-S1 and TRP-like Domains in TRPP Channels Mediates Gating and Functional Regulation by PIP2. *Cell Rep* **22**, 1560-1573

(2018).
266. Singh, S., Syme, C.A., Singh, A.K., Devor, D.C. & Bridges, R.J. Benzimidazolone activators of chloride secretion: potential therapeutics for cystic fibrosis and chronic obstructive pulmonary disease. *J Pharmacol Exp Ther* **296**, 600-611 (2001).
267. Devor, D.C., Singh, A.K., Frizzell, R.A. & Bridges, R.J. Modulation of Cl^- secretion by benzimidazolones. I. Direct activation of a Ca^{2+}- dependent K^+ channel. *Am. J. Physiol* **271**, L775-L784 (1996).
268. Pedarzani, P.*, et al.* Control of electrical activity in central neurons by modulating the gating of small conductance Ca2+-activated K+ channels. *J. Biol. Chem* **276**, 9762-9769 (2001).
269. Ávalos Prado, P.*, et al.* KCNE1 is an auxiliary subunit of two distinct ion channel superfamilies. *Cell* (2020).
270. Wald, D.*, et al.* SIGIRR, a negative regulator of Toll-like receptor-interleukin 1 receptor signaling. *Nat Immunol* **4**, 920-927 (2003).
271. Garlanda, C., Anders, H.J. & Mantovani, A. TIR8/SIGIRR: an IL-1R/TLR family member with regulatory functions in inflammation and T cell polarization. *Trends Immunol* **30**, 439-446 (2009).
272. Sampath, V.*, et al.* SIGIRR genetic variants in premature infants with necrotizing enterocolitis. *Pediatrics* **135**, e1530-1534 (2015).
273. Xiao, H.*, et al.* The Toll-interleukin-1 receptor member SIGIRR regulates colonic epithelial homeostasis, inflammation, and tumorigenesis. *Immunity* **26**, 461-475 (2007).
274. Noris, M.*, et al.* The Toll-IL-1R member Tir8/SIGIRR negatively regulates adaptive immunity against kidney grafts. *J Immunol* **183**, 4249-4260 (2009).
275. Ferenbach, D. & Hughes, J. Macrophages and dendritic cells: what is the difference? *Kidney international* **74**, 5-7 (2008).
276. Hu, J., Winqvist, O., Flores-Morales, A., Wikström, A.C. & Norstedt, G. SOCS2 influences LPS induced human monocyte-derived dendritic cell maturation. *PloS one* **4**, e7178 (2009).
277. Gupta, A.*, et al.* Low Vitamin-D Levels Combined with PKP3-SIGIRR-TMEM16J Host Variants Is Associated with Tuberculosis and Death in HIV-Infected and -Exposed Infants. *PLoS. ONE* **11**, e0148649 (2016).
278. Eckardt, K.U.*, et al.* Evolving importance of kidney disease: from subspecialty to global health burden. *Lancet (London, England)* **382**, 158-169 (2013).
279. Lech, M.*, et al.* Resident dendritic cells prevent postischemic acute renal failure by help of single Ig IL-1 receptor-related protein. *J Immunol* **183**, 4109-4118 (2009).
280. Molgora, M.*, et al.* IL-1R8 is a checkpoint in NK cells regulating anti-tumour and anti-viral activity. *Nature* **551**, 110-114 (2017).
281. Smith, K.D. Toll-like receptors in kidney disease. *Current opinion in nephrology and hypertension* **18**, 189-196 (2009).
282. Grynkiewicz, G., Poenie, M. & Tsien, R.Y. A new generation of Ca^{2+} indicators with greatly improved fluorescence properties. *The Journal of biological chemistry* **260**, 3440-3450 (1985).
283. Wu, J.*, et al.* Red fluorescent genetically encoded Ca2+ indicators for use in mitochondria and endoplasmic reticulum. *Biochem. J* **464**, 13-22 (2014).
284. Chen, N.K.*, et al.* Negative regulatory responses to metabolically triggered inflammation impair renal epithelial immunity in diabetes mellitus. *J Mol Med (Berl)* **91**, 587-598 (2013).
285. Kim, H.*, et al.* Anoctamin 9/TMEM16J is a cation channel activated by cAMP/PKA signal. *Cell calcium* **71**, 75-85 (2018).
286. Kruger, W.A., Monteith, G.R. & Poronnik, P. The plasma membrane Ca(2+)-ATPase: regulation by PSD-95/Dlg/Zo-1 scaffolds. *Int. J. Biochem. Cell Biol* **42**, 805-808 (2010).
287. Schreiber, R., Ousingsawat, J. & Kunzelmann, K. Targeting of Intracellular TMEM16 Proteins to the Plasma Membrane and Activation by Purinergic Signaling. *International journal of molecular sciences* **21**(2020).
288. Reichhart, N.*, et al.* Anoctamin-4 is a bona fide Ca(2+)-dependent non-selective cation channel. *Scientific reports* **9**, 2257 (2019).

289. Warth, R.*, et al.* Molecular and functional characterization of the small Ca^{2+}-regulated K^+ channel (rSK4) of colonic crypts. *Pflugers Archiv : European journal of physiology* **438**, 437-444 (1999).
290. Feske, S., Wulff, H. & Skolnik, E.Y. Ion channels in innate and adaptive immunity. *Annu Rev Immunol* **33**, 291-353 (2015).
291. Giannoudaki, E.*, et al.* SIGIRR Negatively Regulates IL-36-Driven Psoriasiform Inflammation and Neutrophil Infiltration in the Skin. *J Immunol* **207**, 651-660 (2021).
292. Molgora, M., Supino, D., Mantovani, A. & Garlanda, C. Tuning inflammation and immunity by the negative regulators IL-1R2 and IL-1R8. *Immunol Rev* **281**, 233-247 (2018).
293. Ji, Q.*, et al.* Activation of TMEM16A by natural product canthaxanthin promotes gastrointestinal contraction. *FASEB journal : official publication of the Federation of American Societies for Experimental Biology* (2020).
294. Lemos, F.O., Bultynck, G. & Parys, J.B. A comprehensive overview of the complex world of the endo- and sarcoplasmic reticulum Ca(2+)-leak channels. *Biochim Biophys Acta Mol Cell Res* **1868**, 119020 (2021).
295. Kralt, A.*, et al.* Intrinsically disordered linker and plasma membrane-binding motif sort Ist2 and Ssy1 to junctions. *Traffic* **16**, 135-147 (2015).
296. Barreda, D.*, et al.* The Scribble Complex PDZ Proteins in Immune Cell Polarities. *J Immunol Res* **2020**, 5649790 (2020).
297. Marziali, F., Dizanzo, M.P., Cavatorta, A.L. & Gardiol, D. Differential expression of DLG1 as a common trait in different human diseases: an encouraging issue in molecular pathology. *Biol Chem* **400**, 699-710 (2019).
298. Kruger, W.A., Yun, C.C., Monteith, G.R. & Poronnik, P. Muscarinic-induced recruitment of plasma membrane Ca2+-ATPase involves PSD-95/Dlg/Zo-1-mediated interactions. *The Journal of biological chemistry* **284**, 1820-1830 (2009).
299. Luck, K.*, et al.* A reference map of the human binary protein interactome. *Nature* **580**, 402-408 (2020).
300. Maniero, C.*, et al.* ANO4 (Anoctamin 4) Is a Novel Marker of Zona Glomerulosa That Regulates Stimulated Aldosterone Secretion. *Hypertension* **74**, 1152-1159 (2019).
301. Wang, D.Y.*, et al.* The decreased frequency of SIGIRR-positive CD4+ T cells in peripheral blood of patients with SLE and its correlation with disease activity. *Mol Biol Rep* **42**, 423-430 (2015).
302. Trebak, M. & Kinet, J.P. Calcium signalling in T cells. *Nat Rev Immunol* **19**, 154-169 (2019).
303. Babich, A. & Burkhardt, J.K. Coordinate control of cytoskeletal remodeling and calcium mobilization during T-cell activation. *Immunol Rev* **256**, 80-94 (2013).
304. Yanda, M.K., Liu, Q., Cebotaru, V., Guggino, W.B. & Cebotaru, L. Role of calcium in adult onset polycystic kidney disease. *Cellular signalling* **53**, 140-150 (2019).
305. Miyakawa, A.*, et al.* Intracellular calcium release modulates polycystin-2 trafficking. *BMC nephrology* **14**, 34 (2013).
306. Bai, C.X.*, et al.* Formation of a new receptor-operated channel by heteromeric assembly of TRPP2 and TRPC1 subunits. *EMBO reports* **9**, 472-479 (2008).
307. Sammels, E.*, et al.* Polycystin-2 activation by inositol 1,4,5-trisphosphate-induced Ca2+ release requires its direct association with the inositol 1,4,5-trisphosphate receptor in a signaling microdomain. *J Biol. Chem* **285**, 18794-18805 (2010).
308. Hanaoka, K. & Guggino, W.B. cAMP Regulates Cell Proliferation and Cyst Formation in Autosomal Polycystic Kidney Disease Cells. *J Am Soc. Nephrol* **11**, 1179-1187 (2000).
309. Gendron, F.P., Placet, M. & Arguin, G. P2Y(2) Receptor Functions in Cancer: A Perspective in the Context of Colorectal Cancer. *Advances in experimental medicine and biology* **1051**, 91-106 (2017).
310. Grantham, J.J. & Calvet, J.P. Polycystic kidney disease: In danger of being X-rated? *Proceedings of the National Academy of Sciences of the United States of America* **98**, 790-792 (2001).
311. Clarke, L.L.*, et al.* Relationship of a non-cystic fibrosis transmembrane conductance regulator-mediated chloride conductance to organ-level didease in *cftr (-/-)* mice. *Proc.*

Natl. Acad. Sci. USA **91**, 479-483 (1994).
312. Layton, A.T. & Sullivan, J.C. Recent advances in sex differences in kidney function. *American journal of physiology. Renal physiology* **316**, F328-f331 (2019).
313. Michels, G. & Hoppe, U.C. Rapid actions of androgens. *Frontiers in neuroendocrinology* **29**, 182-198 (2008).
314. Couchourel, D., Leclerc, M., Filep, J. & Brunette, M.G. Testosterone enhances calcium reabsorption by the kidney. *Molecular and cellular endocrinology* **222**, 71-81 (2004).
315. Gorczynska, E. & Handelsman, D.J. Androgens rapidly increase the cytosolic calcium concentration in Sertoli cells. *Endocrinology* **136**, 2052-2059 (1995).
316. Metzner, A.*, et al.* A high throughput zebrafish chemical screen reveals ALK5 and non-canonical androgen signalling as modulators of the pkd2(-/-) phenotype. *Scientific reports* **10**, 72 (2020).
317. de Souza Santos, R., Frank, A.P. & Clegg, D.J. The impact of sex and sex hormones on cell function. *Steroids* **128**, 72-74 (2017).
318. Bellott, D.W.*, et al.* Mammalian Y chromosomes retain widely expressed dosage-sensitive regulators. *Nature* **508**, 494-499 (2014).
319. Berrout, J.*, et al.* Function of transient receptor potential cation channel subfamily V member 4 (TRPV4) as a mechanical transducer in flow-sensitive segments of renal collecting duct system. *The Journal of biological chemistry* **287**, 8782-8791 (2012).
320. Liu, S.*, et al.* Eact, a small molecule activator of TMEM16A, activates TRPV1 and elicits pain- and itch-related behaviours. *British journal of pharmacology* **173**, 1208-1218 (2016).
321. Genovese, M.*, et al.* TRPV4 and purinergic receptor signalling pathways are separately linked in airway epithelia to CFTR and TMEM16A chloride channels. *J Physiol* (2019).
322. Tien, J.*, et al.* A comprehensive search for calcium binding sites critical for TMEM16A calcium-activated chloride channel activity. *eLife*, e02772 (2014).
323. Sones, W.R., Davis, A.J., Leblanc, N. & Greenwood, I.A. Cholesterol depletion alters amplitude and pharmacology of vascular calcium-activated chloride channels. *Cardiovasc. Res* **87**, 476-484 (2010).
324. Cipriani, G., Serboiu, C.S., Gherghiceanu, M., Faussone-Pellegrini, M.S. & Vannucchi, M.G. NK receptors, Substance P, Ano1 expression and ultrastructural features of the muscle coat in Cav-1(-/-) mouse ileum. *Journal of cellular and molecular medicine* **15**, 2411-2420 (2011).
325. Ma, K.*, et al.* Ca(2+)-activated Cl(-) channel TMEM16A inhibition by cholesterol promotes angiogenesis in endothelial cells. *J Adv Res* **29**, 23-32 (2021).
326. Kawata, N., Kondo, R., Suzuki, Y. & Yamamura, H. Increased TMEM16A-mediated Ca(2+)-activated Cl(-) currents in portal vein smooth muscle cells of caveolin 1-deficient mice. *Biological & pharmaceutical bulletin* (2022).